Methods in Molecular Biology 1148

Springer Protocols

Sidney Cambridge *Editor*

Photoswitching Proteins

Methods and Protocols

Humana Press

METHODS IN MOLECULAR BIOLOGY

Series Editor
John M. Walker
School of Life Sciences
University of Hertfordshire
Hatfield, Hertfordshire, AL10 9AB, UK

For further volumes:
http://www.springer.com/series/7651

Photoswitching Proteins

Methods and Protocols

Edited by

Sidney Cambridge

Institute of Anatomy and Cell Biology, University of Heidelberg, Heidelberg, Germany

Humana Press

Editor
Sidney Cambridge
Institute of Anatomy and Cell Biology
University of Heidelberg
Heidelberg, Germany

ISSN 1064-3745 ISSN 1940-6029 (electronic)
ISBN 978-1-4939-0469-3 ISBN 978-1-4939-0470-9 (eBook)
DOI 10.1007/978-1-4939-0470-9
Springer New York Heidelberg Dordrecht London

Library of Congress Control Number: 2014936098

Printed on acid-free paper

Humana Press is a brand of Springer
Springer is part of Springer Science+Business Media (www.springer.com)

Preface

During the last three decades, we experienced two major method revolutions in biology—the development of PCR and the introduction of the green fluorescent protein. To my mind, we are now in the midst of another revolution, which is the use of optical approaches in biomedical research. This optical revolution, if you will, is an amalgam of amazingly superior new equipment, including multiphoton and super-resolution microscopes, and an ever-growing zoo of light-responsive molecules, many of whom are biologically active. In particular, researchers are keenly interested in being able to use light for controlling the activity of proteins, the central players in cellular metabolism. There are now several different ways to manipulate proteins with light, including light-sensitive chemical modification of proteins and the use of naturally light-sensitive proteins. Not surprisingly, major efforts are underway to identify novel proteins whose activity is genetically light dependent. In addition, one future goal of the field is to devise a genetically encoded system that can render every protein of choice light-sensitive. If the heavy use of fluorescent proteins and opsin-based channels is any indication, there is a huge market for additional molecular tools, and, presumably, there are many more light-responsive proteins with exciting properties existing in nature that we just have not discovered yet.

This issue of Methods in Molecular Biology on Photoswitching Proteins is timely in its attempt to provide a comprehensive, critical view of the currently available techniques to manipulate proteins with light. The focus, albeit not exclusively, has been on proven applications of photoswitching proteins rather than brand new tools that have not been tested in an experimental setting. Also, the selection of topics in this issue was made to emphasize applications of photoswitching proteins in neurobiology. Optical approaches have been mostly advanced by the neurosciences, where the field was and is in dire need for new tools that allow fast, high-resolution characterization and manipulation of single cells in complex neuronal tissue. And in a "trickle-down effect," many of these optical approaches are now embraced by other fields as well. Apparently, if a method works in neurobiology it works well in other areas too!

With all the available light-responsive molecular tools and fancy microscopes, it is easy to get excited about the possibilities that open up for research in the twenty-first century. It is clear that the future of biomedical research is bright, and it will be fascinating to see where optical approaches can to take us in the upcoming years.

Heidelberg, Germany *Sidney Cambridge*

Contents

Contributors

Virgile Adam • *Université Grenoble Alpes, Institut de Biologie Structurale, Grenoble, France*

Dominique Bourgeois • *Université Grenoble Alpes, Institut de Biologie Structurale, Grenoble, France*

Martin Byrdin • *Université Grenoble Alpes, Institut de Biologie Structurale, Grenoble, France*

Sidney Cambridge • *Institute of Anatomy and Cell Biology, University of Heidelberg, Heidelberg, Germany*

Wagner Steuer Costa • *Buchmann Institute for Molecular Life Sciences, Johann Wolfgang Goethe-University, Frankfurt, Germany*

Matthew K. Daddysman • *Department of Chemistry, University of North Carolina at Chapel Hill, Chapel Hill, NC, USA*

Pietro DeCamilli • *Department of Cell Biology, Yale University School of Medicine, New Haven, CT, USA*

Peter Dedecker • *Department of Chemistry, University of Leuven, Heverlee, Belgium*

Alexander Deiters • *Department of Chemistry, University of Pittsburgh, Pittsburgh, PA, USA*

William P. Dempsey • *Department of Biosystems Science and Engineering, ETH Zurich, Zurich, Switzerland*

Chenxi Duan • *Université Grenoble Alpes, Institut de Biologie Structurale, Grenoble, France*

Christopher J. Fecko • *Department of Chemistry, University of North Carolina at Chapel Hill, Chapel Hill, NC, USA*

Consuelo Fois • *Focus Program Translational Neuroscience (FTN) and Institute for Microscopic Anatomy and Neurobiology, Johannes Gutenberg-University Mainz Mainz, Germany*

Archan Ganguly • *BSB 1029, MC0612, University of California, San Diego, CA, USA*

Charles A. Gersbach • *Department of Biomedical Engineering, Duke University, Durham, NC, USA*

Alexander Gottschalk • *Focus Program Translational Neuroscience (FTN) and Institute for Microscopic Anatomy and Neurobiology, Johannes Gutenberg-University Mainz, Mainz, Germany*

Klaus M. Hahn • *Department of Pharmacology, University of North Carolina at Chapel Hill, Chapel Hill, NC, USA*

Olof Idevall-Hagren • *Department of Cell Biology, Yale University School of Medicine, New Haven, CT, USA*

Ehud Y. Isacoff • *Department of Molecular and Cell Biology and Helen Wills Neuroscience Institute, University of California Berkeley, Berkeley, CA, USA*

Yuji Ishitsuka • *Institute of Applied Physics and Center for Functional Nanostructures, Karlsruhe Institute of Technology, Karlsruhe, Germany*

Andrei V. Karginov • *Department of Pharmacology, University of Illinois at Chicago, Chicago, IL, USA*

Vladimir Korzh • *Institute of Molecular and Cell Biology, Agency for Science, Technology and Research, Singapore, Singapore*

Jana Liewald • *Buchmann Institute for Molecular Life Sciences, Johann Wolfgang Goethe-University, Frankfurt, Germany*
Benjamien Moeyaert • *Department of Chemistry, University of Leuven, Heverlee, Belgium*
Thomas A. Münch • *Centre for Integrative Neuroscience, University Tübingen, Tübingen, Germany*
Marion Mutter • *Centre for Integrative Neuroscience, University Tübingen, Tübingen, Germany*
Karin Nienhaus • *Institute of Applied Physics and Center for Functional Nanostructures, Karlsruhe Institute of Technology, Karlsruhe, Germany*
G. Ulrich Nienhaus • *Institute of Applied Physics and Center for Functional Nanostructures, Karlsruhe Institute of Technology, Karlsruhe, Germany*
Periklis Pantazis • *Department of Biosystems Science and Engineering, ETH Zurich, Zurich, Switzerland*
Lauren R. Polstein • *Department of Biomedical Engineering, Duke University, Durham, NC, USA*
Pierre-Hugues Prouvot • *Focus Program Translational Neuroscience (FTN) and Institute for Microscopic Anatomy and Neurobiology, Johannes Gutenberg-University Mainz, Mainz, Germany*
Hanyu Qin • *Department of Biosystems Science and Engineering, ETH Zurich, Zurich, Switzerland*
Andreas Reiner • *Department of Molecular and Cell Biology and Helen Wills Neuroscience Institute, University of California Berkeley, Berkeley, CA, USA*
Subhojit Roy • *BSB 1030A, MC0612, University of California, San Diego, CA, USA*
Philipp Stawski • *Department of Chemistry, Massachusetts Institute of Technology, Cambridge, MA, USA*
Albrecht Stroh • *Focus Program Translational Neuroscience (FTN) and Institute for Microscopic Anatomy and Neurobiology, Johannes Gutenberg-University Mainz, Mainz, Germany*
Martin Sumser • *Department of Chemistry, Ludwig-Maximilians-Universität München, München, Germany*
Natalia Swietek • *Centre for Integrative Neuroscience, University Tübingen, Tübingen, Germany*
Cathleen Teh • *Institute of Molecular and Cell Biology, Agency for Science, Technology and Research, Singapore, Singapore*
Michael A. Tycon • *Department of Chemistry, University of North Carolina at Chapel Hill, Chapel Hill, NC, USA*
Nina Wittenmayer • *University Medical Center Göttingen, Göttingen, Germany*

Chapter 1

Photoinduced Damage Resulting from Fluorescence Imaging of Live Cells

Matthew K. Daddysman, Michael A. Tycon, and Christopher J. Fecko

Abstract

The widespread application of fluorescence microscopy to study live cells has led to a greater understanding of numerous biological processes. Many techniques have been developed to uniquely label structures and track metabolic pathways using fluorophores in live cells. However, the photochemistry of nonnative compounds and the deposition of energy into the cell during imaging can result in unexpected and unwanted side effects. Herein, we examine potential live cell damage by first discussing common imaging considerations and modalities in fluorescence microscopy. We then consider several mechanisms by which various photochemical and photophysical phenomena cause cellular damage and introduce techniques that have leveraged these phenomena to intentionally create damage inside cells. Reviewing conditions under which intentional damage occurs can allow one to better predict when unintentional damage may be important. Finally, we delineate ways of checking for and reducing photochemical and photophysical damage.

Key words Epifluorescence, Confocal microscopy, Multiphoton microscopy, Photodamage, Ablation, Reactive oxygen species, Radical

1 Introduction

The use of light to interrogate live cell processes has resulted in great mechanistic and structural insight. Fluorescence microscopy has become one of the most widely used light microscopy techniques due to inherent advantages that include selective labeling and imaging of low concentrations of fluorophore [1, 2]. However, the introduction of exogenous fluorophores necessary for fluorescence microscopy inherently modifies the photochemistry of the cell, particularly in the vicinity of the tagged molecule. It is important to be aware of the potential for unnatural cellular damage that can be attributed to these exogenous molecules, which presents as a confounding variable in live cell microscopy experiments. We note that the presence of the fluorophore may have adverse consequences even in the absence of light (e.g., protein inactivation due

Sidney Cambridge (ed.), *Photoswitching Proteins: Methods and Protocols*, Methods in Molecular Biology, vol. 1148,
DOI 10.1007/978-1-4939-0470-9_1,

to the addition of a GFP tag [3, 4]), but this chapter only considers negative photoinduced effects due to imaging the sample.

Damage resulting from fluorescence microscopy can generally be divided into two broad categories, photochemical or photophysical. The likelihood that each type of damage will adversely affect the experiment is determined by the choice of microscopy method and fluorophore, which we refer to using the collective term imaging modality. We begin by reviewing such imaging considerations and then discuss the photochemical and photophysical damage mechanisms in more detail. Finally, we suggest potentials tests for damage and suggest best practices to avoid unwanted photodamage in live cell experiments.

2 Imaging Considerations

2.1 Illumination Parameters

Before discussing potential pitfalls inherent in imaging live cells, we first wish to review important terminology for later reference. The terms energy, power, and intensity describe the strength of the light used to image samples. Although they are closely related quantities, each has a specific meaning that can be important for considering mechanisms of light-induced damage.

Optical microscopy takes advantage of light–matter interactions to gain spatial information about samples. Images result from the absorption, emission, or scattering of individual photons by molecules within the sample. The energy per photon (E) is related to the frequency (ν) or the wavelength (λ) of light by Plank's constant (h):

$$E = h\nu \text{ or } E = \frac{hc}{\lambda}$$

In most fluorescence-based imaging experiments, the wavelength must be selected so that the energy of incident photons matches the gap between the ground state and excited electronic state of the fluorophore. When a fluorophore molecule is excited, it usually relaxes by emitting a photon (fluorescence) but can also relax through other nonradiative pathways that can lead to cellular damage. The SI unit of energy is the Joule (1 kg m^2/s^2), though some optical experiments quote energy in terms of electron-Volts, where $1\ eV = 1.6 \times 10^{-19}$ J.

Power is the rate at which energy is transferred; the SI unit is the Watt (1 J/s). Most optical microscopy experiments utilize light sources whose power output is time independent, such as arc lamps or continuous wave lasers. However, pulsed lasers are used for some specialized types of optical imaging, such as multiphoton microscopy (MPM), because they deliver many photons in a shorter period of time. For example, Ti:sapphire lasers that are most typically used for MPM produce a train of pulses whose duration is ~100 fs separated by dark periods that last for ~10 ns. Other lasers may produce picosecond- or nanosecond-duration pulses. The power of a pulsed laser can be described as either the

time-averaged quantity or the peak power achieved during a single pulse. The time-averaged power is measured over numerous cycles, often using a power meter with a response time much longer than the repetition rate. However, since the "dark period" usually is much longer than the brief flash of light, the time-averaged power is often much lower than the peak power. The peak power, P_{peak}, is approximately given by

$$P_{peak} = \frac{P_{avg}}{\frac{t}{T}}$$

where P_{avg} is the time-averaged power, and t is the length of time that the laser is emitting light per complete cycle of length T. For a Ti:sapphire laser that has a 80 MHz pulse frequency and a 120-fs pulse duration, a time-averaged power of 10 mW (a common value for MPM imaging) corresponds to a peak power of 1,000 W. The peak power is five orders of magnitude larger than the time-averaged power. These large peak powers are leveraged to drive nonlinear transitions in molecules resulting in multiphoton photoexcitation, which can then lead to fluorescence or cellular damage.

Intensity is the measure of power per unit area, and its SI unit is Watts per square meter (often expressed as W/cm^2). In microscopy literature, the intensity is sometimes specified at the focal plane of the objective lens. However, the intensity of a focused beam can be challenging to measure directly, so it is important to note that the quoted values are often estimated based on an expected (theoretical) illuminated area. The actual illuminated area can differ substantially from this calculated value. It is also important to note that the same incident power can result in different intensities when using different objective lenses or in different optical configurations. A tighter focus will increase the intensity with the same incident power. For example, when using a laser scanning microscopy method all of the incident power is focused to a diffraction-limited spot at the focus of the objective lens. This results in a much higher intensity at each point compared to using widefield illumination, in which a much larger field is illuminated somewhat evenly. However, the high intensity used in laser scanning is counteracted by reducing the observation time for each point to a few microseconds, whereas in widefield illumination the entire field of view is illuminated during the whole frame exposure time. Therefore, the total energy delivered to each point in a sample may be similar in widefield and laser scanning microscopies even though the peak intensity is much larger in laser scanning microscopy.

As will be described later, the illumination parameters are critically important in determining the potential photoreactions that occur in a system. Therefore, it is important that these parameters are included in publications. We have noticed that laser powers are sometimes not expressed as useful or reproducible quantities in the

literature, e.g., including a percentage of the maximum laser power, a specific setting on the imaging software, or as the level of current used to operate the laser. Such specifications are not useful for most outside researchers. Even researchers that have the same microscope setup can experience differences in beam alignment and laser (or arc lamp) age that will result in different powers at the objective. Therefore, it is imperative that *all* powers should be measured with a power meter at the objective as part of the experiment and reported along with the objective used so that the experiments can be reproduced by others.

2.2 Imaging Modality

This chapter is primarily concerned with photoinduced damage (both intentional and unintentional) that can occur during optical imaging of biological samples, with a focus on fluorescence microscopy and related photoactivation/photoswitching techniques. Fluorescence microscopy offers the advantage of detecting specific subcellular or molecular components by targeted labeling, but it also offers advantages over other optical microscopy methods that are primarily due to the properties of fluorescence. Fluorescence emission is shifted to wavelengths longer than those required for excitation. This Stokes shift is due to a small amount of energy dissipation that occurs on an ultrafast time scale in the electronically excited state of the fluorophore. The wavelength difference allows the excitation light to be filtered out to produce a background-free emission signal, which is ideal for imaging low concentrations of fluorophore. This is especially important if the molecule to be detected exists in a low copy number inside the cell. However, introducing and exciting an exogenous fluorophore in the cellular system result in potential artificial photochemical pathways that can disrupt cellular processes in nonnative ways. We discuss this possibility in both intentional and unintentional contexts.

The simplest florescence microscopy technique is widefield epifluorescence. In this configuration, the excitation light from an incoherent source is used to illuminate a large area in the focal plane of the objective lens. A portion of the sample fluorescence, which is emitted in all directions, is collected by the same objective lens. The fluorescence is optically separated from the excitation light by a dichroic mirror and bandpass filter before being refocused onto an image sensor. As mentioned above, this method uses relatively low intensity (typical time-averaged intensities are $10–10^2$ W/cm^2) but continuous excitation light (0.1–1-s illumination times). It is useful for basic imaging of thin specimens, but optically thick samples typically require a more specialized method to reduce out-of-focus contributions to the signal. Widefield configurations do not easily allow for selective illumination of small sample regions, a feature desirable for experiments that employ photoswitchable labels. As extensions of conventional widefield techniques, the bourgeoning fields of

single-molecule microscopy and superresolution microscopy have provided a means to extract even more detailed information about biological processes in cells. Given the high signal-to-noise requirements of such experiments, many studies use much higher optical intensities than conventional widefield imaging.

Laser scanning confocal fluorescence microscopy offers increased optical resolution and the ability to target specific regions for photobleaching or photoswitching. It is most commonly applied in a laser scanning configuration in which excitation light from a laser is focused to a point in the sample by the objective lens. This point is raster scanned across the field of view by changing the angle at which the laser light enters the back aperture of the objective lens [5]. Fluorescence from the sample is again collected by the objective lens and separated from the excitation light by a dichroic mirror and bandpass filter. However, light emitted by fluorophores that lie outside the objective lens focal plane is rejected by passing the sample fluorescence through a pinhole before it is detected by a photomultiplier tube. Confocal laser scanning uses higher intensities (typically time-averaged intensities are 10^5–10^6 W/cm^2) but shorter pixel illumination times (typical pixel dwell times of 2–20 μs) than widefield epifluorescence. It is straightforward to illuminate small sample regions by limiting the point scanning area. Confocal detection can also be achieved in a parallel configuration termed Nipkow spinning disk microscopy by using a disk of pinholes, though this method limits the ability to excite small sample regions.

MPM is another laser scanning method that offers resolution similar to confocal microscopy [6]. It is based on multiphoton excitation of fluorophores, which is the process whereby molecules absorb two or more photons simultaneously, yielding an excited state whose energy is approximately the sum of the photon energies. Because the rate of multiphoton absorption depends nonlinearly on the excitation light intensity, imaging conditions are typically chosen so that only fluorophores in the focal volume of the objective lens (the region of highest intensity) have an appreciable excitation probability. The primary advantage of MPM over confocal microscopy is that enhanced axial resolution is achieved in the excitation pathway rather than the imaging pathway. By localizing excitation to the focal point of the objective lens, out-of-plane photobleaching and photodamage are eliminated. However, the large peak intensities necessary for MPM can result in direct absorption by nontarget biomolecules in the cell, triggering collateral cell damage and death (discussed in detail below) [7]. Another advantage of MPM is the use of near-infrared excitation light, which is absorbed and scattered less by biological samples than visible light and has almost no absorption by water. Most MPM systems use femtosecond lasers because they offer extremely

high peak intensities (typically time-averaged intensities are 10^6–10^7 W/cm^2, corresponding to peak intensities of 10^{11}–10^{12} W/cm^2) that are required to drive the nonlinear excitation. A smaller fraction of the incident light is absorbed in MPM as compared with confocal excitation, and the pixel illumination times are similar (typical pixel dwell times of 2–20 μs). Although often referred to in early MPM literature, use of picosecond lasers is less common for two-photon excitation but still prevalent for other forms of nonlinear microscopy.

In addition to the imaging modality, the choice of fluorophore is an important consideration for preventing photodamage in live cell samples. One class of fluorescent dyes is molecular fluorophores, composed of small organic molecules. These molecules are bright and relatively photostable; however, they must be introduced into the cell in some manner to be used in live cell studies. Additionally in studies where specific biomolecules are targeted, the fluorophore molecule must bind chemically to the target. Markers have been engineered that are specific for cellular substructures, targeting incorporation into lipophilic domains for membrane studies or that exhibit high binding affinities to DNA to mark nuclear locations or track genomic processes [8]. Furthermore, since the molecular fluorophore is attached directly to the structure, any production of photochemically reactive species will directly affect the attached molecule. In some cases, tryptophan or endogenous small molecules are used as fluorophores in cells; their use in fluorescence microscopy can cause photodamage similar to nonnative molecules.

Various protein fluorophores exist such as the green florescence protein (GFP) (and various mutations) isolated from *Aequorea* jellyfish [9] and DsRed (and mutations) isolated from *Discosoma striata* coral [10]. These proteins have the key advantage that they can be introduced into an organism's genome through recombinant techniques to be expressed as transgenes, in its native form or fused to a protein of interest. Additionally, fluorescent proteins are typically less phototoxic than molecular fluorophores [11], presumably due to their structure in which the chromophore is buried inside a β-barrel, limiting the release of reactive photochemical by-products [12]. However, the protein must be either transiently or permanently transfected which may be difficult depending on the model organism.

The last class of fluorophore is the quantum dot, a semiconductor fluorophore that is larger (2–20 nm) than an organic or a protein fluorophore. Quantum dots have high quantum efficiencies and are more resistant to photobleaching. However, the large size of the quantum dot limits their introduction into live cells. Thus their primary usage is in single-molecule, in vitro experiments and we will not consider them further.

3 Cellular Damage

3.1 Mechanisms of Damage

Optical imaging of cells or tissue can introduce excess energy that may lead to biological damage of the sample. However, it is important to note that simple exposure to light does not necessarily cause the deposition of optical energy into the sample. For example, transmitted light microscopy is based on phenomena such as scattering and diffraction that typically deposit little or no energy into the sample. On the other hand, fluorescence microscopy and related techniques usually require photon absorption and are thus much more likely to cause photodamage. We note that our discussion is restricted to biological samples that do not contain endogenous species that strongly absorb visible or near-infrared light, such as melanin or hemoglobin.

There are many mechanisms by which light–matter interactions can damage biomolecules, but most fall into one of the two general categories. The first category includes photochemical mechanisms that produce damage via absorption-induced generation of highly reactive chemical species, such as free radicals and reactive oxygen species (ROS). The second category encompasses photophysical mechanisms in which photon absorption modifies the physical properties of the system, such as local heating due to nonradiative relaxation of excited molecules. Damage mechanisms in both categories are important for all forms of fluorescence microscopy techniques, but some imaging methods are more prone to a particular subset, as described below.

In some cases, optical techniques have been developed to intentionally induce specific types of damage in samples. For example, it is sometimes desirable to damage a small portion of genomic DNA, to investigate mechanisms of DNA damage repair [13]. However, it is more often desirable to avoid perturbing samples during optical imaging, so it is important to consider how to avoid introducing unwanted damage and how to determine if photodamage is occurring.

We consider specific photochemical and photophysical mechanisms in more detail below by first introducing several microscopy-based techniques that are specifically intended to generate damage. We then discuss ways to detect and avoid unwanted damage during optical imaging experiments.

3.1.1 Photochemical Mediated Damage

Paramount among the assumptions made in the use of fluorescent reporter molecules is that they do not perturb the system under observation. Unfortunately, this assumption is not always valid. One common source of photodamage arises from chemical reactions of the fluorophore in its lowest energy electronic excited state, which we refer to as photochemical damage. The usual pathway for energy relaxation from this excited state is photon emission, but

there often exist other possible excitation relaxation pathways, such as the chemical reactions discussed below. These reactions can also lead to fluorophore photobleaching, which is a permanent chemical rearrangement of the fluorophore such that fluorescence is no longer the primary relaxation pathway. Most fluorophores undergo 10^5–10^6 excitation cycles before photobleaching. As discussed below, photobleaching may indicate the production of ROS [14, 15]; however, the production of these damaging species may be cryptically occurring even without a visible loss of fluorescence from the sample. In either case, photochemical damage is typically cumulative as it relies upon the net number of excitation events (i.e., the net amount of energy deposited) only and not the rate at which the excitation events occur (i.e., the power or the intensity).

Excited fluorophores can occasionally interact with their solvent environment creating short-lived, damaging radical species capable of destabilizing or destroying other biomolecules. The process begins when molecular fluorophores, excited by appropriate wavelength visible light, are promoted to a singlet excited state. One mode for the energetic relaxation of these species is to emit a photon; however, the high cycling rate induced by high light intensities used in confocal or MPM increases the population of triplet state species (the triplet state quantum yield can be as high as 5 % for some molecular fluorophores). Molecular oxygen, which exists in a triplet ground state configuration, can readily interact with this excited state fluorophore. Energy transfer between these species results in the formation of singlet oxygen, while electron transfer results in the formation of superoxide and a fluorophore radical. All of these species are highly reactive and are generated by the favorable downhill energetics of electron transfer to ground-state oxygen, coupled with the rapid diffusion of molecular oxygen and therefore frequent interactions [15]. These highly unstable species are quickly quenched in aqueous environments leading to the formation of hydroxyl radicals. The short-lived hydroxyl radical is the prime damage-mediating species, resulting in radical-induced damage to proximal biomolecules [16].

The creation of singlet oxygen and radicals has a proximal effect on surrounding biomolecules. The most intuitive directed use of this phenomenon to create damage and inactivate proteins is chromophore-assisted light inactivation (CALI) which inactivates proteins through photochemical damage. CALI has found widespread application in cell biology for selective inactivation of proteins or fragment chromosomes [17]. Original implementations of CALI used organic molecules conjugated to protein-specific antibodies. However, these methods are being replaced by the use of encoded protein markers such as GFP. The encoded protein markers have the advantage of being present in the cell without microinjection and are “background free,” avoiding

potential complications from unbound, excess antibody. However, GFP is not as effective a CALI agent as molecular fluorophores. The GFP chromophore is embedded in a β-barrel structure, isolating the chromophore center from the cellular milieu [12] and limiting singlet oxygen production which is the primary cytotoxic mechanism generated by fluorescent proteins [18]. To counter this problem a more phototoxic GFP variant, KillerRed, was evolved to increase the phototoxicity of GFP by three orders of magnitude [19] [*see* Chapter 15 of this volume]. This protein is an excellent genetically encoded CALI agent. In general, GFP and the normal variants are very good fluorophores for imaging while reducing, but not eliminating, the potential for production of ROS that are common with molecular fluorophores.

ROS are also generated when imaging nucleic acids stained with intercalating dyes. This can lead to widespread genomic damage, the effect of which must be carefully considered when using live cell DNA stains [20]. The formation of damaging hydroxyl radicals proximal to the site of fluorophore incorporation results in species that can attack DNA to produce various forms of oxidative radical photodamage [21], notably single-strand breaks [22, 23]. Single-damage events typically cleave only one strand of the DNA sugar-phosphate backbone [24, 25]; the accumulation of many single-strand breaks leads to double-strand cleavage [26]. Since many proteins involved in DNA replication and repair bind to single-stranded DNA [27–29], the presence of single-strand breaks induced by photoexcitation of intercalating dyes could strongly bias protein–DNA interactions. Additionally, widespread genomic damage can induce apoptotic pathways resulting in cell death. While favorable in emerging cancer treatments, this is likely to induce artifacts in experiments probing native cellular function.

Although the generation of damage-mediating radicals is detrimental for most experiments, it can offer a degree of spatiotemporal user control in instances when initiating cellular damage is desirable [20, 23]. The common DNA intercalating dyes used for in vivo imaging application, such as Hoechst and DAPI, are all capable of selectively targeting DNA for fragmentation [30]. The incorporation of these intercalating dyes enables DNA fragmentation to be initiated at particular wavelengths and in a dose-dependent manner. This is useful for studies of DNA damage and repair mechanisms, where localized photochemical damage can be used to elucidate repair pathways. It has been shown that careful selection of the type of dye and DNA binding mode can be applied to tune the DNA backbone cleavage, biasing damage towards double-strand cleavage or single-strand breaks [31]. For clinical applications, the generation of singlet oxygen by fluorophore sensitization has been leveraged to treat disease states using photodynamic therapy. Here, high-quantum efficiency fluorophores are engineered to absorb at specific wavelengths and are

delivered to biological tissue that is targeted for destruction [32]. Using a myriad of light transducers, such as near-infrared sources with deep tissue penetration or fiber optics for the guidance of visible light, high-intensity light sources can be brought to bear on a limited tissue region. Through the mechanisms explained, apoptotic pathways are initiated following widespread genome and cell membrane disruption; therefore, the conditions mentioned in the above references should be avoided.

Finally, ROS can be generated from other sources in a sample, such as the cell medium. For example, N-2-hydroxyethylpiperazine-N′-2-ethanesulfonic acid (HEPES), a common buffer in cell culture medium, has the unfortunate side effect of producing hydrogen peroxide when used for fluorescence microscopy [33]. Even ambient light can be enough to induce H_2O_2 production and the onset of cell death due to the oxidative stress of the cell culture medium, which was a confounding source of error in cell culture experiments until the mechanism was identified (thus always confirm your buffer system is compatible with your imaging conditions).

3.1.2 Photophysical Mediated Damage

Photophysical damage mechanisms involve excited states that are more energetic than the lowest energy singlet state from which fluorescence typically arises. As examples, this category includes local solvent heating due to the dissipation of excess vibrational energy from the initial (Franck–Condon) fluorophore excited state and free electrons ejected by the fluorophore or solvent as a result of multiphoton ionization. In contrast with photochemical mediated damage, photophysical damage mechanisms typically depend less on the total energy deposited into a sample and more on the intensity. For example, thermal photophysical effects such as localized heating due to excited state vibrational relaxations in the fluorophore can raise the temperature of solvent molecules in the vicinity of the fluorophore for short periods of time. Thermal energy dissipates from the ~femtoliter excitation volume on a nanosecond time scale. Thus, the use of a pulsed excitation laser that transiently raises the local temperature by a few degrees per pulse does not cause appreciable damage if the repetition rate is low enough to allow for thermal relaxation between pulses. However, higher repetition rates (higher powers) may induce severe thermal damage after an equivalent number of excitation pulses. Such thermal damage is more common in laser scanning experiments that use higher powers but can also occur in widefield imaging experiments [34].

Local thermal energy deposition can result in the proximal denaturing of proteins, but in a more extreme case, it can lead to the formation of microbubbles, referred to as cavitation. These microbubbles form from localized solvent expansion creating unstable low-pressure zones that rapidly implode, resulting in subsequent cavitation damage [34]. Depending on the laser spot size

and pixel dwell time, cavitation damage may be restricted to approximately the laser spot region resulting in mechanical damage and bond breaking of proximal biomolecules. In the cases of long dwell times and larger spot sizes, the membrane can become permeable or cell ablation can result. In an imaging context, this damage can create significant artifacts, reduce cell viability, and alter cellular behavior.

Another important photophysical damage mechanism is the formation of highly reactive radical species due to multiphoton ionization of the fluorophore or the solvent (often referred to as solvated electrons). Due to the involvement of a multiphoton process, this mechanism depends nonlinearly on the excitation intensity and is thus typically a problem only for microscopy techniques that used pulsed lasers. In aqueous solution, solvated electrons attack biomolecules in the opposite manner of radical species, causing reductive as opposed to oxidative damage [35]. These chemical pathways have been shown to be equally destructive as, if not more destructive than, oxidative damage. Further, the reduced mass of solvated electrons compared to more typical free radical species confers a larger mean free path of diffusion and therefore larger damage radius. Lipid membranes are especially vulnerable to attack due to the unstable radical fatty acids formed. These residues compromise the cell membrane [36]. If generated inside the cellular confines, nuclear material and mitochondria become vulnerable; damage to either species can initiate cell death.

In some cases, the high peak intensities cause photoionization of the aqueous solvent generating a large population of electrons that exist as plasma. These electrons are capable of absorbing additional light pulses sustaining the plasma and further propagating its production. In water, intensities generated by femtosecond pulsed lasers greater than 1 TW/cm^2 for ultraviolet-B (280–315 nm) light and in the range of 4–10 TW/cm^2 for green light [37] are required to initiate optical breakdown. These high intensities are unlikely to be encountered during most imaging experiments but can be achieved during certain single-molecule techniques (notably optical trapping). However, longer duration laser pulses can reduce this high-intensity threshold, as pico- and nanosecond green laser systems can lower the threshold intensity to sub-TW/cm^2 [38]. Plasma generation has been harnessed for optical tissue microdissection such as creating cuts of DNA strands and microtubules inside of live cells [39–42]. The plasma-mediated ablation occurs only at the focal point of the objective due to the high-photon flux required for off-resonance ionization [34, 43]. In one study, the energy onset of plasma mediation ablation in chromatin and microtubules was systematically confirmed using electron microscopy in addition to the observation of photobleaching with fluorescence microscopy. The onset of ablation occurred at pulse energies of just above 1 nJ at 790 nm and a 1.4 NA objective [41]. The onset of

severe photobleaching occurred at pulse energies slightly lower than 1 nJ; therefore, although photobleaching itself is not a definite indicator of ablation, it can be used to show the likelihood that photophysical damage is occurring.

Cellular components other than typical fluorophores can also be damaged by directly exciting electronic transitions in the biomolecules themselves. Both proteins and nucleic acids absorb in the ultraviolet-C (<280 nm) region of the spectrum. The DNA base thymine readily undergoes a photochemically induced dimerization reaction when exposed to UV-C light. Although these wavelengths are much shorter than the excitations for fluorophores used in fluorescence microscopy, these transitions can be accessed by a higher order nonlinearity when using pulsed lasers in MPM. The nonlinear absorption of biomolecules is dependent on the peak intensity not the net energy, just like nonlinear absorption by fluorophores. The generation of both "UV-like" lesions and single- and double-strand breaks on DNA has been demonstrated for both visible [44, 45] and infrared [46–48] pulsed laser light. In both studies, the required powers to achieve damage were often at least an order of magnitude larger than the powers required for typical MP imaging and therefore are not typically encountered in most MP and confocal microscopy applications. However, the potential for damage in experiments that require brief, intense flashes of light (examples include inducing desired phototransitions in caged proteins, switching of photoactivatable fluorophores, or photobleaching in fluorescence recovery after photobleaching (FRAP)) cannot be ruled out.

3.2 Checking for Cellular Damage Due to Fluorescent Microscopy

In this section, we briefly consider several approaches to detect cellular damage in live cell microscopy. Before doing so, we note that fluorescence-based imaging is likely to cause photodamage in nearly all biological samples, even if the damage is not readily apparent. In many cases, it is possible to detect only relatively large amounts of damage due to a low assay sensitivity or limited dynamic range. Thus, it is important to consider the impact low levels of photodamage could have on experimental results even if undetectable. For example, it is commonplace to locate cell nuclei by imaging samples stained with Hoechst (or similar DNA-associating dyes), but this procedure undoubtedly causes DNA strand breakage as discussed above. Such damage is inconsequential in some types of experiments, but it may have a large impact on experiments intended to probe dynamics of DNA-associating proteins.

Perhaps the simplest method to detect damage is to observe the morphology of cellular structures in initial and final images within an experimental sequence to determine if ablation or cell death has occurred. For example, the use of high-power near-infrared pulses intended for three-photon absorption of DNA creates cavitation bubbles in *Drosophila* salivary glands and destroys

cultured HeLa cells. However, the lower power visible light used to excite DNA via two-photon absorption does not produce such damage [45]. In many cases, light-induced ablation may be much less apparent or even undetectable after recording a single image but may become evident after several frames. Thus, it is advisable to perform control experiments in which a slightly higher excitation power is used or additional images of the same sample are collected. If the final image in such control experiment does not contain unexpected morphological changes, it is generally safe to assume that the actual experimental conditions are acceptable.

Less severe photodamage can often be detected by observing the subsequent growth and division of cell populations that have been used in microscopy experiments. For example, unchecked cell growth without cell division can occur in Chinese hamster ovary (CHO) cells that were exposed to low-intensity NIR pulsed light resulting in oversized cells days after NIR pulsed light exposure [49]. Other qualitative indicators of damage include long-term (hours to days) measures of cell responses like delayed apoptosis [50] or reduction in cell reproductive viability [51, 52].

Although qualitative measures of cell damage are convenient, it is helpful to be aware of cryptic forms of damage that may occur, so various assays have been developed to test for such damage. A large number of cell viability kits are commercially available. One example is the LIVE/DEAD Reduced Biohazard Cell Viability Kit (Molecular Probes) that stains live cells with a green florescent dye while dead or dying cells are stained with a red fluorescent dye. This simple test checks for membrane integrity as a sign of cell viability and can reveal membrane destruction that cannot be resolved using light microscopy. As an example of other damage-specific assays, dyes such as Ni-3,3-diaminobenzidine or Jenchrom px blue (JenLab GmbH) can be used to test for ROS [53]. DNA damage can be assayed using immunohistochemistry with antibodies specific to proteins that are markers for DNA damage, such as γ-H2A.X for single- and double-strand breaks. Antibodies also exist to assay specific types of UV-induced lesions, such as thymine cyclobutane and 6–4 dimers or oxidative stress lesions such as 8-oxoguanine [47].

3.3 Preventing Unwanted Damage in Fluorescent Microscopy

In live cell experiments it is desirable to avoid unintentional photodamage that could potentially bias the results. As stated previously, nearly all fluorescence imaging induces some amount of damage, so it is critical to consider what types and degree of damage are acceptable for a given experiment. It is always prudent to reduce potential damage artifacts by optimizing imaging conditions, as described below, because such changes can also improve the general quality of the results (signal to noise, etc.). However, the addition of additives or other potentially perturbative measures should only be considered when photodamage is likely affecting the experimental outcome. In this case, it is usually beneficial to consider the

type of photodamage or mechanism by which it is produced in order to determine the best approach to reduce its impact.

The best way to prevent unintentional photodamage is to maximize the efficiency of the microscope so that the minimal amount of incident power can be used to image the sample. Rather than resorting to "turning up the power" as a solution for low signal, using a more efficient fluorophore, filters, or better detection hardware can improve signal without increasing the risk of unwanted photoeffects. At a minimum, it is important to ensure that the optical filters are optimal for the excitation and emission spectra of the fluorophore. Unless it is necessary, UV radiation should be well filtered from arc lamp excitation. In general, the longest practical wavelength excitation band should be used for any fluorophore, since it reduces excess energy delivered to the fluorophore (e.g., due to excitation to higher energy electronic states or highly excited vibrational states) and reduces the potential of exciting endogenous fluorophores. To maximize the number of photons collected, single-fluorophore experiments should utilize emission filters with a wide bandpass, while multicolor experiments should use the widest bandpass that still prevents cross talk.

The choice of fluorophore can also be important for preventing photodamage. Some fluorophores have a higher probability than others of producing radicals when excited; this probability can be correlated with the photobleaching rate since the same photochemical mechanisms can cause both damage and bleaching. For example, Alexa 488 is less prone to bleaching and causing photodamage than fluorescein. In addition to photostability, the wavelength range of a fluorophore can affect detection sensitivity and thus photodamage. Photomultiplier tubes used in laser scanning instruments are typically most sensitive in the blue or the green spectral regions, while charge-coupled devices used for widefield imaging experiments are often most sensitive in the red and near-IR spectral region. Choosing the most sensitive detectors and fluorophores that are optimal for the detector wavelength sensitivity is a good way to reduce the amount of incident power and often the amount of photodamage.

Chemical methods can also be undertaken to reduce photodamage. Since one of the most common mediators in producing damage is singlet oxygen, reducing the overall oxygen concentration in the sample can reduce the presence of ROS in the sample. The simplest method is to use deoxygenated buffers and oxygen-impermeable materials, but oxygen depletion agents such as Oxyrase can also accomplish this purpose [54]. Adding antioxidants as radical scavengers is also common in single-molecule experiments and can be used for live cell imaging. For example, compounds such as ascorbate and Trolox can decrease oxidative damage in cells [55]. However, it has also been shown that ascorbate can also introduce DNA damage through other means [31], so it is best to introduce such chemicals only when absolutely necessary.

4 Conclusion

Fluorescence microscopy is a useful tool for imaging and manipulating live cells. High-resolution methods as well as dynamic perturbation [56] and fluctuation spectroscopy [57] have garnered unprecedented structural and mechanistic details, previously only accessible through electron microscopy or in vitro biochemistry. The ability to specifically target cellular substructures for imaging or to genetically encode fluorophores tagged to proteins of interest will continue to expand the applications and utility of fluorescence microscopy. Furthermore, the use of fluorescence microscopy to selectively manipulate live cell metabolism through photoswitching proteins or CALI offers many exciting opportunities for research. However, this growth must be accompanied by a respect for the ways in which the input of optical energy can alter or even destroy a biological system, since deposition of energy into live cells can have unintended consequences for damaging live cell tissue. This damage can cause experimental anomalies that can result in unreliable experimental data or worse, inducing result-altering artifacts leading to incorrect conclusions. Therefore, we recommend caution and consistent reporting of experimental conditions when undertaking florescence microscopy experiments. A good understanding of the amount of energy being deposited is crucial along with an analysis of what the prime absorbers are in a system. This, coupled with limiting the application of ROS generating dye molecules, can significantly reduce the potential for tissue damage. However, it cannot be overemphasized that the best method to prevent damage is a well-configured and optimized microscopy experiment to limit the required optical power.

Acknowledgment

Funding for this work was provided by the National Science Foundation under Grant No. PHY-1150017.

References

1. Stephens DJ, Allan VJ (2003) Light microscopy techniques for live cell imaging. Science 300(5616):82–86. doi:10.1126/science.1082160
2. Lichtman JW, Conchello J-A (2005) Fluorescence microscopy. Nat Methods 2(12): 910–919
3. Giepmans BNG, Adams SR, Ellisman MH, Tsien RY (2006) The fluorescent toolbox for assessing protein location and function. Science 312(5771):217–224. doi:10.1126/science.1124618
4. Wombacher R, Cornish VW (2011) Chemical tags: applications in live cell fluorescence imaging. J Biophotonics 4(6):391–402. doi:10.1002/jbio.201100018
5. Davidovits P, Egger MD (1969) Scanning laser microscope. Nature 223(5208):831–831
6. Denk W, Strickler JH, Webb WW (1990) Two-photon laser scanning fluorescence microscopy. Science 248:73–76
7. Hopt A, Neher E (2001) Highly nonlinear photodamage in two-photon fluorescence microscopy. Biophys J 80:2029–2036
8. Zorov DB, Kobrinsky E, Juhaszova M, Sollott SJ (2004) Examining intracellular organelle

function using fluorescent probes: from animalcules to quantum dots. Circ Res 95(3):239–252. doi:10.1161/01.RES.0000137875.42385.8e

9. Tsien RY (1998) The green fluorescent protein. Annu Rev Biochem 67(1):509–544. doi:10.1146/annurev.biochem.67.1.509
10. Baird GS, Zacharias DA, Tsien RY (2000) Biochemistry, mutagenesis, and oligomerization of DsRed, a red fluorescent protein from coral. Proc Natl Acad Sci U S A 97(22):11984–11989. doi:10.1073/pnas.97.22.11984
11. Surrey T, Elowitz MB, Wolf P-E, Yang F, Fo N, Shokat K, Leibler S (1998) Chromophore-assisted light inactivation and self-organization of microtubules and motors. Proc Natl Acad Sci U S A 95(8):4293–4298
12. Remington SJ (2006) Fluorescent proteins: maturation, photochemistry and photophysics. Curr Opin Struct Biol 16(6):714–721. doi:10.1016/j.sbi.2006.10.001
13. Essers J, Vermeulen W, Houtsmuller AB (2006) DNA damage repair: anytime, anywhere? Curr Opin Cell Biol 18:240–246
14. Halliwell B, Aruoma OI (1991) DNA damage by oxygen-derived species its mechanism and measurement in mammalian systems. FEBS Lett 281:9–19. doi:10.1016/0014-5793(91) 80347-6
15. Schweitzer C, Schmidt R (2003) Physical mechanisms of generation and deactivation of singlet oxygen. Chem Rev 103:1685–1757
16. Sies H (1993) Strategies of antioxidant defense. Eur J Biochem 215(2):213–219. doi:10.1111/j.1432-1033.1993.tb18025.x
17. Jacobson K, Rajfur Z, Vitriol E, Hahn K (2008) Chromophore-assisted laser inactivation in cell biology. Trends Cell Biol 18(9):443–450. doi:10.1016/j.tcb.2008.07.001
18. Ragàs X, Cooper LP, White JH, Nonell S, Flors C (2011) Quantification of photosensitized singlet oxygen production by a fluorescent protein. ChemPhysChem 12(1):161–165. doi:10.1002/cphc.201000919
19. Bulina ME, Lukyanov KA, Britanova OV, Onichtchouk D, Lukyanov S, Chudakov DM (2006) Chromophore-assisted light inactivation (CALI) using the phototoxic fluorescent protein KillerRed. Nat Protoc 1(2):947–953
20. Limoli CL, Ward JF (1993) A new method for introducing double-strand breaks into cellular DNA. Radiat Res 134:160–169
21. Saran M, Bors W (1990) Radical reactions in vivo: an overview. Radiat Environ Biophys 29:249–262
22. Teoule R (1987) Radiation-induced DNA damage and its repair. Int J Radiat Biol 51(4): 573–589
23. Ward JF (1990) The yield of DNA double strand breaks produced intracellularly by ionizing radiation: a review. Int J Radiat Biol 57(6):1141–1150
24. Guo H, Tullius TD (2003) Gapped DNA is anisotropically bent. Proc Natl Acad Sci U S A 100(7):3743–3747
25. Siddiqi MA, Bothe E (1987) Single- and double-strand break formation in DNA irradiated in aqueous solution: dependence on dose and OH radical scavenger concentration. Radiat Res 112:449–463
26. Patrick MH, Rahn RO (1976) Photochemistry and photobiology of nucleic acids. Academic, New York
27. Houten BV, Croteau DL, Vecchia MJD, Wang H, Kisker C (2005) "Close-fitting sleeves": DNA damage recognition by the UvrABC nuclease system. Mutat Res 577:92–117
28. Friedberg EC (2003) DNA damage and repair. Nature 421:436–440
29. Caldecott KW (2008) Single strand break repair and genetic disease. Nat Rev Genet 9:619–631
30. Akerman BTE (1996) Single- and double-strand photocleavage of DNA by YO, YOYO, and TOTO. Nucleic Acids Res 24:1080
31. Tycon MA, Dial CF, Faison K, Melvin W, Fecko CJ (2012) Quantification of dye-mediated photodamage during single-molecule DNA imaging. Anal Biochem 426(1):13–21. doi:10.1016/j.ab.2012.03.021
32. Robertson CA, Evans DH, Abrahamse H (2009) Photodynamic therapy (PDT): a short review on cellular mechanisms and cancer research applications for PDT. J Photochem Photobiol B 96(1):1–8. doi:10.1016/j.jphotobiol.2009.04.001
33. Zigler JSJ, Lepe-Zuniga J, Vistica B, Gery I (1985) Analysis of the cytotoxic effects of light-exposed hepes-containing culture medium. In Vitro Cell Dev Biol 21(5):282–287. doi:10.1007/bf02620943
34. Vogel A, Noack J, Hattman G, Paltauf G (2005) Mechanisms of femtosecond laser nanosurgery of cells and tissues. Appl Phys B 81(8): 1015–1047. doi:10.1007/s00340-005-2036-6
35. Nguyen J, Ma Y, Luo T, Bristow RG, Jaffray DA, Lu Q (2011) Direct observation of ultrafast-electron-transfer reactions unravels high effectiveness of reductive DNA damage. Proc Natl Acad Sci U S A 108:11778

36. Pratt DA, Tallman KA, Porter NA (2011) Free radical oxidation of polyunsaturated lipids: new mechanistic insights and the development of peroxyl radical clocks. Acc Chem Res 44(6): 458–467. doi:10.1021/ar200024c
37. Fan CHSJLJP (2002) Breakdown threshold and localized electron density in water induced by ultrashort laser pulses. J Appl Phys 91: 2530–2536
38. Kong X, Mohanty SK, Stephens J, Heale JT, Gomez-Godinez V, Shi LZ, Kim J-S, Yokomori K, Berns MW (2009) Comparative analysis of different laser systems to study cellular responses to DNA damage in mammalian cells. Nucleic Acids Res 37:e68. doi:10.1093/nar/gkp221
39. König K, Riemann I, Fritzsche W (2001) Nanodissection of human chromosomes with near-infrared femtosecond laser pulses. Opt Lett 26(11):819–821
40. Supatto W, Debarre D, Moulia B, Brouzes E, Martin J-L, Farge E, Beaurepaire E (2005) In vivo modulation of morphogenetic movements in Drosophila embryos with femtosecond laser pulses. Proc Natl Acad Sci U S A 102(4):1047–1052
41. Heisterkamp A, Maxwell IZ, Mazur E, Underwood JM, Nickerson JA, Kumar S, Ingber DE (2005) Pulse energy dependence of subcellular dissection by femtosecond laser pulses. Opt Express 13(10):3690–3696
42. Kuetemeyer K, Rezgui R, Lubatschowski H, Heisterkamp A (2010) Influence of laser parameters and staining on femtosecond laser-based intracellular nanosurgery. Biomed Opt Express 1(2):587–597
43. Vogel A, Venugopalan V (2003) Mechanisms of pulsed laser ablation of biological tissues. Chem Rev 103(2):577–644. doi:10.1021/cr010379n
44. Tycon MA, Chakraborty A, Fecko CJ (2011) Generation of DNA photolesions by two-photon absorption of a frequency-doubled Ti:sapphire laser. J Photochem Photobiol B 102(2):161–168
45. Daddysman MK, Fecko CJ (2011) DNA multiphoton absorption generates localized damage for studying repair dynamics in live cells. Biophys J 101(9):2294–2303
46. Meldrum RA, Botchway SW, Wharton CW, Hirst GJ (2003) Nanoscale spatial induction of ultraviolet photoproducts in cellular DNA by three-photon near-infrared absorption. EMBO Rep 4(12):1144–1149
47. Dinant C, Md J, Essers J, Cappellen WA, Kanaar R, Houtsmuller AB, Vermeulen W (2007) Activation of multiple DNA repair pathways by sub-nuclear damage induction methods. J Cell Sci 120:2731–2740
48. Trautlein D, Deibler M, Leitenstorfer A, Ferrando-May E (2010) Specific local induction of DNA strand breaks by infrared multiphoton absorption. Nucleic Acids Res 38(3):e14. doi:10.1093/nar/gkp932
49. König K (2001) Cellular response to laser radiation in fluorescence microscopes. In: Periasamy A (ed) Methods in cellular imaging. Oxford University Press, Oxford, pp 236–251
50. Tirlapur UK, Konig K, Peuckert C, Krieg R, Halbhuber K-J (2001) Femtosecond near-infrared laser pulses elicit generation of reactive oxygen species in mammalian cells leading to apoptosis-like death. Exp Cell Res 263: 88–97
51. König K, So PTC, Mantulin WW, Gratton E (1997) Cellular response to near-infrared femtosecond laser pulses in two-photon microscopes. Opt Lett 22(2):135–136
52. König K, Becker TW, Fischer P, Riemann I, Halbhuber KJ (1999) Pulse-length dependence of cellular response to intense near-infrared laser pulses in multiphoton microscopes. Opt Lett 24(2):113–115
53. Tirlapur UK, Konig K (2001) Femtosecond near-infrared laser pulse induced strand breaks in mammalian cells. Cell Mol Biol 47(18): OL131–OL134
54. Sacconi L, Dombeck DA, Webb WW (2006) Overcoming photodamage in second-harmonic generation microscopy: real-time optical recording of neuronal action potentials. Proc Natl Acad Sci U S A 103(9):3124–3129. doi:10.1073/pnas.0511338103
55. Altman RB, Terry DS, Zhou Z, Zheng Q, Geggier P, Kolster RA, Zhao Y, Javitch JA, Warren JD, Blanchard SC (2012) Cyanine fluorophore derivatives with enhanced photostability. Nat Methods 9(1):68–71
56. Mueller F, Mazza D, Stasevich TJ, McNally JG (2010) FRAP and kinetic modeling in the analysis of nuclear protein dynamics: what do we really know? Curr Opin Cell Biol 22(3): 403–411. doi:10.1016/j.ceb.2010.03.002
57. Krichevsky O, Bonnet G (2002) Fluorescence correlation spectroscopy: the technique and its applications. Rep Prog Phys 65(2):251–297

Chapter 2

Modification of Purified Proteins with Photochemical Protection Compounds for High-Resolution Photoactivation of Protein Function In Vitro and In Vivo

Sidney Cambridge

Abstract

Specific and targeted photoactivation of protein function inside cells, tissues, or whole organisms can be achieved with reversible inhibition of proteins by conjugation with photolabile protection compounds ("caging"). In vitro caging of proteins is thought to cause sterical or functional hindrance of amino acid side chains that are important for protein activity. Following the modification, the caged protein is introduced into the biological system and high-resolution irradiation ensures specific release of protein function in the desired areas. Here, I describe the entire caging procedure and highlight a few of the caveats of photoactivation in living cells.

Key words Photosensitive protection compounds, Caged proteins, High-resolution photoactivation

1 Introduction

Photosensitive protecting, i.e., caging compounds, have been introduced to biological research more than three decades ago. Originally used in organic chemistry to protect and deprotect growing amino acid chains during peptide synthesis, uncaging of caged, and therefore inactive, molecules has also enjoyed considerable success in living samples. The underlying idea is always that through photoactivation, molecules with biological activity can be controlled with very high spatial and temporal resolution by application of exogenous light. Caging was first used to release ATP upon irradiation [1], and since then researchers managed to cage among others DNAs, RNAs, various small molecules such as neurotransmitters, ions (calcium, protons, etc.), and proteins. For detailed information regarding the rapidly growing collections of caged versions of biologically active molecules, the reader is referred to these two excellent in-depths reviews [2, 3]. The modification of proteins with caging compounds [4] is potentially

Sidney Cambridge (ed.), *Photoswitching Proteins: Methods and Protocols*, Methods in Molecular Biology, vol. 1148,
DOI 10.1007/978-1-4939-0470-9_2,

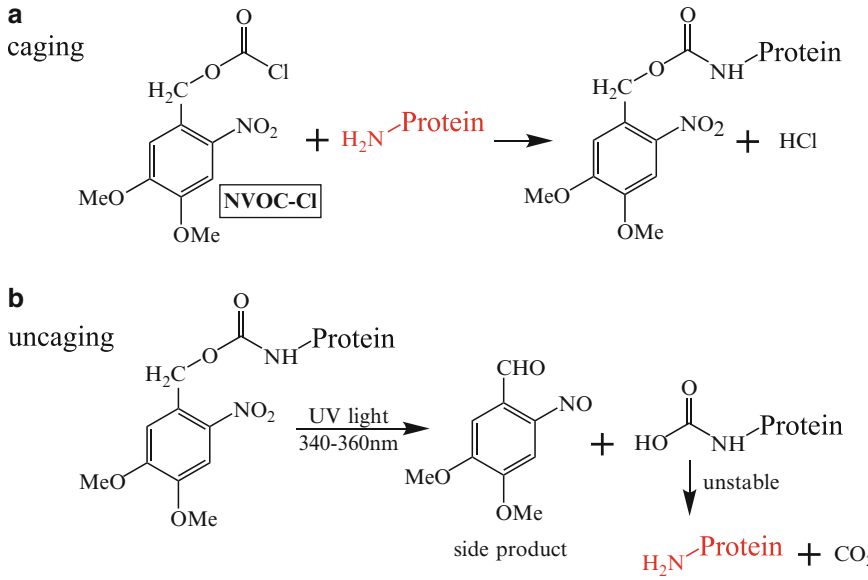

Fig. 1 Caging and uncaging chemistry. (**a**) The commercially available NVOC-Cl preferentially reacts with free amines of lysines at pH 9.5 to form a carbamate linkage. (**b**) UV irradiation photolyzes this linkage to produce a side product and an unstable intermediate which spontaneously decomposes into the original free amine and CO_2

complicated as the functionally important amino acids of a protein may not be known or may be difficult to target. To specifically target a single amino acid, researchers have genetically introduced unnatural amino acids which can then be modified with caging compounds in vitro and in vivo. This elegant approach is not the topic of this chapter but is discussed in this volume by Karginov, Hahn, and Deiters. Caging of proteins can also be achieved by a "shotgun" approach where the protein is mixed in vitro with a reactive caging compound. "Shotgun" caging of proteins is the topic of this chapter. This approach relies on attaining a sufficiently high number of randomly caged side chains for each individual protein molecule. The extent of caging among individual protein molecules may vary within the sample, and so the final probe thus represents a mixture of differently caged proteins whose *collective* activity is blocked through the caging.

Because caging compounds often react with lysines or glutamic/aspartic acids (Fig. 1a), maintaining water solubility becomes an issue as an ionic residue is replaced with a less polar moiety. However, many proteins seem to tolerate moderate levels of caging and their caged versions can even be stored at −20 °C for several months. One chief goal is to determine a concentration for the caging compound that leads to inhibition of protein function while not precipitating too many protein molecules. To optimize the caging parameters, the availability of a simple assay to quickly

determine protein activity after caging is therefore paramount. However, because monitoring the activity of a protein is often not accomplished easily, assaying its binding activity to known binding partners with an enzyme-linked immunosorbent assay (ELISA) is a quick and straightforward alternative. For some proteins such as transcription factors, also a gel-mobility assay to test binding to DNA might be suitable [5]. The author has used standard ELISA analyses to examine the binding of caged function blocking antibodies against BDNF [6]. Since protein binding is a universal prerequisite for protein activity, loss of binding also reflects loss of activity. Therefore, the binding activity of the caged protein can be monitored with an ELISA to assess the extent of its biological activity. To take this a step further, if caging reduces the affinity to the cellular binding partners of the protein, very possibly its affinity to an (commercial) antibody is also reduced. Consequently, one can potentially use antibodies against the protein of interest to follow—at least in a first approximation—how increasing caging concentrations progressively reduce protein activity. So instead of assaying the protein activity after caging, one can coat an ELISA plate with the caged protein and characterize the binding activity of an antibody against this protein. Consequently, the entire procedure from caging the protein to evaluating its (in) activity can thus be executed by inexperienced researchers in a day.

After chemical modification of the caged protein, the sample needs to be introduced into the biological system. I have introduced a caged transcription factor by injection into syncytial Drosophila embryos and a caged antibody against a secreted protein by simply washing it into extracellular milieu of living brain slices. Of course, other means of introducing caged proteins exist such as bead loading or cell-permeant peptide vectors [7, 8]. Following administration of the caged protein to the biological system, uncaging (Fig. 1b) can be performed on any standard fluorescence microscope using DAPI filter sets. Of course, the absorption spectra of the photoremovable protection groups may not fully be excited by the DAPI excitation light, but for a first test, this should be sufficient. If necessary, optical bandpass filters tailored specifically to the uncaging spectrum can always be purchased. The key parameter is being able to deliver adequate levels of photoactivation light without causing significant toxicity. Most biological tissues however appear to tolerate several seconds of DAPI excitation light sufficient for uncaging without any signs of deleterious effects. Spatially resolved uncaging of protein activity at the single-cell level can readily be accomplished with epifluorescence microscopes using high-magnification objectives (40× or 63×) and restriction of the microscope aperture. Even subcellular resolution can be achieved this way or by using scanning one-photon or two-photon microscope setups.

Shotgun caging of proteins and their photoactivation in biological tissue is a comparatively simple approach at the interface of chemistry and biology to address scientific questions that require temporally or spatially resolved protein activity. With ample unmodified protein available, an activity or a binding assay at hand, and an efficient way to administer the caged protein, even inexperienced researchers should be able to advance within a week or two to the experimental stage where the caged protein can be tested with live cells. In light of this, photoswitching proteins after shotgun caging is an attractive and rapid alternative to all genetic experimental procedures.

2 Materials

The caging reaction itself requires only the protein of choice (POC), the caging compound, and a suitable anhydrous organic solvent vehicle for dissolving of the caging compound. Several solvents are listed below which allowed efficient protein caging. The choice of solvent eventually depends on how well the POC tolerates the solvent during the caging reaction and if the biological system may be affected by trace amounts of solvent present in the unpurified or the washed sample. For efficient conjugation with a reactive caging molecule, the POC needs to be provided in a buffer devoid of molecules that could possibly be modified with the photosensitive protection compounds. Any primary amine (-NH2) in millimolar concentrations will block the reaction which therefore excludes TRIS as a possible buffer.

2.1 Caging Reagents

1. POC: Make sure that the POC is provided in a medium devoid of reactive groups such as free amines, azide, or thiols. If you have to resuspend lyophilized protein, a simple buffer containing 20 mM HEPES (pH 7.4)/0.15 M NaCl should be sufficient unless the protein requires ions (Ca^{2+}, Mg^{2+}, etc.) or other molecules for full activity.
2. A commercially available caging compound, NVOC-Cl (6-nitroveratryl chlorofomate; Sigma-Aldrich or FLUKA), is the best option assuming that lysines and arginines are necessary for proper function of the POC. The author is not aware of any other commercially available caging compounds that have been used for protein caging although there is a kit for caging carboxyl groups (Molecular Probes).
3. Anhydrous solvent (*see* **Note 1**): NVOC-Cl hydrolyses in aqueous solution and thus any organic solvent without primary amines or hydroxyl groups should theoretically be applicable. Of course, the eventual reaction will occur in at least 50 %

aqueous solution causing extensive hydrolysis, which is why the caging compound is dissolved in an anhydrous solvent to limit hydrolysis before the actual reaction with the protein. Because alcohols contain hydroxyl groups they cannot be used, leaving 1,4 dioxane, dimethylformamide (DMF), dimethylsulfoxide (DMSO), and perhaps tetrahydrofuran (THF) as the most common water-miscible solvents. The author has used dioxane extensively because it was tolerated very well when injected in large amounts into pre-gastrulation Drosophila embryos. Acetone and chloroform are biologically not suitable.

4. The vessel for the reaction is ideally made of glass because the solvents (DMF!) potentially dissolve plastic tubes. Depending on the type of plastic container, this effect may be quite substantial although standard Eppendorf tubes usually are sufficiently robust for short caging reactions with organic solvents.
5. The caged POC is washed and concentrated with spin columns (e.g., from Centricon). Depending on the molecular size of the POC, the size exclusion of the membrane can be up to 30 kDa. The tolerance of the column when washing samples that contain organic solvents needs to be verified before usage.

2.2 Monitoring the Extent of Caging with ELISA

1. Standard ELISA plates and standard ELISA plate reader (e.g., from ThermoScientific, Tecan, Promega). The plates should be nontransparent, preferably black to reduce light exposure during handling.
2. Antibody against POC.
3. Secondary antibody coupled to reporter enzyme for detection + substrate.
4. Blocking and wash buffers as specified by the manufacturer.
5. Handheld UV lamp.

2.3 Fluorometric Quantification of the Extent of Caging

1. Fluorescamine (Sigma-Aldrich).
2. 50 mM $NaPO_4$, pH 8.5, containing 1 % SDS.
3. Spectrophotometer (e.g., PerkinElmer).

2.4 Uncaging the Caged POC Within a Biological System

1. Standard epifluorescence microscope with DAPI filter set.
2. CMNB-caged fluorescein (Molecular Probes) or other caged fluorescent dye.

2.5 Assessing Postirradiation Cellular Fitness/ Apoptosis Assay

Cell death detection kit (Roche).

3 Methods

The caging reaction can be carried out at room temperature. To protect the caged protein, all subsequent steps should be performed at 4 °C (*see* **Note 2**). Theoretically, the handling of samples at ambient room light should not cause any unspecific uncaging, but as a precaution, dimming the light and covering the samples with aluminum foil are recommended.

It is important that a robust assay to measure protein binding or activity has been established before going ahead with the caging. In vitro binding assays have the advantage that the organic solvents are often tolerated so that the entire sample of the caging reaction can be administered without further washing and purification. The objective of testing protein activity/binding is of course to quickly identify suitable caging/uncaging conditions after varying the reaction time and the different concentrations of POC, caging compound, and solvent.

3.1 The Caging Procedure

To identify a suitable concentration of NVOC-Cl, test three different concentrations: 0.25, 0.5, and 1 mM NVOC-Cl. In previous experiments, 0.5 mM NVOC-Cl was found to inhibit protein function while not reducing protein solubility. However, other concentrations may be more adequate for different proteins. For the first experiment, it is recommended that all three suggested concentrations in addition to a mock treatment without NVOC-Cl are used in parallel for caging and subsequent characterization of the caged proteins.

1. Resuspend (*see* **Note 3**) lyophilized POC in 20 mM HEPES (pH 7.4)/0.15 mM NaCl. If necessary wash the POC twice with copious amounts of buffer (*see* **Note 4**) using spin columns to remove any small molecules in the solution that could possibly react with the caging compound. Follow the company's instructions for using the spin columns. Proteins should preferably be maintained in concentrated solutions (~1 mg/ml) to avoid noticeable degradation, so make sure that the washed sample is not too dilute after the preparation.
2. The pH of the caging reaction is absolutely crucial because it affects with which amino acid side chains the NVOC-Cl preferably reacts. At pH > 9, mostly lysines are targeted, but at physiological pH 7, also thiols and hydroxyl residues could possibly react (*see* **Note 5**). Prepare 0.1 M sodium carbonate buffer to which POC and caging compound will be added later. The pH of the carbonate buffer should be adjusted such that the final pH of the caging reaction is pH 9.5 (*see* **Note 6**). If the POC can tolerate 50 % dioxane, then the reaction can be one volume POC, one volume carbonate buffer, and two volumes caging compound in dioxane. Of course, the volume of

dioxane in the final reaction can be substantially reduced to 10 % and less if necessary.

3. The length of the caging reaction and the concentration of the caging compound correlate as higher concentrations require shorter reaction times. The author is not aware of any systematic analysis to describe the unspecific hydrolysis of NVOC-Cl in aqueous solutions, but there is probably no reactive molecule left after a 30-min incubation. As a starting point, 0.5 mM NVOC-Cl as a final concentration is recommended, but this will have to be investigated for the relevant POC and buffer conditions. Concentration ranges from 0.2 to 2 mM NVOC-Cl have been successfully used for caging various proteins.
4. Although there may not be any reactive caging compound remaining after 30-min incubation at room temperature, the reaction is "stopped" by adding one volume of acidic 0.1 M Tris–HCl. The pH of the TRIS solution was adjusted such that the final pH of the sample was pH 7.4.
5. The sample is then washed with a buffer conducive with subsequent experimental steps keeping in mind that the osmolarity may be important (*see* **Note 7**). If there are no specific requirements, the standard wash buffer of 20 mM HEPES pH 7.4/0.15 mM NaCl can be used. The washed and concentrated caged POC is then aliquoted, snap-frozen with liquid nitrogen, and stored in a non-defrosting –20 °C freezer. A caged version of the transcription factor GAL4VP16 was stable for more than 1 year at –20 °C.

3.2 Characterization of the Caged Protein

The caging reaction replaces charged residues on the surface of proteins with less polar caging compounds. This can have a dramatic effect on the solubility of the caged protein, so monitoring protein solubility when testing different caging conditions is crucial.

3.2.1 1D SDS Polyacrylamide Gel

A straightforward approach to testing solubility is to run the samples on a standard 1D SDS polyacrylamide gel. Proteins that retain water solubility after caging will appear as normal bands in the gel, while proteins that were modified too heavily precipitate and can be pelleted. The staining intensity of the band can then be used to assess the amount of caged soluble protein vs. control mock-treated protein. If a protein is modified on many side chains with the caging compound potentially there may be a shift towards higher molecular weight on the gel. Also, the standard Coomassie stain preferably binds to lysines residues, i.e., those residues to which the NVOC-Cl is conjugated to. Consequently, there may be a reduction in staining intensity compared to control samples although the amount of protein is the same. If the caging interferes with staining, as an alternative, the reader is referred to commercially available staining procedures using silver or zinc for example (e.g., Pierce).

1. After the caging reaction was stopped with acidic Tris buffer, pellet insoluble, caged protein by centrifugation with a table-top centrifuge (10 min at maximum speed, 4 °C).
2. Collect the supernatant. Assuming that the POC is pure, load about 1–2 μg of protein per well onto the gel. Usually, the gels tolerate the organic solvent so that the sample does not have to be washed beforehand.
3. Stain gel with Coomassie stain keeping in mind that caging may reduce staining intensity.
4. Qualitatively assess protein solubility after caging by comparing the signal intensity of the bands.

3.2.2 Uncaging In Vitro

A simple means to uncaging the caged POC in vitro is by irradiation with a handheld UV lamp (4–8 W). These lamps are generally used to look at ethidium bromide-stained DNA agarose gels. Because of their low power output, irradiation times for uncaging need to be quite long, usually around 1–3 h. Irradiations should be performed at 4 °C with the open-lid tubes stuck to the lamp using clay or tape.

3.2.3 ELISA

Binding of the caged POC to its protein substrate is most readily assessed with an ELISA assay. There are many commercially ELISA systems available that rely on a fluorescence 96-well plate reader. The reader is referred to the company's instructions for detailed information about using their system. Thus, the experimental specifics (amount of protein, incubation times, blocking buffers, wash times, etc.) depend on the ELISA system being used, but the basic steps will be as follows: The adhesive surface of the plate is coated with the caged or the mock-treated protein, residual binding sites on the plate are blocked with a BSA blocking buffer or equivalent, and the anti-POC antibody is allowed to bind to its substrate, followed by fluorescence-based detection of the primary anti-POC antibodies using secondary antibodies coupled with an enzyme such as β-galactosidase and a corresponding fluorogenic substrate such as OPC.

3.2.4 Quantifying the Average Number of Caged Lysines

This procedure is based on the fluorogenic reaction of fluorescamine with lysines of the POC. The resulting conjugate fluoresces with a peak of about 485 nm, while the unreacted or the hydrolyzed fluorescamine does not exhibit appreciable fluorescence. The difference in fluorescence between mock-treated POC and caged POC then highlights the extent of caging for the entire sample. Of course, this procedure does not reveal the potential variance in the extent of caging of all individual POC molecules but only the ensemble average. Around 40–60 % of caged lysines in a functionally inhibited POC appears to be a common value.

1. If sufficient amounts of POC are available, cage 10 μg of POC with NVOC-Cl according to the protocol and in parallel perform a control reaction (mock-treat) of 10 μg POC without

NVOC-Cl but with all buffers, organic solvents, etc. the same. Prepare a third sample with all caging reagents except the POC.

2. After 30 min, do not "stop" caging/control reactions with acidic Tris buffer, but instead add 50 mM $NaPO_4$, pH 8.5, containing 1 % SDS to a final volume of 1.5 ml and boil for 3 min.
3. Allow the sample to cool to room temperature, and add 0.5 ml of 0.2 mg/ml fluorescamine in dioxane and incubate for 15 min at room temperature.
4. Using a fluorescence plate reader (390 nm excitation/485 nm emission), analyze the samples. Subtract the value of the sample without the POC as background from the values of the caging reaction and the mock reaction. The ratio of (caged–background)/(mock–background)×100 corresponds to the percentage of caged lysines of the caged POC.

3.3 Introducing the Caged Sample into the System

Biological samples are too diverse to be able to describe a general procedure regarding the introduction of caged proteins into the system. The means by which unmodified POC is administered to the sample should also be adequate for the caged POC. The reader is referred to published protocols describing microinjection and bead loading of proteins into cells [7, 8].

3.4 Uncaging the Caged POC Within a Biological System

3.4.1 Aligning the Microscope optics

A somewhat underappreciated issue with epifluorescence microscope optics is the alignment of the lamp, for example after it has been changed. Most commonly, the adjustment screws at the lamp housing are turned until a uniformly illuminated field, projected onto the ceiling, wall, or a piece of paper, has been achieved. This procedure is sufficient for most applications but does not ensure parallel light beams in the path of the microscope optics. However, for patterned illumination of caged samples, such as a thin stripe, a circle, or more sophisticated patterns such as a letter or a smiley face, it is necessary that all light is aligned in parallel fashion. By introducing a thin metal inset with the shape of the pattern ("smiley face" in Fig. 2, red arrow) into the light path, the adjustment screws are tuned to project the pattern onto a macroscopic surface such as a piece of paper. Misalignment will fail to project the pattern of the inset unless all light beams are in a strictly parallel fashion.

3.4.2 Identifying the Necessary Levels Uncaging Light

A key factor for a good experiment is knowing the amount of light needed for uncaging the POC. Often, the photo-release of active POC and its biological readout may be difficult to assess, and consequently one may not be able to quickly discern if the uncaging procedure was successful or not. To circumvent this problem, one should establish the irradiation parameters with caged fluorescein prior to uncaging POC. The emergence of fluorescein fluorescence upon light exposure is a very rapid and simple means to identify the appropriate light conditions for uncaging in the respective biological system. Living cells can be easily loaded with

Fig. 2 The mechanical shutter and sliding filter holder of a microscope can be used to introduce a thin prefabricated metal plate (here: smiley face; *red arrow*) for patterned illumination of the biological sample (Color figure online)

fluorescein and its derivatives by simply adding it to the medium and allowing the dye to be taken up by the cells [9].

1. Load cells by adding caged fluorescein to the medium at a final concentration of 100 μM and incubate at 37 °C for 20–40 min. Alternatively, inject a 2 mM solution into the cell directly. Wash cells briefly twice with medium.
2. Using transmitted light, choose a region of the sample and limit the to be irradiated area with the microscope aperture.
3. With the GFP/fluorescein filter set, record an image prior to DAPI irradiation.
4. Switch to the DAPI filter set, and either manually or via the software that controls the microscope open the shutter for 2 s and irradiate the sample at the desired area.
5. Switch to the GFP/fluorescein filter set, and assess the levels of fluorescein fluorescence.
6. By adjusting the irradiation times at previously unirradiated areas, determine the minimum irradiation time necessary for full uncaging of fluorescein fluorescence. Use this irradiation time for the first uncaging experiments with caged POC.

3.4.3 Assessing Postirradiation Cellular Fitness

There is a keen awareness that the UV light used for uncaging can be harmful to cells at longer exposure times. Monitoring cell viability before and after irradiation is therefore absolutely necessary although cells seem to tolerate a few seconds of UV light very well. In fact, the neuronal membrane potential, which is very sensitive to perturbance, was not affected in hippocampal brain slices after irradiating for 10 s when 2 s was sufficient for full uncaging [10]. While there are many different ways of assessing cell viability, short and long term, a robust assay would be to monitor apoptosis 24–48 h after irradiation. The author has experience with one commercial kit that produces a green or a red fluorescent signal that can be used in addition to standard antibody stains, but of course, other kits should be suitable as well.

1. Fixate and permeabilize irradiated and control, unirradiated samples for normal immunofluorescence staining. Continue with standard procedure including administration of antibodies and washing steps.
2. After the final washing step, add TUNEL reaction mixture to end-label low-molecular-weight DNA fragments indicative of apoptotic cells (*see* **Note 8**). Incubate for 1 h at 37 °C.
3. Wash sample twice and embed for fluorescence microscopy analysis.

4 Notes

1. Anhydrous solvents may be stored over molecular sieves (3–4 Å) to keep the amount of water molecules in the solution to a minimum. Water causes unspecific hydrolysis of NVOC-Cl which should be avoided prior to the caging reaction. Freshly opened solvent bottles can be considered free of water, so make sure to close the (new) solvent container immediately after use.
2. In case NVOC-Cl had been dissolved in DMSO, remember that the melting point of DMSO is at 18 °C which causes it to become solid on ice or in the fridge.
3. To resuspend lyophilized proteins with aqueous solution avoid producing air bubbles or foam in your sample because this can cause aggregation, oxidation, etc. of proteins. In general, solutions with biological samples should never be handled such that bubbles and foam develop.
4. Use ten times the volume of your sample for washing.
5. Thiol and hydroxyl residues may react with NVOC-Cl but are much more difficult to uncage.
6. The pH adjustments can be done with volumes large enough that the pH can be measured with a standard pH meter.

7. The wash buffer (20 mM HEPES pH 7.4/0.15 mM NaCl) has an osmolarity of 320 mOsm which is near the osmolarity of most biological samples.
8. As a negative control, use only the fluorescently labeled nucleotides without the end-labeling transferase enzyme. For positive control, one can add DNAse I to the sample prior to staining to produce ample free DNA strand ends. Always handle fluorescently stained samples carefully making sure not to expose them to bright light.

References

1. Kaplan JH, Hollis RJ (1980) External Na dependence of ouabain-sensitive ATP:ADP exchange initiated by photolysis of intracellular caged-ATP in human red cell ghosts. Nature 288(5791):587–589
2. Brieke C, Rohrbach F, Gottschalk A, Mayer G, Heckel A (2012) Light-controlled tools. Angew Chem Int Ed Engl 51(34):8446–8476. doi:10.1002/anie.201202134
3. Mayer G, Heckel A (2006) Biologically active molecules with a "light switch". Angew Chem Int Ed Engl 45(30):4900–4921. doi:10.1002/anie.200600387
4. Marriott G (1994) Caged protein conjugates and light-directed generation of protein activity: preparation, photoactivation, and spectroscopic characterization of caged G-actin conjugates. Biochemistry 33(31):9092–9097
5. Cambridge SB, Davis RL, Minden JS (1997) Drosophila mitotic domain boundaries as cell fate boundaries. Science 277(5327):825–828
6. Kossel AH, Cambridge SB, Wagner U, Bonhoeffer T (2001) A caged Ab reveals an immediate/instructive effect of BDNF during hippocampal synaptic potentiation. Proc Natl Acad Sci U S A 98(25):14702–14707. doi:10.1073/pnas.251326998
7. Humphrey D, Rajfur Z, Imperiali B, Marriott G, Roy P, Jacobson K (2007) Introduction of caged peptide/protein into cells using microinjection. CSH protocols 2007:pdb prot4659. doi:10.1101/pdb.prot4659
8. Humphrey D, Rajfur Z, Imperiali B, Marriott G, Roy P, Jacobson K (2007) Introduction of caged peptide/protein into cells using bead loading. CSH protocols 2007:pdb prot4658. doi:10.1101/pdb.prot4658
9. Butcher EC, Scollay RG, Weissman IL (1980) Direct fluorescent labeling of cells with fluorescein or rhodamine isothiocyanate. II. Potential application to studies of lymphocyte migration and maturation. J Immunol Methods 37(2):109–121
10. Cambridge SB, Geissler D, Calegari F, Anastassiadis K, Hasan MT, Stewart AF, Huttner WB, Hagen V, Bonhoeffer T (2009) Doxycycline-dependent photoactivated gene expression in eukaryotic systems. Nat Methods 6(7):527–531

Chapter 3

Optochemical Activation of Kinase Function in Live Cells

Andrei V. Karginov, Klaus M. Hahn, and Alexander Deiters

Abstract

Manipulation of protein kinase activity is widely used to dissect signaling pathways controlling physiological and pathological processes. Common methods often cannot provide the desired spatial and temporal resolution in control of kinase activity. Regulation of kinase activity by photocaged kinase inhibitors has been successfully used to achieve tight temporal and local control, but inhibitors are limited to inactivation of kinases and often do not provide the desired specificity. Here we report detailed methods for light-mediated activation of kinases in living cells using engineered *rap*amycin-*r*egulated kinases in conjunction with a photocaged analog of rapamycin.

Key words Kinase, Phosphorylation, Rapamycin, FKBP12, Caging, Light activation

1 Introduction

Protein kinases play a central role in the regulation of signaling networks critical for cell function. The most common methods for the regulation of kinases include pharmacological inhibitors, overexpression of mutants, and downregulation of protein expression by genetic manipulation or siRNA. These methods are valuable but suffer from numerous limitations. Pharmacological inhibitors are available only for a limited number of kinases and often cannot provide the desired specificity. It is especially difficult to achieve high inhibitor selectivity for a kinase that has several homologs or isoforms. Downregulation or overexpression of kinases provides essentially no temporal resolution and affects function of the whole protein rather than "surgically" regulating catalytic activity alone. The time required for genetic modification to result in altered protein allows the cell to compensate for (and adapt to) the perturbation. More recently, a chemical-genetic approach has overcome some of these limitations by using specifically designed inhibitors for kinases with a drug-sensitizing mutation [1]. However, this method requires separate inhibition or downregulation of the endogenous, wild-type form of the modified kinase, involving

Sidney Cambridge (ed.), *Photoswitching Proteins: Methods and Protocols*, Methods in Molecular Biology, vol. 1148,
DOI 10.1007/978-1-4939-0470-9_3,

elaborate optimization and potentially affecting activity of other endogenous kinases. Importantly, none of these methods enable specific activation of kinases with controlled timing. Several methods that do enable activation are limited to a small subset of kinases that either can be activated by dimerization [2] or can be modified for regulation by high concentrations of imidazole (5 mM) [3]. We have recently developed a new broadly applicable method for engineered allosteric regulation of protein kinases in live cells [4–6]. Insertion of an engineered allosteric switch, the iFKBP domain, at a structurally conserved position within the catalytic domain renders the modified kinase inactive. Treatment with rapamycin or its non-immunosuppresive analogs (iRap, AP21967; Clontech) triggers interaction with a small FKBP–rapamycin-binding (FRB) domain and restores the activity of the kinase (Fig. 1a). The reagents used in this method are either genetically encoded or membrane permeable, enabling ready application in a wide range of systems. Based on the structural similarity of catalytic domains among the most known protein kinases, this method will likely be applicable to a wide variety of kinases. We have already developed *rap*amycin-*r*egulated (RapR) analogs of different kinases, representing both Tyr and Ser/Thr families, namely, FAK, Src, and p38.

To achieve light-mediated control of RapR kinases we generated a photo-activatable analog of rapamycin (*p*hotocaged *rap*amycin (pRap)) [7]. Photo-activatable derivatives of small molecules are typically generated through conjugation of a light-removable protecting group, the so-called caging group, at a site crucial for biological activity of the small molecule [8–18]. Ideally, this renders the molecule completely inactive and unable to induce iFKBP/FRB dimerization, until the caging group is removed through light irradiation, typically with nontoxic [19–21] UV light of 365–405 nm. We constructed the pRap analog by protecting the hydroxyl group at the C-40 position of rapamycin with a sterically demanding, light-removable nitropiperonyloxycarbonyl (NPOC) group (Fig. 1b). Treatment with pRap up to 20 μM does not trigger interaction with FRB and activation of RapR kinase. However, irradiation with 360 nm light leads to rapid pRap uncaging and robust activation of RapR kinase upon interaction with FRB (Fig. 1c) [7]. The experimental details of applying this methodology to the optochemical activation of focal adhesion kinase (FAK) are described here. FAK localizes prominently to focal adhesions in living cells, and we use changes in cell behavior characteristic of this kinase to demonstrate efficient light activation. Similar strategies can also be applied for activation of other RapR kinases. In case a different RapR kinase is used, appropriate modifications to the protocol should be made to test the activity of the kinase. Beyond the activation of kinase function, pRap should be applicable to induce iFKBP/FRB-mediated protein dimerization and thus should provide a general light switch to control of various cellular processes.

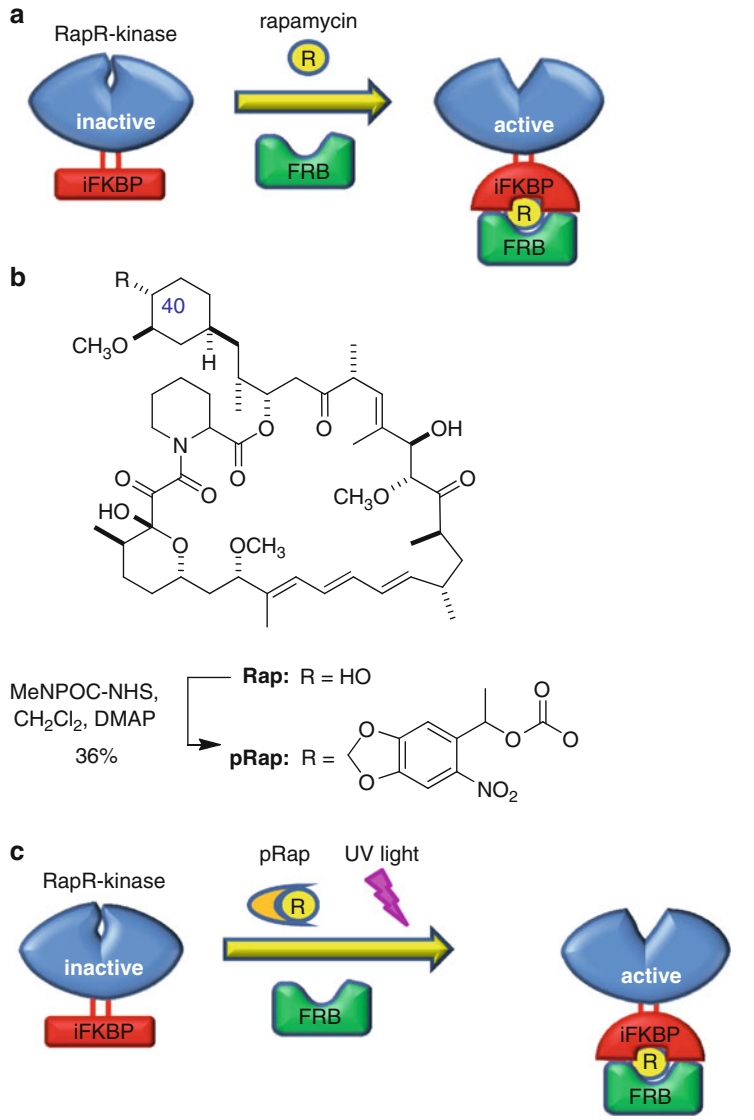

Fig. 1 Engineered control of RapR kinases. (**a**) Schematic of rapamycin-mediated control of kinases. (**b**) Structure of rapamycin (Rap) and synthesis of photocaged rapamycin (pRap) through selective acylation of the C-40 hydroxyl group with methyl-nitro-piperonyloxycarbonyl *N*-hydroxysuccinimide carbonate (MeNPOC-NHS). (**c**) Schematic of the light-induced activation of RapR kinases using pRap

2 Materials

Prepare all buffers and solutions with ultrapure water. Store all buffers at 4 °C unless specified otherwise.

2.1 pRap Synthesis

1. *N*,*N*′-disuccinimidyl carbonate.
2. Dimethylaminopyridine (DMAP).

3. Rapamycin, triethylamine (TEA).
4. Acetonitrile (CH_3CN).
5. Dichloromethane (CH_2Cl_2).
6. Ethyl acetate.
7. Hexanes.
8. TEA.
9. Diisopropylethylamine (DIPEA).
10. Dichloromethane (CH_2Cl_2).

Solvents were distilled and stored over molecular sieves (4 Å) prior to use. TEA, DIPEA, and CH_3CN were distilled from calcium hydride. CH_2Cl_2 was dried by an MB SPS Compact solvent purification system.

2.2 In Vitro Kinase Assay

1. DNA constructs: pEGFP-FRB, pmyc-RapR-FAK plasmids (available at Addgene) dissolved in water or TE buffer (10 mM Tris–HCl, pH 8.0; 1 mM EDTA) at concentrations no less than 200 μg/ml. Store at −20 °C.
2. Cell culture medium: Dulbecco's modified Eagle medium (DMEM, with 4.5 g/l glucose, 4 mM L-glutamine, and 110 mg/l sodium pyruvate) cell culture medium containing 10 % (v/v) fetal bovine serum (FBS) (*see* **Note 1**). Store at 4 °C.
3. Phosphate-buffered saline (PBS): 137 mM NaCl, 10 mM phosphate, 2.7 mM KCl, pH of 7.4. Weigh 8 g of NaCl, 0.2 g of KCl, 1.44 g of Na_2HPO_4, and 0.24 g of KH_2PO_4. Dissolve in 800 ml of water. Adjust pH to 7.4 using HCl. Adjust total volume to 1 l with water.
4. FuGene6 transfection reagent (Promega) (*see* **Note 2**).
5. 6-well tissue culture plates.
6. Cell scraper.
7. Immunoprecipitation: Protein G-coupled agarose beads (Millipore or other manufacturers), 50 % slurry. Store at 4 °C.
8. Antibodies: JL8 anti-GFP antibody (Clontech), Anti-phospho-Tyr31 paxillin antibody (Invitrogen), 4A6 anti-myc antibody (1 mg/ml, Millipore), peroxidase-conjugated secondary antibody. Follow storage conditions recommended by the manufacturer.
9. Reagents and equipment required for SDS-polyacrylamide gel electrophoresis of proteins.
10. Reagents and equipment required for protein transfer onto PVDF membrane.
11. Lysis buffer: 20 mM Hepes–KOH, pH 7.8, 50 mM KCl, 1 mM EGTA, 1 % NP40 (IGEPAL), 1 mM NaF, 0.2 mM Na_3VO_4. Keep on ice (*see* **Note 3**).

12. Wash buffer: 20 mM Hepes–KOH, 50 mM KCl, 100 mM NaCl, 1 mM EGTA, 1 % NP40 (IGEPAL, Sigma-Aldrich), pH 7.8. Keep on ice.
13. Kinase reaction buffer: 25 mM HEPES pH7.5, 5 mM $MgCl_2$, 5 mM $MnCl_2$, 0.5 mM EGTA, 0.005 % BRIJ-35 (nonionic detergent, Fisher BioReagents) (*see* **Note 4**). Keep on ice.
14. Paxillin/ATP mix: 0.1 mM ATP and 0.05 mg/ml purified GST-paxillin N-terminal fragment in kinase buffer (*see* **Note 5**). A protocol for purification of the GST-tagged N-terminus of paxillin has been described elsewhere [22].
15. Rapamycin and pRap: Dissolved in DMSO at 0.25 mM for rapamycin, 1, 5, and 20 mM stocks for pRap. Store at −20 °C.
16. UV irradiation: UVP LMW-20 transilluminator (8 W) (*see* **Note 6**).
17. HEK293 cells (ATCC).
18. 1 mg/ml Bovine serum albumin (BSA) dissolved in lysis buffer (without NaF and Na_3VO_4). Store at −20 °C.

2.3 Components for Live Cell Imaging

1. HeLa cells (ATCC).
2. DNA constructs: pGFP-RapR-FAK and pmCherry-FRB plasmids (Addgene), dissolved in water or TE buffer (10 mM Tris–HCl, pH 8.0, 1 mM EDTA) at concentration no less than 200 μg/ml. Store at −20 °C.
3. FuGene6 transfection reagent (Promega) (*see* **Note 1**).
4. Cell culture medium: DMEM (with 4.5 g/l glucose, 4 mM L-glutamine, and 110 mg/l sodium pyruvate) containing 10 % (v/v) FBS.
5. Live cell imaging medium: L15 Leibovitz Medium (Invitrogen) supplemented with 5 % FBS (*see* **Note 7**).
6. Mineral oil, sterile filtered, suitable for mouse embryo cell culture (Sigma-Aldrich).
7. 25 mm round glass cover slips, 0.13–0.17 mm thick (Fisher Scientific). Store in 70 % ethanol solution.
8. 1 mg/ml Fibronectin stock solution dissolved in 0.5 M NaCl, 0.05 M Tris, pH 7.5 (*see* **Note 8**).
9. Attofluor® cell chamber (Invitrogen) (*see* **Note 9**).
10. 35 mm tissue culture plates.
11. Microscope equipped with an objective-based total internal reflection fluorescence (TIRF) system, a 60× TIRF objective, CCD camera, a high-pressure mercury arc light source, laser lines with excitation at 488 and 590 nm for TIRF imaging, and an open heated chamber (*see* **Note 10**).
12. 5 mM pRap dissolved in DMSO. Store at −20 °C.
13. UV irradiation: UVP UVGL-25 handheld UV lamp (4 W) (*see* **Note 6**).

3 Methods

All centrifugation steps can be performed in a benchtop centrifuge at room temperature unless indicated otherwise.

3.1 pRap Synthesis

3.1.1 Synthesis of α-Methyl-6-Nitropiperonylol Succinimidyl Carbonate (MeNPOC-NHS)

1. 1-(3,4-(Methylenedioxy-6-nitrophenyl) ethanol was synthesized as reported [23], and 200 mg (0.947 mmol) was dissolved in 5 ml of dry CH_3CN (*see* **Note 11**).
2. To the solution were added *N*,*N*′-disuccinimidyl carbonate (485 mg, 1.894 mmol) (*see* **Note 12**) and TEA (0.396 ml, 2.840 mmol).
3. The reaction was stirred at room temperature overnight.
4. The solvent was removed under reduced pressure, and the product was directly purified by column chromatography on silica gel (eluted with hexanes/ethyl acetate 5:1), delivering 296 mg (89 % yield) of MeNPOC-NHS as a light yellow solid.
5. Analytical data: ^{1}H NMR (300 MHz, $CDCl_3$) δ 7.49 (s, 1H), 7.09 (s, 1H), 6.39 (q, J = 6.4 Hz, 1H), 6.14–6.12 (m, 2H), 2.79 (s, 4H), 1.73 (d, J = 6.4 Hz); ^{13}C NMR (100 MHz, $CDCl_3$) δ 168.7, 153.0, 150.8, 148.0, 141.6, 133.2, 105.9, 105.6, 103.5, 76.5, 25.6, 22.3(*see* **Note 25**); high-resolution mass calculated $C_{14}H_{12}N_2NaO_9$ 375.04405, found 375.0430.

3.1.2 Synthesis of MeNPOC-Caged Rapamycin (pRap)

1. Under argon, rapamycin (20.0 mg, 0.022 mmol) was dissolved in dry DCM (0.6 ml) (*see* **Note 11**).
2. DMAP (5.4 mg, 0.044 mmol) (*see* **Note 12**) and MeNPOC-NHS (39.0 mg, 0.109 mmol) were added.
3. The reaction mixture was stirred at room temperature for 24 h.
4. The volatiles were evaporated under reduced pressure, and the product was purified by column chromatography on silica gel (eluted with DCM/ethyl acetate 10:1, 5:1, 2:1, 1:1), delivering 9.1 mg (36 % yield) of pRap as a light yellow solid. No attempts were made to separate the two generated diastereomers.
5. Analytical data: ^{1}H NMR (400 MHz, $CDCl_3$) δ 7.48 (s, 1H), 7.05 (s, 1H), 6.44–6.03 (m, 7H), 5.94–5.83 (m, 1H), 5.60–5.47 (m, 1H), 5.43 (m, 1H), 5.38–5.31 (m, 1H), 5.20–5.08 (m, 1H), 4.50–4.38 (m, 1H), 4.14–4.09 (m, 2H), 3.98–3.73 (m, 2H), 3.67–3.55 (m, 2H), 3.35–3.31 (m, 7H), 3.13–3.03 (m, 5H), 2.87–2.50 (m, 3H), 2.40–2.11 (m, 2H), 2.03–1.52 (m, 15H), 1.47–1.32 (m, 6H), 1.24–0.86 (m, 24H) (*see* **Note 13**); high-resolution mass calculated for $[M+Na]^+$ $C_{61}H_{86}N_2NaO_{19}$ 1173.5723, found 1173.5721.

3.2 Light-Mediated Activation of RapR-FAK Kinase. Assessment of Activity Using an In Vitro Kinase Assay

1. Distribute 10^6 HEK293 cells per well into two 6-well plates (five wells in one plate and three wells in another) in 2 ml DMEM media with 10 % FBS and grow in a 37 °C, 5 % CO_2 incubator overnight. Cells should be 60–80 % confluent for optimal transfection.
2. Using 1:1 ratio co-transfect HEK293T cells with pEGFP-FRB and myc-RapR-FAK (all wells). Perform transfection using FuGene6 reagent according to the manufacturer's recommendations (2 μg of DNA/6 μl FuGene6 per well). Other equivalent transfection methods can also be used (*see* **Note 2**). Incubate in a 37 °C, 5 % CO_2 incubator overnight.
3. On the day of the experiment, prepare protein G-coupled agarose beads for incubation with the 4A6 anti-myc antibody. Transfer 80 μl of bead suspension into a fresh 1.5 ml tube (10 μl of bead suspension is sufficient for each immunoprecipitation (IP) sample, eight IP samples in this experiment) (*see* **Note 14**).
4. Wash beads with 1 ml of lysis buffer (*see* **Note 15**). Resuspend beads in 400 μl of lysis buffer containing 1 mg/ml BSA and add 4 μl of 4A6 antibody (use 0.5 μl of antibody per IP).
5. Incubate beads at 4 °C for 1–2 h. Wash beads two times with 1 ml of lysis buffer (*see* **Note 15**) and resuspend in 400 μl of lysis buffer (50 μl of lysis buffer for each IP). Aliquot 50 μl of beads into fresh 1.5 ml tubes for incubation with cell lysates.
6. Replace media on the transfected cells with 2 ml of fresh DMEM media containing 10 % FBS. For both plates treat cells with three different concentrations of pRap: 1, 5, and 20 μM (add 2 μl of the corresponding stock solution of pRap, one well for each plate, mix by gentle agitation) (*see* **Note 16**).
7. Treat one well of transfected cells with 250 nM rapamycin (2 μl of 0.25 μM stock, positive control) and another well with 2 μl of DMSO (solvent control). Both wells should be in the 6-well dish with five wells of plated and transfected cells. Incubate all cells in a 37 °C, 5 % CO_2 incubator for 10 min.
8. Irradiate plate with five wells of cells with 365 nm light by placing it on a UVP LMW-20 transilluminator for 1 min (*see* **Note 17**). Keep the other plate in the incubator without irradiation; this will be your negative control to be compared to RapR-FAK induced by uncaged pRap.
9. Incubate all cells in a 37 °C, 5 % CO_2 incubator for 1 h.
10. Wash all cells with cold PBS on ice (~3–4 ml of PBS per well) (*see* **Note 18**). Aspirate as much PBS as possible after the wash.
11. Add 300 μl of lysis buffer to each well. Scrape cells from the plate, collect cell lysates into 1.5 ml tubes, and spin for 10 min at 1,000 × *g* and 4 °C.

12. Collect 20 μl of supernatant for protein gel electrophoresis analysis (*see* **Note 19**). Transfer the remaining supernatant into the tubes containing 50 μl of beads prepared in the previous step.
13. Incubate lysates with the beads at 4 °C for 1.5–2 h with constant agitation.
14. Wash beads two times with 0.5 ml of wash buffer and two times with 0.5 ml of kinase buffer (*see* **Note 15**). Remove all buffers from beads after last wash.
15. Add 40 μl of kinase buffer per tube. Resuspend the beads and transfer 20 μl of each sample into a fresh 1.5 ml tube for the kinase reaction.
16. Add 10 μl of paxillin/ATP mix, and incubate for 10 min at 37 °C shaking (*see* **Note 20**).
17. Stop the reaction by the addition of 40 μl 2× Laemmli protein sample buffer. Incubate at 95–100 °C for 5 min. Cool samples to room temperature. Run on a protein SDS-polyacrylamide gel.
18. Perform western blot analysis using a 4A6 anti-myc antibody for detection of myc-FAK variants, anti-phospho-Tyr31 paxillin antibody for assessment of substrate phosphorylation, and anti-GFP JL8 antibody for detection of GFP-FRB (Fig. 2).

3.3 Light-Mediated Activation of RapR-FAK Kinase: Live Cell Imaging

1. Plate 200,000 HeLa cells in a 35 mm tissue culture dish and grow overnight in a 37 °C, 5 % CO_2 incubator. Cell confluency should be 50–70 % the next morning.
2. Co-transfect HeLa cells with 0.5 μg of GFP-FRB plasmid and 1.5 μg of pEGFP-RapR-FAK plasmid using 4 μl of FuGene6 according to the manufacturer's recommendations (*see* **Note 2**). Incubate overnight at 37 °C, 5 % CO_2.

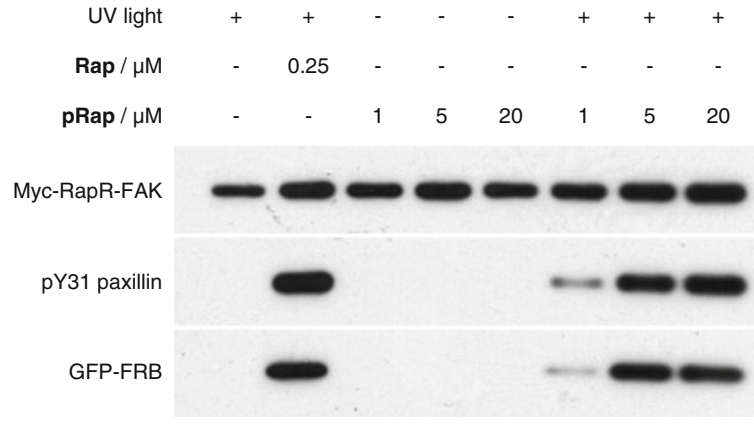

Fig. 2 Light-induced activation of RapR-FAK. Representative results of an in vitro kinase assay. The level of paxillin phosphorylation on Tyr31 (probed with an anti-phospho-Tyr31 paxillin antibody) indicated the kinase activity

3. Place a glass cover slip in 35 mm tissue culture plates or 6-well plates. Wash with 2–4 ml of PBS. Incubate the cover slip in 2 ml of 5 mg/ml fibronectin solution in PBS at 37 °C overnight. Wash the cover slip with PBS, and add 2 ml of DMEM media with 10 % FBS.
4. Plate transfected HeLa cells onto fibronectin-coated cover slip. Incubate in DMEM/10 % FBS medium for 2 h at 37 °C, 5 % CO_2 (*see* **Note 21**).
5. Preincubate mineral oil and L15 media supplemented with 5 % FBS in a tissue culture incubator (37 °C, 5 % CO_2) for at least 1 h before imaging.
6. Wash the cover slip with PBS, and place it in an Attofluor® cell chamber. Add 0.9 ml of L15 Leibovitz Media with 5 % FBS, and cover it with 1 ml of mineral oil (*see* **Note 22**). Place cell chamber onto heated stage of the microscope, and select cells co-expressing GFP-RapR-FAK and mCherry-FRB (*see* **Note 23**).
7. Image cells co-expressing GFP-RapR-FAK and mCherry-FAK, taking images every minute for 120 min. Mix 1 μl of 5 μM pRap solution with 100 μl of L15 Leibovitz Media. Add pRap solution to the cells (final concentration of 5 μM) 30 min after imaging has begun (*see* **Note 24**). Decage pRap 30 min after its addition by placing a UVP UVGL-25 handheld UV lamp 2–3 cm above the cell chamber and irradiating with UV light for 1 min (*see* **Note 17**). Continue imaging for the remaining 60 min. DIC imaging can be used to monitor cell movement and overall changes in cell morphology (i.e., protrusion formation and cell shape) (Fig. 3a). Epifluorescence can be used to monitor RapR-FAK, FRB, or any other fluorescently labeled co-transfected protein. TIRF imaging will reveal translocation of Cherry-FRB to the focal adhesion sites demonstrating interaction between Cherry-FRB and GFP-RapR-FAK induced by uncaging of pRap (Fig. 3b) (*see* **Note 25**).

4 Notes

1. Cell media conditions are determined by the specific cell line used in the experiment. The medium described here is recommended for the HEK293 and HeLa cells used in our experiments.
2. Other transfection reagents can be used. If a different transfection protocol is used, it is recommended to test transfection efficiency before setting up the described experiments. If transfection efficiency is lower than 30 %, either larger quantities of cells should be used or an alternative transfection protocol should be tested.

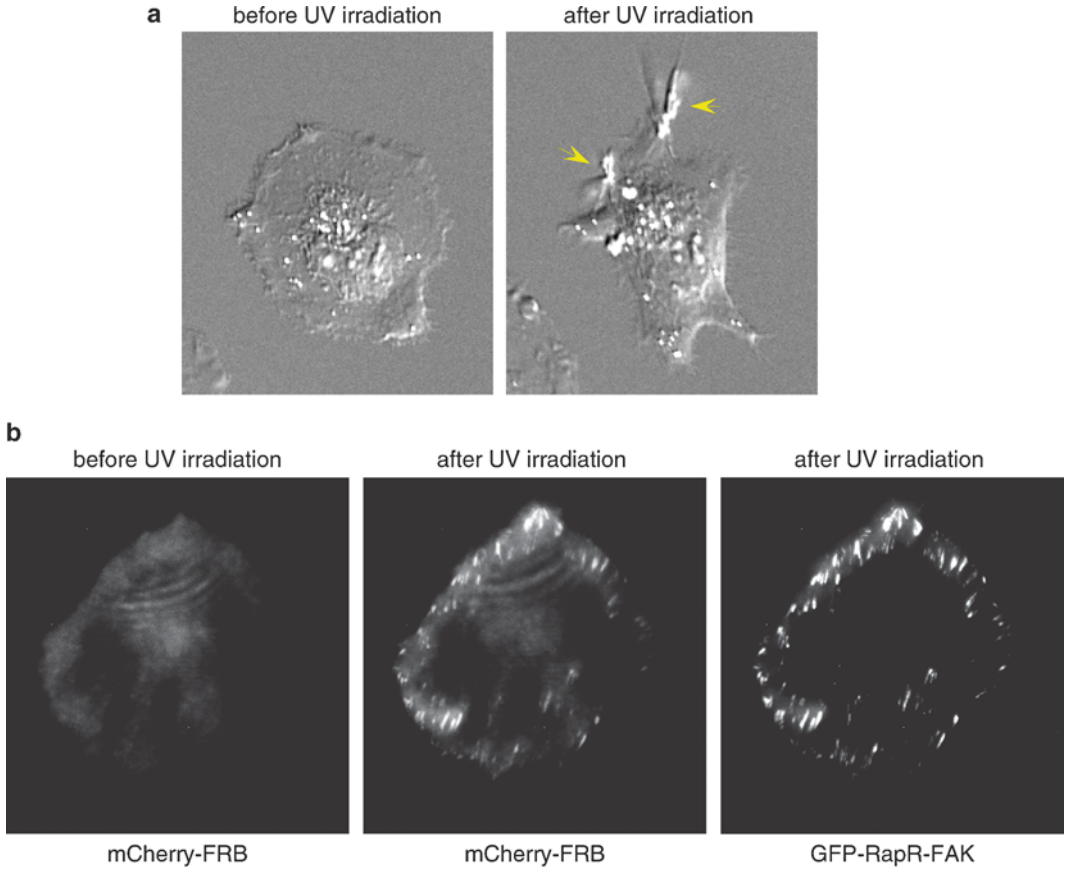

Fig. 3 Effect of light-induced activation of RapR-FAK in live cells and its dimerization with FRB. (**a**) DIC images of HeLa cells expressing GFP-RapR-FAK and mCherry-FRB before and after uncaging of pRap. *Arrows* indicate the formation of large dorsal ruffles stimulated by activated RapR-FAK. (**b**) Localization of mCherry-FRB before and after uncaging of pRap. Images were acquired using TIRF microscopy

3. Buffer containing 20 mM Hepes–KOH, pH 7.8, 50 mM KCl, 1 mM EGTA, and 1 % NP40 should be prepared separately and stored at 4 °C. Sock solutions of 0.5 M NaF and 0.2 M Na_3VO_4 in water should be stored at −20 °C. Complete lysis buffer should be prepared on the day of the experiment and should be stored on ice.
4. Buffer containing 25 mM HEPES pH 7.5, 5 mM $MgCl_2$, 0.5 mM EGTA, and 0.005 % BRIJ-35 should be prepared separately and stored at 4 °C. Stock solutions of $MnCl_2$ (1 M) in water should be stored at −20 °C. If precipitation is observed in $MnCl_2$ solution, then new stock solutions should be prepared. Complete kinase reaction buffer should be prepared on the day of the experiment and stored on ice.

5. Paxillin–ATP mix should be prepared right before the experiment by mixing 100 mM ATP stock solution and stock solution of the purified GST-paxillin N-terminal fragment in kinase buffer. The mixture should be kept on ice.
6. An equivalent UV transilluminator can be used for this experiment, but uncaging efficiency should be determined by irradiating cells for different periods of time.
7. L15 medium (4 °C) and FBS should be stored separately (−20 °C). On the day of the experiment, prepare a fresh mix of L15 medium and FBS. A minimum of 1 ml will be needed per experiment.
8. Fibronectin solution in PBS should be prepared freshly at the time of application.
9. Other inverted epifluorescence microscopes suitable for live cell imaging can be used. The instrument should allow for addition of reagents during cell imaging.
10. We routinely use an Olympus IX-81 microscope equipped with an objective-based TIRF system and a PlanApo N 60× TIRFM objective (NA 1.45). All images are collected using a Photometrix CoolSnap ES2 CCD camera controlled by Metamorph software. The 488 nm line from an omnichrome series 43 Ar/Kr laser and the 594 nm line from a Cobolt Mambo continuous-wave diode-pumped solid-state laser are used for TIRF imaging. Illumination for epifluorescence images was provided from a high-pressure mercury arc light source.
11. All reactions were performed in flame-dried glassware under a nitrogen atmosphere and stirred magnetically unless indicated.
12. All commercially available chemicals and reagents were used without further purification unless indicated.
13. NMR spectra were recorded using Varian Mercury (300 and 400 MHz) instruments.
14. Agarose beads need to be well resuspended before removing an aliquot. The tip of the pipetman tip can be cut in order to prevent it from being clogged by agarose clumps.
15. To wash the agarose beads, add the buffer to the tube, resuspend by vortexing, centrifuge at 1,500 × *g* for 1 min, and remove the supernatant.
16. Adding reagents and mixing media need to be done very carefully, as HEK293 cells may detach if agitated too vigorously.
17. Protect your eyes and skin from irradiation with UV light by wearing appropriate protective goggles, gloves, and lab coat.
18. Add PBS slowly to the side of the well to avoid cell detachment.

19. Run lysate samples on a separate gel. Transfer onto PVDF membrane, and probe with anti-myc and anti-GFP antibody to check the expression of myc-RapR-FAK and GFP-FRB.
20. We recommend to add paxillin/ATP mix to the side of each reaction tube, then spin all tubes briefly at 4,000 × *g* to add the mix to the beads in all reactions simultaneously, and incubate reactions in a thermomixer set to 37 °C.
21. It takes 1–2 h for HeLa cells to attach to the cover slips and spread.
22. Addition of oil on top of the media prevents evaporation but still allows for addition of reagents.
23. A microscope equipped with a motorized stage enables consecutive imaging of several cells by selecting and logging the positions of cells expressing GFP-RapR-FAK and mCherry-FRB. The number of positions depends on the time to take all the images at one position and move to the next one.
24. Mix pRap with the media right before adding it to the cells. Make sure that you penetrate the oil layer when adding pRap to the cells. Imaging the first 30 min without pRap is required to establish a baseline in order to determine if the addition of pRap causes any changes in cell behavior or changes in protein localization.
25. FAK localizes to focal adhesions at the side of the cell where it attaches to the dish. In the absence of active rapamycin, FRB will be diffusely localized throughout the cell.

Acknowledgments

Dr. Karginov, Dr. Hahn, and Dr. Deiters were supported by the NIH (R21 RCA159179A to AVK, R01 GM057464 to KMH, and R01 GM079114 to AD).

References

1. Bishop AC, Buzko O, Shokat KM (2001) Magic bullets for protein kinases. Trends Cell Biol 11:167–172
2. Spencer DM, Wandless TJ, Schreiber SL, Crabtree GR (1993) Controlling signal transduction with synthetic ligands. Science 262: 1019–1024
3. Qiao Y, Molina H, Pandey A, Zhang J, Cole PA (2006) Chemical rescue of a mutant enzyme in living cells. Science 311:1293–1297
4. Karginov AV, Ding F, Kota P, Dokholyan NV, Hahn KM (2010) Engineered allosteric activation of kinases in living cells. Nat Biotechnol 28:743–747
5. Karginov AV, Hahn KM (2011) Allosteric activation of kinases: design and application of RapR kinases. Curr Protoc Cell Biol Chapter 14: Unit 14. 13
6. Dagliyan O, Shirvanyants D, Karginov AV, Ding F, Fee L, Chandrasekaran SN, Freisinger CM, Smolen GA, Huttenlocher A, Hahn KM, Dokholyan NV (2013) Rational design of a ligand-controlled protein conformational switch. Proc Natl Acad Sci U S A 110:6800–6804
7. Karginov AV, Zou Y, Shirvanyants D, Kota P, Dokholyan NV, Young DD, Hahn KM, Deiters A (2010) Light regulation of protein dimerization and kinase activity in living cells

using photocaged rapamycin and engineered FKBP. J Am Chem Soc 133:420–423

8. Riggsbee CW, Deiters A (2010) Recent advances in the photochemical control of protein function. Trends Biotechnol 28:468–475
9. Mayer G, Heckel A (2006) Biologically active molecules with a "light switch". Angew Chem Int Ed Engl 45:4900–4921
10. Young DD, Deiters A (2007) Photochemical control of biological processes. Org Biomol Chem 5:999–1005
11. Deiters A (2010) Principles and applications of the photochemical control of cellular processes. Chembiochem 11:47–53
12. Deiters A (2009) Light activation as a method of regulating and studying gene expression. Curr Opin Chem Biol 13:678–686
13. Tang X, Dmochowski IJ (2007) Regulating gene expression with light-activated oligonucleotides. Mol Biosyst 3:100–110
14. Lawrence DS (2005) The preparation and in vivo applications of caged peptides and proteins. Curr Opin Chem Biol 9:570–575
15. Curley K, Lawrence DS (1999) Light-activated proteins. Curr Opin Chem Biol 3:84–88
16. Lee HM, Larson DR, Lawrence DS (2009) Illuminating the chemistry of life: design, synthesis, and applications of "caged" and related photoresponsive compounds. ACS Chem Biol 4:409–427
17. Dorman G, Prestwich GD (2000) Using photolabile ligands in drug discovery and development. Trends Biotechnol 18:64–77
18. Adams SR, Tsien RY (1993) Controlling cell chemistry with caged compounds. Annu Rev Physiol 55:755–784
19. Dong Q, Svoboda K, Tiersch TR, Monroe WT (2007) Photobiological effects of UVA and UVB light in zebrafish embryos: evidence for a competent photorepair system. J Photochem Photobiol B 88:137–146
20. Schindl A, Klosner G, Honigsmann H, Jori G, Calzavara-Pinton PC, Trautinger F (1998) Flow cytometric quantification of UV-induced cell death in a human squamous cell carcinoma-derived cell line: dose and kinetic studies. J Photochem Photobiol B 44:97–106
21. Robert C, Muel B, Benoit A, Dubertret L, Sarasin A, Stary A (1996) Cell survival and shuttle vector mutagenesis induced by ultraviolet A and ultraviolet B radiation in a human cell line. J Invest Dermatol 106:721–728
22. Lyons PD, Dunty JM, Schaefer EM, Schaller MD (2001) Inhibition of the catalytic activity of cell adhesion kinase beta by protein-tyrosine phosphatase-PEST-mediated dephosphorylation. J Biol Chem 276:24422–24431
23. Lusic H, Deiters A (2006) A New photocaging group for aromatic N-heterocycles. Synthesis 8:2147–2150

Chapter 4

Photoswitching of Cell Surface Receptors Using Tethered Ligands

Andreas Reiner and Ehud Y. Isacoff

Abstract

Optical probing and manipulation of cellular signaling has revolutionized biological studies ranging from isolated cells to intact tissues in the live animal. A promising avenue of optical manipulation is Chemical Optogenetics (or Optogenetic Pharmacology), an approach for engineering specific proteins to be rapidly and reversibly switched *on* and *off* with light. The approach employs synthetic photoswitched ligands, which can be reversibly photo-isomerized to toggle back and forth between two conformations in response to two wavelengths of light. We focus here on the photoswitched tethered ligand (PTL) approach in which the PTL is covalently attached in a site-directed manner to a signaling protein. For this a ligand anchoring site is introduced at a location which allows the ligand to dock only in one of the light-controlled conformations, thus enabling liganding to be rapidly switched. The ligand can be an agonist, antagonist or an active site (or pore) blocker. In principle, orthogonal chemistries of attachment would make PTL anchoring completely unique. However, extremely high specificity of remote control is also obtained by cysteine attachment because of the ligand specificity and precise geometric requirements for liganding. We describe here the design of light-gated ionotropic and metabotropic glutamate receptors, the selection of a site for cysteine placement, the method for PTL attachment, and a detailed protocol of photoswitching experiments in cultured cells. These descriptions can guide applications of Chemical Optogenetics to other receptors and serve as a starting point for use in more complex preparations.

Key words Optogenetics, Light controlled proteins, Ligand-gated ion channels, LiGluR, Photoswitchable tethered ligands, Azobenzene photoswitch, Glutamate receptor, GPCR, mGluR, GluK2, GluR6

1 Introduction

1.1 Photoswitching Proteins with Tethered Ligands

Light-sensitive biomolecules make it possible to control cellular signaling processes in a noninvasive way with exquisite spatial and temporal resolution. Light-controlled proteins that can be expressed in specific cell types or developmental stages, allow to target cells even more precisely and are now used in an array of optogenetic techniques [1–3]. These tools are extremely powerful to control signaling, for instance to probe the role of individual neurons in neuronal circuits and behavior [4, 5].

Sidney Cambridge (ed.), *Photoswitching Proteins: Methods and Protocols*, Methods in Molecular Biology, vol. 1148,
DOI 10.1007/978-1-4939-0470-9_4,

In many cases it is desirable to have reversible photo-control, i.e., photoswitchable proteins, rather than proteins that are irreversibly activated or photo-uncaged by light. Several classes of light-sensitive proteins with endogenous chromophores are found in nature, such as opsins containing retinal, phytochromes containing tetrapyrrole, and BLUF and LOV domains containing flavin cofactors. Opsins that have naturally evolved to function as light-gated G protein-coupled receptors (rhodopsin) or as microbial ion channels (e.g., channelrhodopsin), as well as light-driven pumps (e.g., halorhodopsin and archaerhodopsin) have been successfully transferred to mammalian cells and are now widely used as optogenetic tools [1, 6, 7]. BLUF and LOV domains undergo significant conformational changes upon illumination and can render enzymes light-sensitive [8, 9], while phytochromes have been used, for instance, to photo-control protein association [10].

One of the dreams of optogenetics is to be able to develop a universal approach by which photo-control can be adapted to most native proteins across a wide set of organisms—to create a new optical manipulation layer to proteomics. To achieve this, it is necessary to get around a fundamental aspect of naturally light sensitive systems in which the ability of the protein to associate with the natural chromophore depends on elaborate structural adaptation that cannot be readily engineered into other proteins of interest. This lead to the development of small and robust photo-isomerizable chemicals that can be covalently attached to the accessible surface of a target protein with the idea that the light-driven conformational change in the chemical compound would induce a functional change in the protein.

Several chemical groups can be utilized as photoswitches in this way [11], such as spiropyrans [12, 13], diarylethenes, hemithioindigos [14], thioamids [15], and azobenzenes. Azobenzene derivatives remain by far the most popular photoswitches, since they have excellent photophysical properties and allow robust and efficient switching, *see*, e.g., [16–21].

While photo-control can be achieved by attaching two points of an azobenzene to a protein so that photoswitching applies force and alters the secondary structure [22, 23], the broadest applications have been with photoswitched tethered ligands (PTLs), consisting of a reactive group at one end that attaches selectively to an introduced amino acid, a photo-isomerizable azobenzene, and a ligand for the target protein at the other end. This approach enables a full length protein, with as little as a single amino acid substitution, to become light sensitive. The PTLs provide versatile control over signaling proteins, as they can be designed to function as orthosteric activators (agonists) or inhibitors (antagonists), as allosteric modulators or as active site/pore blockers [24]. The agonist version of this is illustrated in Fig. 1.

PTLs allow robust control of genetically engineered receptors exclusively in the cells to which they were genetically targeted. This makes it possible to selectively probe the role of particular

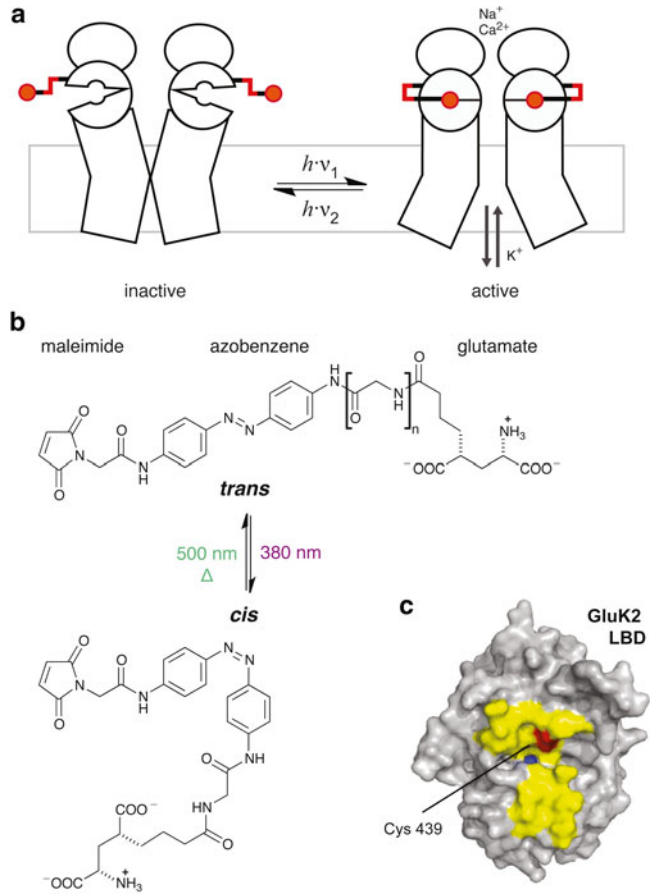

Fig. 1 Optical control of cell surface receptor using photoswitchable tethered ligands. (**a**) Ligand-gated ion channel with tethered ligands that can be reversibly isomerized between an *off* state (*left*) and an *on* state (*right*) with light of specific wavelengths. The ligand can be an agonist (activator), antagonist (inhibitor), or allosteric modulator. (**b**) Structure of the L-MAG ligand family used for the activation of ionotropic glutamate receptors, such as LiGluR. The *m*aleimide group allows covalent attachment to an engineered cysteine residue, the *a*zobenzene serves as *cis*/*trans*-photoswitch and *g*lutamate acts as agonist [29]. Glycine units ($n = 0$, 1, and 2) can be added to increase the linker length (MAG0, MAG1, and MAG2). (**c**) Structure of the ligand binding domain of GluK2 with bound 4-methylglutamate in blue (Protein Data Bank accession code 1SD3 [43]). Of 16 positions tested for MAG attachment (*yellow*), 11 yielded functional receptors and 5 of those permitted photoswitching [41]. The labeling position L439C is shown in *red*. Adapted from refs. [29, 41]

receptors in specific cells or specific subcellular regions. For example, tethered potassium channel blockers can be used generally to control neuronal excitability [25, 26], but they also can be targeted to probe distinct channels, some of which have been implicated in synaptic processing and long-term plasticity in the nervous system. It will be possible to optically manipulate native receptors in their

wild type patterns of expression in knock-in animals. Furthermore, it is possible to use subunit replacement strategies for endowing photo-control on the native protein without the need of a knock-in. This can be achieved by adding a PTL anchoring site to a partner protein that is rendered nonfunctional unless it co-assembles with a native, unmodified target receptor. This Photoswitched Conditional Subunit (PCS) approach was used in conjunction with a PTL pore blocker in the TREK1 K2P channel, which lacks specific soluble blockers, to introduce reversible optical switching, and reveal a previously unknown role in inhibitory synaptic transmission [27, 28].

Tethered agonists and antagonists have also been developed for ionotropic and metabotropic glutamate receptors, iGluRs and mGluRs, respectively. iGluRs, a family of ligand-gated ion channels, and mGluRs, a family of G protein-coupled receptors, are activated by glutamate, the major excitatory neurotransmitter in the mammalian central nervous system. Light-gated versions of the modulatory glutamate receptors that are involved in short- and long-term synaptic plasticity have been made, including kainate receptor GluK2 (iGluR6; LiGluR) and several mGluRs (the LimGluRs) [29–32]. Often the same receptor, or ones that are difficult to distinguish pharmacologically, are found at multiple locations within the same synapse (e.g., in the presynaptic nerve terminal, the postsynaptic dendritic spine, and a local astrocyte process: the three compartments of the tripartite synapse that appear to cross-talk extensively in ways that are not yet understood [33]), which makes it virtually impossible to define their function with soluble compounds. The ability to selectively introduce the PTL anchoring subunit into one of these compartments using genetic targeting combined with the ability to aim light selectively in three dimensions (e.g., [34]) makes it possible to resolve this. This remote PTL-based control of the components of the excitatory synapse has been extended to one of the major classes of modulatory synapses by the production of PTL agonism and antagonism for acetylcholine receptors [17, 35].

1.2 Experimental Strategy

In this section we briefly summarize the design of light-gated glutamate receptors, such as LiGluR.

1.2.1 Design and Characteristics of the MAG Photoswitch

PTLs for glutamate receptors, termed MAGs, encompass three parts: a cysteine-reactive *m*aleimide group, the central *a*zobenzene photoswitch, and a *g*lutamate headgroup that serves as agonist (Fig. 1b). Maleimide reacts with cysteine to form a relatively stable succinimidyl thioether in a Michael-type addition of the thiolate to the maleimide double bond. At pH 6.5–7.5 the reaction remains rather specific for cysteines, while higher pH can facilitate reactions with other nucleophiles, such as amines [36]. Higher pH also accelerates the hydrolysis of both the free maleimide and the conjugated succinimide.

Azobenzene is a molecular photoswitch used in many chemical and technical applications. It has excellent photostability and allows *cis/trans*-photoisomerization over hundreds of switching cycles [31]. The *p,p*-diacylamido substituents in regular MAG lead to favorable optical properties. Near-UV light (370–390 nm) effectively shifts the *trans/*c*is* equilibrium to >90 % *cis* configuration in the photostationary state. Vice versa, 480–530 nm light is effective in populating the *trans* configuration to >85 %. The *trans* form is thermodynamically favored, but at room temperature the thermal relaxation from *cis* to *trans* takes tens of minutes, rendering the switch practically bistable [37]. Other azobenzene substituents [38, 39] can shift the absorption to longer wavelengths and decrease the barrier for thermal relaxation, which can result in spontaneous *cis*-to-*trans* relaxation on experimental timescales.

The MAG ligand headgroup is based on 4-methylglutamate, a known high efficacy agonist of iGluRs [40]. A L-stereochemistry (4*R*) has been found to work with ionotropic glutamate receptors, while mGluRs can be controlled with D-MAGs (4*S*) [32]. The linker length between the azobenzene core and the agonist headgroup has been varied by adding glycine units (Fig. 1b) [37, 41].

1.2.2 Choosing the Receptor and Photoswitch Attachment Sites

The targeted receptor should show robust expression in the desired cell types, e.g., in mammalian cell lines for screening and in neurons for optogenetic applications. Homomeric receptors are usually easier to handle, whereas engineering of subunits that require the formation of heteromers can allow to target native receptor populations [27].

Structural data on the ligand binding region can give information on which ligands might be sterically tolerated, and how the headgroup might be linked to the azobenzene core to not interfere with high affinity binding and receptor activation. In the case of iGluRs, which have LBDs that undergo a pronounced clamshell closure upon agonist binding [42, 43], it was possible to identify an access tunnel for an alkyl linker attached with L-stereochemistry to the 4-position of glutamate (Fig. 1c). In addition, binding site studies, as well as structure–activity relationship studies on pharmacological scaffolds can provide valuable information. Soluble model compounds without a maleimide or azobenzene group can be used to test, whether the designed ligand binds [29], or might be employed as soluble photoswitches [44]. To identify optimal attachment sites, a set of cysteine substitutions around the binding site should be made (Fig. 1c), keeping the overall dimensions (MAGs ~15–30 Å) and the conformational change upon *trans/cis* isomerization in mind. Ideal positions are those, which allow the ligand to reach the binding site in one form, e.g., in the *cis* configuration, but fully prevent binding in the other. For photo-antagonism the structural requirements might be less strict than for agonism, since several ways can be envisaged how the photoswitch could prevent ligand binding or block conformational transitions that lead to activation.

1.2.3 Screening and Validation

To test and compare the PTL performance at different attachment positions a robust and sensitive assay is necessary. Ca^{2+}-imaging has the advantage that many cells can be screened [29, 37], while patch-clamp recordings allow to measure ion channel activation and deactivation in the most direct way [37, 41, 45]. Also G protein-coupled receptor (GPCR) activity may be robustly monitored in this way, using G protein-coupled inwardly rectifying potassium channels [32]. The receptor expression and efficiency of photoswitching can be assessed by applying soluble agonists. It should be kept in mind, however, that mutations around the binding site can affect the affinity for endogenous ligands. Different labeling positions and photoswitch derivatives typically result in a variety of phenotypes, such as full or partial *cis*- and *trans*-agonism or antagonism in different combinations [32, 41]. The application of competitive antagonists is particularly useful to identify *trans*-agonism, as well as to estimate the effective local concentrations of the photoswitch at the binding site [37].

1.3 Photoswitching of LiGluR in HEK Cells

This chapter describes the experimental routine for expressing and photoswitching of LiGluR in HEK cells. The detailed procedure demonstrates the use of the technique with a focus on instrumentation, receptor labeling, and basic photoswitch characterization. The protocol is easy to implement and should serve as guide for adapting PTLs to other receptors or more complex preparations.

LiGluR is a light-gated ionotropic glutamate receptor that can be efficiently switched with L-MAG photoswitches. It is based on the mammalian kainate receptor subunit GluK2 [46, 47], formerly iGluR6, which can form homotetrameric ion channels [48]. It can be robustly expressed in neuronal and non-neuronal cell types and forms a cation-selective ion channel, which under physiological ionic conditions allows a net influx of positive ions, mostly Na^+ [49]. The Ca^{2+}- and Cl^- permeability of GluK2 is largely controlled by the Q/R editing site (621) located in the pore loop [50, 51].

Several LiGluR versions have been designed and the MAG activation mechanism has been characterized in detail [29, 37, 41, 45]. LiGluR can be used to depolarize cells and to induce neuronal firing [30], while an engineered, potassium selective version, Hylighter, can be used to hyperpolarize cells and silence neuronal firing [31]. A key property of regular MAG photoswitches is their bistability on experimental timescales [37]. This means, a brief light pulse of moderate intensity can be used to turn LiGluR *on*, which then will stay in the *on* state until a off light pulse is applied. The extent of LiGluR activation can be finely tuned by the wavelength or the amount of light applied. Fast sub-millisecond switching with high light intensities allows to study the gating of iGluRs in real time [45]. With these favorable properties LiGluR was used for studies in a variety of neurobiological model systems, such as primary neurons [30, 31, 52], astrocytes [53], neuroendocrine cells [54], in the mouse retina [55], the fly neuromuscular junction [56], and zebrafish [4, 30, 31]. Furthermore, viral delivery now allows optogenetic studies in acute brain slices and living animals.

Here we describe the use of patch-clamp recordings, which give the most direct readout and enable detailed characterization. LiGluR and similar tools, however, have been combined in many other experimental settings, such as extracellular recordings [55], imaging techniques with chemical or genetically encoded voltage- or Ca^{2+}-sensors [29, 53], as well as behavioral assays [4, 32, 55].

2 Materials

2.1 DNA Constructs

1. Expression construct for the receptor subunit with an engineered cysteine for MAG attachment, i.e., LiGluR (rat GluK2 L439C) in the pRK5 expression vector [29, 37]. The cytomegalovirus (CMV) promoter gives strong and robust expression in mammalian cell lines. The open reading frame should be preceded by a Kozak consensus sequence and has to include an intact signal peptide sequence (*see* **Note 1**).
2. A wild type expression construct without the engineered cysteine attachment to serve as negative control (*see* **Note 2**). Receptor constructs with different MAG attachment sites [41] can be directly obtained by site-directed mutagenesis [57].
3. Expression construct for a fluorescent marker used to identify transfected cells, e.g., pcDNA3-EGFP.
4. Mini- or midi kit for plasmid purification. Midi preparations often yield higher quality DNA and lower endotoxin levels (*see* **Note 3**).
5. Spectrophotometer for determining the DNA concentration.

2.2 MAG Photoswitch and Chemicals

1. MAG ligands with different linker lengths and stereochemistry have been developed [32, 41] (Fig. 1b). L-MAG0 and L-MAG1 work well in combination with LiGluR and can be obtained from our lab. A red-shifted, spontaneously relaxing MAG ligand has been described as well [39].
2. MAG photoswitches are usually shipped as small powder aliquots (~2 mg), sufficient for ≥120 labeling reactions. The compound should be stored at −20 or −80 °C in the dark and dry, preferably over desiccant (e.g., drierite, *see* **Notes 4** and **5**). The synthesis of the MAG hydrochloride salts, which have good solubility, is described in refs. [29, 37, 41] along with analytical data.
3. Anhydrous, ultrapure DMSO as solvent for stock solutions. Since DMSO is highly hygroscopic it has to be stored moisture free, best in small batches over desiccant (*see* **Notes 4** and **5**).
4. Spectrophotometer for determining the MAG photoswitch concentration.

2.3 Cell Culture

1. Biosafety cabinet (laminar flow hood).
2. Incubator with temperature and CO_2 control (37 °C, 5 % v/v CO_2).

3. Water bath (37 °C).
4. Inverted microscope for cell inspection.
5. Table top centrifuge.
6. Eukaryotic cell lines suitable for the expression of iGluRs and patch-clamp experiments, e.g., human embryonic kidney cells (HEK 293) (*see* **Note 6**). HEK cells are adherent, easy to maintain, allow efficient transfection and have low amounts of endogenous channels interfering with the measurements [58].

   Warning: *Mammalian*, *particularly human cell lines*, *can harbor disease-causing viruses. Consequently*, *cells and materials have to be treated as biohazardous material and have to be handled with proper approval*, *training*, *and care.*
7. Polystyrene cell culture flasks, 25 cm^2, with filter cap, sterile.
8. Polystyrene flat bottom 12-well plates, sterile (fit 18 mm cover glasses).
9. Dulbecco's buffered saline (DPBS) without added Ca^{2+}/Mg^{2+} salts.
10. Dulbecco's modified essential medium (DMEM), high glucose, supplemented with 5 % fetal bovine serum (FBS). Filter-sterilize after serum addition and store at 4 °C (*see* **Note 7**).
11. Trypsin solution (0.25 % with EDTA, e.g., Gibco 25200–114). Optionally, enzyme-free cell dissociation solution (e.g., Sigma, C5914).
12. Transfection reagent with suitable medium supplement (e.g., Lipofectamine® 2000 and Opti-MEM®, Invitrogen).
13. Round cover glasses, 18 mm, thickness ~0.1 mm.
14. Forceps, which allow safe handling of cover glasses.
15. Poly-L-lysine hydrobromide, MW 30,000–70,000 (e.g., Sigma P2636). Prepare a 10 mg/ml stock solution (20×), filter-sterilize, and store 1 ml aliquots at –20 °C.
16. Borate buffer. Prepare a 60 mM borate buffer, pH 8.5, by dissolving 1.5 g boric acid, 2.3 g sodium borate in 500 ml water. Filter-sterilize and store at 4 °C.
17. Distilled water, sterile.
18. Counting chamber (hemocytometer).

2.4 Solutions for Labeling and HEK Cell Patching

1. Extracellular solution: 138 mM NaCl, 1.5 mM KCl, 1.2 mM $MgCl_2$, 2.5 mM $CaCl_2$, 10 mM HEPES, pH 7.3 (NaOH). Prepare a 10× stock solution, filter-sterilize, and store at 4 °C. Before the experiments, dilute to a 1× working solution and supplement with 10 mM glucose (*see* **Note 8**).
2. Intracellular solution: 135 mM K-gluconate, 10 mM NaCl, 2 mM $MgCl_2$, 1 mM EGTA, 10 mM HEPES, pH 7.4 (KOH).

Prepare a 10× stock solution, filter-sterilize, and store at 4 °C (*see* **Note 9**). Before the experiments, dilute to a 1× working solution, supplement with 2 mM Na_2ATP and keep on ice.

3. Concanavalin A (Con A), type IV (e.g., Sigma L7647, *see* **Note 10**). Prepare 20 ml stock solution with 0.3 mg/ml Con A in extracellular solution. The solution can be stored at 4 °C for several weeks.
4. L-Glutamic acid (high purity, e.g., Sigma 49449). Prepare a 100 mM stock in extracellular solution. Readjust to pH 7.3 (NaOH), filter, and store aliquots at −20 °C.
5. Optionally, stock solutions of reducing agents: 10 mM DTT (dithiothreitol) or 1 mM TCEP (*tris*(2-carboxyethyl)phosphine) in extracellular solution [59]. Store aliquots at −20 °C.
6. Optionally, DNQX (6,7-dinitroquinoxaline-2,3-dione) a competitive GluK2 antagonist: 50 mM stock in extracellular solution. Store at −20 °C.

2.5 Imaging and Photoswitch Illumination

1. Inverted microscope with a bright field condenser and epifluorescence light path (*see* Subheading 2.5, **item 6**). For patch-clamp recordings the setup is placed on an air table to reduce vibrations.
2. A Faraday cage should enclose the setup to bar electrical noise. It should be covered with black curtain to block ambient light, which could interfere with photoswitching.
3. For patching on inverted microscopes, 20× or 40× air objectives with long working distances are suitable. Photoswitching with wavelengths <400 nm requires that the objective and all other optical components, including the cover glasses, have significant transmittance in the UV range (*see* **Note 11**).
4. Filter set for imaging GFP or another fluorescent expression marker (*see* Subheading 2.1, **item 3**), including a suitable excitation filter, dichroic mirror, and emission filter. For rapid exchange these filters are usually combined into cubes and mounted in a rotating turret.
5. A standard CCD camera can be used for more sensitive fluorescence detection and easier imaging during patch.
6. Light source for photoswitching with sufficient intensity (*see* **Notes 12** and **13**) in the desired wavelength ranges (e.g., ~375–395 nm for *trans*-to-*cis* and ~488–532 nm for *cis*-to-*trans* isomerization; *see* **Note 11**). Furthermore, the system has to allow rapid switching between the two wavelength ranges, and, preferably, a dark position (*see* **Note 14**). Usually Xe-arc lamps in combination with filter switching systems (e.g., DG-4 with band-pass filters, Sutter Instruments) or monochromators (e.g., Polychrome, Till Photonics) have been used. Solid-state light sources, LED systems, and diode or diode-pumped solid-state

lasers offer now a number of excellent and cost-effective alternatives. Wavelength switching using filters within the microscope should be avoided, since it is often slow and associated with vibrations.

7. The light should be coupled into the epi-fluorescence light path of the microscope. For most light sources, light guides and condenser lenses are available that allow coupling to the back port of the microscope. The coupler should be carefully aligned to yield a centered and uniform illumination in the sample plane [60]. In case the output of the light source cannot be turned off completely, an electromechanical shutter (e.g., Uniblitz) should be added right before the microscope port (*see* **Note 14**). Besides epi-illumination, other illumination schemes can be considered for photoswitching (*see* **Note 15**).
8. A filter cube or filter position should be designated for photoswitching. No further excitation filter is necessary in this cube. The dichroic mirror has to direct both the *on* and *off* wavelengths to the objective, and an emission filter should be added to cut out the excitation light so that it cannot reach the eyepiece or camera (*see* **Note 16**). A fully reflecting mirror (e.g., XF125, Omega Optical) can be installed instead of the dichroic mirror, which gives higher light intensity for photoswitching, but does not allow simultaneous imaging.
9. A plastic shield should be placed in front of the sample stage, as high light intensities can be damaging to the eye (*see* **Note 16**).
10. Powermeter with sensor diode for the UV/VIS-range (e.g., PM100D with S130VC, Thorlabs).
11. Optional: a set of neutral density filters for variation of the light intensity (e.g., XND6PC, Omega Optical).
12. Optional: an amplified photodiode (e.g., PDA25K Thorlabs) or an old photomultiplier tube to record the actual light stimuli (*see* **Note 17**).
13. Optional: a handheld 365 nm UV lamp for affinity labeling.

2.6 Setup for Patch-Clamp Recordings and Accessories

1. Patch-clamp amplifier with headstage, A/D converter, and recording software (e.g., Axopatch 200B, Digidata 1440A and pClamp software, Molecular Devices).
2. Stable 3-axis micromanipulator with amplifier headstage mount (e.g., MP285 from Sutter). The manipulator should be mounted on a rotating base, either on the microscope stage or on a separate stand.
3. Glass micropipette puller (e.g., P-97, Sutter Instruments). A microforge for fire-polishing pipettes is helpful (e.g., MF-830, Narishige), but not absolutely necessary.

4. Pipette glass, borosilicate, thin wall with filament (e.g., G150TF-3, Warner Instruments).
5. Syringe tips for filling micropipettes (e.g., Microfil 28 AWG, MF28G67-5, World Precision Instruments). Alternatively long, soft plastic pipette tips can be used (e.g., Microloader, Eppendorf). A filter (0.2 μM, PES, 13 mm) should be placed between the syringe and tip to remove any dust particles.
6. Handheld pressure meter (e.g., HHP 4205, Omega Engineering) connected to the air tubing at the electrode holder.
7. Ag/AgCl wires for the headstage and reference electrodes. The Ag electrodes can be chlorinated by placing them for 25 min in bleach (sodium hypochlorite).
8. U-shaped KCl salt bridges: glass capillaries are bent into a U-shape using a flame. The salt bridge solution, 3 M KCl in 1 % agarose (electrophoresis grade), is prepared and heated in the microwave. After cooling to ~50 °C a pipette tip is used to fill the glass capillary. After hardening of the agar, the salt-bridges are stored in 3 M KCl at 4 °C.
9. Perfusion chamber for mounting cover glasses (e.g., RC-25 F/PM3, Warner Instruments). Vacuum grease can be used for sealing.
10. Perfusion system: a manual, gravity-driven perfusion system is sufficient for slow perfusion experiments. For this, reservoirs (e.g., 50 ml disposable syringe tubes) are mounted ~30–60 cm above the stage, equipped with stopcocks and flow regulators. The tubings are combined via a manifold (e.g., MP4, Warner Instruments) into a single line, which is attached to the inlet of the perfusion chamber.
11. Vacuum line: a collection bottle and overflow trap is connected to a vacuum line, and a stopcock is added to control the suction. The vacuum line is terminated with a bent syringe needle that is placed in the outlet reservoir of the perfusion chamber. Modeling clay can be used for mounting.

3 Methods

3.1 DNA Preparation

1. Prepare DNA from *E. coli* cultures using standard mini or midi plasmid preparation kits. Elute with sterile elution buffer (*see* **Note 3**).
2. Determine the concentration using a spectrophotometer and $\varepsilon_{260} = 0.02\,(\mu g/ml)^{-1}\,cm^{-1}$. The DNA concentration should be ≥0.4 μg/μl and the A_{260}/A_{280} ratio should be between 1.75 and 1.95.

3.2 Coating Cover Glasses with Poly-L-Lysine

1. Thaw an aliquot of PLL stock solution and dilute it in 20 ml borate buffer (0.5 mg/ml). Fill a sterile 12-well plate with 1.5 ml/well and keep it at 4 °C. This solution can be used for coating several batches of cover glass.
2. Depending on the manufacturer, cover glasses might need washing with nitric acid, HCl, and 70 % ethanol [61].
3. Place one clean cover glass in each PLL well and let them sit for ≥12 h to allow coating. Cover glasses can be stored in the PLL solution at 4 °C until use.
4. Before seeding cells, transfer the cover glasses to a new 12-well plate and wash three times with distilled water (add 1 ml, then aspirate). Soluble excess PLL can have deleterious effects on cell health.
5. Completely remove water and let the cover glasses air dry for 5 min before proceeding with Subheading 3.3, **step 11**.

3.3 Splitting and Seeding HEK Cells

1. For basic cell culture techniques refer to specialized literature [62, 63].
2. Check the quality of the HEK cell culture. Cells should be adherent, not confluent (≤85 % density), have healthy morphology and be free of contaminations. The phenol red indicator should indicate pH 7.2–7.4.
3. Warm DPBS (Ca^{2+}/Mg^{2+}-free), trypsin solution, and DMEM (5 % FBS) to 37 °C in water bath.
4. Gently aspirate the old medium from the cell culture flask.
5. To wash cells, add 8 ml DPBS (per 25 cm^2 flask), let stand for 20 s, and aspirate.
6. Add 3 ml trypsin solution and incubate for 3 min at 37 °C.
7. Cells should detach from the flask, which can be facilitated by tapping. Transfer the cell suspension into a conical 50 ml tube.
8. Centrifuge at 500 × *g* for 3 min. A white cell pellet should be visible.
9. Aspirate the supernatant, add 5 ml DMEM and resuspend the cells by gently pipetting up and down.
10. Count the cell density of the cell suspension.
11. To maintain the HEK cell culture, fill a new 25 cm^2 flask with 7 ml DMEM and add cell suspension (500 µl for splitting the culture 1:10; 1 ml for splitting 1:5).
12. To seed cells, add 1 ml DMEM to the air-dried cover glasses (*see* Subheading 3.2, **step 5**).
13. Add ~40,000 cells (typically 20–80 µl) per cover glass. Distribute the cell suspension by tilting the well plate.
14. Incubate for 12–28 h before proceeding with the transfection.

3.4 HEK Cell Transfection

1. This procedure describes transfection with Lipofectamine 2000 (Invitrogen). See your supplier information for further details.
2. Check cell health before transfection. Cells should be adherent, have healthy morphology and relatively low density (*see* **Note 18**).
3. In case antibiotics or additional serum were added, the medium has to be replaced with DMEM (5 % FBS) (*see* **Note 7**).
4. For each 18 mm cover glass to be transfected, add 2 µl Lipofectamine to 50 µl OPTI-MEM, mix gently, and let stand for 5–10 min.
5. Dilute DNAs into another 50 µl OPTI-MEM for each 18 mm cover glass to be transfected. Typically we use 0.2–0.6 µg of LiGluR vector, and 0.03 µg DNA of the GFP transfection marker per cover glass (*see* **Note 19**).
6. Combine the Lipofectamine and DNA solutions to obtain the transfection mix (i.e., 100 µl/well), mix gently.
7. Let stand for 15–30 min (*see* **Note 19**).
8. Add 100 µl transfection mix to each well and distribute carefully.
9. Place cells in the 37 °C incubator.
10. Replace medium after 6–8 h to remove Lipofectamine, which has cytotoxic effects.
11. Monitor cell health and expression levels for 18–48 h (*see* **Note 18**).

3.5 Setting Up Photoswitch Illumination

1. Establish a fluorescence imaging light path to identify GFP-transfected, fluorescent cells.
2. Establish a photoswitching light path and choose filter or monochromator settings for *on* light, *off* light, and dark conditions (*see* Subheading 3.10, **step 2**). Changes should be triggered electronically and not cause vibration of the patch setup.
3. Check the light intensity (irradiance: power/area) for both the *on*- and *off*-wavelengths using a power meter (*see* **Notes 12** and **13**). Set the power meter to the appropriate wavelength and place the sensor in the light beam exiting the objective. To measure all exiting light, the illuminated area has to be kept smaller than the sensor field.
4. To calculate the irradiance under experimental conditions, e.g., in mW/mm^2, it is further necessary to determine the size of the spot in the focal plane. In case a proper epi-illumination has been established, the illuminated area can be calculated with the spot diameter d given by the objective's field number, FN, and magnification, M: $d = FN/M$. Photographic paper can be used to verify this estimate (*see* **Note 15**).

3.6 Preparing a MAG Stock Solution

1. Dissolve MAG powder aliquot in anhydrous DMSO (*see* **Notes 4** and **5**): let the chemical warm to room temperature, add DMSO (~15 µl per mg) and close the vial to avoid water uptake. The compound readily dissolves into a dark orange solution. If necessary, vortexing, ultrasound, or additional DMSO can be used to facilitate solubilization but not heating.
2. Use a small aliquot to determine the concentration: a 1:2,000 dilution into extracellular solution should allow to determine the stock concentration with a spectrophotometer, i.e., give an absorption in the linear measurement range of $A_{360} = 0.1–1.0$ (1 cm path length). We work with an extinction coefficient of $\varepsilon_{360} = 0.024\ \mu M^{-1}\ cm^{-1}$ to keep the concentration constant across different stock solutions and synthesis batches.
3. Prepare aliquots for use: pipette the volume that is sufficient for one labeling reaction into 1.5 ml vials, e.g., ~0.3 µl of 50 mM stock solution for 300 µl of 50 µM labeling solution. Less concentrated stock solutions can be handled with higher accuracy, the final DMSO concentration in the labeling solution, however, should be kept ≤0.5 % (*see* Subheading 3.7, **step 5**). Store at −20 or −80 °C in the dark, preferably over desiccant. The number of freeze thaw cycles should be kept to a minimum (2–4 cycles) to avoid water uptake.

3.7 Labeling Cells with the MAG Photoswitch

1. Use a 6-well plate for washing and labeling of cover glasses. Label one cover glass at a time.
2. Check health and density of cells.
3. Wash step: transfer the cover glass with cells into a well filled with extracellular solution.
4. Con A treatment: transfer the cover glass into a well filled with Con A in extracellular solution. Incubate for 3 min.
5. In the meantime dilute a MAG aliquot with extracellular solution to yield a concentration of ~50 µM (*see* **Note 5**). For a 18 mm cover glass ≤300 µl solution will be sufficient.
6. Place the cover glass in an empty well and overlay it with the labeling solution.
7. Incubate for 20–40 min in the dark, at room temperature or 37 °C (*see* **Note 20**).
8. Wash thoroughly by transferring the cover glass into a well with 1.5 ml extracellular solution and incubate for 2 min (*see* **Note 21**). Repeat twice.
9. Mount the cover glass in the perfusion chamber and add some extracellular solution.

3.8 Preparation for Patch-Clamp Recordings

1. Pull patch pipettes [64]. For whole-cell HEK recordings the resistance should be 3–6 MΩ when filled with intracellular solution. A medium or short taper is preferable.

2. Set up a pressure line to the electrode holder, with either a mouthpiece or a syringe connected to a stopcock.
3. Place recording chamber with cover glass in the setup. Place the salt bridge between the reservoir and a Petri dish that holds the reference electrode in extracellular solution.
4. Establish a steady perfusion with extracellular solution (~3 ml/min).
5. Fill another perfusion reservoir with 5 mM glutamate in extracellular solution.
6. Neither the sample nor the pipette tip should show any vibration or drift in position.

3.9 Patch-Clamp Recordings

We describe the basic procedure for voltage-clamping HEK cells in the whole-cell configuration [64–66]:

1. Select a single transfected cell using the appropriate fluorescence filter set (e.g., GFP). The cell should have healthy morphology and not start to detach from the cover glass by rounding up (*see* **Notes 19** and **22**) [58].
2. Fill the patch pipette with intracellular solution from the back, while avoiding the formation of air bubbles. Any bubbles should be removed by flicking against the pipette. Dust particles will prevent seal formation.
3. Place the pipette in the electrode holder so that the AgCl wire is in good contact with the solution. The pipette should not be filled to the very top, since solution in the electrode holder can cause electrical noise.
4. Apply positive pressure (~1 psi) to the pipette.
5. Insert the pipette in the bath. The pipette should have a resistance between 3 and 6 MΩ.
6. Using the micromanipulator, place the pipette tip directly above the cell, slightly off center.
7. Adjust the pipette offset while voltage-clamping to 0 mV. Use a test pulse to monitor the resistance and capacitance. The pipette capacitance should be compensated.
8. Change to the filter cube designated for photoswitching, since cell-attached and whole-cell configurations will be particularly sensitive to vibrations.
9. Slowly lower the pipette using the fine coarse setting of the manipulator until the resistance starts to increase sharply, typically after an initial increase of ~0.2 MΩ. Release the pressure and expect seal formation, which can be facilitated by gentle long suction pulses (negative pressure applications). Usually, a seal in the 1–6 GΩ range should form within seconds. Negative holding potentials of −10 to −30 mV can help seal formation.

10. Apply brief suction pulses of increasing strength to break into the cell, i.e., to make the transition from the cell-attached to whole-cell configuration. The break in is accompanied by a sudden decrease of resistance and an increase in capacitance, visible in the test pulse. The leak current should be modest, i.e., the seal ≥100 MΩ. If the seal is lost, repeat the procedure with a new pipette on a new cell.
11. Note the resting potential. Set the voltage-clamp to –75 mV and compensate the series resistance.
12. Turn on the bath perfusion and wait ~2 min to equilibrate the cell interior with the pipette solution.

3.10 Basic Experiments for Photoswitch Validation

1. Photoswitching: run a protocol switching between green light and UV light. This should result in a fully reversible inward current, which turns *on* upon UV illumination and *off* with green light (Fig. 2a). Note the amount of current and timescale of switching. Typically several hundred pA are observed, depending on the expression and labeling efficiency (*see* **Notes 19**, **22**, and **23**).
2. Illumination time: add dark periods to the protocol, i.e., toggle between green-dark-UV-dark-green periods (Fig. 2b). If the illumination periods are sufficiently long, full activation and deactivation should be seen as above. Shorter UV illumination periods will result in partial activation (less photocurrent), shorter green light periods in partial deactivation.
3. Bistability: Regular MAG photoswitches are bistable, as demonstrated by the same protocol. Once the light is turned off, no further activation or deactivation should be seen in the dark (Fig. 2b). If this is not the case, light might be leaking through the illumination system or room light is interfering. Thermal *cis*-to-*trans* relaxation is not visible on the timescale of minutes [37].
4. Wavelength: if the light source allows changing wavelengths, an action spectrum can be reconstructed, reflecting the wavelength dependence of the MAG photostationary state (Fig. 2c, d). The photostationary state will also determine the maximum switching efficacy obtained with different laser lines (*see* **Note 11**).
5. Light intensity: neutral density filters can be used to decrease the light intensity, which will decrease the switching speed. Optimizing the light path, using less narrow band-pass filters or using a higher magnification objective might increase the irradiance (power/area) and will allow to complete switching in less time (*see* **Notes 12** and **13**).
6. Expression and labeling efficiency: perfuse cells with glutamate (Fig. 2a). If GluK2 is present, and the cells were treated with Con A, this should yield a large inward current that returns to baseline when glutamate is washed out (*see* **Note 19**). Perfusion with glutamate also allows to compare the amount of photoswitching to glutamate induced currents (*see* **Note 23**).

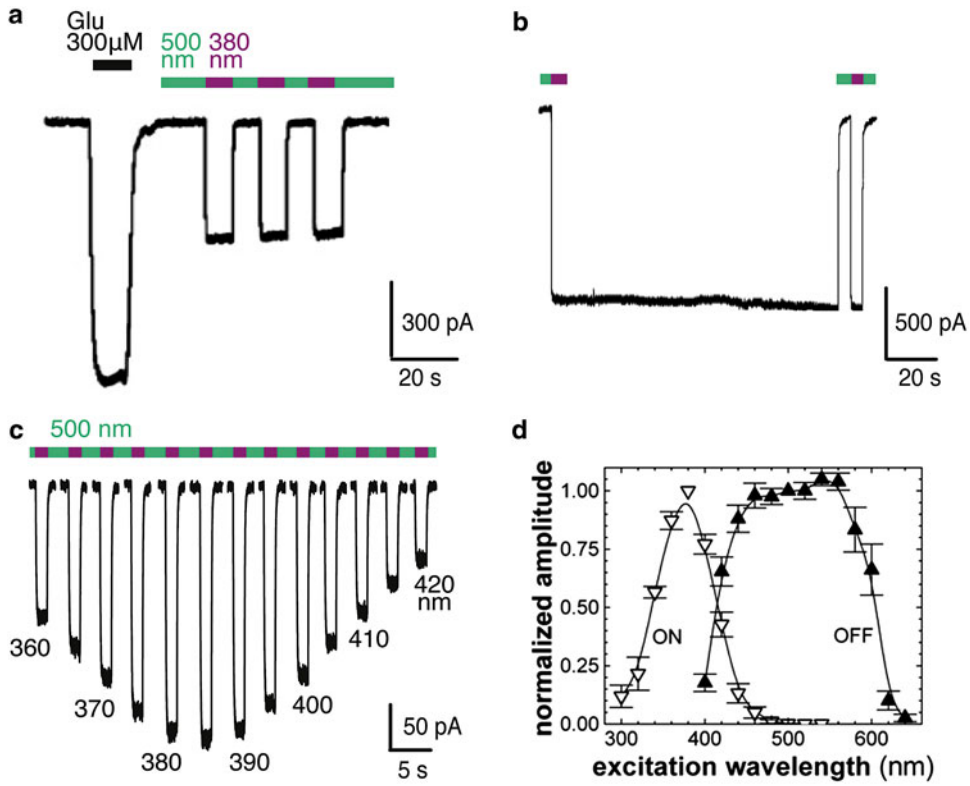

Fig. 2 Photoswitching of LiGluR (GluK2 439C) with L-MAG0. (**a**) Reversible photoswitching and comparison to glutamate-induced currents. (**b**) Bistability of photoswitching as demonstrated by sustained activation in the dark. (**c**, **d**) Wavelength dependence of MAG photoswitching measured with a Polychrome V light source (14 nm bandwidth), *see* [37]. All experiments were performed after incubation in Con A (*see* **Note 10**). Figure 2a reprinted from Volgraf et al. [29]; Fig. 2b, d reprinted from Gorostiza et al. ([37], Copyright (2008) National Academy of Sciences, USA)

7. For controls ensuring that the light induced effects are specific to LiGluR photoswitching *see* **Note 24**. Furthermore, competitive antagonists, such as DNQX (6,7-dinitroquinoxaline-2,3-dione) can be used to suppress LiGluR induced currents, although high concentrations are necessary and may not be able to displace all *cis*-MAG [37]. Light induced artifacts should be easy to identify, since they are likely to correlate with illumination (*see* **Note 25**), whereas MAG photoswitching is bistable (Fig. 2b).
8. Affinity labeling: instead of using rather high ~50 µM MAG concentrations (*see* Subheading 3.6), the high affinity of *cis*-MAG to the ligand binding site can be utilized to increase the effective local concentration for labeling [37]. For this, MAG is pre-irradiated with a handheld 365 nm UV lamp for 3 min directly prior to labeling.

4 Notes

1. The complete coding regions of the constructs should be sequenced on a regular basis. Non-silent point mutations occur frequently and can dramatically affect receptor expression and function.
2. The following control experiments should be considered to ensure that any light-induced effect is due to LiGluR photoswitching: illumination protocols should not induce any currents or signal, (a) in the absence of MAG labeling, (b) in MAG labeled cells that do not express the receptor, and (c) in cells that express a receptor subunit without the cysteine attachment site, i.e., wild type GluK2.
3. For good cell health, the DNA used in transfections should be sterile and free of contaminations, such as endotoxins, RNAses, and EtOH.
4. To avoid water condensation on cold surfaces any vials that were stored at 4 °C or in the freezer should be equilibrated to room temperature before opening.
5. Contamination of MAG powder, DMSO, or stock solutions with even traces of water has to be avoided, as water reacts with the maleimide to products that are no longer cysteine-reactive. Once the MAG stock solution has been diluted in aqueous buffer, it should be immediately used for labeling. Basic pH facilitates the hydrolysis of MAG.
6. Regular HEK 293 cells give ample expression. For even stronger expression, the HEK 293 T cell line, which harbors the SV40 large T-antigen, might be used.
7. Cell cultures can be maintained without antibiotics, if good sterile working practices are used. Many transfection reagents, like Lipofectamine, are not compatible with antibiotics and the continued use of antibiotics facilitates resistant bacterial contaminations. We only use penicillin–streptomycin if necessary.
8. The pH of the extracellular solution is important for cell health and optimal labeling. More basic pH can promote cysteine labeling, but can also increase unspecific labeling of amines [36], as well as hydrolysis (*see* **Note 5**).
9. The osmolarity of the intracellular solution (~290 mOsm) is critical for stable patch-clamp configurations. Observe the cell shape during patching and, if necessary, add some drops of water, 10× intracellular solution, or sucrose. Swelling of cells can indicate high osmolarity, shrinking low osmolarity.
10. Concanavalin A (Con A) is used to suppress ligand-induced desensitization. Con A is a lectin isolated from jack-bean,

Canavalia ensiformis, that binds *N*-glycans present on cell surface proteins and prevents (or reliefs the effects of) desensitization in kainate receptors [67]. A short, minute long incubation period will block desensitization irreversibly, as ConA binds with very high affinity. Photoswitch currents are much larger in the presence of Con A and labeling appears to be more efficient. In the absence of any Con A treatment photoswitching currents will be much smaller, and GluK2 receptors will get fully desensitized, if residual glutamate is present at low concentrations [45].

11. Photoswitching wavelength: to switch as many molecules as possible, wavelengths that populate photostationary states with maximal amounts of the *cis* and *trans* configuration, respectively, should be chosen (*see* Fig. 2c, d) [37]. For regular MAGs, 370–390 nm illumination yields >90 % *cis* configuration. With these wavelengths we did not observe any detrimental effects on cell health. In case of technical limitations, 405 nm light (a popular laser line) can be used, which gives incomplete, but still reasonable activation. To efficiently turn MAG to *trans*, 480–530 nm light can be used (>85 % *trans*). Wavelengths >530 nm favor the *trans* configuration as well, but the absorption of the MAG compounds becomes weak and photoswitching would require more and more light.
12. The light intensity, more precisely the irradiance (power/area, e.g., in mW/mm^2), determines how fast the population of MAG labeled receptors can be isomerized at a given wavelength. The higher the irradiance is, the faster the switching will be (*see* Subheading 3.10, **step 5**). Depending on the wavelength, reasonable fast photoswitching, on the order of $\tau_{switch} > 500$ ms can be achieved with >0.5 mW/mm^2 ($\tau_{switch} \sim 50$ ms with 5 mW/mm^2). High power illumination allows submillisecond photoswitching [45].
13. The irradiance is determined by a number of factors: the power output of the light source, the bandwidth of monochromators or filters, losses in the light path and the size of the illuminated area (in epi-illumination determined by the objective). Decreasing the spot diameter by a factor of 2 can increase the irradiance by a factor of 4.
14. The illumination system should allow to turn off the light within the illumination protocols (dark periods). If necessary, an electromechanical shutter can be installed. Alternatively, "soft shuttering" can be considered, e.g., using the filter changer or monochromator to step to a wavelength region that is either absorbed by a filter or optical components, or that is not absorbed by the MAG photoswitch (red/infrared light). The success of this approach can be tested as described in

Subheading 3.10, **step 3**. Diode lasers can often be turned off electronically.

15. Next to whole-field epi-illumination other options for light delivery exist. Light, e.g., from a diode or light guide, can be directly aimed at the sample, but in most cases the irradiance will be low (large illumination area). TIR (total internal reflection) illumination allows efficient activation [53], as well as patterned illumination with mirror devices [4] or holographic methods [34], as long as the transmittance for the near-UV wavelengths is sufficient. Confocal and point scanning approaches can give very high intensities, but one has to consider that larger areas have to be scanned. Special care has to be taken that the region scanned with the *off* wavelength fully captures the region scanned with the *on* wavelength, and that the intensity per area and time is sufficient. The irradiance is often not as easy to estimate.
16. High light intensities can cause eye damage. Light <430 nm is not well visible, but can nevertheless damage the retina or eye lens. The excitation light should never be directed to the eyepiece, looking into the beam must be avoided and protective eyewear should be used, if necessary.
17. The actual timing and duration of short light pulses (<50 ms) is often determined by the hardware, for instance by delays of signals, light source switching, or shutters. A sufficiently fast, amplified photodiode or a used photomultiplier tube can be used to record the light output directly. It can be installed at any place in the setup where it can capture some stray light.
18. HEK cells are more healthy and easier to transfect at medium cell densities. However, whole-cell recordings should be performed on single cells. Cell density and expression time might therefore require optimization. If necessary, cells can be reseeded onto new cover glasses after transfection, following Subheading 3.3. Instead of trypsin solution, enzyme-free cell dissociation solution (e.g., Sigma C5914) should be used to avoid proteolysis of cell surface receptors.
19. The transfection efficiency can be assessed by the number of fluorescent cells, the amount of fluorescence or the size of glutamate-induced currents. For optimization, the cell density (*see* **Note 18**) or DNA concentration might be increased (*see* **Note 3**), or the incubation period adapted (Subheading 3.4, **step 7**). Antibiotics and serum concentrations >5 % are not compatible with Lipofectamine. If massive cell death occurs after transfection, the amount of Lipofectamine might have to be reduced. High iGluR expression levels can have detrimental effects, as well. In this case, the expression levels and expression time should be reduced, or inhibitors such as DNQX might be added.

20. If labeling affects cell health one should consider using less MAG and/or DMSO. The cells should be moved gently between different solutions to avoid shear forces. If activation through soluble MAG appears to be a problem, labeling can be performed with a solution mainly having a non-permeant cation such as NMDG (*N*-methyl-D-glucamine) and low calcium ion concentration (145 mM NMDG-HCl, 3 mM KCl, 0.5 mM $CaCl_2$, 5 mM $MgCl_2$, 10 mM HEPES, 10 mM glucose (pH 7.3)), instead of extracellular solution.
21. After labeling the cells should be washed thoroughly to remove any unreacted MAG photoswitch, as it might exert unspecific or secondary effects.
22. Weakly fluorescent cells can give large glutamate-induced currents. Strongly fluorescent cells will often have less glutamate receptor expression.
23. If the labeling efficiency is low, more or fresh MAG should be used. The pH of the labeling solution should be controlled and cell health should be monitored (*see* **Note 20**). You might also consider affinity labeling (*see* Subheading 3.10, **step 8**). Cysteines can be oxidized and engage in disulfide bridges. In this case a reduction step can be performed before labeling (after Subheading 3.7, **step 3**): place the cover glass for 2 min in 1 mM DTT (or 100 μM TCEP) in extracellular solution. Wash extensively, at least three times with extracellular solution (after DTT at least five times), before you proceed with labeling. All DTT has to be removed since it reacts with the MAG maleimide group.
24. MAG photoswitches potentially label many cysteines on cell surface proteins, including expressed glutamate receptors. However, photoswitching is specific to labeling of LiGluR at the designated site, as can be demonstrated by proper control experiments (*see* **Note 2**).
25. It should be kept in mind that the amplifier headstage itself might be light sensitive, as noted by the manufacturer of the Axopatch 200B, although we never observed this artifact.

Acknowledgments

We thank all previous and current lab members for their contributions in developing and refining the described photoswitch technologies. Moreover, we thank Richard Kramer and his lab for discussion, and Dirk Trauner and his lab for developing and providing MAG compounds. This work was supported by the National Institutes of Health Nanomedicine Development Center for the Optical Control of Biological Function (2PN2EY018241).

References

1. Miesenböck G (2011) Optogenetic control of cells and circuits. Ann Rev Cell Dev Biol 27:731–758
2. Fenno L, Yizhar O, Deisseroth K (2011) The development and application of optogenetics. Ann Rev Neurosci 34:389–412
3. Szobota S, Isacoff EY (2010) Optical control of neuronal activity. Annu Rev Biophys 39:329–348
4. Wyart C, Del Bene F, Warp E, Scott EK, Trauner D, Baier H, Isacoff EY (2009) Optogenetic dissection of a behavioural module in the vertebrate spinal cord. Nature 461(7262):407–410
5. Tye KM, Deisseroth K (2012) Optogenetic investigation of neural circuits underlying brain disease in animal models. Nat Rev Neurosci 13(4):251–266
6. Zhang F, Vierock J, Yizhar O, Fenno LE, Tsunoda S, Kianianmomeni A, Prigge M, Berndt A, Cushman J, Polle J, Magnuson J, Hegemann P, Deisseroth K (2011) The microbial opsin family of optogenetic tools. Cell 147(7):1446–1457
7. Reiner A, Isacoff EY (2013) The Brain Prize 2013: the optogenetics revolution. Trends Neurosci 36(10):557–560
8. Schröder-Lang S, Schwärzel M, Seifert R, Strünker T, Kateriya S, Looser J, Watanabe M, Kaupp UB, Hegemann P, Nagel G (2007) Fast manipulation of cellular cAMP level by light in vivo. Nat Methods 4(1):39–42
9. Möglich A, Moffat K (2010) Engineered photoreceptors as novel optogenetic tools. Photochem Photobiol Sci 9(10):1286–1300
10. Levskaya A, Weiner OD, Lim WA, Voigt CA (2009) Spatiotemporal control of cell signalling using a light-switchable protein interaction. Nature 461(7266):997–1001
11. Szymański W, Beierle JM, Kistemaker HA, Velema WA, Feringa BL (2013) Reversible photocontrol of biological systems by the incorporation of molecular photoswitches. Chem Rev 113(8):6114–6178
12. Sakata T, Yan Y, Marriott G (2005) Optical switching of dipolar interactions on proteins. Proc Natl Acad Sci U S A 102(13): 4759–4764
13. Kocer A, Walko M, Meijberg W, Feringa BL (2005) A light-actuated nanovalve derived from a channel protein. Science 309(5735): 755–758
14. Lougheed T, Borisenko V, Hennig T, Rück-Braun K, Woolley GA (2004) Photomodulation of ionic current through hemithioindigo-modified gramicidin channels. Org Biomol Chem 2(19):2798–2801
15. Wildemann D, Schiene-Fischer C, Aumüller T, Bachmann A, Kiefhaber T, Lücke C, Fischer G (2007) A nearly isosteric photosensitive amide-backbone substitution allows enzyme activity switching in ribonuclease S. J Am Chem Soc 129(16):4910–4918
16. Kaufman H, Vratsanos SM, Erlanger BF (1968) Photoregulation of an enzymic process by means of a light-sensitive ligand. Science 162(3861):1487–1489
17. Lester HA, Krouse ME, Nass MM, Wassermann NH, Erlanger BF (1980) A covalently bound photoisomerizable agonist: comparison with reversibly bound agonists at electrophorus electroplaques. J Gen Physiol 75(2):207–232
18. Loudwig S, Bayley H (2006) Photoisomerization of an individual azobenzene molecule in water: an on–off switch triggered by light at a fixed wavelength. J Am Chem Soc 128(38): 12404–12405
19. Zhang Y, Erdmann F, Fischer G (2009) Augmented photoswitching modulates immune signaling. Nat Chem Bio 5(10):724–726
20. Schrader TE, Cordes T, Schreier WJ, Koller FO, Dong SL, Moroder L, Zinth W (2011) Folding and unfolding of light-triggered beta-hairpin model peptides. J Phys Chem B 115(18):5219–5226
21. Beharry AA, Woolley GA (2011) Azobenzene photoswitches for biomolecules. Chem Soc Rev 40(8):4422–4437
22. Woolley GA (2005) Photocontrolling peptide alpha helices. Acc Chem Res 38(6):486–493
23. Renner C, Moroder L (2006) Azobenzene as conformational switch in model peptides. ChemBioChem 7(6):868–878
24. Fehrentz T, Schönberger M, Trauner D (2011) Optochemical genetics. Angew Chem Int Ed Engl 50(50):12156–12182
25. Banghart M, Borges K, Isacoff E, Trauner D, Kramer RH (2004) Light-activated ion channels for remote control of neuronal firing. Nat Neurosci 7(12):1381–1386
26. Fortin DL, Dunn TW, Fedorchak A, Allen D, Montpetit R, Banghart MR, Trauner D, Adelman JP, Kramer RH (2011) Optogenetic photochemical control of designer K^+ channels in mammalian neurons. J Neurophysiol 106(1):488–496
27. Sandoz G, Levitz J, Kramer RH, Isacoff EY (2012) Optical control of endogenous proteins with a photoswitchable conditional subunit

reveals a role for TREK1 in GABA(B) signaling. Neuron 74(6):1005–1014

28. Sandoz G, Levitz J (2013) Optogenetic techniques for the study of native potassium channels. Front Mol Neurosci 6:6
29. Volgraf M, Gorostiza P, Numano R, Kramer RH, Isacoff EY, Trauner D (2006) Allosteric control of an ionotropic glutamate receptor with an optical switch. Nat Chem Biol 2(1):47–52
30. Szobota S, Gorostiza P, Del Bene F, Wyart C, Fortin DL, Kolstad KD, Tulyathan O, Volgraf M, Numano R, Aaron HL, Scott EK, Kramer RH, Flannery J, Baier H, Trauner D, Isacoff EY (2007) Remote control of neuronal activity with a light-gated glutamate receptor. Neuron 54(4):535–545
31. Janovjak H, Szobota S, Wyart C, Trauner D, Isacoff EY (2010) A light-gated, potassium-selective glutamate receptor for the optical inhibition of neuronal firing. Nat Neurosci 13(8):1027–1032
32. Levitz J, Pantoja C, Gaub B, Janovjak H, Reiner A, Hoagland A, Schoppik D, Kane B, Stawski P, Schier AF, Trauner D, Isacoff EY (2013) Optical control of metabotropic glutamate receptors. Nat Neurosci 16(4):507–516
33. Perea G, Navarrete M, Araque A (2009) Tripartite synapses: astrocytes process and control synaptic information. Trends Neurosci 32(8):421–431
34. Papagiakoumou E, Anselmi F, Bègue A, de Sars V, Glückstad J, Isacoff EY, Emiliani V (2010) Scanless two-photon excitation of channelrhodopsin-2. Nat Methods 7(10):848–854
35. Tochitsky I, Banghart MR, Mourot A, Yao JZ, Gaub B, Kramer RH, Trauner D (2012) Optochemical control of genetically engineered neuronal nicotinic acetylcholine receptors. Nat Chem 4(2):105–111
36. Hermanson G (2008) Bioconjugate techniques, 2nd edn. Academic Press, San Diego, CA
37. Gorostiza P, Volgraf M, Numano R, Szobota S, Trauner D, Isacoff EY (2007) Mechanisms of photoswitch conjugation and light activation of an ionotropic glutamate receptor. Proc Natl Acad Sci U S A 104(26):10865–10870
38. Mourot A, Kienzler MA, Banghart MR, Fehrentz T, Huber FM, Stein M, Kramer RH, Trauner D (2011) Tuning photochromic ion channel blockers. ACS Chem Neurosci 2(9):536–543
39. Kienzler MA, Reiner A, Trautman E, Yoo S, Trauner D, Isacoff EY (2013) A red-shifted, fast-relaxing azobenzene photoswitch for visible light control of an ionotropic glutamate receptor. J Am Chem Soc 135(47): 17683–17686
40. Zhou LM, Gu ZQ, Costa AM, Yamada KA, Mansson PE, Giordano T, Skolnick P, Jones KA (1997) (2*S*,4*R*)-4-methylglutamic acid (SYM 2081): a selective, high-affinity ligand for kainate receptors. J Pharm Exp Ther 280(1):422–427
41. Numano R, Szobota S, Lau AY, Gorostiza P, Volgraf M, Roux B, Trauner D, Isacoff EY (2009) Nanosculpting reversed wavelength sensitivity into a photoswitchable iGluR. Proc Natl Acad Sci U S A 106(16):6814–6819
42. Armstrong N, Gouaux E (2000) Mechanisms for activation and antagonism of an AMPA-sensitive glutamate receptor: crystal structures of the GluR2 ligand binding core. Neuron 28(1):165–181
43. Mayer ML (2005) Crystal structures of the GluR5 and GluR6 ligand binding cores: molecular mechanisms underlying kainate receptor selectivity. Neuron 45(4):539–552
44. Volgraf M, Gorostiza P, Szobota S, Helix MR, Isacoff EY, Trauner D (2007) Reversibly caged glutamate: a photochromic agonist of ionotropic glutamate receptors. J Am Chem Soc 129(2):260–261
45. Reiner A, Isacoff EY (2014) Tethered ligands reveal glutamate receptor desensitization depends on subunit occupancy. Nat Chem Biol
46. Dingledine R, Borges K, Bowie D, Traynelis SF (1999) The glutamate receptor ion channels. Pharmacol Rev 51(1):7–61
47. Traynelis SF, Wollmuth LP, McBain CJ, Menniti FS, Vance KM, Ogden KK, Hansen KB, Yuan H, Myers SJ, Dingledine R (2010) Glutamate receptor ion channels: structure, regulation, and function. Pharmacol Rev 62(3):405–496
48. Egebjerg J, Bettler B, Hermans-Borgmeyer I, Heinemann S (1991) Cloning of a cDNA for a glutamate receptor subunit activated by kainate but not AMPA. Nature 351(6329):745–748
49. Hille B (2001) Ion channels of excitable membranes, 3rd edn. Sinauer Assoc, Sunderland, USA
50. Egebjerg J, Heinemann SF (1993) Ca^{2+} permeability of unedited and edited versions of the kainate selective glutamate receptor GluR6. Proc Natl Acad Sci U S A 90(2):755–759
51. Burnashev N, Villarroel A, Sakmann B (1996) Dimensions and ion selectivity of recombinant AMPA and kainate receptor channels and their dependence on Q/R site residues. J Physiol 496:165–173
52. Izquierdo-Serra M, Trauner D, Llobet A, Gorostiza P (2013) Optical modulation of neurotransmission using calcium photocurrents through the ion channel LiGluR. Front Mol Neurosci 6:3
53. Li D, Herault K, Isacoff EY, Oheim M, Ropert N (2012) Optogenetic activation of LiGluR-

expressing astrocytes evokes anion channel-mediated glutamate release. J Physiol 590(Pt 4): 855–873

54. Izquierdo-Serra M, Trauner D, Llobet A, Gorostiza P (2013) Optical control of calcium-regulated exocytosis. Biochim Biophys Acta 1830(3):2853–2860
55. Caporale N, Kolstad KD, Lee T, Tochitsky I, Dalkara D, Trauner D, Kramer R, Dan Y, Isacoff EY, Flannery JG (2011) LiGluR restores visual responses in rodent models of inherited blindness. Mol Ther 19(7):1212–1219
56. Kauwe G, Isacoff EY (2013) Rapid feedback regulation of synaptic efficacy during high-frequency activity at the Drosophila larval neuromuscular junction. Proc Natl Acad Sci U S A 110:9142–9147
57. Sambrook J, Russell D (2001) Molecular cloning: a laboratory manual, 3rd edn. CSHL Press, Cold Spring Harbor, USA
58. Thomas P, Smart TG (2005) HEK293 cell line: a vehicle for the expression of recombinant proteins. J Pharmacol Toxicol Methods 51(3):187–200
59. Getz EB, Xiao M, Chakrabarty T, Cooke R, Selvin PR (1999) A comparison between the sulfhydryl reductants tris(2-carboxyethyl)phosphine and dithiothreitol for use in protein biochemistry. Anal Biochem 273(1):73–80
60. Salmon ED, Canman JC (2003) Proper alignment and adjustment of the light microscope. Curr Proto Hum Genet Appendix 3:Appendix 3N
61. Fischer AH, Jacobson KA, Rose J, Zeller R (2008) Preparation of slides and coverslips for microscopy. CSH Protoc 2008:pdb.prot4988
62. ATTC Animal Cell Culture Guide (2012) Tips and techniques for continuous cell lines. American type culture collection, Manassas, VA
63. Freshney R (2010) Culture of animal cells: a manual of basic technique and specialized applications, 6th edn. Wiley-Blackwell, Hoboken, NJ
64. Sakmann B, Neher E (eds) (1995) Single-channel recording, 2nd edn. Plenum Press, New York, USA
65. Sherman-Gold R (ed) (2008) The axon guide: a guide to electrophysiology & biophysics laboratory techniques, 3rd edn. Molecular Devices, Sunnyvale, USA
66. Molleman A (2003) Patch clamping: an introductory guide to patch clamp electrophysiology, 1st edn. Wiley, Chichester, UK
67. Everts I, Villmann C, Hollmann M (1997) *N*-Glycosylation is not a prerequisite for glutamate receptor function but is essential for lectin modulation. Mol Pharmacol 52(5):861–873

Chapter 5

Photocontrol of AMPA Receptors with a Photochromic Ligand

Martin Sumser and Philipp Stawski

Abstract

Photochromic ligands (PCLs), recently introduced by our group as a tool for researchers in neuroscience, offer the ability to control native receptors with light in a reversible fashion without the need for any genetic manipulation. Here we describe the application of the PCL Azo-Tetrazole-AMPA-3 (ATA-3) to reversibly gate native AMPA-receptors with blue light and thereby control the activity of cortical neurons in brain slices.

Key words Photochromic ligand (PCL), Photocontrol, AMPA receptor, ATA-3, Azobenzene

1 Introduction

The light-dependent control of cellular functions has become one of the most valuable tools for neurobiological research. In general, three categories for the optical control of neuronal activity can be defined: (1) caged neurotransmitters, (2) photosensitive proteins, and (3) small molecule photoswitches. While caged compounds are an established method in neuroscientific research, the other tools just emerged during the last decade. Here we focus on photochromic ligands (PCLs), which represent soluble photoswitches, while another chapter (Reiner and Isacoff; this volume) will cover a closely related approach of photosensitizing modified receptors using photoswitchable tethered ligands (PTLs). PCLs represent a photopharmacological method and, as such, do not require any genetic manipulation. In general, these molecules are comprised of three parts: a pharmacophore, a linker, and the photoisomerizable switch which is usually an azobenzene (Fig. 1). While the pharmacophore is designed for the effective interaction with the target receptor, it is the photoisomerizable switch, which changes its configuration upon illumination. This *trans* to *cis* conversion results in an increase/decrease of the affinity of the PCL to its target receptor. For caged compounds the photolabile protecting

Sidney Cambridge (ed.), *Photoswitching Proteins: Methods and Protocols*, Methods in Molecular Biology, vol. 1148,
DOI 10.1007/978-1-4939-0470-9_5,

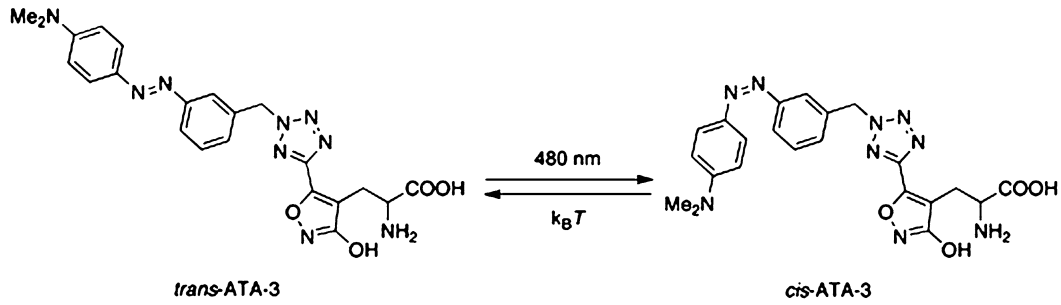

Fig. 1 Structure and photoswitching of ATA-3. Switching of ATA-3 from *trans* (active) to *cis* (inactive) requires light at 480 nm. *cis*-ATA-3 thermally relaxes back to the *trans* configuration without the application of light (k_bT, thermal energy). (Reproduced with permission from Wiley VCH, ref. [1])

group is cleaved to release the pharmacologically active agent. The signaling provided by the photoactivated compound is eventually turned off by the diffusion or active transport away from the irradiated region. In contrast, PCLs are actively turned on and off by irradiation with light of different wavelengths in a reversible fashion. Here we describe the application of ATA-3, an AMPA-specific PCL [1], which is active in the dark (*trans* configuration) and can be turned off by blue light of 480 nm (*cis* configuration). Recently, we introduced several PCLs targeting other glutamate receptors [2], GABA receptors [3], potassium channels [4], and sodium channels [5]. Each PCL exhibits a characteristic action spectrum (spectrum of biological activity) when switching from *trans* to *cis* and vice versa. Importantly, they can be active or inactive in their dark-adapted state (usually the *trans* configuration). By minimal chemical modification, PCLs can be tuned to cover most of the visible range [6]. In general, such red-shifted switches show an enhanced thermal relaxation (i.e., *cis* to *trans*), meaning that they quickly revert to their dark-adapted state after the light has been turned off. This facilitates the experimental setup, so that a single wavelength is sufficient to switch the PCL. The irradiation intensities required to control PCLs are comparable or even less than the ones used to activate channelrhodopsin [7]. Together with the absence of any genetic manipulation this suggests PCLs as excellent candidates for pharmacological restoration of vision [7]. Here however, we focus on the application of ATA-3 in HEK293T cells and brain slices to regulate AMPA receptor activity in vitro with light.

2 Materials

2.1 Cell Culture

1. Dulbecco's phosphate-buffered saline w/o Ca^{2+} and w/o Mg^{2+}.
2. 1× Trypsin–EDTA.
3. DMEM substituted with 10 % of fetal bovine serum (FBS).
4. OptiMEM (Life Technologies).

5. Optifect™ reagent (Life Technologies).
6. Coverslips (VWR, 12 mm, No. 1).
7. Poly-L-Lysine solution (0.1 mg/ml)
8. Expression plasmids coding for GluA2 (L504Y, non-desensitizing mutation) and YFP.
9. External buffer for electrophysiological recordings in HEK293T cells containing: 138 mM NaCl, 1.5 mM KCl, 1.2 mM $MgCl_2$, 2.5 mM $CaCl_2$, 5 mM HEPES, and 10 mM D-glucose, pH 7.4.
10. ATA-3 stock solution: ATA-3 is not commercially available but can be obtained from our lab as part of a cooperation. For the synthesis please refer to [1]. The ATA-3 stock solution contained 200 mM ATA-3 in DMSO.
11. ATA buffer: ATA-3 stock solution diluted in external buffer for electrophysiological recordings to a concentration of 100 μM (*see* **Notes 1–3**).
12. HEK293T cells were obtained from the DSMZ cell collection (www.dsmz.de, ACC-635).
13. 37 % HCl.
14. 65 % HNO_3.
15. 80 % Ethanol.

2.2 Buffers and Reagents for Brain Slices

1. Sucrose buffer (brain slice cutting solution) containing: 87 mM NaCl, 75 mM Sucrose, 25 mM $NaHCO_3$, 2.5 mM KCl, 1.25 mM NaH_2PO_2, 0.5 mM $CaCl_2$, 7 mM $MgCl_2$, 25 mM Glucose, bubbled with 95 % O_2 and 5 % CO_2 (Carbogen, *see* **Note 4**).
2. Artificial cerebrospinal fluid (ACSF) containing: 125 mM NaCl, 26 mM $NaHCO_3$, 2.5 mM KCl, 2 mM $CaCl_2$, 1.25 mM NaH_2PO_4, 1 mM $MgCl_2$, 25 mM D-Glucose, bubbled with 95 % O_2 and 5 % CO_2 (*see* **Note 6**).
3. Intracellular pipette solution containing: 175 mM K-Gluconate, 15 mM KCl, 12.5 mM HEPES, 5 mM NaCl, 5 mM Mg-ATP, 0.5 mM Na_2GTP, pH 7.3 (*see* **Note 5**).
4. ATA buffer: ATA-3 stock solution diluted in ACSF to a concentration of 100 μM (*see* **Notes 1–3**).

2.3 Instrumentation and Equipment

1. Vibratome (e.g., Leica VT1200S or Microm HM-650 V) for preparation of brain slices.
2. Electrophysiology rig (brain slices): Amplifier (HEKA, EPC10 USB) controlled by patchmaster software (HEKA), upright microscope (Nikon, FN-1), perfusion pump (Ismatec), perfusion chamber for slice recordings (Warner Instruments), vibration-isolated table (TMC), CCD-camera (QImaging), micromanipulator (Scientifica), glass capillary puller (Narishige), glass capillaries (Science Products).

3. Electrophysiology rig (HEK293T cells): Differs from the brain slice rig in following positions: Inverted microscope (Leica, DMIL), multi-channel perfusion system (Nanion), perfusion chamber for cover slips (Warner Instruments).
4. Light stimulation (*see* **Note 6**): A monochromator (Till photonics, Polychrome V), equipped with a 150 W xenon arc lamp (Ushio), was coupled to the microscope via a glass fiber (FiberTech, Leoni Fiber Optics). The light was applied through the objective of the microscope onto the cells (*see* **Note 7**). The light power measured as it exits the objective was between 9 and 20 mW/mm^2 depending on the wavelength applied. We used field-of-view illumination to switch the PCL.

3 Methods

All experiments were carried out at room temperature.

3.1 Preparation of GluA2 Expressing HEK293T Cells

1. HEK293T cells are grown in DMEM containing 10 % FBS (at 37 °C and 10 % CO_2, *see* **Notes 8** and **9**).
2. For passaging, wash the cells with DPBS and treat them with trypsin–EDTA for 1 min at 37 °C. After addition of culturing media, dissociate the cells by mechanical shearing using a 10 ml serological pipette. Do not use cells beyond passage number 20.
3. Wash coverslips with acid (12 h conc. HCl, rinse with water, 12 h conc. HNO_3), then rinse with water until the pH is neutral and store in 80 % EtOH. Before use, quickly flame the coverslips with a Bunsen burner to evaporate the ethanol and for sterilization, then place them into a 24-well plate. Coat the coverslips with 50 µl Poly-L-Lysine for 20 min and rinse with sterile DPBS (three times).
4. Dissociate HEK293T cells at 70–80 % confluency and seed them to a total number of 20,000–25,000/coverslip.
5. Transfect adherent cells (typically 9 h after seeding) following the Optifect™ protocol with plasmids coding for GluA2 (L504Y) and YFP as a transfection marker in a 20:1 ratio. The total amount of DNA per coverslip should be 800 ng.

3.2 Patch Clamp Recordings of HEK Cells Expressing GluA2

1. For best expression rates conduct the electrophysiological recordings 24 h post transfection.
2. Under continuous illumination with blue light (480 nm) perfuse the HEK cells with external buffer containing 100 µM ATA-3 (*see* **Notes 10–12**).
3. Pull patch electrodes from glass capillaries to a resistance of 6–8 MΩ.
4. Exclude cells with a series resistance of >20 MΩ from analysis.

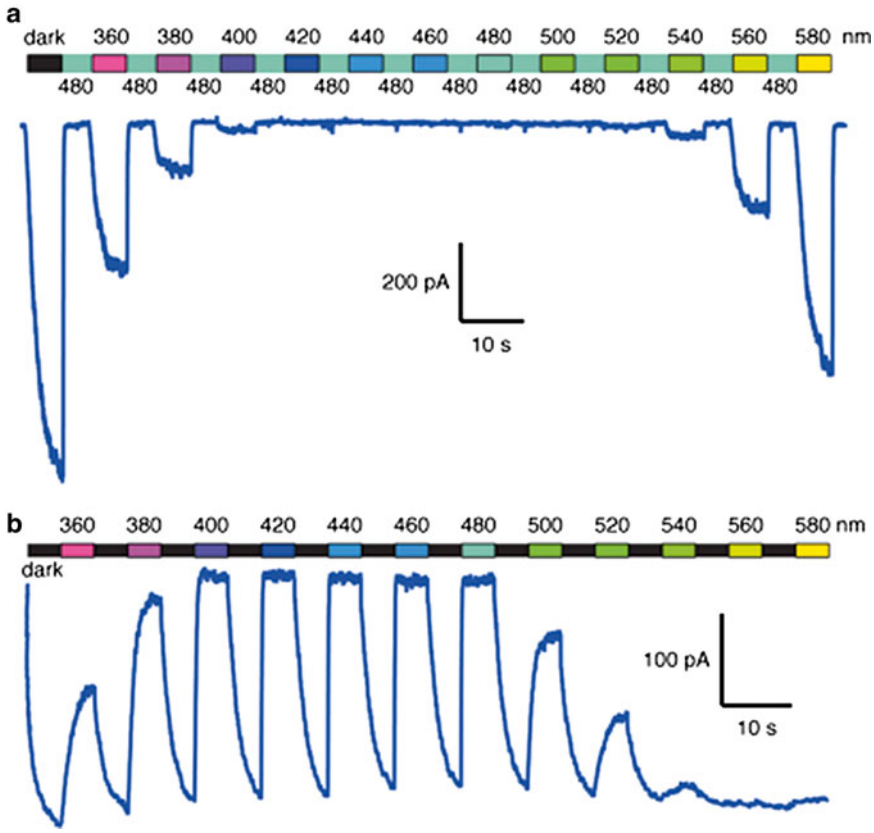

Fig. 2 Voltage clamp recordings of HEK293T cells expressing GluA2 to determine the action spectrum of ATA-3. (**a**) ATA-3-induced currents were evoked by illumination at different wavelengths. Following each wavelength, the current was turned off with 480 nm light to induce the inactive *cis* configuration of ATA-3. Darkness is most effective to induce AMPA-specific currents (**b**) Screening for the most effective wavelength to turn off ATA-3-induced currents. Darkness was intermittently applied with light of increasing wavelengths (360–580 nm). ATA-3-induced currents are most effectively turned off by light in the blue range (420–480 nm). (Reproduced with permission from Wiley VCH, ref. [1])

5. Illicit AMPA receptor-specific currents by switching between blue light (480 nm) and darkness (Fig. 2, *see* **Notes 6** and **13**). The light-induced current can be graded by irradiation with light of different wavelengths (Fig. 2) or by changing the light intensities. To improve switching, bath perfusion may be stopped prior to switching illumination wavelengths to reduce diffusion of the PCL.

3.3 Preparation of Acute Brain Slices

1. After cervical dislocation, remove the brain of wt mice (C57BL/6; P10–P16) and place in ice-cold sucrose buffer. Trim the brain with a sharp blade thereby creating a flat surface and glue it with that side to the cutting chamber. Cut 300 μm thick coronal slices using a vibratome (similar to ref. [8], also *see* **Note 14**).
2. Store the slices in ACSF for 1 h at 34 °C and then for up to 8 h at RT.

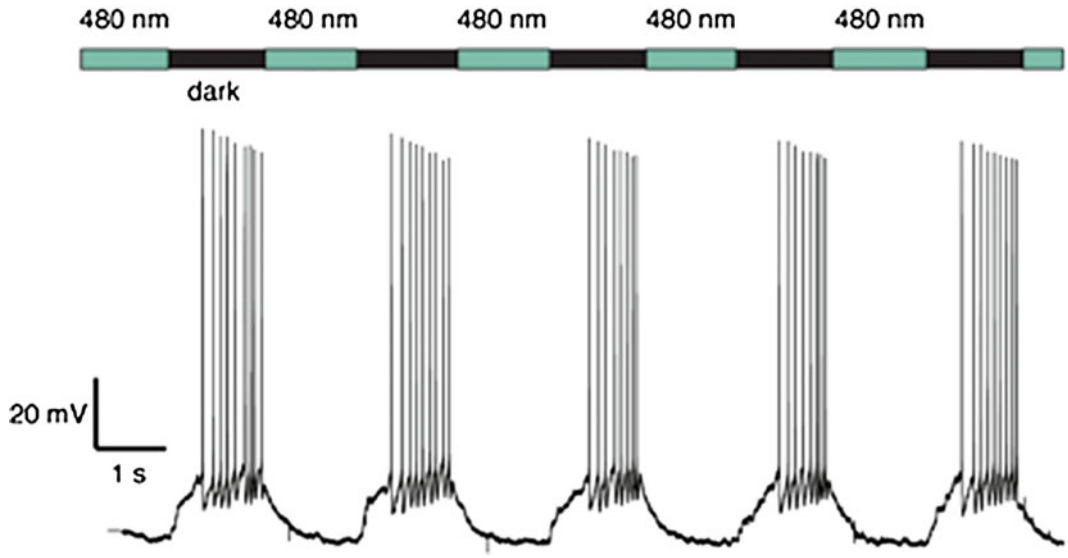

Fig. 3 Current clamp recordings of ex vivo cortical layer 2/3 neurons. Photocontrol of action potential firing by ATA-3 using the most effective illumination as determined in the action spectrum (Fig. 2). (Reproduced with permission from Wiley VCH, ref. [1])

3.4 Patch Clamp Recordings of Cortical Layer 2/3 Neurons

The patch clamp procedure was carried out similar to ref. [8].

1. Place a brain slice into the perfusion chamber. Perfuse the slice under continuous illumination of blue light (480 nm) with external buffer containing 100 μM ATA-3.
2. Pull patch electrodes from glass capillaries to a resistance of 6–8 MΩ.
3. Exclude cells with a series resistance of >20 MΩ from analysis.
4. AMPA receptor-mediated action potential firing (Fig. 3) can be controlled with a light protocol (*see* **Note 6**) switching between darkness (action potential firing) and 480 nm light (no activity).

4 Notes

1. Having the external buffer warmed to 40 °C for 5 min helps to dissolve the DMSO stock solution of the PCL. Keep the final DMSO concentration below 1 %. Routinely, we use 0.1 %.
2. If precipitates form do not filter the solution. We have the experience that most of the compound will be adsorbed by the filter material.
3. The DMSO stock solution must be stored light-protected. We find that storage at RT is best for the integrity of the PCL. The dried powder of the compound is stored at −80 °C.

If possible we recommend to store it under protective atmosphere (e.g., argon).

4. Let the solutions for the brain slice experiments equilibrate with carbogen for at least 15 min.
5. Prepare 10 ml of intracellular solution and store in aliquots at –20 °C.
6. A sophisticated illumination system is not necessarily needed. We could achieve photoswitching using a LED pocket lamp (e.g., Solarforce, Ultrafire) with the appropriate wavelength. In this case the light beam was directly aimed at the perfusion chamber and was not coupled to the microscope. There are remote switches available for which we custom-made a control device to be able to trigger the pocket lamp via a BNC-connector. In addition, standard mercury or metal halide illumination systems (available from all major microscope suppliers) with the appropriate bandpass filters and a shutter can be used.
7. We use the amplifier software Patchmaster to control not only the patch parameters but also to trigger the light pulses.
8. For best transfection results, it is advisable to always passage and seed the cells below a confluency of 80 %.
9. The amount of CO_2 in the incubator sets the pH of the cell culture medium and therefore may vary according to the $NaHCO_3$ content of the DMEM.
10. To remove the PCL solution from your perfusion system, we find that washing the line with 0.1 M HCl solution followed by ddH_2O works best.
11. To reduce the volume in your perfusion line, one should use tubing with a small diameter (inner diameter approx. 0.5–1 mm). We recommend the use of Polyethylen (PE)-tubing and Tygon tubing.
12. To reduce the amount of precious compound needed for the experiment we recommend to recirculate the PCL buffer. In our hands 10 ml of the buffer is sufficient for a whole day of experiments. In addition, it is possible to reuse the buffer for 3 consecutive days, if stored at 4 °C.
13. In general keep the illumination period as short as possible. Any illumination will eventually lead to phototoxic effects due to the formation of reactive oxygen species (ROS).
14. While the process of the brain slice preparation should be sufficiently fast, one should never become hectic and always make precise movements to avoid destroying tissue that you want to record from.

Acknowledgments

This work was supported by the Fonds der Chemischen Industrie (Kekulé fellowship for PS) and the ERC Advanced Grant (CARV: #268795) awarded to Dirk Trauner. We thank Dirk Trauner for the intellectual and financial support of this project.

References

1. Stawski P, Sumser M, Trauner D (2012) A photochromic agonist of AMPA receptors. Angew Chem Int Ed Engl 51:5748–5751. doi:10.1002/anie.201109265
2. Volgraf M, Gorostiza P, Szobota S, Helix MR, Isacoff EY, Trauner D (2007) Reversibly caged glutamate: a photochromic agonist of ionotropic glutamate receptors. J Am Chem Soc 129(2):260–261. doi:10.1021/ja067269o
3. Stein M, Middendorp SJ, Carta V, Pejo E, Raines DE, Forman SA, Sigel E, Trauner D (2012) Azo-propofols: photochromic potentiators of GABA(A) receptors. Angew Chem Int Ed Engl 51(42):10500–10504. doi:10.1002/anie.201205475
4. Banghart MR, Mourot A, Fortin DL, Yao JZ, Kramer RH, Trauner D (2009) Photochromic blockers of voltage-gated potassium channels. Angew Chem Int Ed Engl 48(48):9097–9101. doi:10.1002/anie.200904504
5. Mourot A, Fehrentz T, Le Feuvre Y, Smith CM, Herold C, Dalkara D, Nagy F, Trauner D, Kramer RH (2012) Rapid optical control of nociception with an ion-channel photoswitch. Nat Methods 9(4):396–402. doi:10.1038/nmeth.1897
6. Fehrentz T, Kuttruff CA, Huber FM, Kienzler MA, Mayer P, Trauner D (2012) Exploring the pharmacology and action spectra of photochromic open-channel blockers. Chembiochem 13(12):1746–1749. doi:10.1002/cbic.201200216
7. Polosukhina A, Litt J, Tochitsky I, Nemargut J, Sychev Y, De Kouchkovsky I, Huang T, Borges K, Trauner D, Van Gelder RN, Kramer RH (2012) Photochemical restoration of visual responses in blind mice. Neuron 75(2):271–282. doi:10.1016/j.neuron.2012.05.022
8. Bischofberger J, Engel D, Li L, Geiger JRP, Jonas P (2006) Patch-clamp recording from mossy fiber terminals in hippocampal slices. Nat Protoc 1(4):2075–2081. doi:10.1038/nprot.2006.312

Chapter 6

Photoconversion of CFP to Study Neuronal Tissue with Electron Microscopy

Nina Wittenmayer

Abstract

Being able to use versatile light microscopy on live or fixed samples followed by electron microscopy imaging for high resolution analyses is a challenging goal. The advantage is of course that tracing and localizing fluorescently labeled molecules yields great information about dynamic cellular processes, while electron microscopy of the same sample provides exquisite information about subcellular structures. Here, I describe the straightforward combination of both methods by photoconversion of diaminobenzidine (DAB) through cyan fluorescent protein (CFP) tagged proteins localized to the Golgi apparatus in primary hippocampal neurons.

Key words CFP, DAB, Photoconversion, Neuron, Transmission electron microscopy

1 Introduction

For many cell biological approaches such as localization of molecules in a subcellular environment or visualization of cell dynamics of living cells, the great variety of fluorescent proteins have become the most important tools [1–3]. Despite this success, numerous scientific questions require resolution beyond the light microscopy level. For these specific questions, a combination of light microscopy approaches with electron microscopy are desirable. This can be achieved by diaminobenzidine (DAB) photoconversion of fluorescent proteins such as GFP or CFP (XFP) [4]. As with any illumination of fluorochromes occurs, free oxygen radicals form which in turn photo-oxidize DAB into an electron dense precipitate that can be visualized by classical electron microscopy (EM). In addition to XFPs, other fluorescent probes as fluorescein 5(6)-isothiocyanate (FITC) [5], styryl dyes to label endocytosis of vesicles [6, 7] or photosensitizing molecules [5] were successfully used to photoconvert DAB.

Here, I describe the procedure for DAB photoconversion via pECFP-Golgi, a fusion protein which is targeted to the

Sidney Cambridge (ed.), *Photoswitching Proteins: Methods and Protocols*, Methods in Molecular Biology, vol. 1148,
DOI 10.1007/978-1-4939-0470-9_6,

trans-medial side of the Golgi apparatus in primary hippocampal neurons. The protocol of the procedure starts with a fixed sample, but certainly, prior fluorescence imaging of cellular dynamics would have been possible. After fixation of neurons and selection of a cell of interest with the light microscope, the pECFP-Golgi transfected neuron was illuminated in the presence of DAB and further processed for EM. Because illumination generates oxygen radicals with a very short life-time, the photo-oxidized DAB precipitated and localized in close proximity to the former fluorescent signal of the CFP fusion protein. EM on thin sections revealed the localization of the CFP-Golgi construct at subcompartments of the Golgi apparatus in primary neurons with high resolution.

Thus, DAB photoconversion of fluorescently labeled molecules is a powerful tool to study the location of proteins or molecules with the resolution power of the electron microscope.

2 Materials

Prepare all solutions using ultrapure water (prepared by purifying deionized water to attain a sensitivity of 18 MΩ cm at 25 °C) and analytical grade reagents. Store all reagents at 4 °C unless indicated otherwise.

2.1 DNA Constructs

1. Expression construct of your protein of interest as a fusion protein with cyan fluorescent protein (CFP). Typically eukaryotic expression vectors such as pECFP from Clontech are used. Here, we transfected pECFP-Golgi, a fusion protein consisting of enhanced cyan fluorescent protein (ECFP) and a sequence encoding the N-terminal 81 amino acids of human beta 1,4-galactosyltransferase that contains the membrane-anchoring signal peptide which targets the fusion protein to the *trans-medial* region of the Golgi apparatus (Llopis1998).
2. Maxi kit, preferentially an endotoxin free kit (*see* **Note 1**), for plasmid purification.
3. Spectrophotometer for DNA concentration measurements.

2.2 Calcium Phosphate Transfection of Primary Neurons

1. Laminar flow hood.
2. Water bath (37 °C).
3. Incubator with 37 °C and 5 % v/v CO_2.
4. Inverse microscope with 4× or 10× objectives for analysis of cell health and morphology.
5. Vortexer.
6. Glass-bottom tissue culture dishes (Ibidi GmbH).
7. 1× Phosphate-buffered saline (PBS).

8. Primary hippocampal or cortical neurons which were dissociated and plated 2–4 days before transfection.
9. Opti-MEM® reduced serum medium (Invitrogen).
10. Neurobasal medium.
11. 0.01 % poly-L-lysine (Sigma-Aldrich).
12. 2 M $CaCl_2$ solution: prepare with sterile, distilled water, aliquot and freeze at –20 °C.
13. 2× HBS buffer: 274 mM NaCl, 10 mM KCl, 1.4 mM Na_2HPO_4, 15 mM glucose, 42 mM HEPES, pH 7.02 (NaOH). Prepare with sterile, distilled water and store 2 ml aliquots at –20 °C.
14. Non-autoclaved 2 ml tubes (*see* **Note 2**).

2.3 DAB Photoconversion and Light Microscopy

1. Inverted microscope with a bright field condenser and epifluorescence light path (e.g., Zeiss Axiovert 200 M). The microscope should be equipped with a standard CCD camera, 40× or 63× oil objectives and a filter set for imaging CFP (excitation 436 nm/emission 475 nm) fluorescence.
2. Rectangular diaphragma for light microscopes to confine the DAB photoconverted area of the sample.
3. PIPES buffer: 0.2 M Na–PIPES pH 7.4, 10 mM $CaCl_2$. Weigh 6.05 g PIPES and transfer to a glass or plastic cylinder. Add water to a volume of 70 ml. Mix and adjust pH with 4 N NaOH (*see* **Note 3**). Fill up to 100 ml and store at 4 °C.
4. Fixation buffer: 0.1 M PIPES pH 7.4, 5 mM $CaCl_2$, 1 % glutaraldehyde. Prepare a 1:2 dilution of the 0.2 M PIPES buffer (**step 1**) with water for a small volume such as 10 ml. For a volume of 10 ml, add 0.4 ml of a 25 % glutaraldehyde solution just before fixation of the samples.
5. Washing buffer: 0.15 M PIPES pH 7.4, 7.5 mM $CaCl_2$.
6. Blocking buffer A: 0.1 M PIPES pH 7.4, 5 mM $CaCl_2$, 100 mM potassium cyanide, 100 mM glycine (*see* **Note 4**).
7. Blocking buffer B: 0.1 M PIPES pH 7.4, 5 mM $CaCl_2$, 100 mM ammonium chloride (*see* **Note 5**).
8. Blocking buffer C: 10 mg/ml sodium borohydrate in 0.1 M PIPES pH 7.4 with 5 mM $CaCl_2$ (*see* **Note 5**).
9. DAB solution: 1.5 mg/ml DAB in 0.1 M PIPES pH 7.4, 5 mM $CaCl_2$ (*see* **Note 6**).

2.4 Electron Microscopy

1. BEEM capsules, no 3 (PLANO GmbH), prepare the capsules by cutting of the lid and bottom.
2. 1 % Osmium tetroxide solution (*see* **Note 7**).
3. 85 and 95 % ethanol in water.

4. EPON for embedding of samples: For 50 ml EPON embedding medium mix in an appropriate container with continuous stirring: 26.1 g Epon (Fluka), 12.3 g Epoxy embedding medium hardener DDSA (Fluka) with 16.3 g Epoxy embedding medium hardener MNA (Fluka). To protect the mixture from introduction of water, wipe the stirrer with acetone before use. When all components are mixed homogeneously, add 0.75 ml Epoxy embedding medium accelerator DMP 30 (Fluka), mix, and store aliquots at −20 °C for further use.
5. Hydrofluoric acid.
6. 1 M calcium hydroxide.
7. Microtome.
8. Razor blade.
9. Eyelash on top a wooden stick.
10. Copper grids with 200 mesh.
11. Lead citrate for staining of ultrathin sections: solve 1.33 g lead citrate in 15 ml distilled water. Then add 1.76 g sodium citrate and 15 ml distilled water, shake 1 min and let stand for 30 min. Add 8 ml 1 N NaOH and fill up to a volume of 50 ml. Store the solution 2–3 weeks at 4 °C.
12. Transmission electron microscope.

3 Methods

Carry out all procedures at room temperature unless otherwise specified. Transfect primary hippocampal or cortical neurons using calcium phosphate [8], lipofectamine [9] or use any other method to introduce CFP fusion proteins into neurons at least 24 h before starting DAB photoconversion.

3.1 DNA Preparation

1. Prepare DNA from *E. coli* cultures using an endotoxin free maxi plasmid preparation kit.
2. Using a spectrophotometer to determine DNA concentration and purity by measuring absorbance at 260 nm (A_{260} of 1.0 = 50 µg/ml pure dsDNA). Good-quality DNA will have an A_{260}/A_{280} ratio of 1.7–2.0.

3.2 Calcium Phosphate Transfection of Primary Neurons

1. Dissociated hippocampal cultures are prepared from E19 Wistar rats or E16 mice according to Gosslin & Banker with slight modifications [8]. Neurons are cultured at a density of 40,000 cells/cm² on poly-L-lysine-coated glass-bottom culture dishes. For poly-L-lysine-coating of glass-bottom culture dishes: add 1 ml 0.01 % poly-L-lysine on top of the cover slip and place the dish in the incubator at 37 ° C for 1–2 h.

Afterwards, wash the cover slip three times with sterile 1× PBS, leave a 1 ml drop of 1× PBS on the cover slip and place the dish in the incubator until seeding of cells.

2. Transfect neurons on day 2–4 in vitro (*see* **Note 8**).
3. Check neurons for healthy morphology under the microscope. Neurons should have branched dendrites and should make contacts with surrounding neurons.
4. Warm Opti-MEM® medium to 37 °C in the water bath.
5. The procedure is described for one cell culture dish. Remove the conditioned medium (*see* **Note 9**) of the dish and transfer it to a new, sterile cell culture dish. Immediately add 1.5 ml pre-warmed Opti-MEM® medium to the culture dish with neurons. Return the culture dish with neurons and the cell culture dish with conditioned medium back into the 37 °C incubator.
6. Mix 5.6 µl 2 M $CaCl_2$ with 3 µg DNA and sterile, distilled water in a total volume of 45 µl in a non-autoclaved 2 ml tube. Place the tube on a vortexer and add drop wise 45 µl 2× HBS buffer while shaking. For precipitate formation, let stand for 20 min.
7. Add 90 µl of transfection mixture to the cell culture dish with neurons.
8. Place cells in the 37 °C incubator for 60 min.
9. Meanwhile warm Neurobasal medium to 37 °C in the water bath.
10. To remove the transfection mixture from the neurons (*see* **Note 10**), which causes massive cell death during long incubation times, start washing cells with Neurobasal medium 60 min after adding the transfection mixture.
11. Aspirate the medium off and add 1.5 ml pre-warmed Neurobasal medium. If you transfect more than one dish, work dish per dish to avoid cell death.
12. Remove 1.2 ml of the medium and add pre-warmed Neurobasal medium.
13. Repeat **step 12**.
14. Take the cell culture dish containing conditioned medium out of the 37 °C incubator.
15. Aspirate the Neurobasal medium off, add 1.5 ml conditioned medium to the neurons and place cells in the 37 °C incubator.
16. Verify cell health and CFP expression 18–24 h later.

3.3 DAB Photoconversion

1. Remove cell culture medium and fix transfected neurons with fixation buffer for 20 min at room temperature. Keep cells in the dark to avoid bleaching of CFP fluorescence.
2. Wash cells three times 1 min each with washing buffer.

3. Incubate the cells in blocking buffer A for 80 min in the dark. This step is blocking endogenous enzymes activities (*see* **Note 11**) in cells which cause nonspecific DAB precipitation.
4. Wash neurons three times each for 1 min with washing buffer.
5. Incubate the cells in blocking buffer B for 40 min in the dark to reduce aldehyde-induced autofluorescence (*see* **Note 12**).
6. Wash neurons three times each for 1 min with washing buffer.
7. Incubate the cells in blocking buffer C for 40 min in the dark to reduce aldehyde-induced autofluorescence (*see* **Note 12**).
8. Wash neurons three times each for 1 min with washing buffer.
9. Transfer cell culture dishes on ice and let cool down for 10 min (*see* **Note 13**).
10. Remove washing buffer from the cells and add 2 ml ice-cold DAB solution. Incubate for 3–5 min on ice (*see* **Note 14**). Then immediately transfer the cell culture dish onto the light microscope. Search and select a transfected cell which is suitable for DAB photoconversion and take a phase contrast and fluorescence image (*see* **Note 15**). With a rectangular diaphragm, define the area of the cell of interest and neighboring cells (*see* **Note 16**) as small as possible and illuminate this area 10–12 min with a CFP excitation filter set (peak: 436 nm) (*see* **Note 17**).
11. During 10–12 min illumination, fluorescence fades away until it is completely erased and brownish background staining appears (*see* Fig. 1). At this time point stop the photoconversion reaction by exchanging the DAB solution to washing solution.
12. Wash neurons three times each for 1 min with washing buffer.

3.4 Preparation of Samples for EM

1. Postfix samples in 1 % osmium tetroxide for 30 min on ice. Wash once with distilled water.
2. Dehydrate the samples in graded ethanol series: incubate samples three times for 5 min each time in 85 % ethanol, three times for 5 min each time in 95 % ethanol and three times for 5 min each time in 100 % ethanol.
3. Remove 100 % ethanol from the samples and add EPON only on the glass cover slip of the cell culture dish (*see* Fig. 2). Incubate at 37 °C overnight (*see* **Note 18**).
4. Next day place a BEEM capsule on the DAB-photoconverted area (*see* Fig. 2) which is covered by EPON and incubate 6 h at 60 °C (*see* **Note 19**).
5. Fill up the BEEM capsule with EPON (*see* Fig. 2) and incubate at 60 °C overnight (*see* **Note 20**).
6. Take the glass cover slip surrounding plastic of the cell culture dish off with nippers.

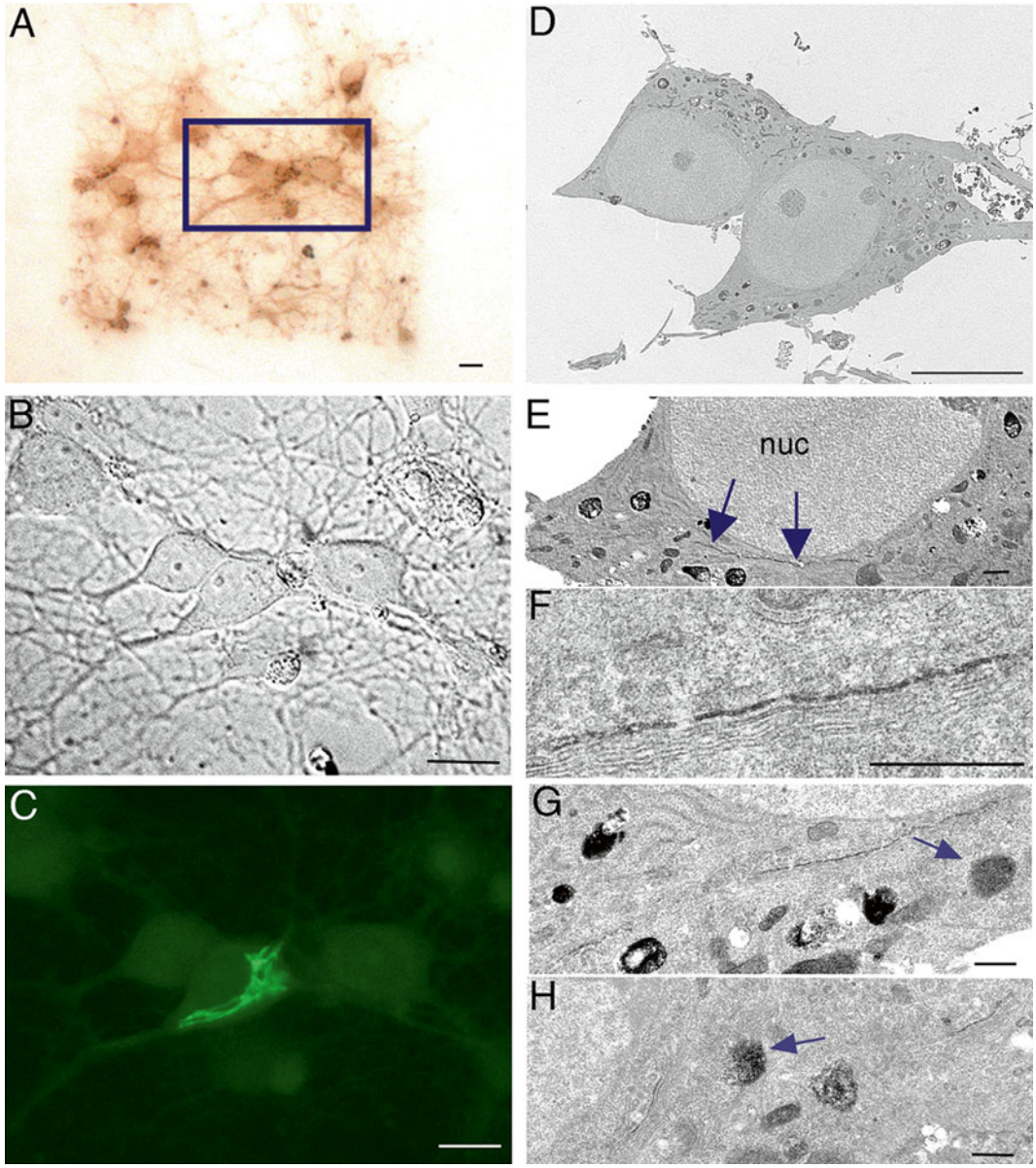

Fig. 1 Primary hippocampal neurons were transfected with pECFP-Golgi, a fusion protein which is targeted to the *trans*-side of the Golgi apparatus at DIV7, photoconversion was carried out at DIV8 and followed by processing for electron microscopy. (**a**) Shows an overview image of the photobleached area. During the DAB photoconversion process fluorescence fades away and background staining appears. (**b**) DIC image of the *boxed area* in (**a**). (**c**) Transfected neuron with fluorescence signals at the Golgi apparatus. (**d**) Overview image of the transfected and a neighboring neuron at the EM level. (**e**, **f**) Higher magnifications clearly reveal dark DAB deposits at the trans-Golgi lamella (*arrows* in (**e**)). (**g**, **h**) Because of DAB photoconversion other dark structures such as mitochondria or autophagic-like vacuoles can appear (*arrows*). *nuc* nucleus, Bars, 15 μm (**a**–**c**), 7.5 μm (**d**), 2.5 μm (**e**), 500 nm (**f**), 1 μm (**g**, **h**)

Fig. 2 (**a**) Glass-bottom cell culture dish. It was filled with EPON embedding medium at the central area which is confined by the glass cover slip (*arrow*). In (**b**) a BEEM capsule was placed on the cover slip (*arrow*) and filled up with EPON embedding medium (**c**) (*arrow*)

7. Remove the glass of the cell culture dish by placing the BEEM capsule with the cover slip in a plastic container filled with hydrofluoric acid for 20–30 min (*see* **Note 21**). Neutralize the sample in 1 M calcium hydroxide.
8. Check with a loupe if all glass was removed. If not repeat **step 7**.
9. Incubation of the sample results in softening of the EPON, therefore incubate the sample again at 60 °C overnight.
10. Remove the plastic of the BEEM capsule with nippers.
11. Trimming: Follow the instructions of the microtome to install the diamond knife and the sample block. Start to trim the EPON block with a razor blade. Trim the block pyramid-like with a trapezoid face. The DAB-photoconverted area appears as a dark spot; therefore keep this spot in the middle of your pyramid-shaped block. The edges of your block should be very straight and without irregularities to guarantee good ultrathin sectioning.
12. Ultrathin sectioning (*see* **Note 22**): Since the monolayer of neurons is very thin compared to EPON-embedded tissue, you have to start immediately with ultrathin sectioning and cannot make semi-thin sections first. Align the knife edge and the block face and fill the knife boat with either filtered distilled water or 10 % ethanol so as to obtain a silvered reflection off the surface of the liquid. Cut individual sections and adjust the section thickness settings until you obtain pale gold to silver sections (*see* **Note 23**). Floating sections are "guided" with an eyelash on top of a wooden stick away from the knife edge. Collect sections by putting the grid under the liquid in the knife boat and then coming up under the sections with the grid. Allow the grids to properly dry on the filter paper before staining with lead citrate.
13. Lead citrate staining: spin the lead citrate solution for 5 min with 17,950 × *g* at room temperature. Put a drop lead citrate solution on parafilm and place the grids with sections upside down on the drop for 1–3 min. With forceps take the grid off

the drop, rinse carefully with distilled water and dry the grid on filter paper (for instance Whatman no. 50). The incubation time on the lead citrate drop has to be tested for each experiment individually. If contrast is low, you can repeat the lead citrate staining.

4 Notes

1. For good cell viability, the DNA should be free of endotoxins.
2. During the autoclaving process, the tubes could be contaminated with endotoxins. Therefore, open a new package of tubes from your supplier under the laminar flow hood and use the tubes directly.
3. Use 4 N NaOH to adjust a pH of 7.4. First adjust the pH to 7.0 to achieve better solubility of PIPES. When PIPES is in solution, adjust the pH to 7.4.
4. Since potassium cyanide is very toxic, prepare a 1 M potassium cyanide stock solution and store aliquots at –20 °C. Prepare a 1 M glycine stock solution and store aliquots at –20 °C. Before use, thaw aliquots of 1 M glycine pH 7.4 and 1 M potassium cyanide and prepare blocking buffer A.
5. It is best to prepare this fresh each time.
6. It is best to prepare this fresh each time. Keep the solution at 4 °C until use and in the dark.
7. Osmium tetroxide is toxic, thus wear gloves and work with a flue while handling osmium tetroxide.
8. This protocol for calcium phosphate transfection of neurons is optimized for transfection at day 2–4 in vitro (DIV2-4).
9. The culture medium is enriched with different factors such as growth factors secreted by glia cells which are present in primary neuronal cultures. The neurons do not tolerate a change of medium and need to be cultured in "their" conditioned medium all the time. Therefore collect the conditioned medium in a new, sterile cell culture dish during the procedure of transfection. Place the dish with conditioned medium in the incubator to adjust the pH to 7.4.
10. Calcium phosphate co-precipitates with DNA into an insoluble precipitate which then is endocytosed by cells. Incubation of neurons for longer time periods than 1 h with the transfection precipitate can cause massive cell death, therefore the transfection precipitate should be washed off the cells timely.
11. Punctuate background staining of peroxisomes and mitochondria can occur during the process of DAB photoconversion. These organelles contain oxidative enzymes, e.g., peroxisomal catalase or cytochrome oxidase, which are activated by aldehyde

fixation [10] and cause DAB precipitation. Incubation with potassium cyanide reduces their enzyme activity.

12. The standard method of fixation for light or electron microscopy is cross-linking by treatment of the sample with aldehydes. The fixative penetrates the cells and cross-link proteins and nucleic acids by forming covalent bonds between adjacent amine-containing groups. Because glutaraldehyde has two reactive aldehyde groups, autofluorescence caused by unreacted aldehyde groups appears. Blocking with amine-containing reagents (e.g., NH_4Cl) or reducing reagents (e.g., $NaBH_4$) can reduce aldehyde-induced autofluorescence.
13. It is very important for the DAB photoconversion process that all solutions and the cell culture dishes are at 10 °C or below. More oxygen dissolves in solutions with higher temperatures and thus causes unspecific DAB precipitation.
14. Pre-incubation of the sample for 3–5 min on ice in DAB solution was sufficient in our experiments. Some groups pre-incubate up to 30 min [11] and/or with oxygen-enriched DAB solution. These are parameters which could be changed to improve the results.
15. Taking a phase contrast image is of high importance. Since we usually do not achieve 100 % transfection efficiency of neurons, the tricky and time consuming part of this method is the identification of the illuminated neuron at the electron microscope. Therefore, a phase contrast image provides you an overview of the neuron selected for photoconversion and neighboring neurons. At the EM, you will find the neuron selected for photoconversion only by its shape and the shape of the surrounding cells.
16. Neighboring neurons without CFP fusion protein expression serve as control for DAB photoconversion of CFP. Control cells do not show any DAB precipitation compared to CFP fusion protein transfected cells.
17. Illumination of CFP or GFP fusion proteins should be carried out with the appropriate filter settings. For CFP fusion proteins use a CFP excitation filter BP436/20 nm and for GFP fusion proteins use a GFP excitation filter BP470/40 nm. The illumination time is variable, depending upon the illumination strength and also upon the DAB penetration into the preparation [4]. DAB photoconversion of CFP fusion proteins required 10–12 min illumination and the neuronal ultrastructure was well preserved at the EM level while illumination of GFP fusion proteins required 30–40 min illumination and ultrastructure of neurons was poor. Thus, we only use CFP fusion proteins for DAB photoconversion in primary hippocampal neurons.

18. Overnight incubation of EPON embedded samples at 37 °C leads to less hardening of the embedding medium which is necessary for the next step (*see* **Note 18**).
19. The DAB photoconverted area appears upon osmium tetroxide fixation as a small black puncta. Place the BEEM capsule onto this puncta, so it is in the middle of the BEEM capsule. Incubation for 6 h at 60 °C leads to complete polymerization of the EPON and afterwards the BEEM capsule can be filled up with EPON.
20. The EPON embedding medium polymerizes and hardens overnight at 60 °C.
21. Check carefully under a microscope if all the glass was removed by the acid. If not it will destroy your diamond knife during ultrathin sectioning. If not incubate again for 20–30 min in acid to remove the remaining glass.
22. If you are not experienced with ultrathin sectioning it is highly recommended to first get help and training from experienced researchers.
23. The interference color of sections serves as the index of its approximate thickness. Sections with a silver interference color have a thickness of 90 nm and gold-colored sections have a thickness of 150 nm. The estimation of section thickness based on these colors is reliable to within a range of 10–20 nm.

References

1. Lippincott-Schwartz J, Patterson GH (2009) Photoactivatable fluorescent proteins for diffraction-limited and super-resolution imaging. Trends Cell Biol 19(11):555–565
2. Ward TH, Lippincott-Schwartz J (2006) The uses of green fluorescent protein in mammalian cells. Methods Biochem Anal 47:305–337
3. Giepmans BN, Adams S R, Ellisman MH, Tsien RY (2006) The fluorescent toolbox for assessing protein location and function. Science 312(5771):217–224
4. Grabenbauer M et al (2005) Correlative microscopy and electron tomography of GFP through photooxidation. Nat Methods 2(11): 857–862
5. Pellicciari C et al (2013) Ultrastructural detection of photosensitizing molecules by fluorescence photoconversion of diaminobenzidine. Histochem Cell Biol 139(6):863–871
6. Harata N, Ryan TA, Smith SJ, Buchanan J, Tsien RW (2001) Visualizing recycling synaptic vesicles in hippocampal neurons by FM 1-43 photoconversion. Proc Natl Acad Sci U S A 98(22):12748–12753
7. Opazo F, Rizzoli SO (2010) Studying synaptic vesicle pools using photoconversion of styryl dyes. J Vis Exp. 36
8. Dresbach T et al (2003) Functional regions of the presynaptic cytomatrix protein bassoon: significance for synaptic targeting and cytomatrix anchoring. Mol Cell Neurosci 23(2):279–291
9. Ohki EC, Tilkins ML, Ciccarone VC, Price PJ (2001) Improving the transfection efficiency of post-mitotic neurons. J Neurosci Methods 112(2):95–99
10. Fahimi HD, Baumgart E (1999) Current cytochemical techniques for the investigation of peroxisomes. A review. J Histochem Cytochem 47(10):1219–1232
11. Meiblitzer-Ruppitsch C et al (2008) Electron microscopic visualization of fluorescent signals in cellular compartments and organelles by means of DAB-photoconversion. Histochem Cell Biol 130(2):407–419

Chapter 7

Light-Inducible Gene Regulation with Engineered Zinc Finger Proteins

Lauren R. Polstein and Charles A. Gersbach

Abstract

The coupling of light-inducible protein–protein interactions with gene regulation systems has enabled the control of gene expression with light. In particular, heterodimer protein pairs from plants can be used to engineer a gene regulation system in mammalian cells that is reversible, repeatable, tunable, controllable in a spatiotemporal manner, and targetable to any DNA sequence. This system, Light-Inducible Transcription using Engineered Zinc finger proteins (LITEZ), is based on the blue light-induced interaction of GIGANTEA and the LOV domain of FKF1 that drives the localization of a transcriptional activator to the DNA-binding site of a highly customizable engineered zinc finger protein. This chapter provides methods for modifying LITEZ to target new DNA sequences, engineering a programmable LED array to illuminate cell cultures, and using the modified LITEZ system to achieve spatiotemporal control of transgene expression in mammalian cells.

Key words Optogenetics, Transcription, Gene regulation, Gene expression, Zinc finger protein, Protein engineering, Genetic engineering, Synthetic biology, Gene circuits

1 Introduction

The growing complexity of scientific research requires the development of advanced gene regulation systems. The ability to easily manipulate gene expression with spatial and temporal control in a tunable and reversible manner is critical to many potential applications in gene therapy, regenerative medicine, tissue engineering, metabolic engineering, synthetic biology, and basic research. The most common gene regulation systems are controlled by the presence of a small molecule such as an antibiotic or steroid analogue [1–9]; however, because small molecules quickly diffuse throughout tissues and cell culture, these systems cannot be used to achieve spatial control over gene regulation. Furthermore, the small molecule must be removed from the system to reverse its effect, making it difficult to dynamically control gene expression for some applications.

Sidney Cambridge (ed.), *Photoswitching Proteins: Methods and Protocols*, Methods in Molecular Biology, vol. 1148,
DOI 10.1007/978-1-4939-0470-9_7,

Recently, the emerging field of optogenetics has provided tools to engineer gene regulation systems that are controlled by light rather than small molecules, thus enabling precise spatiotemporal genetic control [10, 11]. Several of these systems have been reported to modulate transcription of an exogenous transgene by the presence of blue [12–17] or red [18–20] light. This makes gene activation and deactivation easier and faster compared to conventional systems, and it also eliminates the possibility of pleiotropic effects due to a chemical activator molecule. In general, most of these systems take advantage of plant proteins that form a homo- or heterodimer when illuminated by a specific wavelength of light (Fig. 1). Fusion of one of the plant dimerizing proteins to a DNA binding protein, such as the GAL4 DNA-Binding Domain, localizes that plant protein to the corresponding DNA target sequence.

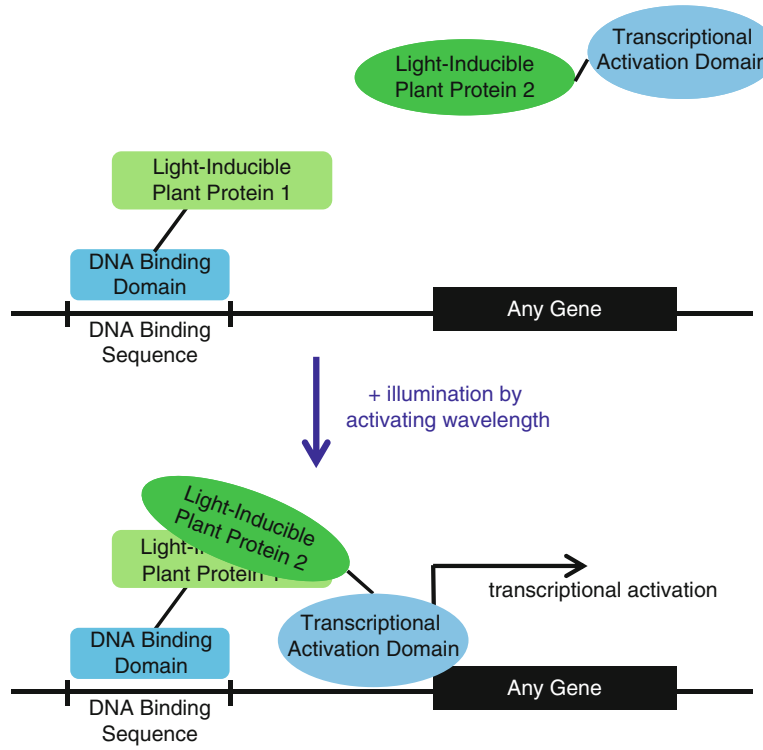

Fig. 1 Schematic of a general light-inducible gene regulation system. Many light-inducible gene regulation systems take advantage of homo- or heterodimerization between two light-inducible plant proteins. The first plant protein ("Light-Inducible Plant Protein 1") is usually fused to a DNA-binding domain, such as the GAL4 DNA-binding domain, which localizes the fusion protein to the DNA-binding domain's target DNA sequence. This target DNA sequence is located upstream of a gene of interest. The second plant protein ("Light-Inducible Plant Protein 2") is usually fused to a transcriptional activation domain, such as VP16. In the presence of an activating wavelength of light, the two light-inducible plant proteins interact, which translocates the transcriptional activation domain to the gene of interest and activates transcription

Fusion of the other plant protein to a transcriptional activation domain, such as the herpes simplex virus protein VP16 [21, 22], results in translocation of the activation domain to the DNA binding sequence upon illumination at the activating wavelength. This then activates transcription of a transgene located downstream of the DNA binding sequence.

We engineered a system that can regulate any transgene under the control of any arbitrary promoter sequence using blue light [23]. This system, Light-Inducible Transcription using Engineered Zinc finger proteins (LITEZ), takes advantage of the interaction between GIGANTEA (GI) and the Light-Oxygen-Voltage (LOV) domain of FKF1 [24]. These two proteins exist in the *Arabidopsis thaliana* plant and form a heterodimer in the presence of blue light (450 nm). In the LITEZ system, GI is fused to the N-terminus of a synthetic zinc finger protein (GI-ZFP), which makes this system unique because the ZFP is highly programmable and can theoretically be engineered to bind any desired DNA sequence through a variety of different techniques [25–38]. The other protein domain, LOV, is fused to three tandem copies of the minimal VP16 activation domain (LOV-VP16) [21, 22, 24]. When expressed in cells, GI-ZFP localizes to the ZFP target DNA sequence upstream of the transgene. In the presence of blue light, LOV binds to GI, which translocates VP16 to the gene of interest and activates transcription. Engineering of the ZFP provides the opportunity to target GI-ZFP to any DNA sequence. This flexibility in design enables the regulation of novel synthetic promoters, the use of multiple orthogonal promoters in a single cell, and potentially the ability to control natural endogenous promoters using blue light.

The following protocol describes the steps for engineering and using any GI-ZFP for light-inducible activation of a transgene in a spatiotemporal, reversible, repeatable, and tunable manner. It is assumed that a functional ZFP has already been engineered and determined to be active in the cell type or species of interest as a direct fusion to an activation domain, repression domain, or endonuclease. Many protocols have been published for designing, building, and testing novel ZFPs targeted to new sequences by a variety of methods [25–38], and online webservers have been created to facilitate this process [31, 33, 39–41]. Novel ZFPs are available commercially through Sigma-Aldrich, and many ZFPs are also available through the Addgene nonprofit plasmid repository (www.addgene.org) [37, 38]. A complete volume of *Methods in Molecular Biology* has also been published dedicated to this subject [42].

2 Materials

2.1 Construction of GI-ZFP Expression Plasmid

1. Polymerase chain reaction (PCR) primers: The 3′ end of these primers must be designed to anneal to the cDNA encoding the particular ZFP that will be cloned downstream of GI. For the

forward primer (NotI-ZFP fwd), replace the "N" sequence shown below with a sequence that has a melting temperature of 55–60 °C (about 14–21 base pairs long) and is homologous to the leading strand of the target ZFP gene, starting with the ATG start codon. It also may be necessary to add one or two additional base pairs between the *Not*I restriction endonuclease site and the homologous sequence to keep the ZFP in frame with the upstream GI gene once it is cloned into the final vector (*see* **Note 1**). For the reverse primer (XbaI-ZFP rev), replace the "N" sequence with a sequence that has a melting temperature of 55–60 °C and is homologous to the antisense strand of the target ZFP gene. Make sure to include the stop codon in this homologous sequence. If desired, an epitope tag, such as HA or FLAG for ensuring expression or localization by western blot or immunofluorescence staining, can also be cloned between the GI and ZFP genes without affecting the activity of the fusion protein. To insert an epitope tag, insert the leading strand sequence of the epitope tag between the "ATG" and the next (fourth) base pair of the sequence that is homologous to the ZFP in the NotI–ZFP fwd primer. Ensure that the downstream ZFP gene remains in frame after adding the epitope tag.

(a) NotI-ZFP fwd: 5′-taagcggccgcaNNNNNNNNNNNN-3′ (*see* **Note 2**).

(b) XbaI-ZFP rev: 5′-ttctagaNNNNNNNNNNNN-3′ (*see* **Note 3**).

2. Expression plasmid pcDNA3-GI-ZFP2: This construct contains a Cytomegalovirus (CMV) immediate early promoter driving expression of a gene encoding GI-ZFP2 [23]. This plasmid can be obtained from Addgene (Plasmid 42215).
3. Restriction endonucleases and appropriate buffers: *Not*I and *Xba*I.
4. Sequencing primers (*see* **Note 5**):

   (a) CMV fwd: 5′-ATTGACGCAAATGGGCGGTAGGCG TGT-3′.

   (b) GI fwd 1: 5′-GCTGTTGCTAATGGAGCTG-3′.

   (c) GI fwd 2: 5′-CCACTGCAACCTCCTATC-3′.

   (d) GI fwd 3: 5′-GGACTCCATGGAGTTACAGT-3′.

   (e) GI fwd 4: 5′-AGCCTTGGATCGCCAAAG-3′.

   (f) GI fwd 5: 5′-ACTGGGAAGCTCACAGCTT-3′.

5. Standard equipment and reagents for agarose gel electrophoresis.
6. Standard equipment and reagents for purification of DNA from agarose gels following electrophoresis, such as the QIAquick Gel Extraction Kit (Qiagen).

7. Standard equipment and reagents for purification of PCR products, such as the QIAquick PCR Purification Kit (Qiagen).
8. Calf intestinal alkaline phosphatase (CIP).
9. T4 DNA Ligase and appropriate buffer.
10. Chemically competent Stbl3 *E. coli* (Invitrogen) (*see* **Note 4**).
11. LB-Agar plates containing 100 μg/mL ampicillin for bacteria culture.
12. LB media containing 100 μg/mL ampicillin.
13. Standard equipment and reagents for purification of bacterial plasmid DNA, such as the Qiagen Spin Miniprep Kit.

2.2 Construction of Reporter Plasmid

1. Reporter plasmid pGL3-Basic-9xSeq2-Luc: This plasmid contains nine copies of the DNA binding site for GI-ZFP2 (5′-AAACTGCAAAAG-3′) upstream of a minimal CMV promoter and luciferase gene [23]. This plasmid can be obtained from Addgene (Plasmid 42214).
2. Oligonucleotides: The oligonucleotides below will be annealed and phosphorylated to create an insert containing three GI-ZFP DNA binding sites. Replace $(N)_n$ with the target binding sequence of the GI-ZFP and $(N')_n$ with the sequence that is antiparallel to the target binding sequence of the GI-ZFP. The double-stranded DNA product that will result from annealing these oligonucleotides contains sticky overhangs at the 5′ and 3′ ends that are compatible with ligation to DNA cleaved by *Xho*I and *Bgl*II endonucleases (*see* **Note 6**).
   (a) GI-ZFP binding fwd: 5′-tcgag$(N)_n$gtcgag$(N)_n$gtcgag$(N)_n$a-3′.
   (b) GI-ZFP binding rev: 5′-gatct$(N')_n$ctcgac$(N')_n$ctcgac$(N')_n$c-3′.
3. Sequencing primer hCMV rev: 5′-GAGCTCTGCTTATATA GACCTCCC-3′.
4. Restriction endonucleases and appropriate buffers: *Xho*I and *Bgl*II.
5. Reagents Subheading 2.1, **steps 5–13**.

2.3 Construction of a Programmable LED Light Array

1. 12 Blue LEDs centered on a wavelength of 450 nm (*see* **Note 7**).
2. 6 × 4 × 2″ project enclosure box (Radio Shack).
3. Arduino™ Uno Microcontroller.
4. BuckPuck AC Driver (700 mA).
5. Male and female wire connectors (MOLEX).
6. Soldering iron.
7. Electrical wire.

8. Wire stripper.
9. Wire cutters.
10. Copper-terminal printed circuit board.
11. Lexan™ plexiglass.
12. 12 VDC, 1.0 A power supply.
13. USB cable.
14. Silicone glue.

2.4 Measurement of LITEZ Activity

1. Mammalian cell line that can be readily transfected, such as HeLa or HE293T cells.
2. Lipofectamine 2000 Reagent (Invitrogen), or other suitable transfection reagent.
3. OptiMEM® Reduced Serum Media (Life Technologies).
4. DMEM supplemented with 10 % Fetal Bovine Serum (FBS).
5. DMEM supplemented with 10 % FBS and 1 % penicillin/streptomycin (P/S).
6. 0.25 % trypsin.
7. 2 × 24-well tissue culture treated plates.
8. Transfection plasmids:
   (a) pcDNA3-GI-ZFP.
   (b) pcDNA3-LOV-VP16 (can be obtained from Addgene (Plasmid 42499, [24])).
   (c) Reporter plasmid.
   (d) "Empty" expression plasmid (i.e., a plasmid containing a promoter but no expressed gene).
9. Lamp containing red flood lights (*see* **Note 8**).
10. Luciferase assay reagents, such as the Bright-Glo Luciferase Assay System (Promega).

2.5 Patterning Gene Expression Using LITEZ

1. *Green fluorescent protein* (GFP) cDNA.
2. Reporter construct engineered in Subheading 3.2 or pGL3-Basic-9xSeq2-Luc.
3. Polymerase chain reaction (PCR) primers:
   (a) GFP fwd: 5′-ACCATGGTGAGCAAGGGCGA-3′.
   (b) GFP rev: 5′-CCTCTAGATTACTTGTACAGCTCGTC C-3′.
4. Sequencing primer hCMV fwd: 5′-TAGGCGTGTACGGT GGG-3′.
5. Restriction endonucleases and appropriate buffers: *Nco*I and *Xba*I.
6. Reagents Subheading 2.1, **steps 5–13**.

7. Lipofectamine 2000 Reagent (Invitrogen), or other suitable transfection reagent.
8. OptiMEM® Reduced Serum Media (Life Technologies).
9. DMEM supplemented with 10 % FBS.
10. DMEM supplemented with 10 % FBS and 1 % P/S.
11. 0.25 % trypsin (Life Technologies).
12. 35 mm glass-bottom tissue culture dish (MatTek Corporation, Ashland, MA).
13. Transfection plasmids:
    (a) pcDNA3-GI-ZFP.
    (b) pcDNA3-LOV-VP16.
    (c) Reporter plasmid.
    (d) An "empty" expression plasmid (i.e., a plasmid containing a promoter but no expressed gene).
    (e) A plasmid that constitutively expresses dsRed or another fluorophore distinguishable from GFP (we used phUbC-dsRed, which is a plasmid containing the *dsRed* gene expressed under the human Ubiquitin C (hUbC) promoter).
14. Lamp containing red flood lights (*see* **Note 8**).
15. Photomask, such as one designed using computer software (i.e., AutoCAD®) and fabricated using a 3D printer (*see* **Note 9**).
16. Black electrical tape.
17. 1× phosphate-buffered saline (PBS).
18. 4 % paraformaldehyde in PBS (PFA).
19. Epifluorescence inverted microscope, such as the Zeiss Axio Observer Z1 fluorescence microscope.

3 Methods

3.1 Construction of GI-ZFP Expression Plasmid

1. Amplify the target ZFP gene via PCR using XbaI-ZFP fwd and NotI-ZFP rev primers.
2. Isolate the PCR product by gel electrophoresis and subsequent column purification using the QIAquick Gel Extraction Kit according to the manufacturer's directions.
3. Digest the purified PCR product and pcDNA3-GI-ZFP2 with restriction endonucleases *Not*I and *Xba*I. Also add the appropriate amount of CIP to the digestion reaction containing pcDNA3-GI-ZFP2 (we use 1 μl in 50 μl total volume). Allow the digestion to proceed for 1–3 h.
4. Isolate the 8,858 base-pair digestion product from pcDNA3-GI-ZFP2 via gel electrophoresis and subsequent column

purification using the QIAquick Gel Extraction kit. Purify the PCR digest reaction using the QIAquick PCR Purification kit according to the manufacturer's directions.

5. Ligate the purified PCR digestion product into the purified pcDNA3-GI-ZFP digestion product using T4 DNA Ligase (*see* **Note 10**). Incubate at room temperature for 1 h or overnight.
6. Transform 50 μl of chemically competent Stbl3 cells with 4 μl of the ligation reaction. Spread cells on ampicillin-containing LB-agar plates and culture overnight at 37 °C.
7. Inoculate 5 mL of LB media containing 100 μg/mL ampicillin with one colony from the ampicillin-containing LB-agar plates, and culture 12–16 h with shaking at 37 °C.
8. Purify plasmid DNA from the bacterial culture using a plasmid purification kit, such as the Qiagen Spin Miniprep Kit.
9. Verify the new construct by sequencing with CMV fwd, GI fwd 1, GI fwd 2, GI fwd 3, GI fwd 4, and GI fwd 5 primers.

3.2 Construction of Reporter Plasmid

1. Anneal GI-ZFP binding fwd and GI-ZFP binding rev oligonucleotides: Combine 500 ng of each oligonucleotide and 1× T4 DNA Ligase Buffer in water to a final volume of 50 μl. Heat sample in a thermal cycler to 95 °C for 2 min, then cool to 25 °C over a period of 45 min. Add 1 μl of T4 PNK and incubate at 37 °C for 30 min. Sample can be stored overnight at 4 °C (*see* **Note 11**).
2. Digest pGL3-Basic-9xSeq2-Luc with restriction endonucleases *Xho*I and *Bgl*II. Also add the appropriate amount of CIP to this digestion reaction (we use 1 μl in 50 μl total volume). Allow the digestion to proceed for 1–3 h.
3. Isolate the 4,863 base-pair digestion product via gel electrophoresis and subsequent column purification using the QIAquick Gel Extraction kit. Purify the PCR digest reaction using the QIAquick PCR Purification kit.
4. Ligate the annealed DNA product from **step 1** into the purified pGL3-Basic-9xSeq2-Luc digestion product using T4 DNA Ligase (*see* **Note 10**). Incubate at room temperature for 1 h or overnight.
5. Repeat Subheading 3.1, **steps 5–8**.
6. Verify the new construct by sequencing with the hCMV rev primer.

3.3 Construction of a Programmable LED Array

1. Cut the printed circuit board into a rectangle that fits inside the project enclosure box.
2. Connect four blue LEDs in series onto the printed circuit board using the soldering iron and electrical wire. When soldering the LEDs to the circuit board, create a line running down one of

the long edges of the board. Solder a second series of four LEDs along the opposite long edge of the printed circuit board. Solder the third and final series of four LEDs down the center of the circuit board. Space the LEDs to the dimensions of a 12-well tissue culture plate such that each LED is positioned approximately where the center of each well would be located.

3. Connect the three series of LEDs in parallel: solder the three wires at the anodic terminal of the circuit together (one from each LED series). Also solder the three wires at the cathodic terminal of the circuit together. Place the circuit board with attached LED array into the project box.
4. Extend the anodic and cathodic terminals by soldering a long piece of wire to each terminal. Cut a hole in the side of the project box and pass the wires through the hole to the outside of the box. Connect the free ends of these wires to a male wire connector, keeping track of which wire is the cathode and which is the anode. The wire connector enables separation of the LED array from the BuckPuck AC Driver and Arudino™ UNO microcontroller, allowing easy installation into an incubator while keeping the electrical control components outside of the humidity of the incubator environment.
5. Cut two new wires and install them into the female wire connector.
6. Fit the female wire connector into the male wire connector to determine which wire in the female connector connects to the anode and which connects to the cathode. Solder the cathodic wire from the female wire connector to the "LED (−)" pin and the anodic wire to the "LED (+)" pin of the BuckPuck AC Driver. An electrical diagram for this LED circuit can be seen in Fig. 2.
7. Strip both ends of a new piece of wire. Solder one end onto the "Ctrl" pin of the BuckPuck AC Driver, and insert the other end into the "Pin 13" port of the Arduino™ UNO microcontroller. Wires can simply be stripped and inserted into the Arduino™ UNO microcontroller ports or soldered into the ports for a sturdier connection.
8. Strip a new piece of wire on both ends, and solder one end onto the "Vin (+)" pin of the BuckPuck AC Driver. Insert the other end into the "Vin" port of the Arduino™ UNO microcontroller.
9. Strip a new piece of wire on both ends, and solder one end onto the "Vin (−)" port of the BuckPuck AC Driver. Insert the other end into the "GND" port on the Arduino™ Uno microcontroller.
10. Cut the Lexan™ plexiglass to the dimensions of the project enclosure box, and glue the Plexiglass to the top of the box using silicone glue.

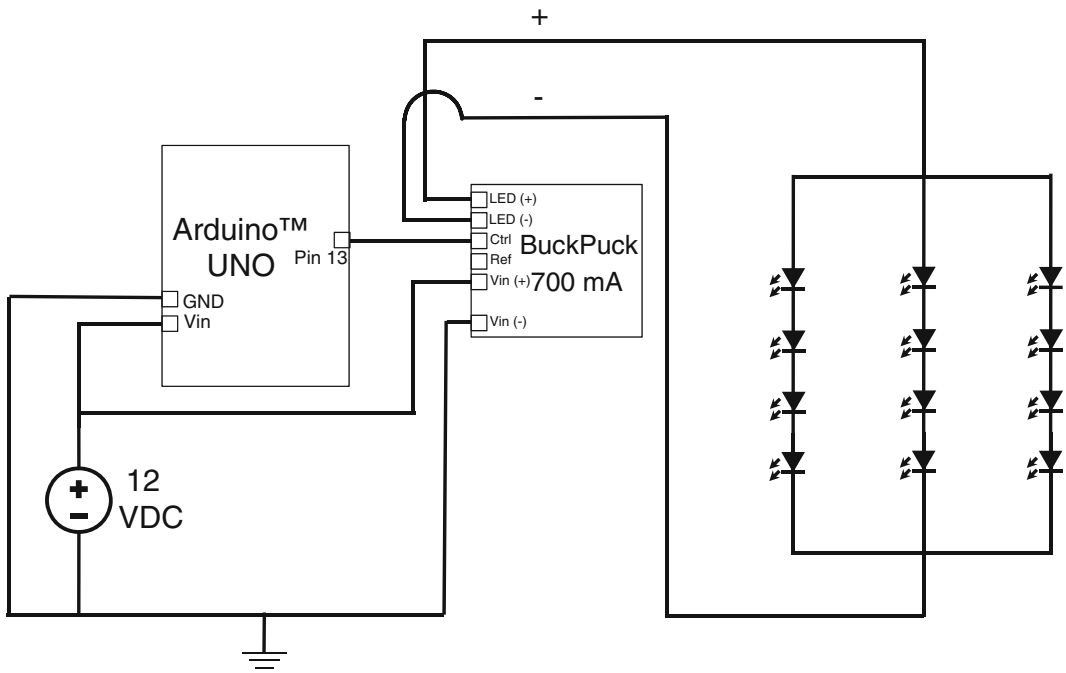

Fig. 2 Circuit diagram for a custom 3 × 4 LED array controlled by an Arduino UNO® microcontroller

11. To program the LED array, download the Arduino™ coding software (available free for download at http://arduino.cc/en/main/software). Design a computer code that will pulse the LED array as desired (*see* **Note 12**). Install the LED code onto the Arduino™ UNO Microcontroller by connecting the Arduino™ board to the computer via a USB cable and following the manufacturer's uploading instructions.
12. To use the LED array, disconnect the Arduino™ UNO microcontroller from the computer. Place the LED array inside the incubator and run the wires connected to the male wire connector out through the incubator's port (usually located in the back wall of the incubator with a plug—ensure the plug is reinserted into the incubator port to maintain environmental conditions). Place the Arduino™ UNO microcontroller and BuckPuck AC Driver outside of the incubator. Insert the male wire connector into the female wire connector, and plug the 12 VDC, 1.0 A power supply into the Arduino™ UNO microcontroller power port. Plug the other end of the power supply into an electrical outlet. The programmed code should now run on the LED array.

3.4 Measurement of LITEZ Activity

1. The day before transfection (Day 0), seed cells into wells of 2 × 24-well plates such that confluency will be ~80 % in 24 h. If using HeLa cells, seed 160,000 cells/well. Make sure to seed and incubate cells in medium that does not contain antibiotic; presence of antibiotic during transfection will decrease transfection efficiency and cell viability.

2. The next day (Day 1), transfect cells according to the transfection reagent manufacturer's instructions. We transfected each well of HeLa cells using 2 μl of Lipofectamine 2000 reagent and 800 ng total plasmid DNA in 100 μl OptiMEM Reduced Serum Medium. Conditions that should be included are as follows:
   (a) Control 1: mock transfected cells (cells that receive no plasmid or an "empty" expression plasmid).
   (b) Control 2: reporter construct only (*see* **Note 13**).
   (c) Control 3: reporter construct + pcDNA3-LOV-VP16.
   (d) Control 4: reporter construct + pcDNA3-GI-ZFP (*see* **Note 14**).
   (e) Experimental sample: reporter construct + pcDNA3-LOV-VP16 + pcDNA3-GI-ZFP (*see* **Note 15**).
3. Wrap both plates in aluminum foil to shield cells from exposure to light.
4. Exchange the media containing transfection reagent with fresh media 4–6 h post-transfection (cells can now be incubated in media that contains antibiotic). While this media change is not necessary for some cell types, other cell types will die if left overnight in the transfection reagent-containing medium. Make sure to work with cells under a dim red safelight so as to avoid activating the LITEZ system during cell manipulation.
5. Wrap one plate in foil and return to the incubator. Place the other plate on top of the upward-facing LED array (Fig. 3).

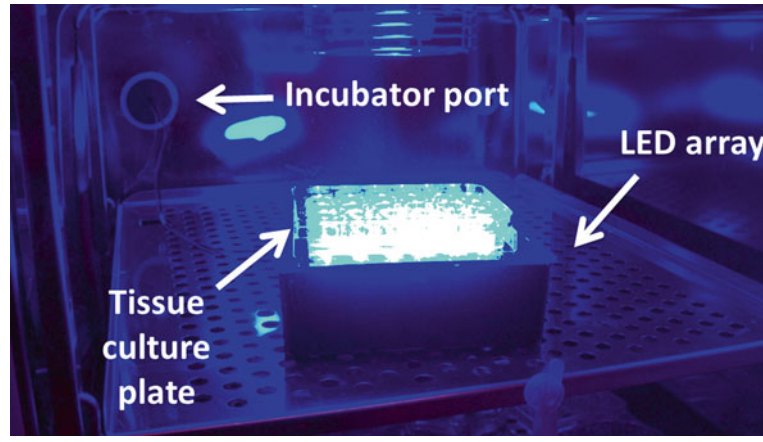

Fig. 3 Illumination of cells inside an incubator. A 24-well plate containing cells transfected with the LITEZ system was placed atop an upward-facing LED array inside an incubator. The wire extension connected to the male wire connector was connected through the back of the incubator via the incubator port. The male wire connector was then plugged into the female wire connector outside of the incubator

We typically wait 12–24 h after transfection to achieve stable protein expression levels and then turn on the LED array to initiate blue light-induced activation of the luciferase reporter gene (*see* **Note 16**).

6. Measure luciferase activity at desired time points using a luciferase assay kit, such as the Promega Bright-Glo Luciferase Assay System, according to the manufacturer's instructions. Compare luciferase activity between cells that received illumination to cells that did not receive illumination, as well as between the different control and sample conditions.

3.5 Patterning Gene Expression Using LITEZ

1. Amplify the cDNA of GFP using the GFP fwd and GFP rev primers (*see* **Note 17**).
2. Isolate the PCR product via gel electrophoresis and subsequent column purification using the QIAquick Gel Extraction kit.
3. Digest the purified PCR product and the reporter plasmid with restriction endonucleases *Nco*I and *Xba*I. Also add the appropriate amount of CIP to the digestion reaction containing the reporter plasmid (we use 1 μl in 50 μl total volume). Allow the digestion to proceed for 1–3 h.
4. Isolate the 3,366 base-pair digestion product via gel electrophoresis and subsequent column purification using the QIAquick Gel Extraction kit. Purify the PCR digest reaction using the QIAquick PCR Purification kit.
5. Ligate the purified PCR digestion product into the purified reporter construct digestion product using T4 DNA Ligase. Incubate at room temperature for 1 h or overnight.
6. Repeat Subheading 3.1, **steps 5–8**.
7. Verify the new construct by sequencing with the hCMV fwd primer.
8. The day before transfection (Day 0), seed cells into glass-bottom 35 mm dishes such that confluency will be ~80 % in 24 h. If using HE293T cells, seed 1.8×10^6 cells/dish. Make sure to seed and incubate cells in media that does not contain antibiotic; presence of antibiotic during transfection will decrease transfection efficiency and cell viability (*see* **Note 18**).
9. The next day (Day 1), transfect cells according to the transfection reagent manufacturer's instructions. We transfected each dish of HEK293T cells using 10 μl of Lipofectamine 2000 reagent and 2 μg total plasmid DNA in 250 μl OptiMEM Reduced Serum Medium. We transfected cells with 200, 120, 120, 120, and 1,440 ng of reporter plasmid, LOV-VP16, GI-ZFP, hUbC-dsRed, and empty plasmid, respectively.
10. Wrap dish in aluminum foil to shield cells from exposure to light.

11. Exchange the media containing transfection reagent with fresh media 4–6 h post-transfection (cells can now be incubated in media that contains antibiotic). Make sure to work with cells under a dim red safelight so as to avoid activating the LITEZ system during cell manipulation.
12. Cover the sides and top of the dish with black electrical tape to prevent light from illuminating cells through the sides and top of the dish (cells should only be able to be illuminated by light passing up through the photomask at the bottom of the dish). Place the dish on top of the photomask. The tape can also be used to secure the plate onto the photomask. Place the plate and photomask on top of the upward-facing LED array, and turn on the LED array 12–24 h after transfection to initiate blue light-induced activation of the GFP reporter gene.
13. To image patterned GFP expression, remove dish at desired time point. Carefully rinse cells 2× with PBS, and then fix cells in 4 % PFA for 10 min.
14. Rinse cells 2× with PBS and image using a fluorescence microscope. Compare dsRed and GFP expression levels; while all transfected cells should express dsRed, only the cells illuminated through the photomask should express GFP (Fig. 4). We acquired images using the scan and stitch feature of the Zeiss Axio Observer Z1 fluorescence microscope (5× magnification). Images were analyzed using ImageJ software.

4 Notes

1. One easy way to ensure this is to first perform the cloning procedure in silico using software such as SerialCloner®; if the cloning process causes the ZFP to be out of frame, add one or two base pairs to correct the frame.
2. The NotI-ZFP fwd primer contains three random base pairs followed by the *Not*I restriction enzyme recognition site. The first three base pairs enable the *Not*I restriction enzyme to bind the DNA and cleave at the restriction site.
3. The XbaI-ZFP rev primer contains one random base pair followed by the *Xba*I restriction site. Unlike *Not*I, *Xba*I only requires one extra base pair to achieve acceptable DNA cleavage efficiency. Information on how many base pairs different restriction endonucleases require upstream of their target site for efficient DNA cleavage can be found at: https://www.neb.com/tools-and-resources/usage-guidelines/cleavage-close-to-the-end-of-dna-fragments.
4. Chemically competent Stbl3 *E. coli* have been engineered for reduced recombination in the presence of direct repeat

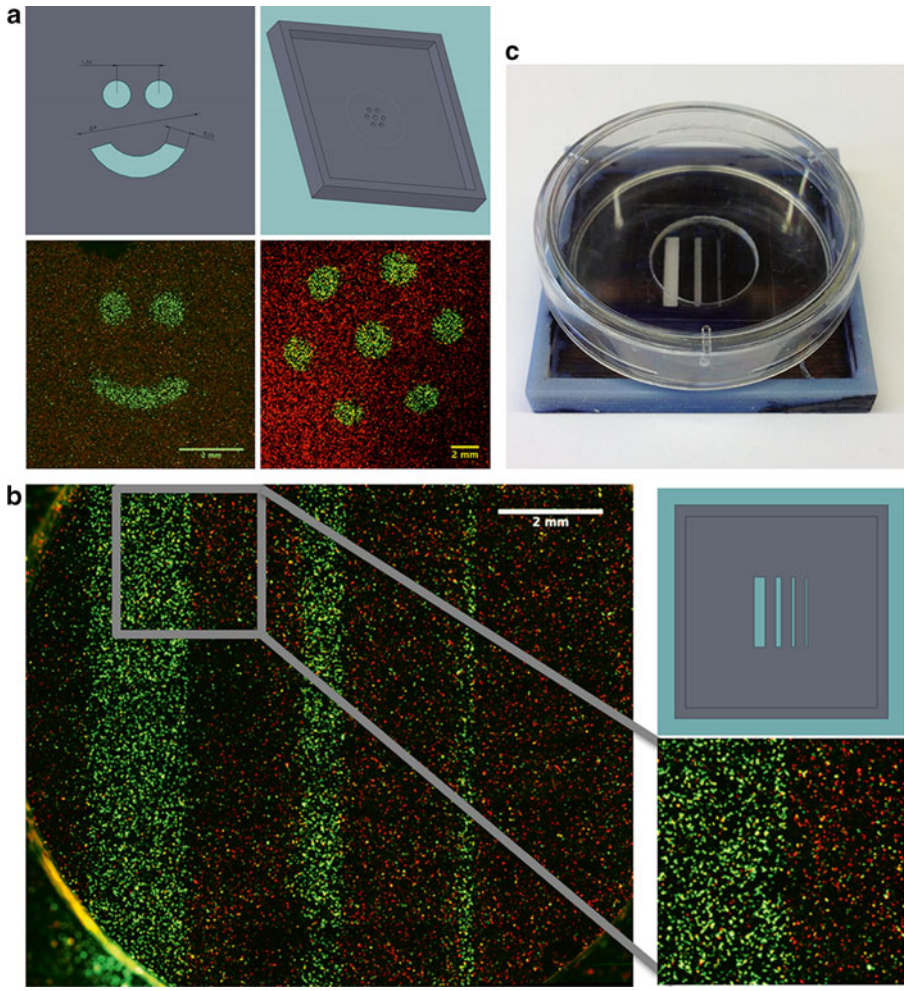

Fig. 4 Patterned green fluorescent protein (GFP) expression using LITEZ. (**a**) HEK293T cells were illuminated with blue light through a photomask in the shape of a happy face or dot array pattern. *Top* two images show the AutoCAD® images used to design and fabricate the photomasks using a 3D printer. *Bottom* two images show resulting pattern of GFP-expressing cells when illuminated through the corresponding photomask. All cells were transfected with a plasmid that constitutively expressed dsRed. (**b**) HEK293T cells were illuminated through a photomask containing slits with widths of 2, 1, 0.5, and 0.3 mm. Features as small as 0.5 mm were readily achievable. *Inset* (**b**, *lower right*) shows the sharp contrast of GFP-positive and -negative cells at the border of the 2 mm slit. (**c**) Photograph of a glass-bottom 35 mm dish on top of the photomask containing slits of various widths. The photomasks were painted black to decrease reflectance. Reprinted with permission from ref. 23. Copyright 2012 American Chemical Society

sequences, such as those found in ZFPs or in promoter sequences containing multiple copies of a DNA-binding protein's target site (i.e., pGL3-Basic-9xSeq2-Luc).

5. While it is highly recommended that the entire GI-ZFP gene is sequenced for clone verification, only the GI fwd 5 primer is necessary to verify the sequence of the inserted ZFP gene.

6. Greater number of ZFP binding sites in the reporter plasmid will increase the level of gene expression when the system is activated by blue light [23]. If it is desired to have more than three GI-ZFP binding sites in the reporter plasmid, perform a PCR reaction using the following primers:

   GI-ZFP binding fwd: 5′-gaggagctcgag$(N)_n$gtcgag$(N)_n$gtcgag $(N)_n$gtcgag$(N)_n$a-3′.

   GI-ZFP binding rev: 5′-ctcctcagatct$(N')_n$ctcgac$(N')_n$ctcgac $(N')_n$ctcgac$(N')_n$ctc-3′.

   GI-ZFP outside PCR fwd: 5′-gaggagctcgag$N_1N_2N_3N_4N_5$-3′, where N_i is the *i*th base pair of the GI-ZFP forward binding sequence, starting from the 5′ end.

   GI-ZFP outside PCR rev: 5′-ctcctcagatct$N'_1N'_2N'_3N'_4N'_5$-3′, where N'_i is the *i*th base pair of the sequence antiparallel to the GI-ZFP binding sequence, starting from the 3′ end.

   Perform PCR using 0.1 μl of each of the four primers listed above. This PCR step will create double-stranded oligonucleotides of different lengths due to misannealing of the GI-ZFP binding fwd and GI-ZFP binding rev primers. Purify the PCR reaction using a PCR purification kit. Digest the purified PCR product with *Xho*I and *Bgl*II, purify the digestion product using a PCR purification kit, and then ligate this product into the purified pGL3-Basic-9xSeq2-Luc digestion product from **step 2**. Screen clones by sequencing until a clone containing the desired number of binding sites is found. This protocol should yield clones containing up to nine GI-ZFP binding sites (we found one clone containing nine binding sites and another clone containing seven binding sites by screening about 25 clones by colony PCR [43]).

   Alternatively, commercial gene synthesis can be used to generate the desired insert of DNA-binding sites.

7. We used Blue Rebel LEDs centered on a wavelength of 470 nm that were pre-soldered to a Saber 10 mm square base (Luxeon® Star LEDs). LOV domains typically have a relatively broad absorbance spectrum around 450 nm [44, 45], so an LED of the exact 450 nm wavelength is not required. We have achieved similar levels of activation using LEDs centered at 447.5 and 470 nm.

8. Cells expressing the LITEZ constructs must be manipulated under a red "safelight." Working with cells under white light may activate the system. Red and blue light are at opposite ends of the visible light spectrum, and so red light will not induce GI/LOV binding.

9. The photomask can be made using a 3D printer (Fig. 4) or simply by cutting a pattern out of foil or other opaque material.

For precision and repeatability between experiments, a 3D printer or other method for automated photomask fabrication is preferred.

10. When setting up the ligation reaction, add the PCR insert and pcDNA3-GI-ZFP backbone to the reaction in a 3:1 (insert:backbone) molar ratio. If cloning fails, it is likely that the Ligase Buffer was not fresh; obtain fresh buffer and try the reaction again. If cloning still fails, increase the insert: backbone ratio to 5:1 or more.
11. Alternatively, the annealing reaction can be placed in a heat block at 90–95 °C for 3–5 min. After heating, turn off the heat block and allow the sample to cool to room temperature in the heat block.
12. For assistance writing a computer code, there are free sample codes on the Arduino™ website designed for controlling LEDs. Furthermore, the code used to control the LITEZ system can be obtained from the authors upon request; in our published experiments we used a code that pulses the light for 3 s every 3 min [23].
13. This sample is important because it reveals the background expression of luciferase from the reporter construct alone. To facilitate comparison across all samples, make sure to keep the total amount of transfected DNA constant across all samples; thus, if samples that receive only reporter construct will be transfected with 80 ng of the reporter, make sure to also transfect this "reporter only" sample with 720 ng of "empty" expression plasmid DNA.
14. Controls three and four reveal activation of the reporter by the GI-ZFP or LOV-VP16 alone. There should not be any significant activation of the reporter in these samples when compared to cells that only received the reporter construct.
15. It may be necessary to optimize the ratio of transfected reporter construct, pcDNA3-LOV-VP16, and pcDNA3-GI-ZFP for different cell lines. In HeLa cells, we found that a ratio of 1:1:3 (reporter construct:pcDNA3-LOV-VP16:pcDNA3-GI-ZFP) was optimal.
16. In the original LITEZ manuscript [23], the LED array was set to pulse "on" for 3 s every 3 min. This illumination regimen may require optimization for different cell types, GI-ZFPs, and applications.
17. Genes other than GFP can be used to pattern gene expression as long as the gene product can be visually imaged by microscopy or immunofluorescence staining. Other example reporter genes include *beta-galactosidase*, *alkaline phosphatase*, and fluorescent proteins other than GFP.

18. To increase resolution of activated and nonactivated cells at the borders of the pattern, perform the experiment using media that does not contain phenol red or other colorimetric pH indicator; light will diffract less in clear media.

Acknowledgments

Ricardo E. Dolmetsch provided the original GI and LOV-VP16 plasmid constructs and Carlos F. Barbas, III provided ZFP constructs used to characterize the original LITEZ system. Graeme O'Connell and Chandra Tucker assisted in the design and programming of the custom LED array. This research was funded by an NSF CAREER Award (CBET-1151035), NIH Director's New Innovator Award (1DP2-OD008586), NIH 1R01-DA036865, and a Ralph E. Powe Junior Faculty Enhancement Award from Oak Ridge Associated Universities. L.R.P. was supported by an NIH Biotechnology Training Grant to the Duke Center for Biomolecular and Tissue Engineering (T32GM008555) and the Duke Biomedical Engineering McChesney Fellowship.

References

1. Gossen MFS, Bender G, Muller G, Hillen W, Bujard H (1995) Transcriptional activation by tetracyclines in mammalian cells. Science 268(5218):1766–1769
2. No D, Yao TP, Evans RM (1996) Ecdysone-inducible gene expression in mammalian cells and transgenic mice. Proc Natl Acad Sci U S A 93(8):3346–3351
3. Rivera VM, Clackson T, Natesan S, Pollock R, Amara JF, Keenan T, Magari SR, Phillips T, Courage NL, Cerasoli F Jr, Holt DA, Gilman M (1996) A humanized system for pharmacologic control of gene expression. Nat Med 2(9):1028–1032
4. Beerli RR, Schopfer U, Dreier B, Barbas CF 3rd (2000) Chemically regulated zinc finger transcription factors. J Biol Chem 275(42):32617–32627. doi:10.1074/jbc.M005108200
5. Fussenegger M, Morris RP, Fux C, Rimann M, von Stockar B, Thompson CJ, Bailey JE (2000) Streptogramin-based gene regulation systems for mammalian cells. Nat Biotechnol 18(11):1203–1208. doi:10.1038/81208
6. Weber W, Fux C, Daoud-el Baba M, Keller B, Weber CC, Kramer BP, Heinzen C, Aubel D, Bailey JE, Fussenegger M (2002) Macrolide-based transgene control in mammalian cells and mice. Nat Biotechnol 20(9):901–907. doi:10.1038/nbt731
7. Dent CL, Lau G, Drake EA, Yoon A, Case CC, Gregory PD (2007) Regulation of endogenous gene expression using small molecule-controlled engineered zinc-finger protein transcription factors. Gene Ther 14(18):1362–1369. doi:10.1038/sj.gt.3302985
8. Magnenat L, Schwimmer LJ, Barbas CF 3rd (2008) Drug-inducible and simultaneous regulation of endogenous genes by single-chain nuclear receptor-based zinc-finger transcription factor gene switches. Gene Ther 15(17):1223–1232. doi:gt200896 [pii] 10.1038/gt.2008.96
9. Schwimmer LJ, Gonzalez B, Barbas CF 3rd (2012) Benzoate X receptor zinc-finger gene switches for drug-inducible regulation of transcription. Gene Ther 19(4):458–462. doi:10.1038/gt.2011.112
10. Pathak GP, Vrana JD, Tucker CL (2013) Optogenetic control of cell function using engineered photoreceptors. Biol Cell 105(2):59–72. doi:10.1111/boc.201200056
11. Muller K, Weber W (2013) Optogenetic tools for mammalian systems. Mol Biosyst 9(4):596–608. doi:10.1039/c3mb25590e
12. Yazawa M, Sadaghiani AM, Hsueh B, Dolmetsch RE (2009) Induction of protein–protein interactions in live cells using light. Nat Biotechnol 27(10):941–945, http://www.nature.com/nbt/journal/v27/n10/suppinfo/nbt.1569_S1.html

13. Kennedy MJ, Hughes RM, Peteya LA, Schwartz JW, Ehlers MD, Tucker CL (2010) Rapid blue-light-mediated induction of protein interactions in living cells. Nat Methods 7(12):973–975, http://www.nature.com/nmeth/journal/v7/n12/abs/nmeth.1524.html—supplementary-information
14. Ye H, Baba MD-E, Peng R-W, Fussenegger M (2011) A synthetic optogenetic transcription device enhances blood-glucose homeostasis in mice. Science 332(6037):1565–1568. doi:10.1126/science.1203535
15. Ohlendorf R, Vidavski RR, Eldar A, Moffat K, Moglich A (2012) From dusk till dawn: one-plasmid systems for light-regulated gene expression. J Mol Biol 416(4):534–542. doi:10.1016/j.jmb.2012.01.001
16. Wang X, Chen X, Yang Y (2012) Spatiotemporal control of gene expression by a light-switchable transgene system. Nat Methods 9(3):266–269, http://www.nature.com/nmeth/journal/v9/n3/abs/nmeth.1892.html—supplementary-information
17. Konermann S, Brigham MD, Trevino AE, Hsu PD, Heidenreich M, Cong L, Platt RJ, Scott DA, Church GM, Zhang F (2013) Optical control of mammalian endogenous transcription and epigenetic states. Nature 500(7463):472–476
18. Shimizu-Sato S, Huq E, Tepperman JM, Quail PH (2002) A light-switchable gene promoter system. Nat Biotechnol 20(10):1041–1044
19. Levskaya A, Lim WA, Voigt CA, Weiner OD (2009) Spatiotemporal control of cell signalling using a light-switchable protein interaction. Nature 461(7266):997–1001
20. Muller K, Engesser R, Metzger S, Schulz S, Kampf MM, Busacker M, Steinberg T, Tomakidi P, Ehrbar M, Nagy F, Timmer J, Zubriggen MD, Weber W (2013) A red/far-red light-responsive bi-stable toggle switch to control gene expression in mammalian cells. Nucleic Acids Res 41(7):e77. doi:10.1093/nar/gkt002
21. Beerli RR, Dreier B, Barbas CF 3rd (2000) Positive and negative regulation of endogenous genes by designed transcription factors. Proc Natl Acad Sci U S A 97(4):1495–1500. doi:10.1073/pnas.040552697 040552697 [pii]
22. Beerli RR, Segal DJ, Dreier B, Barbas CF 3rd (1998) Toward controlling gene expression at will: specific regulation of the erbB-2/HER-2 promoter by using polydactyl zinc finger proteins constructed from modular building blocks. Proc Natl Acad Sci U S A 95(25): 14628–14633
23. Polstein LR, Gersbach CA (2012) Light-inducible spatiotemporal control of gene activation by customizable zinc finger transcription factors. J Am Chem Soc 134(40):16480–16483. doi:10.1021/ja3065667
24. Yazawa M, Sadaghiani AM, Hsueh B, Dolmetsch RE (2009) Induction of protein–protein interactions in live cells using light. Nat Biotechnol 27(10):941–945. doi:nbt.1569 [pii] 10.1038/nbt.1569
25. Pabo CO, Peisach E, Grant RA (2001) Design and selection of novel Cys2His2 zinc finger proteins. Annu Rev Biochem 70:313–340. doi:70/1/313 [pii] 10.1146/annurev.biochem.70.1.313
26. Beerli RR, Barbas CF 3rd (2002) Engineering polydactyl zinc-finger transcription factors. Nat Biotechnol 20(2):135–141. doi:10.1038/nbt0202-135
27. Maeder ML, Thibodeau-Beganny S, Osiak A, Wright DA, Anthony RM, Eichtinger M, Jiang T, Foley JE, Winfrey RJ, Townsend JA, Unger-Wallace E, Sander JD, Muller-Lerch F, Fu F, Pearlberg J, Gobel C, Dassie JP, Pruett-Miller SM, Porteus MH, Sgroi DC, Iafrate AJ, Dobbs D, McCray PB Jr, Cathomen T, Voytas DF, Joung JK (2008) Rapid "open-source" engineering of customized zinc-finger nucleases for highly efficient gene modification. Mol Cell 31(2): 294–301. doi:10.1016/j.molcel.2008.06.016
28. Sander JD, Dahlborg EJ, Goodwin MJ, Cade L, Zhang F, Cifuentes D, Curtin SJ, Blackburn JS, Thibodeau-Beganny S, Qi Y, Pierick CJ, Hoffman E, Maeder ML, Khayter C, Reyon D, Dobbs D, Langenau DM, Stupar RM, Giraldez AJ, Voytas DF, Peterson RT, Yeh JR, Joung JK (2011) Selection-free zinc-finger-nuclease engineering by context-dependent assembly (CoDA). Nat Methods 8(1):67–69. doi:10.1038/nmeth.1542
29. Gonzalez B, Schwimmer LJ, Fuller RP, Ye Y, Asawapornmongkol L, Barbas CF 3rd (2010) Modular system for the construction of zinc-finger libraries and proteins. Nat Protoc 5(4):791–810. doi:10.1038/nprot.2010.34
30. Carroll D, Morton JJ, Beumer KJ, Segal DJ (2006) Design, construction and in vitro testing of zinc finger nucleases. Nat Protoc 1(3):1329–1341. doi:nprot.2006.231 [pii] 10.1038/nprot.2006.231
31. Gupta A, Christensen RG, Rayla AL, Lakshmanan A, Stormo GD, Wolfe SA (2012) An optimized two-finger archive for ZFN-mediated gene targeting. Nat Methods 9(6):588–590. doi:10.1038/nmeth.1994
32. Bhakta MS, Segal DJ (2010) The generation of zinc finger proteins by modular assembly. Methods Mol Biol 649:3–30. doi:10.1007/978-1-60761-753-2_1

33. Bhakta MS, Henry IM, Ousterout DG, Das KT, Lockwood SH, Meckler JF, Wallen MC, Zykovich A, Yu Y, Leo H, Xu L, Gersbach CA, Segal DJ (2013) Highly active zinc-finger nucleases by extended modular assembly. Genome Res 23(3):530–538. doi:10.1101/gr.143693.112
34. Thibodeau-Beganny S, Maeder ML, Joung JK (2010) Engineering single Cys2His2 zinc finger domains using a bacterial cell-based two-hybrid selection system. Methods Mol Biol 649:31–50. doi:10.1007/978-1-60761-753-2_2
35. Zhu C, Gupta A, Hall VL, Rayla AL, Christensen RG, Dake B, Lakshmanan A, Kuperwasser C, Stormo GD, Wolfe SA (2013) Using defined finger-finger interfaces as units of assembly for constructing zinc-finger nucleases. Nucleic Acids Res 41(4):2455–2465. doi:10.1093/nar/gks1357
36. Perez-Pinera P, Ousterout DG, Brown MT, Gersbach CA (2012) Gene targeting to the ROSA26 locus directed by engineered zinc finger nucleases. Nucleic Acids Res 40(8):3741–3752. doi:gkr1214 [pii] 10.1093/nar/gkr1214
37. Perez-Pinera P, Ousterout DG, Gersbach CA (2012) Advances in targeted genome editing. Curr Opin Chem Biol 16(3–4):268–277. doi:S1367-5931(12)00076-2 [pii] 10.1016/j.cbpa.2012.06.007
38. Sander JD, Yeh JR, Peterson RT, Joung JK (2011) Engineering zinc finger nucleases for targeted mutagenesis of zebrafish. Methods Cell Biol 104:51–58. doi:10.1016/B978-0-12-374814-0.00003-3
39. Mandell JG, Barbas CF 3rd (2006) Zinc Finger Tools: custom DNA-binding domains for transcription factors and nucleases. Nucleic Acids Res 34(Web Server issue):W516–W523. doi:34/suppl_2/W516 [pii] 10.1093/nar/gkl209
40. Sander JD, Maeder ML, Reyon D, Voytas DF, Joung JK, Dobbs D (2010) ZiFiT (Zinc Finger Targeter): an updated zinc finger engineering tool. Nucleic Acids Res 38 (Web Server issue):W462–W468. doi:10.1093/nar/gkq319
41. Fu F, Sander JD, Maeder M, Thibodeau-Beganny S, Joung JK, Dobbs D, Miller L, Voytas DF (2009) Zinc Finger Database (ZiFDB): a repository for information on C2H2 zinc fingers and engineered zinc-finger arrays. Nucleic Acids Res 37(Database issue):D279–D283. doi:gkn606 [pii] 10.1093/nar/gkn606
42. Engineered Zinc Finger Proteins (2010) Methods in Molecular Biology. 649
43. Packeiser H, Lim C, Balagurunathan B, Wu J, Zhao H (2013) An extremely simple and effective colony PCR procedure for bacteria, yeasts, and microalgae. Appl Biochem Biotechnol 169(2):695–700. doi:10.1007/s12010-012-0043-8
44. Kasahara M, Swartz TE, Olney MA, Onodera A, Mochizuki N, Fukuzawa H, Asamizu E, Tabata S, Kanegae H, Takano M, Christie JM, Nagatani A, Briggs WR (2002) Photochemical properties of the flavin mononucleotide-binding domains of the phototropins from Arabidopsis, rice, and Chlamydomonas reinhardtii. Plant Physiol 129(2):762–773. doi:10.1104/pp. 002410
45. Nash AI, McNulty R, Shillito ME, Swartz TE, Bogomolni RA, Luecke H, Gardner KH (2011) Structural basis of photosensitivity in a bacterial light-oxygen-voltage/helix-turn-helix (LOV-HTH) DNA-binding protein. Proc Natl Acad Sci U S A 108(23):9449–9454. doi:10.1073/pnas.1100262108

Chapter 8

Manipulation of Plasma Membrane Phosphoinositides Using Photoinduced Protein–Protein Interactions

Olof Idevall-Hagren and Pietro DeCamilli

Abstract

Phosphoinositides, the phosphorylated products of inositol phospholipids, play critical regulatory roles in cell physiology. The elucidation of their functions will greatly benefit from the methodology to manipulate their local concentrations within membranes with high spatial and temporal precision. Recently developed genetically encoded and light-regulated dimerization modules, in combination with the use of fluorescence-tagged lipid-binding domains and live-cell imaging, provide an attractive means to achieve this goal. Here we describe a protocol for blue light-dependent conversion of one phosphoinositide species into another based on the light-regulated dimerization between cryptochrome 2 (CRY2) and its ligand, CIB1. We describe the development of these tools using the dephosphorylation of plasma membrane phosphatidylinositol 4,5-bisphosphate (PI(4,5)P2) as an example and show how they can be used to rapidly and reversibly deplete the plasma membrane of this lipid. We also provide instructions for image analysis. The CRY2–CIB1 dimerization method has also already been adapted for the acute and spatially restricted generation of PI(3,4,5)P_3 in the plasma membrane. More generally, this methodology should be broadly applicable to studies of the spatiotemporal regulation of membrane lipid metabolism in many types of cells.

Key words Optogenetics, Cryptochrome, Lipids, Phosphatidylinositol, Inositol 5-phosphatase, PI 3-kinase, Total internal reflection fluorescence microscopy, Confocal microscopy, Rapamycin

1 Introduction

Phosphoinositides (PIs) are the signalling membrane phospholipids that derive from the phosphorylation of phosphatidylinositol on the inositol group. Phosphatidylinositol is synthesized in the ER and is then distributed to all other membranes of the secretory and endocytic pathway and to the plasma membrane, where it undergoes reversible phosphorylation on the 3, 4, and 5 positions to generate seven different PIs. The heterogeneous distribution and abundance of each of the PIs in various membranes, and in specific microdomains within membranes, help control organelle identity and function [1–4]. The generation, interconversion, and degradation of the different PI species are the result of the consorted action

Sidney Cambridge (ed.), *Photoswitching Proteins: Methods and Protocols*, Methods in Molecular Biology, vol. 1148,
DOI 10.1007/978-1-4939-0470-9_8,

of inositol kinases and phosphatases as well as phospholipases. These are cytosolic enzymes that translocate to cellular membranes or specific microdomains within membranes in response to specific cues. Such regulation may occur very rapidly and can result in ten-fold concentration changes of a specific PI within seconds. For this reason, measurements and manipulations of these lipids aimed at elucidating their functions should ideally be achieved with high spatial and temporal control. Biochemical detection techniques based on radiotracer labelling, chromatography, or mass spectrometry yield quantitative information and can be optimized to distinguish between all different PI isomers. However, these methods have important limitations: large numbers of cells are required to obtain a sufficient signal and repeated measurements cannot be made from the same sample [5]. In addition no spatial resolution can be achieved. These shortcomings preclude the detection of compartmentalized signals, short-lasting transients, oscillations, and other complex time courses that characterize many signalling systems.

During the last decade, the development of genetically encoded fluorescence biosensors for single-cell detection of PIs has greatly improved our understanding of PI lipid signalling. These sensors comprise fluorescent proteins fused to protein modules with specific PI binding properties. Analysis of fluorescent reporter protein localization and stimulus-induced translocation provides information about the intracellular distribution and changes in relative levels of a particular lipid [6]. However, in order to understand the role of specific PIs in the regulation of cell function, it is imperative to be able to manipulate their levels. To date, most studies on PI functions have relied on pharmacological or genetic perturbations of the enzymes responsible for PI synthesis or degradation. Although powerful, both these techniques have certain limitations. Small-molecule inhibitors only exist for a few of the PI-metabolizing enzymes, and off-target effects cannot be excluded. Genetic manipulations, such as knockout, knockdown, and overexpression, involve long-term changes that may result in adaptive changes in lipid levels that can complicate the interpretation of an experiment. More recently, methods that rely on chemicals to acutely induce protein dimerization have been developed. Fusing a PI-metabolizing enzyme module to FKBP and a membrane-targeting signal to FRB allows control of enzyme recruitment to a specific membrane upon addition of the drug rapamycin, which induces dimerization of FKBP and FRB [7, 8]. This approach, although very powerful, has some limitations, such as the requirement of a cofactor (rapamycin or rapalogues) and the irreversible nature of the dimerization. Moreover, this technique makes manipulations at the single-cell or subcellular level difficult, although still possible [9]. To address these shortcomings, dimerization systems controlled by light instead of chemicals have been developed and to date there exist at least four such systems: PhyB–PIF, GIGANTEA–FKF1, cryptochrome 2 (CRY2)–CIB1, and AsLOV2 (*see* Table 1) [10–14].

Table 1
Properties of light-inducible dimerization systems

System	Motif size (aa)	Light sensor	Bait	Association kinetics	Dissociation kinetics	Activation light	Fluorophore compatibility	Reference
FKF1-GIGANTEA	619 + 1173	N-term	N-term	Min	Irreversible	405 nm	GFP, YFP, RFP, iRFP	[10]
CRY2–CIB1	612 + 335	N/C-term	N-term	<5 s	5–10 min in the dark	405–488	YFP, RFP, iRFP	[12, 15]
PhyB–PIF6	650 + 100	N-term	C-term	<5 s	<10 s at 750 nm	650	BFP, CFP, YFP, GFP, RFP	[11]
LOV domains	~140	C-term	N/A	<5 s	<10 s at 568–640 nm	458	RFP, iRFP	[13]

The table shows properties of the four most commonly used light-inducible dimerization/activation systems. Motif size indicates length of components in number of amino acids. Light sensor indicates where in the fusion protein the light sensor must be located (N- or C-terminal). Bait indicates where in the fusion protein the bait must be located (N- or C-terminal). Association kinetics indicates the time required for saturated dimerization/activation to occur when illuminated with light of the optimal wavelength. Dissociation kinetics indicates the reversibility of the reaction. Fluorophore compatibility lists commonly used fluorescent proteins that are compatible with the dimerization system (i.e., can be visualized without inducing dimerization or activation)

Properties that vary amongst the different light-dependent dimerization systems may be of importance for their successful application. Such properties include dimerization module size and orientation, wavelength of activation light, absorption spectrum of the photochrome, and on/off kinetic characteristics of the dimerization pair (*see* Table 1 for a non-exhausting list of dimerization pairs and their properties).

We have used, and described here, the minimal interaction modules of the CRY2–CIB1 system, referred to henceforth as CRY2–CIBN, because of their relative small size and of their absorption spectrum that allows induction of dimerization by visible light (405–488 nm) using lasers typically found on most standard fluorescence microscopes [12, 15]. The dimerization is also spontaneously reversible upon interruption of blue light illumination, thus helping control the specificity of the physiological effects observed. Additionally, reversibility allows multiple rounds of experiments from the same biological sample, e.g., recruitment in the absence or the presence of a drug. In particular, we focus here on the application of this technique to the acute recruitment of an inositol 5-phosphatase module to the plasma membrane to induce dephosphorylation of PI(4, 5)P_2 and PI(3,4,5)P_3. As we have recently reported, the system allowed the validation of the critical role of these phosphoinositides in endocytosis, actin cytoskeleton dynamics, ion channel permeability, and endoplasmic reticulum–plasma membrane interactions [15]. We have also shown that the CRY2–CIBN dimerization system can be used to recruit endogenous PI3 kinase by blue light illumination to the plasma membrane by fusing CRY2 to a PI3 kinase catalytic subunit-interacting region [15] (*see* Fig. 2b).

2 Materials

2.1 Cell Culture and Transfection

1. Cell culture facility equipped with laminar flow hood.
2. Water bath set to 37 °C.
3. Cell culture incubator (5 % CO_2).
4. Hemocytometer (or similar equipment for cell counting).
5. MatTek dishes (no. 1 or 1.5, MatTek Corp., Ashland, MA).
6. Poly-D-lysine (MW 70,000–150,000): Prepare 2 mg/mL stock solution in sterile water and store at −70 °C. Prepare the working solution at 0.1 mg/mL in sterile water.
7. Cell culture medium: DMEM (4.5 g/L D-glucose), 10 % (vol/vol) heat-inactivated fetal bovine serum, 2 mM L-glutamine. Sterile filter the medium using 0.22 μm pore size (e.g., Stericup Millipore Express Plus 0.22 μm). Store at +4 °C.
8. Sterile PBS.
9. 0.25 % Trypsin–EDTA solution (Life technologies).
10. OptiMEM-I supplemented with 10 % FBS and sterile filtered.

Table 2
Commonly used phosphoinositide-binding protein domains

Phosphoinositide	Domain	Protein	Reference
PI3P	FYVE	Hrs	[17, 18]
	FYVE	EEA1	[18, 19]
PI4P	PH	OSBP	[20]
	PH	Fapp1	[21]
	PH	OSH2	[22]
	P4M	GOLPH3	[23–25]
		DrrA/SidM	
PI5P	PHD	ING2	[26]
$PI(3,4)P_2$	PH	Tapp1	[27]
	PH	P47phox	[28]
	PH	Akt/PKB	[29]
$PI(4,5)P_2$	PH	PLCδ1	[30]
	PX	Tubby	[31]
$PI(3,5)P_2$	PROPPIN	Atg18p	[32]
$PI(3,4,5)P_3$	PH	GRP1	[33]
	PH	Btk	[34]
	PH	ARNO	[35]
	PH	Akt/PKB	[29]

11. For transient transfection of HeLa or COS-7 cells, use Lipofectamine 2000 reagent and OptiMEM I (Life technologies) (*see* **Note 1**). The Lipofectamine 2000 reagent should be mixed gently before use.
12. Plasmid DNA encoding the optogenetic modules and PI biosensors (*see* Table 2).
13. Opaque box where to place the MatTek dishes with transfected cells to avoid exposure to light.

2.2 Fluorescence Microscopy

– Experimental buffer: 125 mM NaCl, 4.9 mM KCl, 1.3 mM $MgCl_2$, 1.2 mM $CaCl_2$, 25 mM HEPES, 3 mM glucose, pH adjusted to 7.40 with 2 M NaOH. Prepared fresh on the day of experiments.

– Spinning disc confocal or total internal reflection fluorescence (TIRF) microscope located in a darkroom: A confocal microscope allows z-direction sectioning and is required for analysis of PI lipids in intracellular organelles, whereas a TIRF microscope is better for imaging the plasma membrane, at least in flat cells.

  • Spinning disc confocal microscope: Systems suitable for live-cell imaging are available from all major microscope manufacturers. We use the Improvision UltraVIEW VoX system from Perkin-Elmer, built around a Nikon Ti-E inverted microscope equipped with PlanApo objectives (60×1.45-NA and 100×1.45-NA) and a fluorescence

recovery after photobleaching (FRAP) module that allows focal illumination.

- TIRF microscope: These microscopes utilize objectives with high NA (>1.4) to generate evanescent wave excitation that selectively illuminates fluorophores close to the interface between cover slip and adherent cell (i.e., the plasma membrane), and they are available from most major microscope manufacturers. We use a setup built around a Nikon TiE microscope provided by Andor technology (Belfast, Northern Ireland).

– Light sources, filters, and wavelength selection:

- Diode-pumped solid-state lasers are common light sources for excitation of fluorescent proteins (available from, e.g., Coherent, Spectraphysics, or Cobolt). CRY2–CIBN dimerization can be induced using a blue light-emitting laser (405–488 nm). We typically use 488 nm. For excitation of fluorophores compatible with CRY2–CIBN (i.e., fluorophores that can be visualized without inducing dimerization; *see* Table 1) we use 561 nm (for mRFP- and mCherry-tagged proteins) and 640 nm (for iRFP-tagged proteins) lasers.
- Appropriate excitation filters are the following: 488 nm/10 nm half bandwidth (for induction of dimerization), 560 nm/20 nm half bandwidth (for mRFP/mCherry excitation), and 630 nm/20 nm half bandwidth (for iRFP excitation). Alternatively, an acousto-optical tunable filter (AOTF) can be used for selection of excitation light. Appropriate emission filters are the following: 625 nm long pass for mRFP/mCherry and 690 nm long pass for iRFP. Filters and mirrors can be obtained from Chroma Technology (Rockingham, VT), Omega Optical (Brattleboro, VT), or Semrock (Rochester, NY). Multichannel recordings will require a filter changer, which can be obtained from, e.g., Sutter Instruments (Novato, CA).
- A sensitive, electron-multiplying charge-coupled device (EM-CCD) camera for spinning disc confocal or TIRF microscopes can be obtained from, e.g., Andor Technology, Hamamatsu, or Roper Scientific.
- Data acquisition and analysis software are usually included with commercial systems. We use the free ImageJ software (http://rsb.info.nih.gov/ij) for off-line analysis (see below).

2.3 Choice of Dimerization Pairs

The protocol described here uses a fusion of the catalytic domain of the human inositol 5-phosphatase OCRL (amino acids 234–539) to the C-terminal side of the PHR domain of *Arabidopsis thaliana* CRY2 (amino acids 1–498 in the full-length protein). The construct is also N-terminally tagged with mCherry for microscopic detection (*see* Fig. 1a for schematic drawing). The catalytic domain of OCRL,

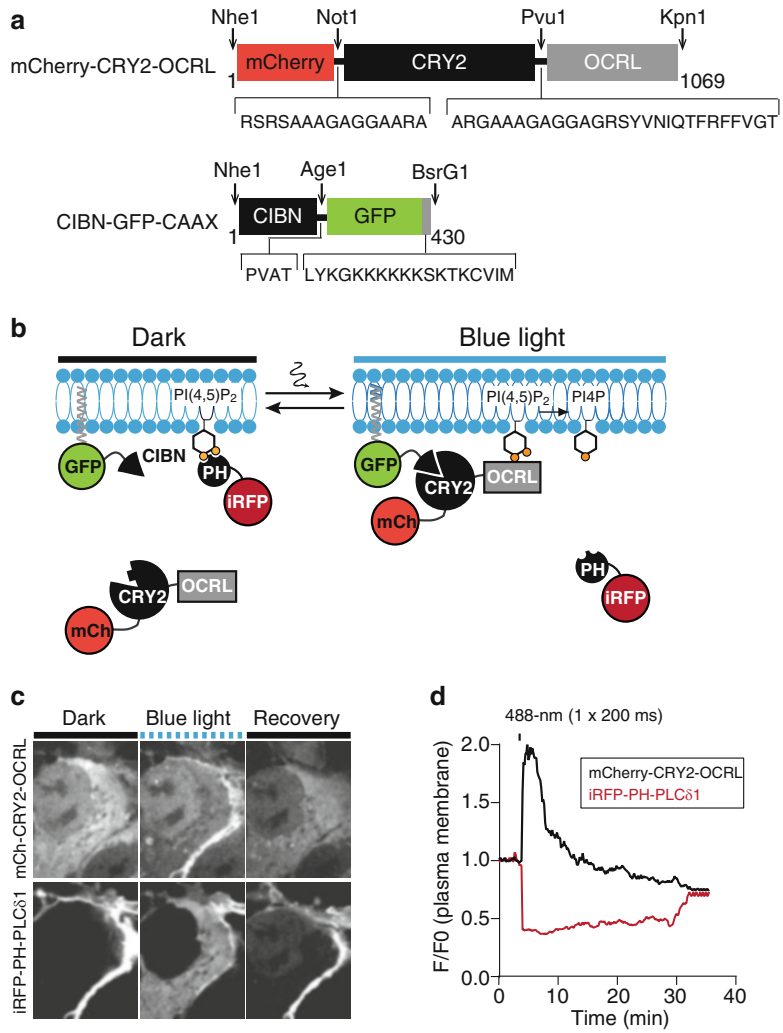

Fig. 1 (**a**) Schematic illustration mCherry-CRY2-OCRL and CIBN-GFP-CAAX showing restriction enzymes used for cloning and size and composition of linker regions between the modules in the fusion proteins. (**b**) Drawing illustrating the principle of blue light-induced dimerization between CRY2 and CIBN for the dephosphorylation of PI(4,5)P_2 at the plasma membrane. (**c**) Confocal micrographs of a COS-7 cell subregion expressing CIBN-GFP-CAAX (not shown), mCherry-CRY2-OCRL (*top row*), and the PI(4,5)P_2 biosensor iRFP-PH-PLCδ1 (*bottom row*). Under basal conditions (no blue light illumination) mCherry-CRY2-OCRL is cytoplasmic and iRFP-PH-PLCδ1 is bound to PI(4,5)P2 at the plasma membrane (*left column*). Upon illumination by a single, 200 ms blue light pulse (*middle column*), mCherry-CRY2-OCRL is activated and binds to CIBN-GFP-CAAX at the plasma membrane where it dephosphorylates PI(4,5)P2 and causes dissociation of iRFP-PH-PLCδ1. Upon interruption of blue light illumination, both reactions are reversed (*right column*). (**d**) Time course of the blue light-induced PI(4,5)P2 dephosphorylation shown in (**b**). Notice the almost identical kinetics of mCherry-CRY2-OCRL and iRFP-PH-PLCδ1 fluorescence changes upon blue light illumination but the much slower reassociation of iRFP-PH-PLCδ1 with the plasma membrane upon interruption of the illumination

which dephosphorylates PI(4, 5)P_2 and PI(3,4,5)P_3 at the 5 position, can easily be replaced by other catalytic domains or proteins of interest using standard molecular biology techniques. As plasma membrane bait for CRY2 we used the N-terminal region of *Arabidopsis thaliana* cryptochrome-interacting basic helix–loop–helix protein 1 (CIBN) with a C-terminal GFP-tag containing the myristoylation motif from KRas (*see* Fig. 1a, b). Similar to the CRY2 fusion, the membrane-targeting motif can be replaced to target CIBN to any membrane of interest. In the dark, the CRY2 fusion protein is cytosolic and the CIBN fusion protein is anchored to the plasma membrane. Upon blue light illumination, CRY2 translocates to the plasma membrane (*see* Fig. 1b). Initially, we explored the possibility of using CRY2 as the membrane bait and CIBN fused to the 5-phosphatase module, but this modality was not efficient in PI(4, 5)P_2 dephosphorylation, possibly due to steric problems at the plasma membrane.

3 Methods

3.1 Preparation of Poly-D-Lysine-Coated Dishes

1. Prepare a 1× (0.01 mg/mL) working solution of poly-D-lysine (PDL) by diluting the 20× stock solution in sterile H_2O.
2. Place a 200 μL drop of PDL in the center of the dish, and leave it for at least 30 min at room temperature.
3. Remove the PDL, and rinse the dish twice with sterile water. It is important not to let the PDL dry on the dish.
4. After the last washing step, remove as much water as possible and allow the dish to dry in a laminar flow bench with the lids of dishes open (*see* **Note 2**). This can be done either just before plating cells or at an earlier time point, as long as the coated dishes are stored at a sterile location.

3.2 Cell Culture and Choice of Cell Lines

We have performed most of our experiments so far in HeLa and COS-7 cells, but efficient CRY2–CIBN dimerization has been further confirmed in hepatocytes (HepG2), adipocytes (NIH-3T3), chromaffin cells (PC-12), neuroblastoma cells (SH-SY5Y and N2a), HEK293 cells, macrophages (RAW264.7), and mouse primary cortical neurons. All cell culture work is done in a laminar flow bench using appropriate sterile techniques.

1. Preheat complete cell culture medium, sterile PBS, and trypsin solution to 37 °C on a water bath or a bead bath.
2. Remove the flask with cells from the incubator, and aspirate medium.
3. Wash cells once with 10 mL sterile PBS solution and aspirate.

4. Add 3 mL trypsin solution to the cells and return to the incubator for 3 min or until all cells have detached from the bottom of the cell culture flask.
5. Add 7 mL of complete culture medium and pipet up and down with a serological pipette. Transfer the 10 mL to a sterile 13 mL Falcon tube.
6. Count the cells using a hemocytometer or a similar device.
7. Prepare a new flask by adding 12 mL complete culture medium and 500 μL (1:20 split) of the cell suspension. Mix by pipetting up and down, and place the flask in the incubator.
8. Calculate the number of cells needed. We typically seed HeLa or COS-7 cells at a density of 50,000–100,000 cells per dish to use for transfection the next day (*see* **Note 3**).
9. Pipette a volume corresponding to the number of cells needed for the experiments from the cell suspension and transfer to a new 15 mL Falcon tube.
10. Spin the tube at 1,000 × *g* for 5 min to pellet the cells. Aspirate the supernatant.
11. Resuspend the pellet in cell culture medium (2 mL per dish) and add 2 mL to each of the previously coated MatTek dishes. Put the dishes in the cell culture incubator, and allow the cells to settle for 12–24 h before transfection.

3.3 Transient Transfection and Co-transfection

Choice of transfection technique may vary depending on the cell type to be transfected. In this chapter we describe transfection of HeLa and COS-7 cells that typically yields 80–90 % transfected cells.

1. Warm OptiMEM-I supplemented with 10 % FBS to 37 °C using a water bath or a bead bath.
2. For each MatTek dish to be transfected combine 125 μL OptiMEM with 3 μL Lipofectamine 2000 in an Eppendorf tube and gently tap the tube to mix. Let sit for 5 min at room temperature (*see* **Note 1**).
3. For each MatTek dish to be transfected combine 125 μL OptiMEM with <3 μg high-quality plasmid DNA encoding mCherry-CRY2-OCRL, CIBN-GFP-CAAX, and iRFP-PH-PLCδ1 in an Eppendorf tube and tap the tube to mix (*see* **Notes 4** and **5**).
4. Combine the contents of the two tubes, tap gently to mix, and let sit for 20 min at room temperature.
5. Remove the MatTek dishes with adherent cells from the incubator, aspirate the culture medium, and replace it with 750 μL OptiMEM. Put the cells back in the incubator.

6. After 20 min, add 250 μL DNA–liposome mixture to each MatTek dish, swirl the dish to mix, and incubate in the cell culture incubator for 3 h.
7. Warm complete cell culture medium to 37 °C using a water or a bead bath.
8. Terminate the transfection by aspirating the transfection reaction medium, wash cells once with 1 mL complete culture medium, and add 2 mL complete culture medium.
9. Allow 14–20 h for expression.

3.4 Preparing Cells for Imaging

1. Rinse the cells on the MatTek dish once with the experimental buffer, add 2 mL new buffer to the dish, and incubate for 30–60 min in a 37 °C incubator to allow cells to adapt to basal conditions in the experimental buffer (*see* **Note 6**).
2. From this point on, avoid exposing the cells to light since illumination, even of low intensity, might promote the interaction between the light-sensitive dimerization pair and thus affect the levels of the PIs of interest. We keep cell dishes in an opaque plastic container.
3. Mount the dish on the stage of a fluorescence microscope. We use a custom-built temperature-controlled culture dish holder to maintain 37 °C throughout the experiment (similar setups are available from, e.g., Warner Instruments, Hamden, CT). The temperature control is not necessary for the light-induced dimerization, but lowering the temperature to, e.g., room temperature might affect processes controlled by the PIs being modulated.

3.5 Imaging of Cells and Induction of Dimerization

1. Use the eyepieces of the microscope to locate cells expressing the fluorescence-tagged constructs. Avoid exposing cells to blue-green light (wavelengths <514 nm) since such light will induce dimerization of the light-regulated PI-metabolizing enzymes. Although the dimerization reaction is reversible within a few minutes after interruption of the illumination, it may take longer time for the cells to reverse any biological changes induced by the translocation of the PI-metabolizing enzymes. For this reason, it is recommended to co-transfect cells with fluorescence-tagged CRY2 fusion construct and/or fluorescence-tagged reporters for the PIs to be modulated and to use the fluorescence from these fusion proteins to assess the functionality of the system (for example images *see* Figs. 1c and 3c). Once this has been determined, one can use CRY2 fusion proteins without fluorescence tags which will allow simultaneous dual-color live-cell imaging using co-expressed red (e.g., mRFP or mCherry) and far-red (e.g., iRFP) fusion proteins to study biological questions of interest.

2. When selecting cells to image, choose cells that express low to intermediate levels of the fluorescent proteins (*see* **Note 7**). If the CRY2 fusion protein carries a fluorescent tag, make sure that its localization is cytoplasmic at the beginning of the experiment and that there is little or no localization at the periphery (plasma membrane) of the cell since this indicates preexisting dimerization which might impact on the interpretation of the experiment (*see* **Note 8** and Fig. 1c). When setting up these experiments for the first time, it is recommended to co-transfect a reporter of the lipids being studied (*see* Table 2 for a non-exhausting list of lipid-binding protein modules) (*see* **Note 9**).
3. Project the image onto the EM-CCD camera.
4. Adjust acquisition parameters, such as exposure time and signal gain, to appropriate levels (*see* **Note 10**). Do this for all excitation light sources to be used for imaging.
5. Set parameters for the dimerization-inducing light source (405–488 nm). Avoid exposing the cells to this light since even very-low-intensity light is sufficient to induce efficient dimerization. For spinning disc confocal microscopy experiments, we typically use 10 % laser output (controlled by an AOTF but can also be obtained by placing neutral density filters in the laser light path) from a 50 mW diode-pumped solid-state laser projected through a 60× (1.45-NA) objective and 200-ms exposure time (*see* **Note 10**).
6. Acquire pre-stimulatory images with the EM-CCD camera every 1–30 s (depending on the need for fast acquisition or long-term imaging) for 5–10 min using fluorophores compatible with CRY2–CIBN (*see* Table 1).
7. Illuminate the sample with blue light to induce dimerization (*see* **Note 11**).
8. Reverse the reaction induced by blue light by interrupting the blue light illumination, and keep recording fluorescence using non-blue light for 10–30 min (*see* **Note 12**).
9. For certain experiments, global blue light illumination (as described above) can be replaced by focal illumination. This will allow plasma membrane recruitment of mCherry-CRY2-OCRL, and hence manipulation of PI lipids, with subcellular precision. We use a commercially available FRAP unit to target a subcellular structure with 405-nm laser light (*see* **Note 13** and Fig. 2a).

3.6 Image Analysis

1. Analyze changes in relative fluorescence in individual cells using off-line software. Several different software suitable for such analysis are available (e.g., Volocity from Improvision, MetaMorph from Molecular Devices, or ImageJ by W.S. Rasband, http://rsb.info.nih.gov/ij). Below we describe a simple way performing the analysis in ImageJ.

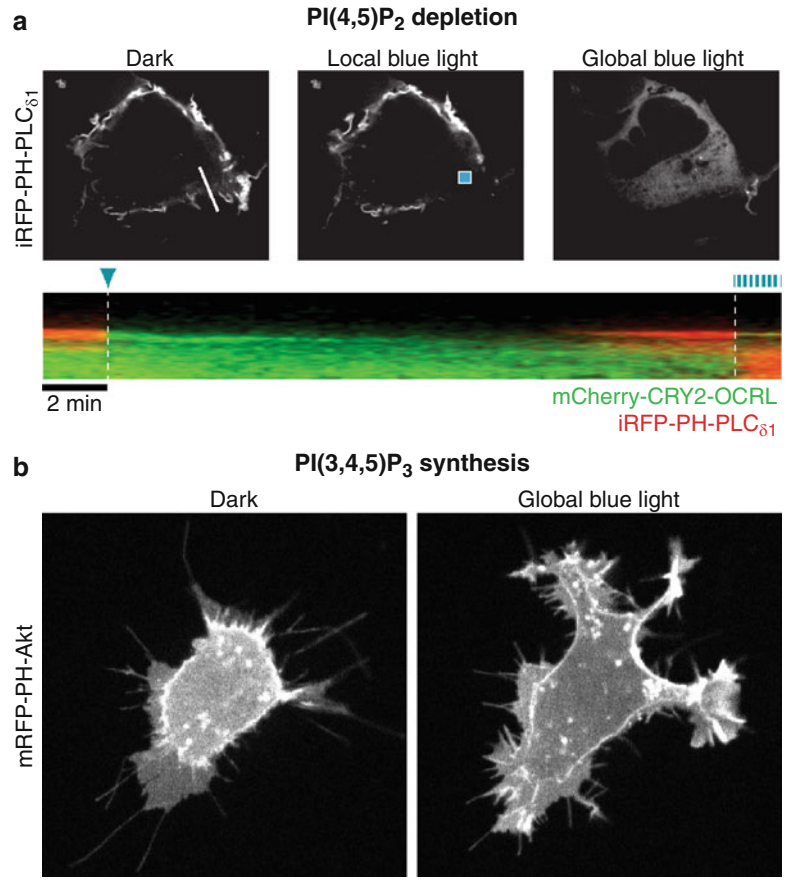

Fig. 2 (**a**) Confocal micrographs of a single COS-7 cell expressing CIBN-GFP-CAAX (not shown), mCherry-CRY2-OCRL (not shown), and iRFP-PH-PLCδ1 before blue light illumination, immediately after 500 ms focal blue light illumination (*blue square*), and 30 s after subsequent global blue light illumination. Kymograph below is drawn along the *white line* and shows iRFP-PH-PLCδ1 in *red* and mCherry-CRY2-OCRL in *green*. (**b**) Confocal micrograph of a PC-12 cell expressing CIBN-GFP-CAAX (not shown), CRY2-iSH2 (a PI3 kinase-binding module; not shown), and the $PI(3,4,5)P_3$ reporter mRFP-PH-Akt (shown) before and following 15 min of blue light illumination. Notice the pronounced expansion of cellular membrane following PI3 kinase recruitment to the plasma membrane

2. Open the image files. Make sure that each recorded wavelength is opened as a separate stack of images (mCherry-CRY2-OCRL and iRFP-PH-PLCδ1).
3. Determine what parameters to measure from the images (analysis/set measurements). Usually it is sufficient to record mean grey values (the average fluorescence within a defined region) as well as the minimum and maximum grey values. This will reveal if any pixels within the defined region are saturated.

4. Draw a region in a part of the mCherry-CRY2-OCRL image where there are no fluorescent cells, and use this to define background fluorescence. Save the coordinates for this region in the region of interest (ROI) manager (analyze/tools/ROI manager) by pressing the "Add" button.
5. To measure the background fluorescence in the image stack, activate the region drawn above and plot the Z-axis profile for that region (image/stacks/plot Z-axis profile). Copy the data points in the displayed graph, and paste them into an Excel spreadsheet. These are the background values for that specific wavelength.
6. Repeat the process for the other wavelength (iRFP-PH-PLCδ1).
7. For confocal microscopy images, the simplest way to assess plasma membrane translocation of mCherry-CRY2-OCRL and dissociation of the lipid-binding biosensor (iRFP-PH-PLCδ1) is to quantify the changes in cytoplasmic fluorescence by defining an ROI inside the cell expressing mCherry-CRY2-OCRL that excludes the nucleus and the plasma membrane. Alternatively, ROI can be defined over the plasma membrane either manually or with the help of a segmentation algorithm. This can be a difficult method because the profile of the plasma membrane may change over the time course of an experiment, in particular after cell stimulation (e.g., ruffles).
8. In TIRF microscopy images, an ROI over the cell will always show fluorescence in the plasma membrane and translocation or dissociation is simply recorded as changes of intensity (*see* Fig. 3c) (*see* **Note 14**).
9. Add the drawn region to the ROI manager.
10. Measure the fluorescence intensity change within the region by plotting the Z-axis profile, as described above for the background. Copy the data points to the spreadsheet.
11. Transfer the same region onto the iRFP-PH-PLCδ1 images by activating that window and clicking on the coordinates for the region in the ROI manager. Repeat as in **step 10**.
12. Repeat **steps 7–10** for all cells in the image stack.
13. In Excel, subtract the background fluorescence for each wavelength from the cellular fluorescence point by point to obtain the actual fluorescence (F) (*see* **Note 15**).
14. Define an initial fluorescence value (typically an average of the fluorescence from ten frames just prior to blue light illumination) for each wavelength and cell from the calculated F-values, and define this as F_0.
15. To get the normalized fluorescence for each wavelength and cell, divide the background-corrected fluorescence (F) with the initial fluorescence (F_0) and plot this as a function of time (*see* Fig. 3a, b for examples).

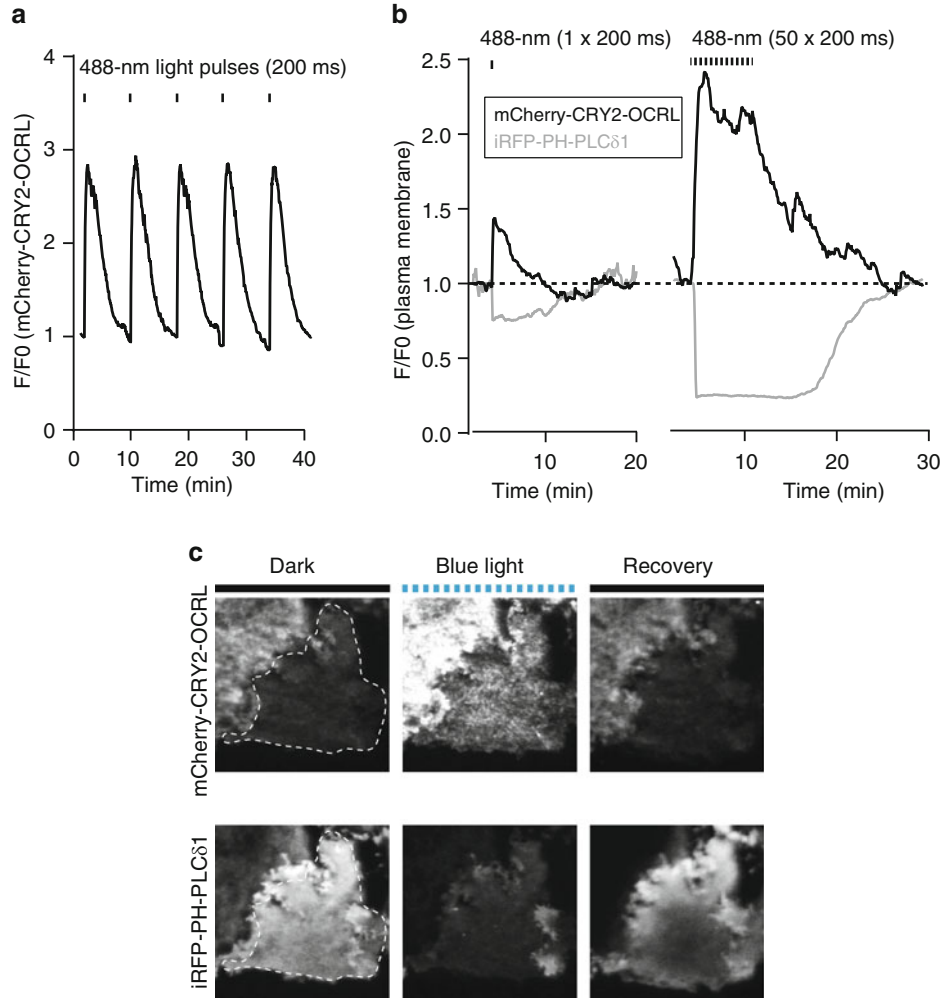

Fig. 3 (**a**) TIRF microscopy recordings from a single COS-7 cell expressing CIBN-GFP-CAAX and mCherry-CRY2-OCRL. The cell was exposed to brief (200 ms) 488 nm light pulses (throughout the whole cell) with 8-min intervals, and mCherry-CRY2-OCRL fluorescence was recorded every 2 s. The data are plotted as fluorescence divided by initial fluorescence after subtraction of background (F/F_0) for mCherry-CRY2-OCRL, and the increase in fluorescence represents translocation and binding of mCherry-CRY2-OCRL to CIBN-GFP-CAAX at the plasma membrane. Notice the reversibility and reproducibility of the dimerization reaction. (**b**) Dual-color TIRF microscopy recordings from a single COS-7 cell expressing CIBN-GFP-CAAX, mCherry-CRY2-OCRL, and iRFP-PH-PLCδ1 following illumination of cells with 488 nm laser light delivered through the evanescent field. Notice that using this illumination regime, several subsequent blue light pulses are required to achieve maximal plasma membrane binding of mCherry-CRY2-OCRL and loss of plasma membrane iRFP-PH-PLCδ1. (**c**) Representative TIRF microscopy images from the plots in (**b**) showing plasma membrane translocation of mCherry-CRY2-OCRL (seen as an increase in fluorescence within the evanescent field) and corresponding loss of iRFP-PH-PLCδ1 fluorescence upon blue light illumination as well as the reversibility upon interruption of the illumination

4 Notes

1. This protocol typically yields 80–90 % transfection efficiency 24 h after transfection. The best results are obtained if the cells are allowed to grow on coated dishes for 24 h prior to transfection. Obviously, other methods for transfection can be used. For example, electroporation (e.g., using Lonza Nucleofection) or virus-mediated gene transfer is highly efficient in a large variety of cell types.
2. As an alternative to PDL, cover slips can be coated with, e.g., collagen or fibronectin. Many cell lines will adhere and spread on the MatTek dishes without coating, but we recommend coating especially for TIRF microscopy imaging, since this allows the cells to adhere more firmly to the substrate and thus give a more even "footprint" within the evanescent field excitation light.
3. The number of cells to seed depends on the cell line being used. For optimal transfection using this protocol, the cell confluence on the dish should be 40–50 % on the day of transfection (lower confluence may be OK). This will give roughly 70 % confluence on the day of imaging, which will allow the imaging of multiple cells at the same time while still being able to identify individual cells.
4. All plasmids used for transfection must be of high quality. Our experience is that the quality of plasmid DNA correlates positively with the scale of production. We therefore recommend producing plasmid DNA from at least 200 mL bacterial cultures (corresponding to a standard "maxi-prep" DNA purification) using commercially available kits from, e.g., Qiagen or Macherey-Nagel.
5. This protocol requires the transfection of multiple plasmids into cells. For transfection of the two dimerization components (CIBN-GFP-CAAX and mCherry-CRY2-OCRL) we use roughly equimolar amounts of the two plasmids, which for a 1 mL transfection reaction is 1 μg CIBN-GFP-CAAX and 1.5 μg mCherry-CRY2-OCRL. In addition, we include 0.5 μg iRFP-PH-PLCδ1 as a reporter of plasma membrane PI(4, 5) P2, making the total amount of cDNA in the reaction 3 μg. If necessary, additional plasmids can be added to the transfection reaction. We have found that Lipofectamine 2000 is toxic to the cells at concentrations >3 μg/mL, even if just incubated together with the cells for 3 h, and we do not recommend increasing the concentration above this even if the total amount of plasmid DNA exceeds 3 μg.

6. For some cell types and applications longer preincubation time in serum-free culture medium may be required (up to several hours), since serum contains factors that may, e.g., stimulate PI3 kinase and formation of PI(3,4,5)P_3.
7. There will be a large variability between cells in the expression level of the fluorescent proteins. High levels of PI-binding proteins can interfere with processes in the cells. Choose cells with relatively low expression levels but not so low that the signal-to-noise ratio is compromised. The fluorescence collected from the cells expressing the biosensor should be well above the autofluorescence from non-transfected cells. Also avoid cells with large brightly fluorescent patches, as this often reflects abnormal aggregation of (possibly misfolded) proteins. Note that in some cell types, the CRY2 fusion protein may form aggregates in the cell cytoplasm. Avoid imaging such cells if possible although, in our experience, efficient CRY2–CIBN dimerization is still observed in such cells. In COS-7 and HeLa cells we typically observe successful dimerization in >90 % of transfected cells.
8. Even when kept in complete darkness, there may be some basal dimerization occurring. This can be observed with spinning disc confocal microscopy as an accumulation of mCherry-CRY2-OCRL at the periphery of the cell (the plasma membrane) where the bait CIBN-GFP-CAAX is localized even before illumination of the sample with blue light. By co-transfecting the cells with a marker for the substrate PI lipid (in this case PI(4, 5)P2) it is possible to observe if this basal dimerization is associated with loss of the substrate lipid at the plasma membrane (*see* Fig. 1c). Cells that show strong basal dimerization and loss of substrate lipid should not be further imaged.
9. It is important to keep in mind that certain PI-binding protein domains (sensors) often do not recognize all pools of the specific PI because of (1) competition with endogenous effectors or (2) the requirement of co-receptors (such as membrane proteins) whose subcellular distribution does not overlap with that of the specific PI. For example, the PH-PLCδ1 domain is a PI(4, 5)P_2 that labels very efficiently and nearly selectively PI(4, 5)P_2 in the plasma membrane, although there is evidence for the presence of this phospholipid also on intracellular membranes. *See* ref. [16] for a more thorough discussion on these limitations.
10. Select camera exposure time and gain settings so that no pixels in the image will be saturated. It is important to consider that the fluorescence intensity might change severalfold during an experiment when mCherry-CRY2-OCRL or PI biosensor redistributes between different cellular compartments (*see* Figs. 1d and 3a, b). It is good to keep the exposure times as

short as possible without compromising the signal-to-noise ratio, since excessive exposure to excitation light may result in photobleaching and phototoxic effects. If the fluorescence collected from the cells is very low, it is possible with most EM-CCD cameras to combine charges in adjacent pixels to form 1 pixel in a process named binning. This will enhance the signal at the expense of optical resolution. On the contrary, if the signal is too bright, it indicates an excessive excitation light intensity. Reduce the laser power or attenuate the light with neutral density filters in the excitation beam path. The laser beam should be completely blocked with a shutter between image captures to avoid adverse effects of the light on the specimen.

11. The free diffusion of mCherry-CRY2-OCRL in the cell cytoplasm is very high, and a brief blue light pulse (200 ms) delivered throughout the whole cell (as with a spinning disc confocal microscope) is sufficient to induce saturated CRY2–CIBN interactions within 5 s. This reaction is then spontaneously reversed within minutes upon interruption of blue light illumination, and repeated blue light illumination causes cycles of shuttling of mCherry-CRY2-OCRL between the cytoplasm and the plasma membrane (*see* Fig. 3a). When imaging cells by TIRF microscopy, CRY2–CIBN dimerization can be induced either by whole-cell blue light illumination or evanescent wave blue light illumination. The latter will selectively activate mCherry-CRY2-OCRL molecules in the volume of the cytosol close to the "footprint" of the cell and promote more efficient and faster interaction with CIBN-GFP-CAAX molecules located in this cell region. This results in a preferential loss of PI(4, 5)P_2 in the region of the plasma membrane facing the substrate. We have found that approximately 20 light pulses (200 ms in duration and 4 s apart) must be delivered to induce maximal depletion of PI(4, 5)P_2 from the region of the plasma membrane visible in the TIRF plane, as at each pulse, non-activated mCherry-CRY2-OCRL enters the field of illumination (*see* Fig. 3b, c).

12. Part of the usefulness of the CRY2–CIBN system for manipulating cellular PI lipids is the reversible nature of the interaction. A single 488, 200 ms blue light pulse delivered throughout the cells is generally sufficient to induce efficient plasma membrane recruitment of mCherry-CRY2-OCRL and nearly complete loss of plasma membrane PI(4, 5)P_2. If no further pulses are given, mCherry-CRY2-OCRL starts to spontaneously dissociate from the plasma membrane within 30 s and the reaction is completely reversed within minutes. If PI(4, 5)P_2 is monitored at the same time, the loss of the lipid follows very closely the plasma membrane association kinetics of mCherry-CRY2-OCRL, but the recovery of the lipid is significantly slower, probably due to time required for resynthesis

from its precursor lipid PI4P (*see* Fig. 1d). When required, depletion of PI(4, 5)P_2 levels at the plasma membrane can be maintained for extended periods of time by applying blue light pulses every 30 s (*see* Figs. 1d and 3b). Pulsatile illumination is preferred over continuous illumination to minimize photobleaching and phototoxic effects. Temporal parameters may need to be adjusted when using different microscopic modalities (e.g., spinning disc confocal versus TIRF) or when using dimerization pairs involving inositol phosphatases other than OCRL or involving inositol kinases. For example, when using the CRY2–CIBN system to recruit endogenous PI3 kinase to the plasma membrane [15], this reaction is much slower and requires extended periods of blue light illumination to ensure maximum synthesis of PI(3,4,5)P_3 at the plasma membrane.

13. Focal recruitment of mCherry-CRY2-OCRL onto CIBN-GFP-CAAX positive plasma membrane works best in flat cells or in cell processes. In both cases, the locally activated cytosolic mCherry-CRY2-OCRL will first bind nearby CIBN-GFP-CAAX before being able to diffuse over longer distances. When using a FRAP unit for induction of local CRY2–CIBN interactions, very-low-intensity laser light should be used. We typically use 2 % output (controlled by the AOTF) from a 50 mW 405-nm DPSS laser. In most cases, a single 200 ms blue light pulse will be sufficient to locally recruit mCherry-CRY2-OCRL and to observe local loss of plasma membrane PI(4, 5)P_2 (*see* Fig. 2a). In fact, repeated illumination may cause activation of a too large fraction of mCherry-CRY2-OCRL molecules that will diffuse throughout the cell cytoplasm and change globally plasma membrane PI(4, 5)P_2 levels. Attempts to use membrane-targeted CRY2 as the bait together with a cytosolic CIBN-5-phosphatase domain have so far proven unsuccessful. Fine-tuning of the dimerization system may eventually allow to use this modality successfully.
14. Some cell types exhibit profound membrane ruffling or other morphological changes, which can alter the area of membrane contact with the cover slip, especially after stimulation. In a TIRF microscope, such morphological changes can induce a fluorescence change that might be misinterpreted as translocation of mCherry-CRY2-OCRL or lipid biosensors. It is therefore important to perform control experiments to ensure that an observed fluorescence change is indeed due to biosensor translocation. This can be achieved by repeating the experiment and replacing the PI-binding biosensor with a nonspecific membrane-targeted fluorescent protein or using a catalytically inactive 5′-phosphatase module. The translocation response can also be confirmed with confocal microscopy. In the described protocol, the GFP fluorescence from CIBN-GFP-CAAX can be

used as a reference signal during stimulation (blue light illumination). Its fluorescence remains stable over the time course of the experiment (we have imaged cells for up to 6 h) since it is permanently anchored to the plasma membrane through a lipid anchor and loss of PI(4, 5)P_2 does not seem to affect this localization, at least over the time ranges used.

15. The expression levels of the fluorescent proteins will vary greatly from cell to cell. To compare cells with each other in terms of kinetics and magnitude of responses it is therefore necessary to normalize the fluorescence in each cell to its initial fluorescence (F/F_0).

Acknowledgments

The development of the methodology described here was supported in part by funding from the National Institutes of Health (NIH) (NS36251, DK082700, DA018343, and DK45735) (P.D.C.) and by a postdoctoral fellowship from the Swedish Research Council (O.I-H.). The authors thank Chandra Tucker and Matthew Kennedy for the generous gift of reagents.

References

1. Di Paolo G, De Camilli P (2006) Phosphoinositides in cell regulation and membrane dynamics. Nature 443:651–657
2. Simonsen A, Wurmser AE, Emr SD et al (2001) The role of phosphoinositides in membrane transport. Current Opin Cell Biol 13:485–492
3. Vicinanza M, D'Angelo G, Di Campli A et al (2008) Function and dysfunction of the PI system in membrane trafficking. EMBO J 27: 2457–2470
4. Balla T, Szentpetery Z, Kim YJ (2009) Phosphoinositide signaling: new tools and insights. Physiology (Bethesda) 24:231–244
5. Rusten TE, Stenmark H (2006) Analyzing phosphoinositides and their interacting proteins. Nat Methods 3:251–258
6. Varnai P, Balla T (2007) Visualization and manipulation of phosphoinositide dynamics in live cells using engineered protein domains. Pflugers Arch 455:69–82
7. Suh BC, Inoue T, Meyer T et al (2006) Rapid chemically induced changes of PtdIns(4,5)P2 gate KCNQ ion channels. Science 314: 1454–1457
8. Varnai P, Thyagarajan B, Rohacs T et al (2006) Rapidly inducible changes in phosphatidylinositol 4,5-bisphosphate levels influence multiple regulatory functions of the lipid in intact living cells. J Cell Biol 175:377–382
9. Umeda N, Ueno T, Pohlmeyer C et al (2011) A photocleavable rapamycin conjugate for spatiotemporal control of small GTPase activity. J Am Chem Soc 133:12–14
10. Shimizu-Sato S, Huq E, Tepperman JM et al (2002) A light-switchable gene promoter system. Nat Biotechnol 20:1041–1044
11. Levskaya A, Weiner OD, Lim WA et al (2009) Spatiotemporal control of cell signalling using a light-switchable protein interaction. Nature 461:997–1001
12. Kennedy MJ, Hughes RM, Peteya LA et al (2010) Rapid blue-light-mediated induction of protein interactions in living cells. Nat Methods 7:973–975
13. Strickland D, Yao X, Gawlak G et al (2010) Rationally improving LOV domain-based photoswitches. Nat Methods 7:623–626
14. Tucker CL (2012) Manipulating cellular processes using optical control of protein–protein interactions. Prog Brain Res 196:95–117
15. Idevall-Hagren O, Dickson EJ, Hille B et al (2012) Optogenetic control of phosphoinositide metabolism. Proc Natl Acad Sci U S A 109:E2316–E2323
16. Varnai P, Balla T (2006) Live cell imaging of phosphoinositide dynamics with fluorescent protein domains. Biochim Biophys Acta 1761: 957–967

17. Gillooly DJ, Morrow IC, Lindsay M et al (2000) Localization of phosphatidylinositol 3-phosphate in yeast and mammalian cells. EMBO J 19:4577–4588
18. Gaullier JM, Simonsen A, D'Arrigo A et al (1998) FYVE fingers bind PtdIns(3)P. Nature 394:432–433
19. Patki V, Lawe DC, Corvera S et al (1998) A functional PtdIns(3)P-binding motif. Nature 394:433–434
20. Levine TP, Munro S (1998) The pleckstrin homology domain of oxysterol-binding protein recognises a determinant specific to Golgi membranes. Curr Biol 8:729–739
21. Levine TP, Munro S (2002) Targeting of Golgi-specific pleckstrin homology domains involves both PtdIns 4-kinase-dependent and -independent components. Curr Biol 12: 695–704
22. Roy A, Levine TP (2004) Multiple pools of phosphatidylinositol 4-phosphate detected using the pleckstrin homology domain of Osh2p. J Biol Chem 279:44683–44689
23. Dippold HC, Ng MM, Farber-Katz SE et al (2009) GOLPH3 bridges phosphatidylinositol-4-phosphate and actomyosin to stretch and shape the Golgi to promote budding. Cell 139:337–351
24. Wood CS, Schmitz KR, Bessman NJ et al (2009) PtdIns4P recognition by Vps74/GOLPH3 links PtdIns 4-kinase signaling to retrograde Golgi trafficking. J Cell Biol 187:967–975
25. Brombacher E, Urwyler S, Ragaz C et al (2009) Rab1 guanine nucleotide exchange factor SidM is a major phosphatidylinositol 4-phosphate-binding effector protein of Legionella pneumophila. J Biol Chem 284: 4846–4856
26. Gozani O, Karuman P, Jones DR et al (2003) The PHD finger of the chromatin-associated protein ING2 functions as a nuclear phosphoinositide receptor. Cell 114:99–111
27. Dowler S, Currie RA, Campbell DG et al (2000) Identification of pleckstrin-homology-domain-containing proteins with novel phosphoinositide-binding specificities. Biochem J 351:19–31
28. Karathanassis D, Stahelin RV, Bravo J et al (2002) Binding of the PX domain of p47(phox) to phosphatidylinositol 3,4-bisphosphate and phosphatidic acid is masked by an intramolecular interaction. EMBO J 21:5057–5068
29. Gray A, Van Der Kaay J, Downes CP (1999) The pleckstrin homology domains of protein kinase B and GRP1 (general receptor for phosphoinositides-1) are sensitive and selective probes for the cellular detection of phosphatidylinositol 3,4-bisphosphate and/or phosphatidylinositol 3,4,5-trisphosphate in vivo. Biochem J 344(Pt 3):929–936
30. Stauffer TP, Ahn S, Meyer T (1998) Receptor-induced transient reduction in plasma membrane PtdIns(4,5)P2 concentration monitored in living cells. Curr Biol 8:343–346
31. Santagata S, Boggon TJ, Baird CL et al (2001) G-protein signaling through tubby proteins. Science 292:2041–2050
32. Dove SK, Piper RC, McEwen RK et al (2004) Svp1p defines a family of phosphatidylinositol 3,5-bisphosphate effectors. EMBO J 23: 1922–1933
33. Klarlund JK, Rameh LE, Cantley LC et al (1998) Regulation of GRP1-catalyzed ADP ribosylation factor guanine nucleotide exchange by phosphatidylinositol 3,4,5-trisphosphate. J Biol Chem 273:1859–1862
34. Varnai P, Rother KI, Balla T (1999) Phosphatidylinositol 3-kinase-dependent membrane association of the Bruton's tyrosine kinase pleckstrin homology domain visualized in single living cells. J Biol Chem 274:10983–10989
35. Venkateswarlu K, Oatey PB, Tavare JM et al (1998) Insulin-dependent translocation of ARNO to the plasma membrane of adipocytes requires phosphatidylinositol 3-kinase. Curr Biol 8:463–466

Chapter 9

A Roadmap to Applying Optogenetics in Neuroscience

Consuelo Fois, Pierre-Hugues Prouvot, and Albrecht Stroh

Abstract

Optogenetics allows for the specific manipulation of the activity of genetically defined cell populations in the CNS. Yet, it requires effective gene delivery, light stimulation, and readout strategies. Here, we provide a roadmap aimed at guiding the experimenter in the process of establishing an optogenetic approach tailored to a given research hypothesis in the field of neuroscience.

Key words Optogenetics, Viral gene transfer, Neuroscience, Light stimulation, ChR2

1 Introduction

Advancement of our understanding of neuronal network dynamics in health and disease requires the investigation of defined populations of neurons and their interactions in the intact central nervous system (CNS). Up to now, neuronal circuits have been mainly probed by electric stimulation, not allowing for selectivity towards genetically defined neuronal populations. Alternative strategies such as microinjection of neurotransmitters (e.g., GABA) are limited to spatially constrained applications in a controlled setting.

However, probing the specific contribution of genetically defined neuronal populations to network function is pivotal for furthering our knowledge of network dynamics and for the development of effective therapy strategies. The discovery of a rapidly gated light-sensitive cation channel channelrhodopsin-2 (ChR2) suitable for noninvasive control of neuronal activity has made it possible to optically control membrane depolarization on the millisecond timescale in genetically defined neurons [7]. ChR2 is a transmembrane protein derived from the green alga *Chlamydomonas reinhardtii* [32]. It consists of an opsin with seven transmembrane helices and the covalently bound chromophore retinal. Upon absorption of a photon the retinal undergoes a *trans–cis*-isomerization, opening the channel pore and leading to an influx of cations.

Sidney Cambridge (ed.), *Photoswitching Proteins: Methods and Protocols*, Methods in Molecular Biology, vol. 1148,
DOI 10.1007/978-1-4939-0470-9_9,

ChR2 is an entirely genetically encoded actuator, in contrast to optochemical approaches requiring exogenously added photosensitive ligands. It incorporates strategies of genetic expression with optical stimulation into a single-component system, at least in mammalian cells. Recent advancements of the optogenetic toolbox also allow for the effective inhibition of genetically defined neuronal cell populations in vivo, by activation of the bacterial proton pump Arch or the chloride pump NpHR with green laser light [9, 15]. These methods have the potential for rebalancing disturbed neuronal circuitry by activation or inhibition of endogenous neuronal sub-circuits.

Yet, establishing a meaningful and effective optogenetic approach will only succeed given a comprehensive experimental design covering several levels of expertise, starting with the choice of opsin, gene delivery, and illumination methods. Here, we aim at providing a general roadmap to the design of an optogenetic experiment tailored to the scientific question the experimenter wants to address. Clearly, this roadmap cannot be exhaustive, but rather it should give a condensed overview of the most critical aspects. Moreover, we chose to focus on applications of optogenetics in rodents, representing the majority of currently published studies. Nonetheless it should be noted that optogenetics significantly contributed to neuroscience research in invertebrates [33] and non-human primates [10].

We subdivided this "beginner's optogenetics manual" in four levels highlighted in Fig. 1: (1) *Modulation*, (2) *Delivery*, (3) *Light source*, and (4) *Readouts*. On each level, the experimenter needs to make critical choices, determining the success and validity of the optogenetic approach in addressing the specific research hypothesis. We only included tried-and-tested methods on each level, and discuss the key aspects that need to be considered. Naturally, we cannot provide a detailed experimental manual on how to practically implement all those methods in the lab, but rather we would like to focus on three main aspects: virus injection, functional characterization of opsins, and Readout strategies.

2 Experimental Design

2.1 Modulation

Designing an optogenetic approach starts by choosing the type of opsin best suited for modulating activity of the respective neuronal or non-neuronal cell population.

There are three main classes of opsins: (1) depolarizing cation channels, (2) hyperpolarizing light-driven pumps, and (3) light-sensitive G-protein-coupled receptors (GPCRs) directly affecting intracellular signaling.

The main characteristics of key opsins are depicted in Fig. 2. Note, that this figure is not exhaustive, but includes those opsins that are best suited for getting started with optogenetics, as they

Fig. 1 Roadmap of the design of an optogenetics experiment

display low cytotoxicity and high photocurrents. In addition, the respective stimulation paradigms are already well established.

Choosing the appropriate opsin requires defining the cell type that should be optogenetically modulated. The choice of opsin depends on whether the experiment is, e.g., targeting fast spiking

OPSIN		KEY FEATURES	PEAK ACTIVATION λ	τoff (off kinetics)	REFS.
FAST EXCITATORY (BLUE/GREEN)					
ChR2		• First version • From *Chlamydomonas reinhardtii*	470 nm (blue)	10 ms	(Boyden et al., 2005; Nagel et al., 2003)
ChR2 (H134R)*		• Slower channel closure kinetics • Reduced desensitization • Mammalian codon (higher expression)	470 nm (blue)	18 ms	(Gradinaru et al., 2007; Nagel et al., 2005)
ChETAs*	ChR2 (E123A)	• Faster channel closure kinetics • Reduced photocurrent	470 nm (blue)	4 ms	(Berndt et al., 2011; Gunaydin et al., 2010)
	ChR2 (E123T)		500 nm (green)	4,4 ms	
	ChR2 (E123A/T159C)		500 nm (green)	8 ms	
ChIEF *		• Higher photocurrent • Reduced light sensitivity • Chimera(ChR1+ChR2→ChEF +Ile170Val→ChIEF)	450 nm (blue)	~ 10 ms	(Lin et al., 2009)
FAST EXCITATORY (YELLOW/RED)					
C1V1		• Slow channel closure kinetics • Enhanced photocurrent • Chimera (ChR1 and VChR1)	540 nm (green)	156 ms	(Fenno et al., 2011; Yizhar et al., 2011)
C1V1ChETA (E122T/E162T)		• Faster channel closure kinetics • 2P excitable • Enhanced photocurrent • Chimera (ChR1+VChR1)	545 nm (green)	34-38 ms	(Yizhar et al., 2011)
BISTABLE MODULATION (SFOs STEP FUNCTION OPSINS)					
ChR2 (C128A)		• Minute time scale deactivation kinetics • Yellow light terminates blue light triggered photocurrent	470 nm activation (blue) 590 nm deactivation (yellow)	42 sec	(Berndt et al., 2009; Yizhar et al., 2011)
ChR2 (D156A)				414 sec (6.9 min)	
ChR2 (C128S/D156A)				1740 sec (29 min)	
INHIBITORY (GREEN /YELLOW)					
Arch/ArchT		• Proton pump • From *Halorubrum sodomense*	566 nm (green)	n/a	(Chow et al., 2010)
INHIBITORY (YELLOW/RED)					
eNpHR3.0		• Chloride pump • Enhanced photocurrents (compared to eNpHR and eNpHR2.0) • ER export motif and neurite trafficking sequence from Kir2.1 K^+ channel • From *Natromonas pharaonis*	590 nm (yellow)	n/a	(Fenno et al., 2011; Gradinaru et al., 2010)
BIOCHEMICAL SIGNALING, G-Protein Coupled Receptors					
Rh-CT(5-HT1A)		• ↑ Gi/o- protein signaling • ↑ cAMP • Chimera (5-HT1A C-terminal + RO4)	485 nm (blue)	n/a	(Oh et al., 2010)
Opto-α1AR		• ↑ Gq-protein signaling • ↑ IP3, DAG • Chimera (bovine rhodopsin + adrenergic GPCR)	500 nm (green)	n/a	(Airan et al., 2009; Fenno et al., 2011)
Opto-β1AR		• ↑ Gs-protein signaling • ↑ cAMP • Chimera (bovine rhodopsin + adrenergic GPCR)	500 nm (green)	n/a	

*Compared to ChR2

Fig. 2 Spectral and kinetic properties of opsins

interneurons versus sparse firing principle neurons. A key determinant is the characteristic time constant, τ, defined by the internal closure kinetics of the channel. For example, even a brief stimulation of 5 ms of the opsin C1V1 will result in a depolarization of the neuronal membrane substantially longer than the light pulse due to the τ of 156 ms. Consequently, this opsin would certainly

not be capable of inducing action potential trains of frequencies above 5 Hz. Therefore, the desired stimulation protocol needs to be determined first, followed by the choice of opsin. In our view, if, e.g., cortical pyramidal neurons need to be stimulated with typical frequencies of 10 Hz or below, ChR2 (H134R) would be the most appropriate opsin, as it shows the best compromise between high photocurrent, sufficient expression levels, and low cytotoxicity.

For reliable induction of action potentials at a high frequency, use fast variants. For bistable optogenetic modulation in the range of seconds to minutes, step function opsins (SFO) would be the choice.

Importantly, it has to be considered that expressing high numbers of exogenous membrane proteins, irrespective of the choice of opsin, will affect both membrane properties and neuronal physiology, this is of particular relevance in long-term studies [31]. Pumps, on the other hand, are the only option when aiming at inhibition of neuronal activity, requiring an active light-driven transport of ions against their electrochemical gradient. Both pumps highlighted here, ArchT and eNpHR3.0, enable efficient inhibition of neuronal activity in vivo [9, 15].

For directly modulating intracellular signal transduction, light-sensitive GPCRs should be employed [2]. This approach is promising also for the activation of non-neuronal cell populations, such as astrocytes.

2.2 Delivery

Clearly, the cell type specificity represents the key advantage of optogenetics compared to electrical stimulation methods. Optogenetics achieves specificity of manipulation by transferring the gene for the optogenetic actuator combined with a cell type specific promoter. Differential gene expression governed by promoters represents the fundamental mechanism underlying the morphological and functional diversity of neuronal networks.

There are three main approaches to enable opsin expression in postmitotic neurons: viral gene transfer, transgenic animals, and in utero electroporation. Viral gene transfer and in utero electroporation typically yield a spatially restricted expression of the opsin depending on the virus titer, injected volume, and the time point and location of electroporation. In transgenic animals, typically a brain-wide expression is achieved [53]. This might pose a problem of specificity, as, e.g., in the Thy1-ChR2 transgenic mouse line [5] both cortical and subcortical structures are expressing ChR2, and a cortical optogenetic stimulation would inevitably also stimulate fibers of passage.

Here, we will focus on viral methods of gene transfer, as those can be implemented easy in the lab, not requiring extensive training or additional instrumentation. Mainly lentiviral or adeno-associated-viral (AAV) vectors have been used to deliver opsins in post mitotic neurons as well as non-neuronal cells such as embryonic stem cells [45].

Table 1
AAV promoters and their cell-type specificity

Adeno-associated virus (AAV)		
Promoter	**Cell type-specificity**	**Refs.**
EF1-α	Ubiquitous	[19]
CMV	Ubiquitous	[11, 19]
OT	MCN (magnocellular neurons)	[23]
CaMKIIα	Excitatory neurons	[26, 47]
hSynI	Panneuronal	[10]
hThy1	Panneuronal	[10]
hGFAP	Astrocytes	[25, 26]

The third generation AAVs has key advantages, such as lower biosafety level, low immunogenicity, reliability, and also wide availability through academic and commercial vendors (*see* Subheading 3.2). Therefore, for beginners in optogenetics, we do not recommend setting up virus production capabilities.

Besides the promoter, cell type specificity is determined by the serotype of the virus. The serotypes yielding pan-neuronal expression and most commonly used are serotypes 2 and 5.

However, due to the low packaging capacity of the AAVs, only a limited number of promoters can be used to directly drive opsin expression, *see* Table 1.

In addition, many cell type specific promoters, especially those specific for interneurons, result in low expression rates, which may not suffice for effective optogenetic modulation, especially in vivo. This can be addressed by using the Cre/loxP system, where the opsin and a strong ubiquitous promoter are inverted and the construct is double floxed with two loxP sequences. In a second plasmid the enzyme Cre recombinase is under the control of the weak cell-specific promoter. Injecting both viruses (typical ratio 1 Cre:4 opsin) results in a recombination selectively in the target cell and the opsin is expressed under the control of the strong ubiquitous promoter [8].

A successful virus injection depends on the type of injection method: automatic injection or manual injection. The automatic injection method employs an automatic injector such as Nanoliter 2010 Injector from WPI (WPI World precision instruments, Inc. Sarasota, FL, USA). Manual injection is performed using a large volume syringe (50 ml is preferable) connected with a plastic tubing to a glass graduated pipette with ring marks made of borosilicate glass (HIRSHMANN Louisville, KY, USA).

The advantage of the automatic method is that the experimenter can precisely control the injection speed and the pressure

applied to the liquid containing the virus, provided that the pipettes are normalized and their resistance remains constant. However, the main drawback of this method is the inability to directly monitor whether the liquid is actually injected, particularly as clogging of the pipette cannot be avoided at all times.

Manual injection can be more reliable as the injection procedure can be directly observed, ensuring that the liquid is correctly injected, but it lacks precise control over the injection speed and pressure applied to the liquid.

2.3 Light Source

The choice of light source is as crucial as the choice of the opsin in the design process of your experiment. It is also possibly the largest investment needed to implement optogenetics. Two main categories need to be considered: the light sources that allow selective single cell stimulation (mainly 2-photon-based approaches) and those that are capable of stimulating larger cellular ensembles (1-photon approaches).

We will start with single photon light sources. Those light sources are easy to implement and do not require advanced knowledge in optics.

We would recommend visible light lasers (vendors include Coherent, Santa Clara USA; Qioptics, Fairport, USA; Newport, Irvine USA).

Pros	Cons
• High and tunable power • Collimated beam easy to focus in an optic fiber or microscope • Defined wavelength	• Expensive • Not suitable for direct head mounting

A cheaper and also promising alternative to lasers are laser diodes, currently available in blue (473–488 nm) and green (532 nm)(OSRAM, Munich, Germany; Newport Irvine USA), but they do not provide a collimated beam.

LEDs (available at all the above-mentioned manufacturers) are the smallest devices among light sources for optogenetics. They have mostly been used for behavioral studies as they can be fixed directly to the head of the animal, even including batteries [50] or can be connected to an external power source [27]. LEDs may pose problems with regards to bimodal optogenetic control due to the broad spectrum, e.g., when combining ChR2 and ArchT, expressed in different cell types but within one brain region.

Pros	Cons
• Cheap • Small (awake behaving animal possible)	• Need to be collimated • Heating issues • Broad wavelength

At the junction of one photon and two photon excitation are one photon holographic scanless excitation approaches, developed by the group of Valentina Emiliani [30] and commercialized by Intelligent Imaging Innovations (PHASOR, 3I Denver, USA). This approach enables the experimenter to choose multiple points of illumination in 3D and to focus the laser light with very high lateral (0.3 μm) and axial (1.2 μm) resolution, resulting in single cell but also subcellular excitation. This technique has not been established in vivo yet.

For two photon excitation there are currently three established approaches and all of them allow single cell stimulation in vivo and use a Ti:Sapphire mode locked laser for excitation. The first method is to use spiral scanning to achieve sufficient photon density. Scanning the cell body in a spiral manner results in a larger effective dwell time on the area of the cell compared to standard scanning; thereby achieving the opening of a larger number of light-gated channels and increasing the likelihood to elicit action potentials [40]. Still, the evoked currents are significantly smaller than those evoked by single photon excitation. Additionally, to elicit sufficient photocurrents, the diameter of the beam can be increased by underfilling the back aperture of the objective, e.g., by using a diaphragm in the light path (*see* **Notes 7** and **8**).

The second approach is to use a two photon excitable construct such as the C1V1 variants or ChR1 [35]. These opsins are modified for increased excitability at 1,100 nm with a Ti:Sapphire laser. Here, a conventional scanning pattern on the cell soma is sufficient to induce large amplitude photocurrents without increasing the size of the focal spot.

The third option is two photon holography [37, 48]. Here, a pattern of illumination in 3D is created (multiple zones on multiple focal planes) with very high spatial resolution, by manipulating the focus and the phase of a two-photon laser beam. It is not yet commercially available.

2.4 Readouts

The choice of readouts of optogenetic modulation serves two purposes that need to be considered independently from each other: first, the effect of light stimulation on neuronal activity needs to be defined and dose–effect curves established (Fig. 3). This is of crucial importance in order to determine the optimal virus titer, injection method, promoter strength, and light source. In our view, a combination of high-resolution confocal imaging and single cell electrophysiology is most appropriate.

Second, once optogenetic procedures have been established, the readout that is best suited to actually address the research question needs to be determined. Here, the experimenter needs to consider several limitations and pitfalls involved in implementing optogenetics, e.g., the Becquerel effect at high light intensities (see below). Here, we will provide an overview of the most commonly used readout methods and their limitations from an optogenetics perspective.

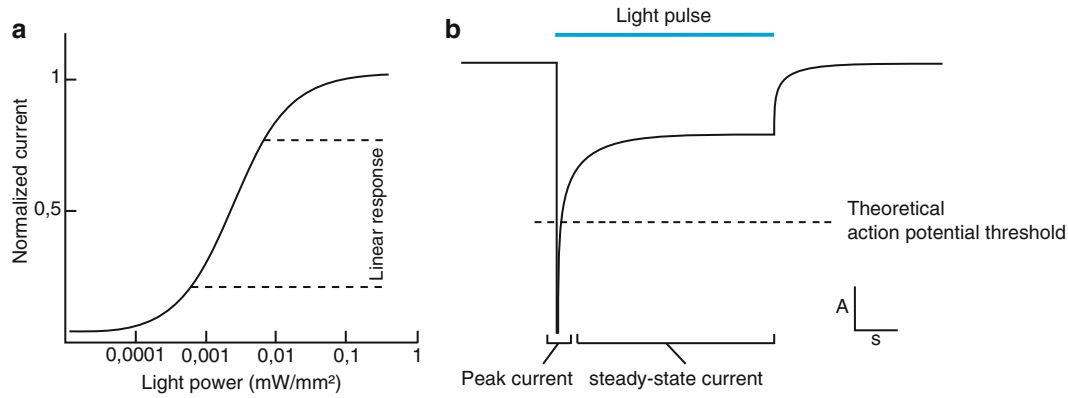

Fig. 3 (**a**) Typical dose–response curve for an excitatory opsin, adapted from ref. [39]. For the subsequent effective and low-impact optogenetic experiment, choose a light power density in the linear section of the dose–response curve. (**b**) Schematic light evoked inward currents in a ChR2 expressing cell in voltage clamp (light pulse indicated by *blue bar*) adapted from [45]. Note that this current is bimodal with a brief peak current followed by a steady state current. The peak current exhibits inactivation (*see* **Note 13**) (Color figure online)

2.4.1 Electrophysiology

Electrophysiology still represents the gold standard in assessing sub- and suprathreshold neuronal activity on cellular level [42]. Electrophysiological recordings can be performed either in a single neuron using the patch clamp approach or in neural assemblies by Local Field Potential (LFP) recording techniques. Combining electrophysiology using metal electrodes with optogenetics may result in the Becquerel effect [18]. The Becquerel effect or photoelectric effect occurs if only a section of a metal electrode is strongly illuminated, thereby inducing a current [18].

Patch clamp permits recording of neuronal electrical activity with high temporal resolution in the kHz range. Extracellular single unit recordings using glass pipettes (cell attached or whole cell) can be easily combined with optogenetics without any interference resulting from light stimulation.

LFPs reflect the population activity of neuronal circuitry. However, two common issues with LFP recordings are the lack of spatial specificity [21] and the Becquerel effect when using metal electrodes (*see* **Notes 11** and **12**).

To easily combine electrophysiology and optogenetics, a hybrid device ("optrode") has been developed that combines light delivery and electrical recordings [14].

A further enhancement of this device consists of a tapered coaxial optical electrode and a 100 element microelectrode array (MEA) [49].

Just recently, an improved design for simultaneous patch-clamp recordings and light stimulation has been proposed. This device, which is called "optopatcher" enables whole cell patch-clamp recordings simultaneously with direct illumination using a fiber within the recording pipette. The optopatcher eliminates the need of an additional manipulator and, importantly, enables spatially accurate, stable, and reproducible illumination [22].

2.4.2 Optical/Magnetic Imaging

Imaging methods capable of directly monitoring neuronal activity include, among others, Ca^{2+} imaging using fluorescent Ca^{2+} indicators [43]. The intracellular Ca^{2+} concentration is tightly regulated and is mainly controlled by the release and reuptake into intracellular Ca^{2+} stores such as the endoplasmatic reticulum and by in- and outflux through voltage-gated Ca^{2+} channels in the neuronal membrane. Amplitudes of intracellular Ca^{2+} transients in neurons are linearly correlated to the number of action potentials [41]. In order to monitor Ca^{2+} concentrations, fluorescence indicators changing their fluorescence emission upon binding with Ca^{2+} are already well established. This includes both acutely injected synthetic indicators, such as Oregon Green BAPTA-1 (Invitrogen, Life Technologies, UK), and genetically encoded indicators such as GCaMP5 [3]. By using 2-photon microscopy in vivo following bolus loading with Ca^{2+} indicators, the activity of small neuronal populations—microcircuits—can be monitored with cellular resolution [16]. In the context of combining optical detection of neuronal population activity and optogenetics—all optical physiology—we recently showed that an optical fiber-based recording and stimulation system allows for optogenetic stimulation and simultaneous readout of network function of neurons in sensory cortices in vivo [44]. Using this approach, we probed the initiation of thalamocortical slow waves.

Recently, optogenetics has been combined with blood oxygenation level dependent (BOLD) fMRI giving rise to opto-fMRI [26]. This allows for a global assessment of specific optogenetically induced activation and inhibition on global neuronal activity. It has to be noted, however, that BOLD fMRI is correlated to neuronal activity by the process of neurovascular coupling, and thus cannot be interpreted as a quantitative measure of neuronal activity [29].

2.4.3 Behavioral

Behavioral testing enables the assessment of high cognitive functions. A certain behavior occurs as a result of the physiological interaction between the organism and the environment but is also be dependent on pathological conditions. Optogenetics in awake animals allows the investigation of the impact of genetically and spatially defined neuronal subpopulations on a specific behavior. By the use of small diameter optic fibers, opsins expressed in any brain region of a freely moving animal can be stimulated. Optogenetics has been used to study narcolepsy and sleep-wake transitions [1], reward-related behavior [46, 51], memory [20], fear conditioning, anxiety [20, 47], and Parkinson's disease [13, 24].

3 Experimental Procedures

Here, we describe the key procedures that need to be implemented for a basic optogenetic experiment in neuroscience. We omit all steps that can be easily outsourced when using standard opsins and promoters, such as cloning and virus production.

3.1 Modulation

The plasmids of all opsins listed in Fig. 2 are available directly from the researchers (*see* References). As stated above, for an experiment aiming at modulating excitatory neurons, we recommend commencing with ChR2(H134R). Start by stimulating ChR2 expressing neurons with brief pulse trains, at pulse durations of 5 ms, and an interpulse interval of 8 s, to allow recovery of the peak current (*see* Fig. 3b). Light power density for ChR2 should range at 1–10 mW/mm^2, but ideally a dose–response curve will be established, even more so for recently established opsins, *see* Fig. 3a and Subheading 4. Stimulate the opsins with light power densities in the linear section of the input–output correlation; *see* Subheading 3.3 for the calculation of the effective power density and Subheading 3.4 for measuring the light-induced currents.

3.2 Delivery: Manual Virus Injection

Several academic facilities, namely the vector core facility of the University of North Carolina (http://genetherapy.unc.edu/services.htm) or the University of Pennsylvania (http://www.med.upenn.edu/gtp/vectorcore/), provide both AAVs and Lentiviruses, encoding for various opsins, so a typical experiment does not require in-house virus production capabilities. However, even though these virus preparations have shown to be very reliable and of high quality, we strongly recommend to test each new batch. Inject at least three different virus titers and assess the functional expression by a combination of confocal imaging and electrophysiology (*see* Subheading 3.4).

Here, we provide a step-by-step procedure on manual virus injection in rodents.

3.2.1 Preparation

1. Sterilize all surgical equipment (Hot Bead Sterilizers, FST, Inc., North Vancouver, British Columbia, Canada).
2. Anesthetize the mouse with 8–10 μl/g bodyweight Ketamin/Xylaxin (50–20 mg/ml) intraperitoneally.
3. Monitor the animal until reflexes are gone (tail pinch, eye lid).
4. Continuously monitor the body temperature by a rectal probe (ATC-1000DC Temperature Controller, WPI). The body temperature should be kept at 37 °C by placing the animal on a heating plate and the respiration rates at 80–100 breaths per minute.

5. Shave the head of the animal (Electric razor or Hydroxide-based hair removal topical cream).
6. Position the animal in a stereotactic frame (e.g., from Stoelting Co, Wooddale, IL, USA; or Kopf Instruments, Tujunga, CA, USA). Fix the animal's upper teeth on a bite bar, place the ear bars inside the ear canal, and make sure that the skull is firmly stabilized. All the procedures are performed with the aid of a dissecting microscope (e.g., Leica Microsystems, Olympus, Zeiss).
7. Apply ointment (Bepanthen, Bayer AG, Leverkusen, Germany) to the eyes to avoid dehydration.
8. Apply local anesthetics to the skin (Xylocaine gel 2 %, Astra Zeneka GmbH, Wedel, Germany).
9. Perform a midline scalp incision of around 1 cm with a scalpel.
10. Identify the cranial sutures (bregma and lambda) and center the stereotactic frame according to those reference points.
11. Determine the position of the subsequent craniotomy based on stereotaxic coordinates of the targeted brain region (see stereotaxic brain atlas, e.g., [36].
12. Perform a small craniotomy with a dental drill (Ultimate XL-F. NSK, Tochigi, Japan) using a 0.5 mm burr (Komet Dental, Lemgo, Germany). The craniotomy size has to be as small as possible to reduce tissue damage and infections, so aim for a craniotomy with a diameter not larger than the drilling burr itself.
13. Thin the skull until the bone is moving when gently pressed with pointed forceps, avoid drilling too deep.
14. With a thin injection needle (30 G) lift the remaining piece of bone while trying to avoid injuring the dura and damaging the brain parenchyma. Put a drop of physiological solution (ACSF, PBS, or physiological solution 0.9 %) on top of the cranial opening to avoid dehydration of the tissue. In case of bleeding it is useful to use a surgical sponge (Gelfoam, absorbable gelatin compressed sponge, Pfizer, New York) to stop it and to remove the blood before coagulation from the brain surface without damaging the tissue.

3.2.2 Injection

1. Pull a graduated pipette with a standard puller (e.g., Sutter Instruments, Novato, CA, USA) resulting in a long thin shaft and a tip of 45 μm outer and 15 μm inner diameter.
2. Connect the glass pipette to the tubing and attach it to the cannula holder of the stereotactic frame.
3. Transfer 1 μl of virus-containing liquid on a piece of parafilm, from now on work as fast as possible to avoid virus evaporation and degradation.

4. Insert the tip of the glass pipette into the virus drop and apply negative pressure with the syringe until 600–800 nl of the virus solution are taken up.
5. When imaging needs to be performed in the targeted area, perform injections at a 45° angle, to avoid tissue damage by the injection canal directly dorsal of the injected region.
6. Place the pipette near the cranial opening.
7. Set the x-y-z controller to 0 before piercing the dura and insert the pipette to the desired depth.
8. Start injecting the virus as slow as possible, typically 1 min/100 nl. After injecting the desired amount of virus (200–400 nl) wait 2 min to allow the liquid to diffuse into the tissue.
9. Slowly remove the pipette.
10. Sew the skin incision.
11. Move the animal onto a heating plate in a cage to keep the body temperature at 37 °C until it recovers from the anesthesia and monitor for 24 h, apply post surgery analgesics (Metacam 0.5 mg/ml. Boheringer, Ingelheim, Germany).

The entire procedure can take from 40 to 90 min depending on the targeted brain regions.

3.3 Light Source: Determining Light Power Density

The next step is to characterize the light density distribution in the illuminated brain area. First, the light power at the tip of the optic fiber or at the focus of the objective needs to be determined, e.g., by a photodiode coupled to a power meter (Newport, Thorlabs, Newton, NJ, USA). Second, the penetration depth needs to be measured, e.g., when targeting layer V neurons in mouse cortex, this would be around 700 μm. Light absorption and scattering in the tissue can be modeled by the Kubelka-Munk equation to provide an order of magnitude estimation of the light density in the depth of the tissue [4]. Briefly, the transmitted fraction through a scattering medium is $T = 1/(S \times z + 1)$, where S is the scattering coefficient (typically 11.2 mm^{-1} for mouse brain and 10.3 mm^{-1} for rat brain), T is the transmitted fraction, and z is the penetration depth in mm. At a given depth the effective light power is then $P_z = P_0 \times T$, where P_0 is the initial power and T the transmitted fraction calculated earlier.

Yet, the key parameter determining the effectiveness of opsin activation is the power density, in mW/mm^2 (*see* **Notes 9** and **10**).

The power density is defined as the light power divided by the surface of the illuminated area. Note, that in case of optic fibers, the geometry of the light beam has to be taken into account, which is dependent on the numerical aperture of the fiber.

The size of your illumination spot can be determined as follows:

1. Pipette a solution of a fluorescent dye such as HPTS or fluorescein in a glass cuvette and place it under the microscope.
2. Capture an image of the focus spot with a CCD camera mounted on the microscope. Measure the lateral and axial spread of the spot if using a focused light source. If using optic fibers, insert the fiber into the cuvette and measure the angle at which the light spreads.

3.4 Readouts: Verifying Expression and Functionality

Once the viral constructs have been injected or the transgenic mouse lines established, the specificity of the optogenetic procedures has to be established. First, the expression profile of the opsins needs to be evaluated. This is particularly important for the virus injected and in utero electroporated animals as variability can be high. It is less significant in the case of transgenic mouse lines, as typical expression profiles have already been determined. Second, the functionality of the opsins needs to be assessed by electrophysiology.

3.4.1 Confocal

High-resolution confocal imaging is the recommended method to assess opsin expression [44]:

1. Transcardially perfuse the animal with ice-cold 4 % paraformaldehyde (PFA) in phosphate-buffered saline (PBS).
2. Extract the brain and incubate it in 4 % PFA overnight.
3. Wash the brain in PBS twice before transferring it to 30 % sucrose solution (in PBS) at 4 °C.
4. Slice the brain including the injected region.
5. Stain the slices with a fluorescent Nissl stain (e.g., Neuro Trace, Invitrogen) to stain the neuronal nuclei and enable the calculation of a ratio of opsin-expressing cells.
6. Perform fluorescent microscopy using a 10× or 4× objective to assess the area of expression (typically ranging at 0.3 and 0.5 mm laterally in mouse brain depending on the serotype and the amount injected).
7. Verify the membrane localization of the opsins using a 40× or 63× objective. Certain fluorescent proteins fused to the opsins have a tendency to aggregate and form clusters within the cell, this is not problematic as long as there is still strong membrane-bound expression (*see* **Notes 5** and **6**).

3.4.2 Electrophysiology

In order to design an effective stimulation paradigm, three aspects need to be considered: First, the light power density threshold for activation. For that, a dose–response curve needs to be determined (Fig. 3), *see* Subheading 3.3 for determining the light power density.

To determine the light-induced currents, the opsin-expressing cell needs to be patched in whole cell voltage clamp mode and the light power modulated stepwise.

Second, the characteristic recovery time of your construct needs to be quantified, if it is not already described in the literature (*see* **Note 13**). Third, the dimension of the area of activation needs to be assessed:

1. Center the light source on the soma of a patched cell, optically stimulate and record the spikes in order to calculate the spiking probability.
2. Displace the light source stepwise laterally.
3. Measure the effective distance from the cell until the spike probability returns to control levels. This is the effective diameter of the stimulated area [37].
4. Repeat this by moving the focus of the light in dorsoventral direction to measure the axial dimension, in case of using focal activation. For optic fibers, vary the depth of implantation (*see* ref. [44], Suppl. fig. 5 for further details).

4 Notes

1. Membrane-bound expression can be improved by using translocation strategies that employ targeting of the opsin to the membrane [15].
2. Using a 2PA construct (in which the opsin is separated from the XFP) allows for easier counting of the cells as the XFP becomes cytosolic [38], but the evaluation of the correct trafficking of the opsin can be problematic.
3. The red fluorophore mCherry has a tendency to aggregate intracellularly.
4. If planning long-term experiments it might be important to additional check for abnormal development of neurons [31].
5. If the opsins do not exhibit membrane-bound expression the problem might be due to the viral constructs. Check that the fluorophor is fused to the opsin by sequencing the plasmid, if this is not the case, cytoplasmic staining can be expected. If it is fused and still low membrane-bound expression is detected, include a membrane targeting sequence.
6. For an effective optogenetic modulation, the opsins have to be expressed in high numbers; however, the cellular physiology should be affected as little as possible. A first indicator of the right level of expression is the absence of cells that died from overexpression. Those are recognizable by the bright small

fluorescent spots in the vicinity of the shadow of the soma. If only these spots are to be seen and no intact cells expressing the construct, most likely the virus titer has been too high.

7. Arc lamps provide suitable wavelengths and light powers for optogenetic stimulation if used with the correct set of filters. Yet, they are often subject to flickering, causing unwanted changes in the output power.
8. Be wary that underfilling the back aperture of the objective will increase the axial size of the focal spot much more than the lateral size. Importantly, increasing the diameter of the focal spot prevents imaging and stimulation with the same light path. One can use a diaphragm in the light path (which also decreases the power output as a part of the beam is blocked) to change the diameter of the parallel beam entering the objective.
9. To experimentally determine the light attenuation in *z-direction*, one can place tissue slices of different thicknesses between the light source and the power meter.
10. Alternatively if using a two photon microscope a fluorescent sample (either a plastic slide, fluorescent agarose or an actual fluorescent brain slice) can be bleached and subsequently imaged. Thereby the bleached area can be quantified in all three dimensions.
11. Control experiments:
    (a) Perform recordings in wild type (WT) animals and apply light at the same wavelength and power density as used in opsin-expressing animals.
    (b) If conducting virus injection perform experiments in animals injected with a virus encoding only the fluorophore; to control for unspecific effects of the expression of exogenous proteins to neuronal functionality.
12. To ensure recording of neuronal activity rather than light-evoked artifacts there are several potential measures:
    (a) Reduce the exposed metal surface by placing the metal electrode inside a glass electrode.
    (b) Use indium tin oxide (not affected by Becquerel effect) instead of tungsten microelectrodes.
    (c) Use silicon probes.
    (d) Reduce the light pulse width.
    (e) Change the illumination angle.

13. If not described in the literature characterize the kinetics of de-inactivation of the opsin [45]. This can be done in slice as the measurement is translatable to the in vivo situation:
    (a) Patch an opsin expressing cell in voltage clamp mode.
    (b) Illuminate the cell for a relatively long time (0.5 s), resulting in a bimodal current with a peak and a steady state component (Fig. 3b), followed by a second pulse after 1 s.
    (c) Increase the intervals between the light pulses from 1 to 10 s, in 1 s increments.
    (d) The time required to restore the initial amplitude of the peak current is the de-inactivation time of the construct.

References

1. Adamantidis AR, Zhang F, Aravanis AM, Deisseroth K, de Lecea L (2007) Neural substrates of awakening probed with optogenetic control of hypocretin neurons. Nature 450: 420–424
2. Airan RD, Thompson KR, Fenno LE, Bernstein H, Deisseroth K (2009) Temporally precise in vivo control of intracellular signalling. Nature 458:1025–1029
3. Akerboom J, Chen TW, Wardill TJ, Tian L, Marvin JS, Mutlu S, Calderon NC, Esposti F, Borghuis BG, Sun XR et al (2012) Optimization of a GCaMP calcium indicator for neural activity imaging. J Neurosci 32:13819–13840
4. Aravanis AM, Wang LP, Zhang F, Meltzer LA, Mogri MZ, Schneider MB, Deisseroth K (2007) An optical neural interface: in vivo control of rodent motor cortex with integrated fiberoptic and optogenetic technology. J Neural Eng 4:S143–S156
5. Arenkiel BR, Peca J, Davison IG, Feliciano C, Deisseroth K, Augustine GJ, Ehlers MD, Feng G (2007) In vivo light-induced activation of neural circuitry in transgenic mice expressing channelrhodopsin-2. Neuron 54:205–218
6. Berndt A, Schoenenberger P, Mattis J, Tye KM, Deisseroth K, Hegemann P, Oertner TG (2011) High-efficiency channelrhodopsins for fast neuronal stimulation at low light levels. Proc Natl Acad Sci U S A 108:7595–7600
7. Boyden ES, Zhang F, Bamberg E, Nagel G, Deisseroth K (2005) Millisecond-timescale, genetically targeted optical control of neural activity. Nat Neurosci 8:1263–1268
8. Cardin JA, Carlen M, Meletis K, Knoblich U, Zhang F, Deisseroth K, Tsai LH, Moore CI (2009) Driving fast-spiking cells induces gamma rhythm and controls sensory responses. Nature 459:663–667
9. Chow BY, Han X, Dobry AS, Qian X, Chuong AS, Li M, Henninger MA, Belfort GM, Lin Y, Monahan PE, Boyden ES (2010) High-performance genetically targetable optical neural silencing by light-driven proton pumps. Nature 463:98–102
10. Diester I, Kaufman MT, Mogri M, Pashaie R, Goo W, Yizhar O, Ramakrishnan C, Deisseroth K, Shenoy KV (2011) An optogenetic toolbox designed for primates. Nat Neurosci 14: 387–397
11. Dittgen T, Nimmerjahn A, Komai S, Licznerski P, Waters J, Margrie TW, Helmchen F, Denk W, Brecht M, Osten P (2004) Lentivirus-based genetic manipulations of cortical neurons and their optical and electrophysiological monitoring in vivo. Proc Natl Acad Sci U S A 101:18206–18211
12. Fenno L, Yizhar O, Deisseroth K (2011) The development and application of optogenetics. Ann Rev Neurosci 34:389–412
13. Gradinaru V, Mogri M, Thompson KR, Henderson JM, Deisseroth K (2009) Optical deconstruction of parkinsonian neural circuitry. Science 324:354–359
14. Gradinaru V, Thompson KR, Zhang F, Mogri M, Kay K, Schneider MB, Deisseroth K (2007) Targeting and readout strategies for fast optical neural control in vitro and in vivo. J Neurosci 27:14231–14238

15. Gradinaru V, Zhang F, Ramakrishnan C, Mattis J, Prakash R, Diester I, Goshen I, Thompson KR, Deisseroth K (2010) Molecular and cellular approaches for diversifying and extending optogenetics. Cell 141: 154–165
16. Grienberger C, Konnerth A (2012) Imaging calcium in neurons. Neuron 73:862–885
17. Gunaydin LA, Yizhar O, Berndt A, Sohal VS, Deisseroth K, Hegemann P (2010) Ultrafast optogenetic control. Nat Neurosci 13: 387–392
18. Han X, Qian X, Bernstein JG, Zhou HH, Franzesi GT, Stern P, Bronson RT, Graybiel AM, Desimone R, Boyden ES (2009) Millisecond-timescale optical control of neural dynamics in the nonhuman primate brain. Neuron 62:191–198
19. Jakobsson J, Ericson C, Jansson M, Bjork E, Lundberg C (2003) Targeted transgene expression in rat brain using lentiviral vectors. J Neurosci Res 73:876–885
20. Johansen JP, Hamanaka H, Monfils MH, Behnia R, Deisseroth K, Blair HT, LeDoux JE (2010) Optical activation of lateral amygdala pyramidal cells instructs associative fear learning. Proc Natl Acad Sci U S A 107: 12692–12697
21. Kajikawa Y, Schroeder CE (2011) How local is the local field potential? Neuron 72:847–858
22. Katz Y, Yizhar O, Staiger J, Lampl I (2013) Optopatcher – an electrode holder for simultaneous intracellular patch-clamp recording and optical manipulation. J Neurosci Methods 214:113–117
23. Knobloch HS, Charlet A, Hoffmann LC, Eliava M, Khrulev S, Cetin AH, Osten P, Schwarz MK, Seeburg PH, Stoop R, Grinevich V (2012) Evoked axonal oxytocin release in the central amygdala attenuates fear response. Neuron 73:553–566
24. Kravitz AV, Freeze BS, Parker PR, Kay K, Thwin MT, Deisseroth K, Kreitzer AC (2010) Regulation of parkinsonian motor behaviours by optogenetic control of basal ganglia circuitry. Nature 466:622–626
25. Lawlor PA, Bland RJ, Mouravlev A, Young D, During MJ (2009) Efficient gene delivery and selective transduction of glial cells in the mammalian brain by AAV serotypes isolated from nonhuman primates. Mol Ther 17:1692–1702
26. Lee JH, Durand DR, Gradinaru V, Zhang F, Goshen I, Kim DS, Fenno LE, Ramakrishnan C, Deisseroth K (2010) Global and local fMRI signals driven by neurons defined optogenetically by type and wiring. Nature 465(7299): 788–792
27. Lee SH, Kwan AC, Zhang S, Phoumthipphavong V, Flannery JG, Masmanidis SC, Taniguchi H, Huang ZJ, Zhang F, Boyden ES et al (2012) Activation of specific interneurons improves V1 feature selectivity and visual perception. Nature 488: 379–383
28. Lin JY, Lin MZ, Steinbach P, Tsien RY (2009) Characterization of engineered channelrhodopsin variants with improved properties and kinetics. Biophys J 96:1803–1814
29. Logothetis NK, Pauls J, Augath M, Trinath T, Oeltermann A (2001) Neurophysiological investigation of the basis of the fMRI signal. Nature 412:150–157
30. Lutz C, Otis TS, DeSars V, Charpak S, DiGregorio DA, Emiliani V (2008) Holographic photolysis of caged neurotransmitters. Nat Methods 5:821–827
31. Miyashita T, Shao YR, Chung J, Pourzia O, Feldman DE (2013) Long-term channelrhodopsin-2 (ChR2) expression can induce abnormal axonal morphology and targeting in cerebral cortex. Front Neural Circuit 7:8
32. Nagel G, Szellas T, Huhn W, Kateriya S, Adeishvili N, Berthold P, Ollig D, Hegemann P, Bamberg E (2003) Channelrhodopsin-2, a directly light gated cation-selective membrane channel. Proc Natl Acad Sci USA 100: 13940–13945
33. Nagel G, Brauner M, Liewald JF, Adeishvili N, Bamberg E, Gottschalk A (2005) Light activation of channelrhodopsin-2 in excitable cells of Caenorhabditis elegans triggers rapid behavioral responses. Curr Biol 15:2279–2284
34. Oh E, Maejima T, Liu C, Deneris E, Herlitze S (2010) Substitution of 5-HT1A receptor signaling by a light-activated G protein-coupled receptor. J Biol Chem 285:30825–30836
35. Packer AM, Peterka DS, Hirtz JJ, Prakash R, Deisseroth K, Yuste R (2012) Two-photon optogenetics of dendritic spines and neural circuits. Nat Methods 9:1202–1205
36. Paxinos G, Franklin KBJ (2001) The Mouse Brain in Stereotaxic Coordinates, 2nd edn. Academic Press, San Diego
37. Papagiakoumou E, Anselmi F, Begue A, de Sars V, Gluckstad J, Isacoff EY, Emiliani V (2010) Scanless two-photon excitation of channelrhodopsin-2. Nat Methods 7:848–854
38. Prakash R, Yizhar O, Grewe B, Ramakrishnan C, Wang N, Goshen I, Packer AM, Peterka DS, Yuste R, Schnitzer MJ, Deisseroth K (2012) Two-photon optogenetic toolbox for fast inhibition, excitation and bistable modulation. Nat Methods 9:1171–1179

39. Prigge M, Schneider F, Tsunoda SP, Shilyansky C, Wietek J, Deisseroth K, Hegemann P (2012) Color-tuned channelrhodopsins for multiwavelength optogenetics. J Biol Chem 287:31804–31812
40. Rickgauer JP, Tank DW (2009) Two-photon excitation of channelrhodopsin-2 at saturation. Proc Natl Acad Sci U S A 106:15025–15030
41. Rochefort NL, Jia H, Konnerth A (2008) Calcium imaging in the living brain: prospects for molecular medicine. Trends Mol Med 14:389–399
42. Sakmann B, Neher E (1984) Patch clamp techniques for studying ionic channels in excitable membranes. Ann Rev Physiol 46: 455–472
43. Stosiek C, Garaschuk O, Holthoff K, Konnerth A (2003) In vivo two-photon calcium imaging of neuronal networks. Proc Natl Acad Sci U S A 100:7319–7324
44. Stroh A, Adelsberger H, Groh A, Ruhlmann C, Fischer S, Schierloh A, Deisseroth K, Konnerth A (2013) Making waves: initiation and propagation of corticothalamic ca(2+) waves in vivo. Neuron 77:1136–1150
45. Stroh A, Tsai HC, Wang LP, Zhang F, Kressel J, Aravanis A, Santhanam N, Deisseroth K, Konnerth A, Schneider MB (2011) Tracking stem cell differentiation in the setting of automated optogenetic stimulation. Stem Cells 29:78–88
46. Stuber GD, Britt JP, Bonci A (2012) Optogenetic modulation of neural circuits that underlie reward seeking. Biol Psychiatry 71: 1061–1067
47. Tye KM, Prakash R, Kim SY, Fenno LE, Grosenick L, Zarabi H, Thompson KR, Gradinaru V, Ramakrishnan C, Deisseroth K (2011) Amygdala circuitry mediating reversible and bidirectional control of anxiety. Nature 471:358–362
48. Vaziri A, Emiliani V (2012) Reshaping the optical dimension in optogenetics. Curr Opin Neurobiol 22:128–137
49. Wang J, Wagner F, Borton DA, Zhang J, Ozden I, Burwell RD, Nurmikko AV, Van WR, Diester I, Deisseroth K (2012) Integrated device for combined optical neuromodulation and electrical recording for chronic in vivo applications. J Neural Eng 9:016001
50. Wentz CT, Bernstein JG, Monahan P, Guerra A, Rodriguez A, Boyden ES (2011) A wirelessly powered and controlled device for optical neural control of freely-behaving animals. J Neural Eng 8:046021
51. Witten IB, Lin SC, Brodsky M, Prakash R, Diester I, Anikeeva P, Gradinaru V, Ramakrishnan C, Deisseroth K (2010) Cholinergic interneurons control local circuit activity and cocaine conditioning. Science 330:1677–1681
52. Yizhar O, Fenno LE, Prigge M, Schneider F, Davidson TJ, O'Shea DJ, Sohal VS, Goshen I, Finkelstein J, Paz JT et al (2011) Neocortical excitation/inhibition balance in information processing and social dysfunction. Nature 477:171–178
53. Zeng H, Madisen L (2012) Mouse transgenic approaches in optogenetics. Prog Brain Res 196:193–213

Chapter 10

Salvaging Ruins: Reverting Blind Retinas into Functional Visual Sensors

Marion Mutter, Natalia Swietek, and Thomas A. Münch

Abstract

Blindness is one of the most devastating conditions affecting the quality of life. Hereditary degenerative diseases, such as retinitis pigmentosa, are characterized by the progressive loss of photoreceptors, leading to complete blindness. No treatment is known, the current state-of-the-art of restoring vision are implanted electrode arrays. As a recently discovered alternative, optical neuromodulators, such as channelrhodopsin, allow new strategies for treating these diseases by imparting light-sensitivity onto the remaining retinal neurons after photoreceptor cell death. Retinal degeneration is a heterogeneous set of diseases with diverse secondary effects on the retinal circuitry. Successful treatment strategies have to take into account this diversity, as only the existing retinal hardware can serve as substrate for optogenetic intervention. The goal is to salvage the retinal ruins and to revert the leftover tissue into a functional visual sensor that operates as optimally as possible. Here, we discuss three different successful approaches that have been applied to degenerated mouse retina.

Key words Visual restoration, Optogenetics

1 Retinal Restoration

Genetic mutations can have dramatic effects on the visual system. About 15 million people worldwide are affected by inherited retinal degenerative diseases [1]. One prominent example is Retinitis pigmentosa (RP) with around 30,000 patients in Germany alone (http://www.pro-retina.de/netzhauterkrankungen). The loss of vision is caused by a progressive degeneration of the rod photoreceptor and subsequently of the cone photoreceptors [2, 3] (Fig. 1). Characteristic symptoms are the loss of night vision in adolescence, loss of peripheral vision in young adulthood, and loss of central vision later in life [4]. Several approaches to treat this disease are being tested, ranging from virus-vector mediated gene therapy [5] to implantable electrical chips to stimulate surviving retinal neurons [6, 7]. Gene therapy aims at inserting a functional copy of the affected gene sequence to restore proper cell functionality.

Sidney Cambridge (ed.), *Photoswitching Proteins: Methods and Protocols*, Methods in Molecular Biology, vol. 1148,
DOI 10.1007/978-1-4939-0470-9_10,

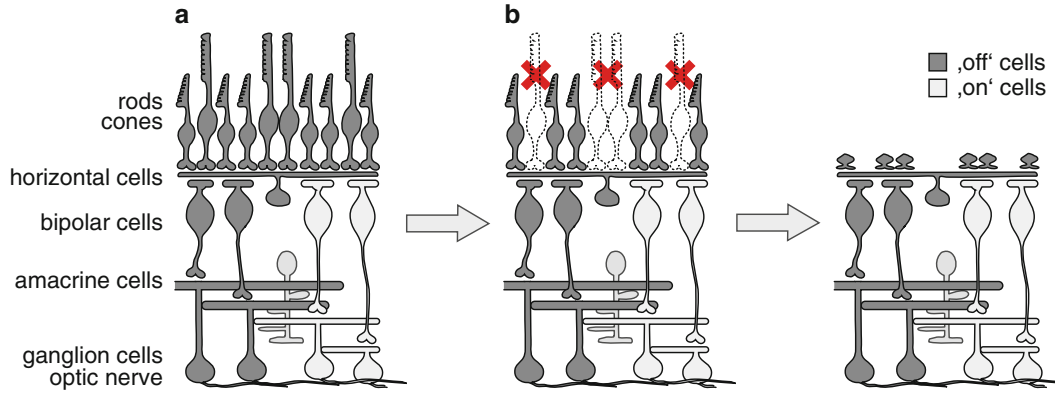

Fig. 1 Schematic representation of retinal degeneration in the mammalian retina. (**a**) Overview of the retinal layout. Vision begins with light reception by specialized cells, the photoreceptors (rods and cones), who convert light into electrical signals. Rod photoreceptors provide for sensitivity in dim light, whereas cone photoreceptors are active in bright light [35]. Several types of bipolar cells transmit the signal from photoreceptors to ganglion cells, which sent the preprocessed visual information to cortical areas through the optic nerve. Bipolar cells can be grouped in two categories: ON bipolar cells depolarize in response to light, OFF bipolar cells hyperpolarize to light. Accordingly, there are ON, OFF, and ON–OFF ganglion cells depending on the input they get from bipolar cells. Inhibitory interneurons modulate synaptic transmission between photoreceptors and bipolar cells (horizontal cells) and between bipolar cells and ganglion cells (amacrine cells). Although there are only two synaptic processing steps inside the retina, the retina performs substantial information processing: more than a dozen different representations of the incoming images are transmitted in parallel along the optic nerve. (**b**) Progressive retinal degeneration. A high number of genetic mutations can lead to retinal degeneration, often occurring in photoreceptors or the retinal pigment epithelium [1]. Often, rod photoreceptors are directly affected and degenerate first. This results in impaired vision and night blindness. The loss of rod photoreceptors is followed by degenerating cone photoreceptors. Depending on the severity of the phenotype, this can lead to partial loss of vision or total blindness. In humans, this process can take up to decades. Even in total blindness, cone photoreceptors can sometimes survive, even if they are not light-sensitive anymore. Schematic representation of retina based on [32] doi: 10.1371/journal.pone.0081278.g001 (CC-BY license)

However, due to the diversity of underlying genetic mutations, with diverse secondary effects on the retinal circuitry [8], the complexity of this strategy was highly underestimated [9]. More than 50 genes and 3,000 mutations were identified [3], demanding personalized gene analysis and virus production for each patient.

Alternatively, a new promising approach is optogenetics. The general idea is to restore light sensitivity in degenerated retinas with the help of light sensitive proteins. The unifying property of these proteins is that they are able to directly transform light into an electrical signal without the need of an additional signaling cascade (Fig. 2). One of the most widely used optogenetic proteins so far is channelrhodopsin-2 (ChR-2), originally found in the unicellular green algae *Chlamydomonas reinhardtii* [10]. These algae are able to detect light gradients in their surrounding and adjust their position to optimize photosynthesis by using at least two channelrhodopsins: ChR-1 and ChR-2 [11]. Both are light-gated unselective

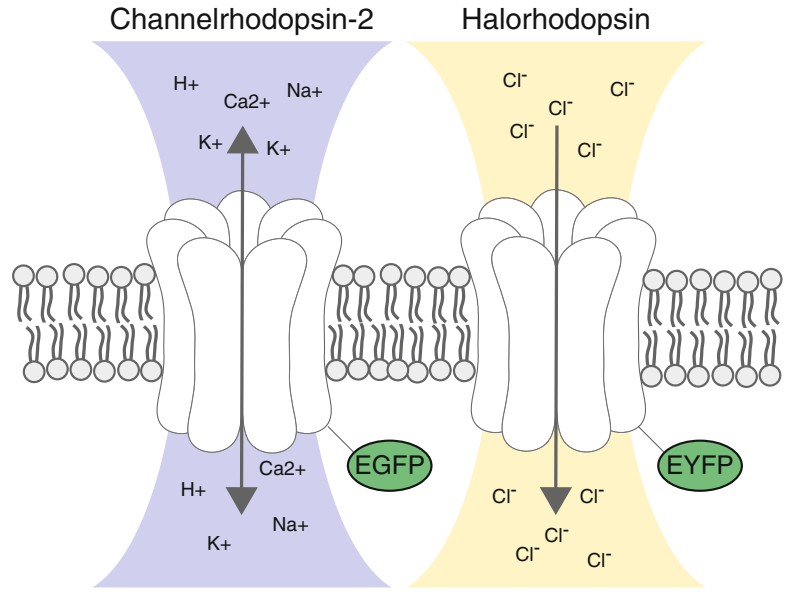

Fig. 2 Schematic drawing of the two optogenetic proteins channelrhodopsin-2 and halorhodopsin. Optogenetic proteins transform light energy into electric signals. They differ in spectral sensitivity, ion selectivity, and kinetic properties. Here we show two examples that have successfully been used in retinal restoration approaches. Channelrhodpsin-2 depolarizes cells in response to blue light (peak sensitivity 480 nm). This light-activated cation channel was originally found in *Chlamydomonas reinhardtii* [11]. In contrast, halorhodopsin responds best to yellow light (580 nm) and hyperpolarizes the cell due to its chloride pump function [14]

cation channels, with a broad conductance for H^+, Na^+, K^+, and Ca^{2+} ions [12]. The light-induced depolarization of the cells is maximal at the peak absorbance of 500 nm (ChR-1) and 470 nm (ChR-2) [13]. A different optogenetic tool with antagonistic action is halorhodopsin (eNpHR), a light-activated chloride pump that hyperpolarizes the target cell [14]. The peak wavelength sensitivity of eNpHR is at 580 nm [15]. Both ChR-2 and eNpHR have fast kinetic properties with deactivation time constants of about 10 ms and 4 ms, respectively [15]. Consequently, they can translate light information within the visible spectrum at sufficient temporal resolution and therefore are well suited for visual restoration.

In the following we describe three successful approaches of optogenetic vision restoration in the degenerated retina. These three studies can be considered milestones in the field. In general, research on optogenetic vision restoration always consists of two experimental steps:

Step 1: Expression of the optogene in the retina.
This includes the choice of optogene, the design of the delivery construct and method, and the choice of experimental model (e.g., a particular mouse line).

Info Box
Rhodopsin

Rhodopsin consists of a protein (opsin, a 7-transmembran protein) with a covalently bound chromophore (retinal) [16]. The retinal, which is a derivate of vitamin A, undergoes a conformational change upon photon absorption. In vertebrate rhodopsins, the retinal isomerizes from 11-cis to the all-trans conformation, resulting in a conformational change of the opsin [16]. This activates a G-protein based phototransduction signaling cascade. After activation, the retinal detaches from the opsin, a process known as bleaching, and has to be replaced with a new 11-cis retinal [17]. In contrast to this, the retinal bound to microbial rhodopsins photoisomerizes from the all-trans to the 13-cis conformation [18]. Again, the conformational change results in a cascade of structural changes of the opsin. Finally this leads to ion transport (halorhodopsin), channel opening (channelrhodopsin), or interaction with signaling transducers ("non-channel" rhodopsins) [19]. An important difference is that in microbial channelrhodopsins, the retinal remains covalently bound to the opsin and regenerates thermally [20].

Step 2: Evaluation of successful vision restoration.
The success of vision restoration is usually assessed at the level of histology (expression level), physiology (responses of expressing cells, the retina or the cortex to light) and behavior. In addition, some studies deal with biosafety aspects of expressing a foreign gene in the retina.

By using the three milestone studies as examples, we will highlight and describe these different methodological approaches used in the field.

1.1 Approach 1: Expressing ChR-2 in Ganglion Cells (Fig. 3a)

Bi and colleagues were the first to successfully restore visual function by expressing ChR-2 in the retina [21]. They achieved ChR-2 expression mainly in retinal ganglion cells, the output neurons of the retina which normally transmit the preprocessed visual information to higher brain areas. The reasoning for treating cells in the inner retinal layer was that they survive for many years after the death of photoreceptors [22]. Bi et al. convincingly showed that formerly blind retinas become light sensitive again and that the visual signals are transferred to the visual cortex.

1.1.1 Methodological Concepts

Step 1: Expression
Bi et al. designed a construct containing the gene sequence for a GFP-tagged ChR-2. They combined it with an unspecific basal promotor for β-actin (CAG) and the expression enhancing element WPRE (woodchuck hepatitis post-transcriptional regulatory element). For transfection, Bi et al. used adeno-associated viruses (AAV). Viruses have the useful property that they insert genetic sequences into host cells. Recombinant AAV are the most popular

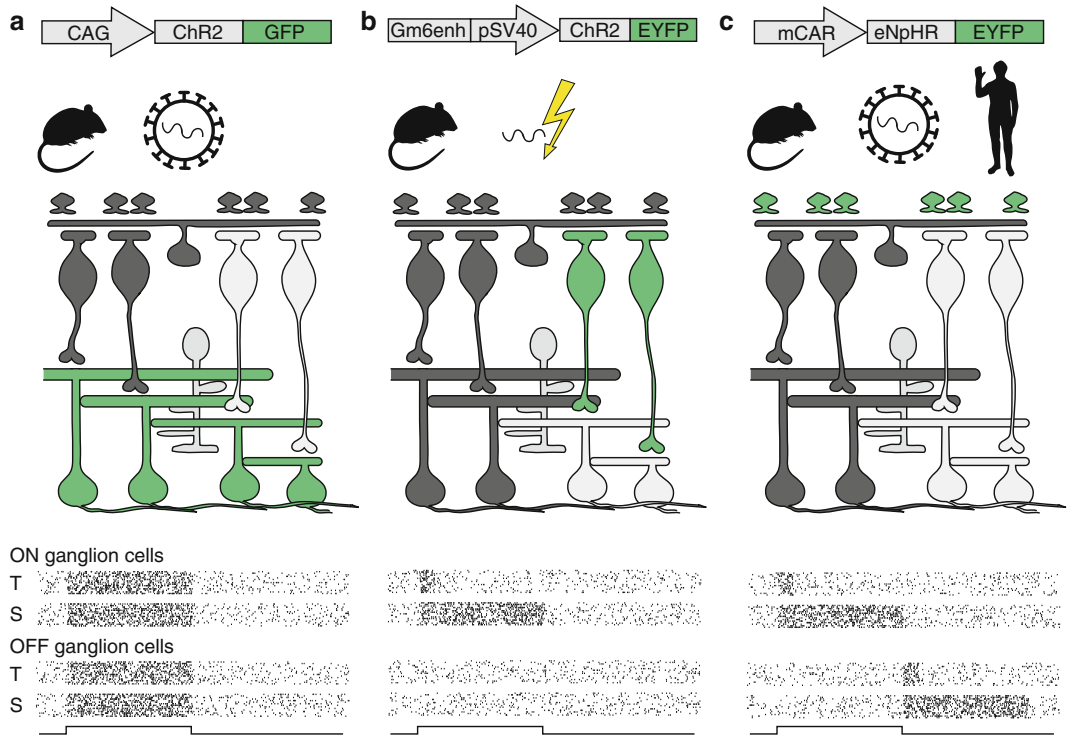

Fig. 3 Different visual restoration strategies with optogenetic proteins. Overview of the transfection methods and applied constructs (*top*), target cells in the retina (*middle*), and resulting response characteristics of ganglion cells (*bottom*, *ticks* represent action potentials as they would be recorded during many repetitions of the same stimulus), as they were applied by Bi et al. [21] (**a**), Lagali et al. [27] (**b**) and Busskamp et al. [30] (**c**). (**a**) ChR-2-GFP expressed in retinal ganglion cell after intravitreal injection of an adeno-associated virus. This strategy leads to sustained light responses in all expressing ganglion cells, independent of their natural response properties. (**b**) ChR-2-EYFP targeted to ON-bipolar cells by using a cell type specific enhancer. The construct was integrated into the retina by subretinal injection of the plasmid, followed by electroporation. This strategy faithfully restored many response characteristics of ON ganglion cells, including transient *T* and sustained *S* responses, but failed to elicit responses in OFF ganglion cells. (**c**) eNpHR-EYFP targeted to leftover cones by using a cell type specific promoter after subretinal injection of an adeno-associated virus. Expression was also achieved in postmortem human retina. This strategy faithfully restored most features of retinal processing, including appropriate responses in ON and OFF ganglion cells. Schematic representation of retina based on [32] doi: 10.1371/journal.pone.0081278.g001 (CC-BY license)

virus type for clinical studies. They have a very low oncogenic risk for the patients because all viral coding sequences have been removed [23]. Bi et al. demonstrated the expression and functionality of optogenetic proteins in retinas of wild type mice as well as in a mouse model for retinal degeneration. There are several visually impaired mouse strains, some of them especially designed for a better understanding of the pathogenesis of retinitis pigmentosa in humans [24]. A commonly used model is the retinal degenerating mouse model (rd1) with a well-known

genetic background. These mice have a fast and progressive retinal degeneration starting around post-natal day 8 (P8), leading to complete blindness around P30 [25]. The AAV containing the CAG-ChR2-WPRE construct was injected into the vitreous in the eye.

Step 2: Evaluation

Three to four weeks after intravitreal virus injection, all treated eyes showed bright GFP fluorescence. Even after 12 months the signal was mainly detected in the plasma membrane of retinal ganglion cells, confirming the successful expression of ChR-2-GFP. More importantly, the expressed ChR2 construct was functional: ChR-2-GFP expressing cells were responding to light stimuli, mostly at the peak sensitivity of 470 nm, both in wild type and rd1 ganglion cells, as identified through single-cell voltage clamp recordings. The currents evoked by ChR-2 were strong enough to depolarize the membrane and evoke action potentials. Consequently, Bi et al. were able to show activation of a large number of ganglion cells in transduced retinas with the help of microelectrode array (MEA) recordings. MEAs allow simultaneous extracellular recordings from a population of neurons. In the living animal, the light-evoked signal was transmitted to the brain, as demonstrated by the presence of visually evoked potentials in the visual cortex (V1). In summary, Bi et al. were the first to restore light sensitivity in blind mice (rd1).

In the study of Bi et al., all ganglion cells expressing ChR-2 were activated at the onset of light, consistent with the depolarizing effect of ChR. However, this presumably also included OFF-type ganglion cells, which would normally not be activated at light onset but at light offset. In normal vision, the retina does not simply relay a 1-to-1 image of the outside world to higher visual centers. Instead, many different features of the stimulus (contrast, movement, color, optic flow, etc.) are extracted, encoded, and sent in parallel over the optic nerve [26]. Simply making ganglion cells light sensitive does not restore this retinal preprocessing of visual information.

1.2 Approach 2: Expressing ChR-2 in ON Bipolar Cells (Fig. 3b)

In a first step to restore not only light sensitivity but also computational abilities of the retina, Lagali et al. targeted ON bipolar cells to express ChR-2 [27]. Bipolar cells are a class of retinal interneurons that normally integrate the signals of photoreceptors and forward them to retinal ganglion cells. Physiologically, they come in two flavors, ON and OFF bipolar cells, which de- or hyperpolarize in response to light. Targeting ON bipolar cells with ChR therefore maintains the natural response polarity of the cells. In addition, the natural antagonistic inhibition of ON visual channels

from OFF bipolar cell circuits can be avoided. Lagali et al. demonstrated that these treated retinas not only were responsive to light but also that certain types of image processing (e.g., center–surround antagonism, transient and sustained responses) were restored. In addition, they were able to show that the treated mice regained visual guided behavior.

1.2.1 Methodological Concepts

Step 1: Expression

Lagali et al. used a construct that put YFP-tagged ChR-2 under the control of an ON bipolar cell specific enhancer sequence (metabotropic glutamate receptor mGluR6). Currently, there are no AAV serotypes that can efficiently infect bipolar cells in the retina. Instead of viral transfection, Lagali et al. used in vivo electroporation of the vector into the retina. For this, the naked plasmid is injected subretinally, and then driven into cells by short electrical pulses that permeabilize the plasma membrane [28, 29]. Again, rd1 mice were used as a model system for retinal degeneration and restoration approaches. Like in the study of Bi et al., no detrimental effects could be observed when ChR-2 was expressed in wild type retinas.

Step 2: Evaluation

In the electroporated areas, Lagali et al. found around 7 % of all ON bipolar cells expressing ChR-2, stable for at least 6 months. Convincingly, they were able to measure with MEA recordings short latency spike activity as a response to light stimulation in treated rd1 mice but not in control animals. Lagali et al. could demonstrate that certain aspects of retinal processing were maintained in treated retinas. For example, even though ChR-2 itself and the expressing neurons are known to respond to light in a sustained fashion, i.e., they stay depolarized for as long as the light is on, ganglion cell responses in treated retina were both sustained and transient, as in healthy retina. Furthermore, center–surround antagonism could be demonstrated, which is one hallmark of retinal processing. This implies that inhibitory circuits are triggered and properly activated by the ChR-expressing bipolar cells. Indeed, whole cell patch clamp recordings from ganglion cells revealed not only light evoked excitatory inputs but also inhibitory inputs. In addition, the approach of Lagali et al. avoided improper activation of OFF ganglion cells at light onset, while at the same time it could not achieve their proper activation at light offset.

Lagali et al. were able to show visually evoked responses in the cortex of treated rd1 mice, and continued experiments to test whether ChR-2 vision could also induce behavioral responses in otherwise blind rd1 mice. In fact, ChR-2/rd1

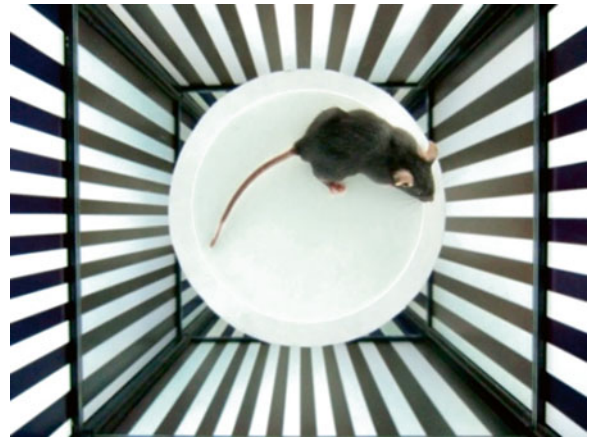

Fig. 4 Behavioral assessment with a virtual optokinetic drum [36]. The freely moving mouse is sitting on an elevated platform in the middle of the arena. The arena consists of four monitors, presenting a virtual cylinder with rotating *black* and *white stripes*. Mirrors on top and at the bottom elongate the stimulus. The mouse reflexively follows the rotating stripe pattern with head movements. The optokinetic reflex is used as a direct behavioral test whether an animal can see the pattern and to determine visual acuity and contrast sensitivity of the subject

mice passed the dark/light box test measured by increasing activity in the light period. Additionally, these mice showed an enhanced performance in the optokinetic reflex task in comparison to the control rd1 group. This behavioral experiment is based on the optokinetic reflex which causes the subject to follow rotating stripe pattern with eye and head movements. To trigger this reflex, the freely moving mouse is exposed to a rotating grating (Fig. 4). The behavioral tests indicated that optogenetically treated mice not only had light sensitivity but also a certain degree of vision leading to behavioral improvements.

1.3 Approach 3: Expressing NpHR in Cones (Fig. 3c)

Many retinal degenerative diseases primarily affect rod photoreceptors. Cones, on the other hand, remain functional for a longer time. Even when they become nonfunctional later in the disease progression, often they remain as living—albeit light-insensitive—neurons in the outer retina. There, they can serve as target for optogenetic intervention. Furthermore, targeting a neuron that early in the visual pathway raises the hope that visual processing in the retinal network can be maximally restored. This strategy was followed by Busskamp et al. in 2010 [30].

In photoreceptors, photon absorption triggers a signaling cascade ending in the hyperpolarization of the cells. Therefore the hyperpolarizing properties of halorhodopsin are in line with photoreceptor light responses.

1.3.1 Methodological Concepts

Step 1: Expression

Busskamp and his colleagues tried three different promoters to drive YFP-tagged NpHR expression in cones, of which the mouse cone arrestin-3 (mCar) promoter worked best. As models for retinal degeneration they chose two different mouse models, rd1 mice as in the previous studies, and a Cnga3-Rho double knockout mouse, which has nonfunctional cones (Cnga3 is a model for stationary night blindness); and nonfunctional degenerating rods [31]. Like Bi et al., they used AAV to insert the genetic construct into the target cells. Expression was stable for up to 8 months in the remaining photoreceptors, even though they were degenerating.

For the first time, Busskamp et al. also demonstrated translational aspects of the optogenetic approach to treating blindness. For this they used postmortem human retina, obtained from the cornea bank in Amsterdam, Netherlands. To keep the retina alive for several days, tissue was kept in culture and supplied with enriched medium, especially adapted to the needs of neuronal cells. For a fast and strong expression, they used a different viral vector, lentiviruses, to transduce the mCar-eNpHR-EYFP-WPRE construct into the retina. Lentiviruses release double-stranded RNA sequences into the host cell, together with a reverse transcriptase to translate RNA in DNA. The gene sequence is then integrated into the host genome resulting in stable long-term expression but also in a higher oncogenic risk. The big advantage of lentiviruses is that they can also infect nondividing cells very efficiently. After treating cultured postmortem human retina, they were able to detect high NpHR protein expression in photoreceptors after only 1–2 days incubation time.

Step 2: Evaluation

Whole cell patch clamp recordings of cone photoreceptors in mice showed very strong responses while cone photoreceptors of the blind control group (untreated or only EGFP treated) did not respond to light stimulation. As expected for halorhodopsin, photoreceptors responded best around 580 nm. One important prerequisite for the cone approach to work is that the synapses between inner and outer retina are still functional, despite the strongly altered cone morphology in these retinae. Busskamp et al. demonstrated this by successfully recording light-triggered activity from the ganglion cells. Amazingly, a large range of naturally occurring activity of ganglion cells could be demonstrated, ranging from the proper activation of ON and OFF ganglion cells, center–surround antagonism, and even complex image processing like direction-selective responses which requires nonlinear neural computations involving excitatory and inhibitory interneurons in the retina.

Behaviorally, the treated blind mice performed significantly better in the dark/light box as well as in the optomotor reflex test. However, this was only true for rd1 mouse model, not for the Cnga3/Rho mouse model. Presumably this is owed to the fact that the latter mice have never had functional vision during development, since both photoreceptor classes are nonfunctional, while rd1 animals have functional vision for a brief period before the rapid retinal degeneration kicks in.

Electrophysiological recordings of cone photoreceptors in the cultured postmortem human retina showed that these cells were responding to light stimuli, while in control retinas, photoreceptors were not responding any more.

2 Discussion/Future Possibilities

Optogenetic vision restoration is a highly promising approach for treating blindness. The studies described above have demonstrated that the idea is feasible. Furthermore, they illustrate the wide spectrum of methods that have to be applied for a complete study of optogenetic vision restoration, from molecular cloning, virus production, virus injection, electroporation, electrophysiology (patch clamp—MEA—cortical recordings), behavioral testing and tissue culture. This review was meant to give an overview of this diversity of methods. Each of these methods has its own complexity and could easily fill its own method chapter.

Convincingly, all three studies were able to show the potential of restoring vision in retinal degeneration mouse models. On the electrophysiological level, the "blind" retina was reliably responding to light stimuli. Moreover, the treated mice were showing light evoked behavioral responses. But there is still a long way to go to adapt the system for human retina. Here, Busskamp et al. laid the foundation by resensitizing cultured human retinal tissue. He and his colleagues showed first results on expression and function of optogenetic proteins in postmortem human retinal photoreceptors.

However, there are general differences between the native visual system and the optogenetically restored vision that have to be considered for future approaches. One striking difference is the lack of light adaptation. Because of adaptation, our own visual system can support vision over a range of about a dozen orders of intensity magnitude. In contrast, with optogenetics one can activate cells only over a relatively restricted range of light intensities, spanning between two and three orders of magnitude [27]. The behavioral experiments described above have shown that it is generally possible to elicit light-induced behavior in optogenetically treated mice, but high light intensities were necessary to do so. What distinguishes normal vision from optogenetic vision is however not so much the biophysical response properties and sensitivity of the individual molecular light sensors

(rhodopsins in both cases), but rather the machinery with which their responses are translated into cellular activity [32]. Thus, improved constructs should be more light sensitive, to work also under dimmer daylight conditions. One promising candidate is the newly discovered channelrhodopsin variant CatCh, with a ~70-fold increased light sensitivity compared to wild-type ChR2 due to increased Ca^{2+} permeability [33]. This is one of several examples for successful engineering of channelrhodopsins with enhanced properties. Another interesting candidate for future vision restoration approaches is the tandem protein vChR2–ChR1 with the benefit of a combined wavelength sensitivity, covering the full visible range of 400–600 nm [34].

Importantly, there is still a lack of knowledge about the human retina on the functional level. Most of the findings about the wiring and the properties of the computational network were made in laboratory animals. To develop and improve directed treatment approaches, it will be important to study the human retina directly.

References

1. Gargini C, Terzibasi E, Mazzoni F, Strettoi E (2007) Retinal organization in the retinal degeneration 10 (rd10) mutant mouse: a morphological and ERG study. J Comp Neurol 500(2):222–238. doi:10.1002/cne.21144
2. Delyfer MN, Leveillard T, Mohand-Said S, Hicks D, Picaud S, Sahel JA (2004) Inherited retinal degenerations: therapeutic prospects. Biol Cell 96(4):261–269. doi:10.1016/j.biolcel.2004.01.006
3. Daiger SP, Sullivan LS, Bowne SJ (2013) Genes and mutations causing retinitis pigmentosa. Clin Genet 84:132. doi:10.1111/cge.12203
4. Hartong DT, Berson EL, Dryja TP (2006) Retinitis pigmentosa. Lancet 368(9549):1795–1809. doi:10.1016/S0140-6736(06)69740-7
5. Acland GM, Aguirre GD, Ray J, Zhang Q, Aleman TS, Cideciyan AV, Pearce-Kelling SE, Anand V, Zeng Y, Maguire AM, Jacobson SG, Hauswirth WW, Bennett J (2001) Gene therapy restores vision in a canine model of childhood blindness. Nat Genet 28(1):92–95. doi:10.1038/88327
6. Stingl K, Bartz-Schmidt KU, Besch D, Braun A, Bruckmann A, Gekeler F, Greppmaier U, Hipp S, Hortdorfer G, Kernstock C, Koitschev A, Kusnyerik A, Sachs H, Schatz A, Stingl KT, Peters T, Wilhelm B, Zrenner E (2013) Artificial vision with wirelessly powered subretinal electronic implant alpha-IMS. Proc Biol Sci 280(1757):20130077. doi:10.1098/Rspb.2013.0077
7. Zrenner E (2002) Will retinal implants restore vision? Science 295(5557):1022–1025. doi:10.1126/science.1067996
8. Boye SE, Boye SL, Lewin AS, Hauswirth WW (2013) A comprehensive review of retinal gene therapy. Mol Ther 21(3):509–519. doi:10.1038/mt.2012.280
9. Flannery JG, Greenberg KP (2006) Looking within for vision. Neuron 50(1):1–3. doi:10.1016/j.neuron.2006.03.027
10. Nagel G, Ollig D, Fuhrmann M, Kateriya S, Musti AM, Bamberg E, Hegemann P (2002) Channelrhodopsin-1: a light-gated proton channel in green algae. Science 296(5577):2395–2398. doi:10.1126/science.1072068
11. Nagel G, Szellas T, Huhn W, Kateriya S, Adeishvili N, Berthold P, Ollig D, Hegemann P, Bamberg E (2003) Channelrhodopsin-2, a directly light-gated cation-selective membrane channel. Proc Natl Acad Sci U S A 100(24):13940–13945. doi:10.1073/pnas.1936192100
12. Tsunoda SP, Hegemann P (2009) Glu 87 of channelrhodopsin-1 causes pH-dependent color tuning and fast photocurrent inactivation. Photochem Photobiol 85(2):564–569. doi:10.1111/j.1751-1097.2008.00519.x
13. Berthold P, Tsunoda SP, Ernst OP, Mages W, Gradmann D, Hegemann P (2008) Channelrhodopsin-1 initiates phototaxis and photophobic responses in Chlamydomonas by immediate light-induced depolarization. Plant Cell 20(6):1665–1677. doi:10.1105/tpc.108.057919
14. Lanyi JK (1990) Halorhodopsin, a light-driven electrogenic chloride-transport system. Physiol Rev 70(2):319–330
15. Fenno L, Yizhar O, Deisseroth K (2011) The development and application of optogenetics.

Annu Rev Neurosci 34:389–412. doi:10.1146/annurev-neuro-061010-113817

16. Grobner G, Choi G, Burnett IJ, Glaubitz C, Verdegem PJ, Lugtenburg J, Watts A (1998) Photoreceptor rhodopsin: structural and conformational study of its chromophore 11-cis retinal in oriented membranes by deuterium solid state NMR. FEBS Lett 422(2):201–204
17. Burns ME, Baylor DA (2001) Activation, deactivation, and adaptation in vertebrate photoreceptor cells. Annu Rev Neurosci 24:779–805. doi:10.1146/annurev.neuro.24.1.779
18. Yizhar O, Fenno LE, Davidson TJ, Mogri M, Deisseroth K (2011) Optogenetics in neural systems. Neuron 71(1):9–34. doi:10.1016/j.neuron.2011.06.004
19. Zhang F, Vierock J, Yizhar O, Fenno LE, Tsunoda S, Kianianmomeni A, Prigge M, Berndt A, Cushman J, Polle J, Magnuson J, Hegemann P, Deisseroth K (2011) The microbial opsin family of optogenetic tools. Cell 147(7):1446–1457. doi:10.1016/j.cell.2011.12.004
20. Haupts U, Tittor J, Bamberg E, Oesterhelt D (1997) General concept for ion translocation by halobacterial retinal proteins: the isomerization/switch/transfer (IST) model. Biochemistry 36(1):2–7. doi:10.1021/bi962014g
21. Bi A, Cui J, Ma YP, Olshevskaya E, Pu M, Dizhoor AM, Pan ZH (2006) Ectopic expression of a microbial-type rhodopsin restores visual responses in mice with photoreceptor degeneration. Neuron 50(1):23–33. doi:10.1016/j.neuron.2006.02.026
22. Flannery JG, Farber DB, Bird AC, Bok D (1989) Degenerative changes in a retina affected with autosomal dominant retinitis pigmentosa. Invest Ophthalmol Vis Sci 30(2):191–211
23. Petersen-Jones SM (2012) Viral vectors for targeting the canine retina: a review. Vet Ophthalmol 15(Suppl 2):29–34. doi:10.1111/j.1463-5224.2012.01054.x
24. Chang B, Hawes NL, Pardue MT, German AM, Hurd RE, Davisson MT, Nusinowitz S, Rengarajan K, Boyd AP, Sidney SS, Phillips MJ, Stewart RE, Chaudhury R, Nickerson JM, Heckenlively JR, Boatright JH (2007) Two mouse retinal degenerations caused by missense mutations in the beta-subunit of rod cGMP phosphodiesterase gene. Vision Res 47(5):624–633. doi:10.1016/j.visres.2006.11.020
25. Bowes C, Li T, Danciger M, Baxter LC, Applebury ML, Farber DB (1990) Retinal degeneration in the rd mouse is caused by a defect in the beta subunit of rod cGMP-phosphodiesterase. Nature 347(6294):677–680. doi:10.1038/347677a0
26. Gollisch T, Meister M (2010) Eye smarter than scientists believed: neural computations in circuits of the retina. Neuron 65(2):150–164. doi:10.1016/j.neuron.2009.12.009
27. Lagali PS, Balya D, Awatramani GB, Munch TA, Kim DS, Busskamp V, Cepko CL, Roska B (2008) Light-activated channels targeted to ON bipolar cells restore visual function in retinal degeneration. Nat Neurosci 11(6):667–675. doi:10.1038/nn.2117
28. Matsuda T, Cepko CL (2004) Electroporation and RNA interference in the rodent retina in vivo and in vitro. Proc Natl Acad Sci U S A 101(1):16–22. doi:10.1073/pnas.2235688100
29. Matsuda T, Cepko CL (2007) Controlled expression of transgenes introduced by in vivo electroporation. Proc Natl Acad Sci U S A 104(3):1027–1032. doi:10.1073/pnas.0610155104
30. Busskamp V, Duebel J, Balya D, Fradot M, Viney TJ, Siegert S, Groner AC, Cabuy E, Forster V, Seeliger M, Biel M, Humphries P, Paques M, Mohand-Said S, Trono D, Deisseroth K, Sahel JA, Picaud S, Roska B (2010) Genetic reactivation of cone photoreceptors restores visual responses in retinitis pigmentosa. Science 329(5990):413–417. doi:10.1126/science.1190897
31. Huber G, Beck SC, Grimm C, Sahaboglu-Tekgoz A, Paquet-Durand F, Wenzel A, Humphries P, Redmond TM, Seeliger MW, Fischer MD (2009) Spectral domain optical coherence tomography in mouse models of retinal degeneration. Invest Ophthalmol Vis Sci 50(12):5888–5895. doi:10.1167/iovs.09-3724
32. Mutter M, Münch T (2013) Strategies for expanding the operational range of channelrhodopsin in optogenetic vision. PLoS One 8:e81278. doi:10.1371/journal.pone.0081278
33. Kleinlogel S, Feldbauer K, Dempski RE, Fotis H, Wood PG, Bamann C, Bamberg E (2011) Ultra light-sensitive and fast neuronal activation with the Ca(2)+-permeable channelrhodopsin CatCh. Nat Neurosci 14(4):513–518. doi:10.1038/nn.2776
34. Kleinlogel S, Terpitz U, Legrum B, Gokbuget D, Boyden ES, Bamann C, Wood PG, Bamberg E (2011) A gene-fusion strategy for stoichiometric and co-localized expression of light-gated membrane proteins. Nat Methods 8(12):1083–1088. doi:10.1038/nmeth.1766
35. Cepko C (2010) Neuroscience. Seeing the light of day. Science 329(5990):403–404. doi:10.1126/science.1194086
36. Benkner B, Mutter M, Ecke G, Munch TA (2013) Characterizing visual performance in mice: an objective and automated system based on the optokinetic reflex. Behav Neurosci 127:788–796. doi:2013-29457-001 [pii] 10.1037/a0033944

Chapter 11

Photoactivated Adenylyl Cyclases as Optogenetic Modulators of Neuronal Activity

Wagner Steuer Costa, Jana Liewald, and Alexander Gottschalk

Abstract

In recent years, optogenetic methods became invaluable tools, particularly in neurobiological research. Most prominently, optogenetic methods utilize microbial rhodopsins to elicit neuronal de- or hyperpolarization. However, other optogenetic tools have emerged that allow influencing neuronal function by different approaches. In this chapter we describe the use of photoactivated adenylyl cyclases (PACs) as modulators of neuronal activity. Using *Caenorhabditis elegans* as a model organism, this chapter shows how to measure the effect of PAC photoactivation by behavioral and electrophysiological assays, as well as their significance to neurobiology.

Key words Photoactivated adenylyl cyclase, PAC, *Caenorhabditis elegans*, Tracker, Electrophysiology

1 Introduction

Caenorhabditis elegans is a ~1 mm long transparent nematode with known genomic sequence [1]. It is cultivated on *E. coli* OP50 bacteria and has a generation time of 3–4 days at 20 °C [2]. Neurobiology studies are further facilitated by the eutelic nature of the animal, the low cell count of 302 neurons (about 30 % of all cells), and the known connectivity pattern [3]. These properties allow a relatively easy adoption of optogenetic methods compared to the effort needed in other model organisms.

A collection of optogenetic methods has been developed for spatiotemporal control of neuronal firing with a minimum invasive approach in *C. elegans* [4, 5]. The majority of applications use microbial rhodopsins or their derivates. Widely known examples are Channelrhodopsin-2, a blue light-activated cation channel, and Halorhodopsin, a yellow light-activated chloride pump [6–9]. However, these proteins do not activate or inhibit neuronal activity in an entirely natural manner, but rather override any intrinsic

Sidney Cambridge (ed.), *Photoswitching Proteins: Methods and Protocols*, Methods in Molecular Biology, vol. 1148,
DOI 10.1007/978-1-4939-0470-9_11,

signal being processed by the neuron or population of neurons of interest, thus perturbing circuit function. They thus do not allow to simply accentuate intrinsic activities of a circuit.

Expression of photoactivated adenylyl cyclases (PACs), like the *Euglena* PACα (EuPACα) or *Beggioatoa* PAC (bPAC) [10–14] in the neurons of interest may overcome the deficits of canonical optogenetic tools, because they do not evoke neurotransmitter release per se, like depolarization does. Rather, cAMP can affect neuronal firing through at least two different pathways: Via PKA-mediated phosphorylation [15] of downstream targets that affect synaptic vesicle docking and priming through presently ill-defined mechanisms, and via Epac, an exchange protein activated by cAMP [16]. Thus, intrinsic activity will lead to the release of more transmitter than usual, and consequently circuit activity becomes accentuated and behaviors are increased, in a coordinated fashion.

EuPACα and bPAC each contain two (in EuPACα) or one (in bPAC) "blue light sensor using FAD" (BLUF) domains [17], as well as two or one adenylyl-cyclase domains [12, 13], respectively. They form dimers, and upon BLUF domain activation by absorption of a photon, they generate cAMP from ATP. BLUF domain activation by light is reversible and does not lead to degradation of the PAC. Light sensitivity, kinetics, and enzymatic parameters, as well as dark activity levels differ for different PACs. Blue light thus will lead to a more or less rapid and robust increase in cAMP levels. Generally, EuPAC has a comparably high dark activity, rapid onset of light-induced cAMP production, and comparably low light sensitivity, while bPAC is highly light sensitive, produces more overall cAMP and has very low dark activity, but responds more slowly to light onset (bPAC: $\tau off = 12.3$ s; $K_M = 3.7 \pm 0.4$ μW/mm² in TRIS–HEPES buffer [13]). Work by Yoshikawa et al. showed that, in vitro, EuPACα is only active as long as it is exposed to blue light [18]. Pulsed photoactivation of PACs results in lower cAMP production and this has to be taken into account when designing experiments, but is also a means to finely control the induced increase in cAMP concentration. The effects of cAMP may be long-lasting in vivo, with the duration of the signal depending on the activity of, among others, phosphodiesterases, Epacs, and protein kinase A. EuPAC expression levels need to be well-controlled to avoid any compensatory mechanisms in response to constantly elevated cAMP levels due to its dark activity [10]. Working with bPAC is complicated by its high light sensitivity, as ambient light levels have to be kept very low to avoid unwanted (pre-) activation before the actual experiment (our unpublished observations). Furthermore, fusion constructs of PACs with fluorescent proteins, for instance, have been reported, but addition of a fusion tag to the BLUF domain may lead to protein inactivation (our unpublished observations).

PACs have been successfully used to study different model systems (not only in neurobiology), for instance: *Aplysia*, *Caenorhabditis*

elegans, *Drosophila melanogaster*, *Escherichia coli*, cultured insect cells (Sf9, *Spodoptera frugiperda*), *Toxoplasma gondii*, and *Xenopus* spinal neurons in culture [10, 11, 19–24].

This chapter describes how to assess experimental readouts after PAC photo-stimulation in neurons and potentially whole neural networks, by example of the *C. elegans* cholinergic neurons. These neurons are critically regulating *C. elegans* locomotion, by providing excitatory signals to both muscles and GABAergic neurons, the latter of which inhibit muscles on the opposite side of the body, thus evoking a body bend coordinately with the action of the cholinergic neurons [25]. Cholinergic motor neurons are essential for *C. elegans* crawling on solid substrate, as well as for it swimming in liquid. Here we assess electrophysiological and behavioral changes upon PAC activation, for example the swimming behavior of *C. elegans* with periodic swimming locomotion (thrashing) of a wavelength about twice the length of the animal.

Application of a specific PAC as an optogenetic tool depends on its kinetic properties compared to the expected outcome of the optogenetic experiment as well as its dark activity. Furthermore PACs may be used to investigate signaling cascades activated by cAMP itself, since cAMP has many modes of action and, by the time of writing, these are still not fully understood.

2 Materials

Prepare all solutions using double-distilled water and analytical grade reagents. Prepare and store all reagents at room temperature unless indicated otherwise.

2.1 Common Materials

1. "KPO_4"-*Buffer*: 1 M KH_2PO_4, 1 M K_2HPO_4, pH 6.
2. *NGM*: 0.3 % (w/v) NaCl, 1.7 % (w/v) Agar, 0.25 % (w/v) Trypton/Pepton, 1 mM $CaCl_2$, 1 mM $MgSO_4$, 25 mM "KPO_4"-Buffer, 0.0005 % (w/v) Cholesterol (in ethanol), autoclaved.
3. Aluminum foil.

2.2 Analyses of Behavior in Liquid

1. *M9 Buffer*: 20 mM KH_2PO_4, 40 mM Na_2HPO_4, 85 mM NaCl, 1 mM $MgSO_4$.
2. 96-well microtiter plate filled with 80 µl NGM and 80 µl M9 for the assay (*see* **Note 1**).
3. Regulatable blue light source (450–490 nm) with a maximum intensity output of about 1 mW/mm^2, in the objective/microscope focal plane, for photo-activation of PAC (*see* **Note 2**).
4. Stereomicroscope: SMZ 645 (Nikon, Japan) equipped with a red optical cast plastic filter (2″ × 2″, #43-946, Edmund Optics, Germany) for red background light (*see* **Note 3**).

5. Thumb counter.
6. Video camera for recording of experiment (i.e., Canon G9 with adapter for stereomicroscope).

2.3 Analyses of Behavior on Solid Substrate

1. 6.5 cm wide petri dish.
2. Leica MZ 16 F with Excite light source and filters, or equivalent, equipped with an 8 bit grayscale camera of at least 640 × 480 pixel resolution.
3. Computer with a running installment of "OptoTracker" software (*see* **Note 4**) [26, 27]. Install OptoTracker from our web site [http://www.biochem.uni-frankfurt.de/index.php?id=236]. The software runs on MatLab 2007 or higher including the Image Acquisition and the Image Processing Toolboxes. The computer needs a parallel port for transistor-transistor logic (TTL) communication with the shutter present at the light source.

2.4 Electrophysiology

1. *C. elegans* Ringer's (CR): 150 mM NaCl, 5 mM KCl, 5 mM $CaCl_2$, 1 mM $MgCl_2$, 10 mM glucose, 15 mM HEPES (pH 7.35), ~340 mOsm, sterile filtered (filter pore size 0.22 μm). Store at 4 °C.
2. *Collagenase solution*: 0.5 mg/ml collagenase (C-5138, Sigma, Germany) diluted in CR. Store at −20 °C.
3. *Pipette solution*: 120 mM KCl, 20 mM KOH, 4 mM $MgCl_2$, 5 mM TES pH 7.2, 0.25 mM $CaCl_2$, 4 mM Na_2ATP, 36 mM sucrose, 5 mM EGTA, ~315 mOsm. Store at −20 °C.
4. *Histoacryl blue glue*: A cyanoacrylic tissue adhesive (B. Braun Aesculap, Germany).
5. *Dental wax square ropes*: #50094491, Heraeus, USA.
6. *Sylgard coated cover glass*: Combine the two components of Sylgard 184 (Dow Corning, USA)—silicone elastomer base (9 ml) and curing agent (1.5 ml)—and mix them very thoroughly. Position a 25 mm circular cover glass at the bottom of a small petri dish (for easier transport) and put it on a plane surface. Add ~400 μl of the Sylgard mixture in the middle of the cover glass. Wait for 10–30 min while the mixture is slowly spreading on the cover glass surface forming a thin coating (Fig. 1) (*see* **Note 5**). For curing the petri dish with the cover glass should be closed (to avoid dirt) and put into a drying cabinet at 60 °C for ~8 h. Prepare 30–50 Sylgard coated cover glasses at a time and store them at room temperature in a closed box to avoid them getting dusty.
7. *Recording chamber*: Various recording chambers are commercially available but they are usually very expensive. Our recording chamber was custom manufactured in the university machine shop. It was made of Plexiglas (10 × 5 × 0.5 cm) with a circular hole in the middle (∅ 25 mm; tapered at an angle of

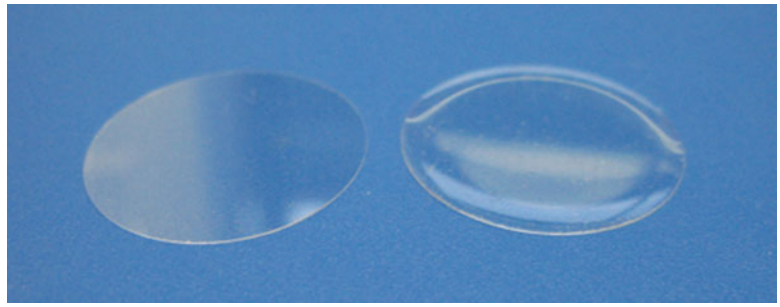

Fig. 1 Cover glass before (*left*) and after (*right*) coating with Sylgard. Sylgard eases the process to glue and dissect the animal

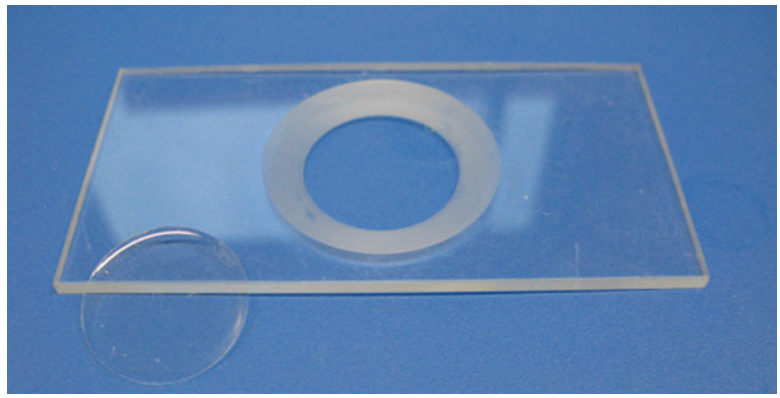

Fig. 2 Recording chamber and a Sylgard coated cover glass (*front left*)

ca. 30° on one side) (Fig. 2). Close off the backside of the chamber with a 50 mm circular cover glass. Connect cover glass and Plexiglas by pipetting ~200 µl of liquid Paraffin, melted at 80 °C, in between. To allow better spreading of the Paraffin, the backside of the chamber can once again be put onto a hot plate (80 °C) for a few seconds. The Paraffin will melt again quickly to completely and evenly fill the space between the chamber and the cover glass by capillary action. Use a Q-tip to remove any Paraffin that leaked inside the cavity of the recording chamber before it resolidifies.

8. *Borosilicate glass capillaries*: Filament-containing glass capillaries with an outer diameter of 1 mm (#1B100F-4, WPI, Germany) are used to produce gluing, dissection, extraction, and patch pipettes. Use a laser-based micropipette puller (P-2000, Sutter Instrument, USA) to fabricate pipettes with the required tip opening (see below). Always prepare several pipettes of each type (~8–20) to have extra ones in case of problems. (a) Gluing pipette: tip ∅ ~4 µm. (b) Incision pipette: tip ∅ ~1–2 µm. (c) Extraction pipette: tip ∅ ~30 µm. (d) Patch

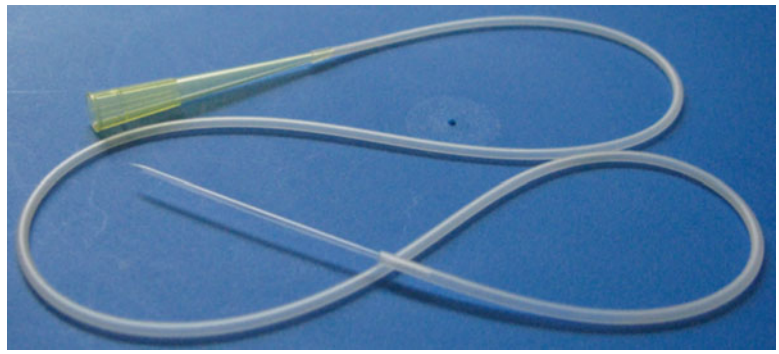

Fig. 3 Glue applicator consists of a needle linked to a pipette tip by a polyethylene tube. Mouth air pressure is used to fill the needle with glue and to glue the dissected animal to the dish

pipette: tip ∅ ~3 μm, resistance 4–7 MΩ. The patch pipettes should always be pulled anew on the day of the experiment and should then be fire-polished (Micro Forge MF-830, Narishige, Japan). Type a–c pipettes are connected via polyethylene tubing to a yellow pipette tip which is used to apply mouth-pressure (Fig. 3).

9. *Stereomicroscope*: Stemi 2000 (Zeiss, Germany) with a 5× zoom range and equipped with 20× oculars and an auxiliary objective (2×, #455028).
10. *Inverted microscope*: Axioskop 2 FS plus (Zeiss, Germany) with 2.5× air and 40× water-immersion objectives, respectively.
11. *Micromanipulator*: Stereomicroscope - Mk1 (Singer Instruments, UK); Inverted microscope - PCS-5000 (Burleigh, USA).
12. *Patch-clamp amplifier*: EPC 10 (HEKA, Germany) controlled by data acquisition software Patchmaster which can be operated on a regular PC.
13. *LED lamp*: KSL-70 (470 nm, 8 mW/mm^2), Rapp OptoElectronic (Germany).
14. *Electrophysiology rig* (Fig. 4):
    (a) Anti-vibration isolating lab table.
    (b) Motorized platform (Gibraltar, Burleigh, USA).
    (c) Inverted microscope.
    (d) Micromanipulator.
    (e) Amplifier.
    (f) PC.
    (g) Faraday cage.
15. *Mini Analysis software*: Can be downloaded at http://www.synaptosoft.com/MiniAnalysis/ (Synaptosoft, USA; purchase charge applies).

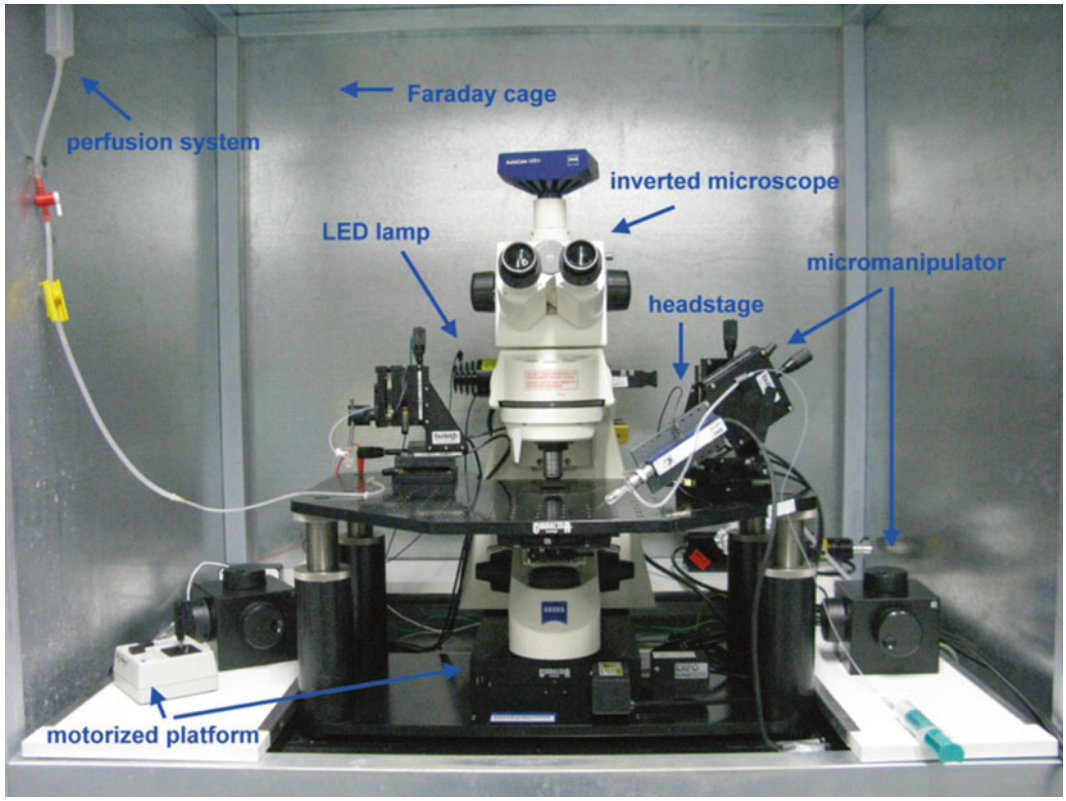

Fig. 4 Electrophysiology setup detailing the different components

3 Methods

3.1 Analyses of Behavior in Liquid

1. Transfer ten animals about 24 h after L4-stage to a well. Animals should be without or with only a minimum of OP50 bacteria.
2. Wait 15 min to allow animals to adapt to the new environment.
3. Acquire a video of the experiment (*see* **Note 6**). For PAC expressed in cholinergic neurons (strain ZX785: *lite-1*(*ce314*); *zxEx513*[*punc-17*::*GFP*::*PACa*; *pelt-2*::*mCherry*]) [10] the protocol used is 20 s without blue light followed by 20 s photoactivation and again 20 s without blue light.
4. Play the video in slow motion while counting the amount of thrashes an animal does in a defined time bin (i.e., 10 s). PACs photoactivation enhances activity in cholinergic neurons, resulting in a behavioral change.
5. Repeat **steps 1–4** for each strain and condition to be tested at least thrice (*see* **Note 7**).
6. Calculate the thrashing frequency and statistical significances in the statistics program of your choice (e.g., Origin, Prism, Excel).

3.2 Analyses of Behavior on Solid Substrate

1. Prepare assay plates 2 days before experiment. Pour 8.5 ml autoclaved NGM in a 6.5 cm wide petri dish (*see* **Note 8**).
2. Transfer approximately 20 animals about 24 h after L4-stage to an assay plate (*see* **Note 9**).
3. Wait 15 min (*see* **Note 10**), meanwhile prepare the tracker software.
4. Start MatLab and run OptoTracker. During the first run, add a user and create a new program in the main interface. Open the settings for the VideoCapture module and store the timing protocol as wanted. Here, we start recording 15 s prior to the 25 s illumination pulse followed by additional 15 s without illumination. We set in options "capture time" and "capture every" the value to 1 min. Set the "capture path" to the folder into which the video should be stored. Set a file name for the video to be acquired and save the changes. Open the settings for the Shutter module and set 15 s delay, "light for" to 25 s and "wait" to 15 s. The "repeat" option is set to one.
5. Position the animals in the focus of the camera and open the VideoCapture module. Select preview video to see a live image. Ensure that animals are in focus and with good contrast to the background before starting recording (*see* **Note 11**).
6. After recording all movies, start the WormTracker module settings. Set the size of the animals as well as their maximal velocity, minimal track length, and size change. Choose auto thresholding to allow WormTrack to adjust the thresholding into black and white automatically. Save the options and exit the preferences (*see* **Note 12**).
7. Start the WormTracker module and add the movies to the job list with their absolute system path, the file name is set without its end number. The numbers in start and end are set to the last numbers in the file name. For example, in the sequence of five movies named N2_1 … N2_5, the file name will be "N2_," start will be 1 and end 5. Start the tracking progress and visually monitor if the tracker did recognize the animals in the progress plot (*see* **Note 13**).
8. Start the WormAnalyzer settings and select the output properties to be analyzed and displayed. Set the camera sampling ratio and pixel size in the first run of these settings. Chose a smoothening sliding window size (*see* **Note 14**). Set the reversal and pirouette identification thresholds as necessary. Select whether data should be automatically exported to Excel tables, save the changes, and exit the settings menu.
9. Start the WormAnalyzer module and load the track file created by WormTracker as well as the corresponding movie. Visually check the recognized tracks by scrolling through the upper slider and delete invalid tracks (*see* **Note 15**). Select the Tracks

menu and click "Analyze All Tracks" to score all available tracks. Save the file to append the analysis to the tracks file. Select in the Tracks menu "Export to excel" and there the export to "Excel table" (first option). All data analyzed will be exported to an Excel file, one track per table.

10. Use your program of choice for analysis of relevant data.

3.3 Electrophysiology

Whole cell patch clamp recordings are carried out on body wall muscle cells of dissected *C. elegans* expressing PAC in cholinergic neurons (strain ZX785: *lite-1*(*ce314*); *zxEx513*[*punc-17*::*GFP*::*PACa*; *pelt-2*::*mCherry*])[10] (*see* **Notes 16** and **17**).

1. Insert a Sylgard-coated cover glass in the cavity of the recording chamber and fix it inside the chamber with two small pieces of dental wax attached to the sides of the chamber. Fill the cavity with ~2 ml CR. Using a stereomicroscope and a pick wire, position one adult nematode in the center of the cover glass.
2. Apply Histoacryl Blue through a gluing pipette and glue the animal's tail down to the cover glass (Fig. 5). This keeps the

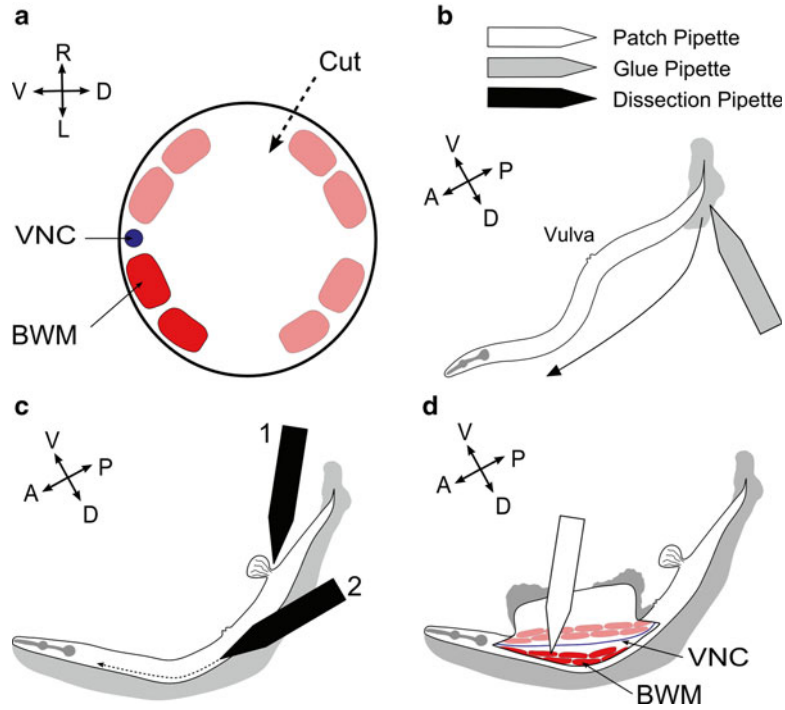

Fig. 5 Scheme for the dissection procedure. (**a**) *C. elegans* cross section with the ventral nerve cord (VNC) and body wall muscle (BWM) cells as well as the cut direction depicted. The aim is to measure the BWM cells nearest to the VNC. (**b**) The glue is applied from the tail to the head of the animal. (**c**, **d**) The posterior part of the animal is punctured with the dissection pipette (1) in order to reduce the hydrostatic pressure. A second (2) cut opens a cuticle flap, this is then glued to the ventral side of the animal. Patch the BWM cells as shown

nematode from swimming away. Try to glue it down at the center of the cover glass (*see* **Note 18**). Afterwards the nematode can be glued along the dorsal cuticle (*see* **Note 19**).

3. Make a single puncture behind the vulva to release the hydrostatic pressure from the nematode's body (Fig. 5). This will force out some of the viscera which would otherwise hinder your view during the actual incision. Make a lateral longitudinal incision in the dorsal cuticle with the help of a Mk1 micromanipulator and an incision pipette. Start in front of the vulva and stop just before the pharynx starts. Clear the viscera from the area of the incision using an extraction pipette. Finally glue the cuticle flap to the side to make the muscle cells easily accessible (*see* **Note 20**).
4. Enzymatically remove the basement membrane overlying the muscle cells by incubating the preparation with collagenase solution for 10 s and afterwards wash three times with CR. From now on the cells are only viable for ~10–15 min so you have to continue quickly and without interruption.
5. Position the recording chamber on the motorized platform of the inverted microscope. Use the 2.5× objective to search for the dissected nematode and align it in a direction where the muscle cells can easily be accessed by the patch pipette. Fill the patch pipette with pipette solution, attach it to the chlorinated silver wire of the headstage and immerse its tip into the CR of the recording chamber. Position the bath electrode in the CR as well. Check the pipette's resistance on the Patchmaster software—it should be between 4 and 7 MΩ. Switch to the 40× objective. Then carefully place the patch pipette onto one of the ventral medial body wall muscle cells using the micromanipulator. As soon as the patch pipette gets in touch with the cell membrane the pipette's resistance will slightly increase. Apply suction to the patch pipette via the tubing at the headstage to achieve a tight connection between pipette and cell membrane. You can verify the quality of your seal by monitoring the pipette resistance which is displayed on the amplifier software. As soon as a GigaΩ seal is achieved (500 MΩ–20 GΩ) a short but strong suction is applied to remove the patch of membrane inside the patch pipette and to achieve whole cell configuration.
6. Choose voltage clamp mode in the amplifier software and clamp the body wall muscle cell to a holding potential of −60 mV. Exclude muscle cells which have leak currents larger than 200 pA from recordings. Before the actual start of the recording keep the preparation in complete darkness for ~4 min.
7. Within your recording the pre-illumination period should be at least 30 s so you can analyze a reliable control value for amplitude and frequency of miniature postsynaptic currents (mPSCs)

before PAC activation. The LED lamp is controlled via TTL by the amplifier software. *n* value should be at least 7. Stimulate PAC in the cholinergic neurons by shining blue LED light (470 nm) onto the preparation, e.g., 45 s. The discrepancy to the tracker protocol is derived from the reliability of tracker experiments. Longer protocols for tracking are more susceptible to omega-turns (a specific locomotion motif, i.e., a reversal with sharp directional change, during the body resembles the Greek letter Ω) and such might corrupt later analysis. Such timing constraint also exists in electrophysiology: the time that the muscle cell is alive and responsive. Experimental protocols should be designed taking these information into account.

8. Analysis of mPSC amplitudes and frequencies is done by MiniAnalysis software (Synaptosoft, USA). First of all, the raw data need to be transferred from the Patchmaster software to MiniAnalysis. Therefore, the Patchmaster data need to be concerted. Export each sweep in "Igor Binary" (.itx) format. With the ABF Utility software (included with MiniAnalysis), convert the Igor Binary file to an ABF file (.abf). This data format can then be loaded and analyzed by the MiniAnalysis software. Choose a threshold of ~10 pA. It is advisable to inspect the results of the automatic peak detection since some mPSCs might be omitted or there might be artifacts which are detected as real signals.

4 Notes

1. We use these volumes for easier pipetting. Be sure to coat the well with NGM, the animals will stick to the plastic without it. M9 volumes may be lower for video acquisition, restraining the movement in *Z*-axis. Pay attention to evaporation of buffer at low volumes.
2. The intensity of 1 mW/mm^2 is usually used for Channelrhodopsin 2 photoactivation. We successfully tried different blue light sources: filtered HBO 50 lamp light (Zeiss, Germany; 450–490 nm); filtered LCD projector light (450–490 nm); DPSS laser illumination (Pusch OptoTech, Baden-Baden, Germany; 473 nm, 25.6 mW/mm^2), or a LED lamp (KSL-70, Rapp OptoElectronic, Hamburg, Germany; 470 nm, 8 mW/mm^2). Depending on the PAC used, it may be necessary to use lower intensity during photoactivation.
3. The red filter is positioned to allow only red light as background light during the measurement. Cover any possible, unfiltered source of light with aluminum foil. This is crucial, as unfiltered light might photoactivate PAC even before the actual start of your experiment. Work in a dark room protected from

sun light. Our dark room for PAC measurements has a blue light background intensity below 25 nW/mm^2.

4. There is a variety of worm tracker software available on-line. We use different trackers depending on the task. Here we show the usage of OptoTracker [26], an enhancement of the Parallel Worm Tracker [27] capable of photostimulation during video acquisition at a low cost. For a review on the different trackers *see* ref. [28]. A microscope-less alternative is the Multi Worm Tracker [29].
5. If the amount of mixture is not enough to fill the entire surface add a little more of the mixture. If there are any air bubbles in the Sylgard coating try to remove them with a pipette tip. The nematodes move more slowly on Sylgard than on glass which facilitates gluing. Furthermore, the Sylgard coat helps the glue to adhere to the cover glass and it provides a basis for cleansing clogged glue pipettes.
6. The experimental protocol depends on the expected outcome. Video acquisition eases the process of thrashing quantification. Without it, one should measure only one animal at a time. There are specialized automated acquisition and analysis software alternatives in the scientific community [30].
7. Pay attention not to photostimulate neighboring wells, in case more than one group of animals is transferred at a time to the 96-well plate. Use of a black-walled, clear-bottom 96-well plate and tight covering with aluminum foil of unutilized wells prevents unwanted photostimulation. A further option is to prepare different 96-well plates and only expose one group of animals at a time to the blue stimulation light.
8. Assay plates should be made with care; air bubbles, variation in volume and surface irregularities on the NGM will decrease the quality of the tracked data. Fresh plates are kept for 1 day at room temperature to allow NGM solidification and surface drying; they can be stored for up to 2 weeks at 4 °C. If OP50 seeded plates are necessary, cover the whole plate with OP50 and then remove as much liquid as possible with a pipette. Let the OP50 dry for about 2 h before use; this might take longer for freshly poured NGM plates.
9. All transfers must be made without blue light illumination. Use a red optical cast plastic filter (2″×2″, #43-946, Edmund Optics, Germany) for red background light. Transfer the animals first to an unseeded plate and allow them to crawl for some minutes before transferring them to the assay plate. This will minimize the amount of OP50 carried over to the assay plate. Bacteria in the assay plate can change the behavior of the animals and challenge the tracking software. Tracking experiments on an OP50 seeded assay plate work best with a very thin bacterial lawn without humps or impurities on the surface.

10. Worm transfer does change the animal's behavior for some minutes. *C. elegans* takes between 5 and 10 min to adapt to the new plate.
11. The contrast of the animal relative to the background is an essential issue. The OptoTracker can track dark objects on bright background and vice versa. An even background illumination is necessary; otherwise the tracker will not recognize animals either at the center or periphery of the image.
12. The size options define which objects will be treated as animals. Impurities as dark colored grains of same relative size will be tracked as if they were immobile animals. We emphasize the necessity to have clean, good quality assay plates without air bubbles in the NGM, as well as good quality background light and even illumination. Furthermore, the maximum size allows the WormTracker software to ignore when two animals collide. The minimum track length allows WormTracker to ignore poor light conditions, animals that flicker in the thresholded image, as well as animals that enter and exit the field of view often.
13. In case WormTracker does not recognize the animals correctly, stop the tracking procedure and start the WormTracker preferences anew. Adjust the allowed animal size for a broader range and change the correction factor of the auto thresholding algorithm.
14. Although the smoothening window filters the output graph, it may distort the results. For instance, time critical responses to light stimuli may be smoothed out during this procedure. We use a window size of 1 (no smoothing) in the first run of the analysis software and compare it to bigger smoothing windows. We only use the smoothed data where there is no fast change in behavior. For example, a change in behavior that takes 2 s will not be smoothed out with a window size of 200 ms, a response in the first 250 ms in contrast will.
15. Although the tracker can filter the tracks automatically through the WormTracker settings, we do confirm visually that only valid tracks are used for the statistics. There is an issue when deleting the last track: the slider bar will disappear. Save the tracks file and reload it, it will be updated and the slider will be functional.
16. Following dissection, the body wall muscle cells stay viable only for a short time (~10–15 min). Therefore, you should prepare your experiments very well and have everything needed readily available.
17. When working with PAC it is extremely important that all working steps are carried out using lowest necessary intensity of surrounding light to minimize pre-activation. Thus, animals should be kept in the dark and the petri dish they are

cultivated on should be wrapped in aluminum foil. When conducting the dissection and the actual experiments the room should be darkened (as much as possible). Use only red light lamps whenever you need a certain amount of light to conduct experiments. The intensity of standard bright field illumination should be reduced to a level at which it is still possible to do all necessary experimental work. A red optical cast plastic filter (2″ × 2″, #43-946, Edmund Optics, Germany) in the optical path additionally prevents transmission of wavelengths below 550 nm and therefore reduces blue light illumination of PAC. The front opening of the Faraday cage should also be light shielded with a thick curtain—keeping in mind that other light sources such as PC monitors, will emit a certain amount of light.

18. If the animal is glued near the border of the cavity it might be difficult or even impossible to access the nematode with the patch pipette at subsequent experimental steps. The glue polymerizes when it gets in contact with water. Thus, you have to maintain a continuous mouth-pressure as long as the gluing pipette is in the solution since otherwise the pipette tip will be plugged.
19. It is important to apply the right amount of glue. If you use too little glue, the animal will detach when you do the incision. If you use too much glue you might later on have problems accessing the body-wall muscle cells with the patch pipette.
20. Use as little glue as possible for this and try not to drag the cuticle.

References

1. Errata (1998) Genome sequence of the nematode C. elegans: a platform for investigating biology. The C. elegans Sequencing Consortium [published errata appear in Science 1;283(5398):35 and 1999 Mar 26;283(5410):2103 and 1999 Sep 3;285(5433):1493] (1998). Science 282(5396): 2012–2018
2. Brenner S (1974) The genetics of Caenorhabditis elegans. Genetics 77(1): 71–94
3. White JG, Southgate E, Thomson JN, Brenner S (1986) The structure of the nervous system of the nematode Caenorhabditis elegans. Philos Trans R Soc Lond B Biol Sci 314(1165): 1–340
4. Husson SJ, Gottschalk A, Leifer AM (2013) Optogenetic manipulation of neural activity in C. elegans: from synapse to circuits and behaviour. Biol Cell 105(6):235–250. doi:10.1111/boc.201200069
5. Xu X, Kim SK (2011) The early bird catches the worm: new technologies for the Caenorhabditis elegans toolkit. Nat Rev Genet 12(11):793–801. doi:10.1038/nrg3050
6. Nagel G, Brauner M, Liewald JF, Adeishvili N, Bamberg E, Gottschalk A (2005) Light activation of channelrhodopsin-2 in excitable cells of Caenorhabditis elegans triggers rapid behavioral responses. Curr Biol 15(24):2279–2284
7. Zhang F, Wang LP, Brauner M, Liewald JF, Kay K, Watzke N, Wood PG, Bamberg E, Nagel G, Gottschalk A, Deisseroth K (2007) Multimodal fast optical interrogation of neural circuitry. Nature 446(7136):633–639. doi:10.1038/nature05744
8. Liewald JF, Brauner M, Stephens GJ, Bouhours M, Schultheis C, Zhen M, Gottschalk A (2008) Optogenetic analysis of synaptic function. Nat Methods 5(10):895–902
9. Liu Q, Hollopeter G, Jorgensen EM (2009) Graded synaptic transmission at the Caenorhabditis elegans neuromuscular junction. Proc Natl Acad Sci U S A 106(26): 10823–10828

10. Weissenberger S, Schultheis C, Liewald JF, Erbguth K, Nagel G, Gottschalk A (2011) PACalpha–an optogenetic tool for in vivo manipulation of cellular cAMP levels, neurotransmitter release, and behavior in Caenorhabditis elegans. J Neurochem 116(4):616–625. doi:10.1111/j.1471-4159.2010.07148.x
11. Bucher D, Buchner E (2009) Stimulating PACalpha increases miniature excitatory junction potential frequency at the Drosophila neuromuscular junction. J Neurogenet 23(1–2):220–224. doi:10.1080/01677060802441356
12. Schroder-Lang S, Schwarzel M, Seifert R, Strunker T, Kateriya S, Looser J, Watanabe M, Kaupp UB, Hegemann P, Nagel G (2007) Fast manipulation of cellular cAMP level by light in vivo. Nat Methods 4(1):39–42
13. Stierl M, Stumpf P, Udwari D, Gueta R, Hagedorn R, Losi A, Gartner W, Petereit L, Efetova M, Schwarzel M, Oertner TG, Nagel G, Hegemann P (2011) Light modulation of cellular cAMP by a small bacterial photoactivated adenylyl cyclase, bPAC, of the soil bacterium Beggiatoa. J Biol Chem 286(2):1181–1188. doi:10.1074/jbc.M110.185496
14. Ryu MH, Moskvin OV, Siltberg-Liberles J, Gomelsky M (2010) Natural and engineered photoactivated nucleotidyl cyclases for optogenetic applications. J Biol Chem 285(53):41501–41508
15. Gross RE, Bagchi S, Lu X, Rubin CS (1990) Cloning, characterization, and expression of the gene for the catalytic subunit of cAMP-dependent protein kinase in Caenorhabditis elegans. Identification of highly conserved and unique isoforms generated by alternative splicing. J Biol Chem 265(12):6896–6907
16. Tada M, Gengyo-Ando K, Kobayashi T, Fukuyama M, Mitani S, Kontani K, Katada T (2012) Neuronally expressed Ras-family GTPase Di-Ras modulates synaptic activity in Caenorhabditis elegans. Genes Cells 17(9):778–789. doi:10.1111/j.1365-2443.2012.01627.x
17. Iseki M, Matsunaga S, Murakami A, Ohno K, Shiga K, Yoshida K, Sugai M, Takahashi T, Hori T, Watanabe M (2002) A blue-light-activated adenylyl cyclase mediates photoavoidance in Euglena gracilis. Nature 415(6875):1047–1051
18. Yoshikawa S, Suzuki T, Watanabe M, Iseki M (2005) Kinetic analysis of the activation of photoactivated adenylyl cyclase (PAC), a blue-light receptor for photomovements of Euglena. Photochem Photobiol Sci 4(9):727–731
19. Nagahama T, Suzuki T, Yoshikawa S, Iseki M (2007) Functional transplant of photoactivated adenylyl cyclase (PAC) into Aplysia sensory neurons. Neurosci Res 59(1):81–88. doi:10.1016/j.neures.2007.05.015
20. Bellmann D, Richardt A, Freyberger R, Nuwal N, Schwarzel M, Fiala A, Stortkuhl KF (2010) Optogenetically induced olfactory stimulation in drosophila larvae reveals the neuronal basis of Odor-Aversion behavior. Front Behav Neurosci 4:27. doi:10.3389/fnbeh.2010.00027
21. Yasukawa H, Konno N, Haneda Y, Yamamori B, Iseki M, Shibusawa M, Ono Y, Kodaira K, Funada H, Watanabe M (2012) Photomanipulation of antibiotic susceptibility and biofilm formation of Escherichia coli heterologously expressing photoactivated adenylyl cyclase. J Gen Appl Microbiol 58(3):183–190
22. Ntefidou M, Ludtke T, Ahmad M, Hader DP (2006) Heterologous expression of photoactivated adenylyl cyclase (PAC) genes from the flagellate Euglena gracilis in insect cells. Photochem Photobiol 82(6):1601–1605. doi:10.1562/2006-04-06-RA-867
23. Hartmann A, Arroyo-Olarte RD, Imkeller K, Hegemann P, Lucius R, Gupta N (2013) Optogenetic modulation of an adenylate cyclase in Toxoplasma gondii demonstrates a requirement of the parasite cAMP for host-cell invasion and stage differentiation. J Biol Chem 288(19):13705–13717. doi:10.1074/jbc.M113.465583
24. Nicol X, Hong KP, Spitzer NC (2011) Spatial and temporal second messenger codes for growth cone turning. Proc Natl Acad Sci U S A 108(33):13776–13781. doi:10.1073/pnas.1100247108
25. Von Stetina SE, Treinin M, Miller DM 3rd (2006) The motor circuit. Int Rev Neurobiol 69:125–167
26. Husson SJ, Costa WS, Wabnig S, Stirman JN, Watson JD, Spencer WC, Akerboom J, Looger LL, Treinin M, Miller DM 3rd, Lu H, Gottschalk A (2012) Optogenetic analysis of a nociceptor neuron and network reveals ion channels acting downstream of primary sensors. Curr Biol 22:743–752. doi:10.1016/j.cub.2012.02.066
27. Ramot D, Johnson BE, Berry TL Jr, Carnell L, Goodman MB (2008) The parallel worm tracker: a platform for measuring average speed and drug-induced paralysis in nematodes. PLoS ONE 3(5):e2208
28. Husson SJ, Steuer Costa W, Schmitt C, Gottschalk A (2012) Keeping track of worm trackers. In: Hobert O (ed). doi:10.1895/wormbook.1.150.1
29. Swierczek NA, Giles AC, Rankin CH, Kerr RA (2011) High-throughput behavioral analysis in C. elegans. Nat Methods 8(7):592–598. doi:10.1038/nmeth.1625
30. Buckingham SD, Sattelle DB (2009) Fast, automated measurement of nematode swimming (thrashing) without morphometry. BMC Neurosci 10:84. doi:10.1186/1471-2202-10-84

Chapter 12

Structural Basis of Photoswitching in Fluorescent Proteins

Chenxi Duan, Virgile Adam, Martin Byrdin, and Dominique Bourgeois

Abstract

Fluorescent proteins have revolutionized life sciences because they allow noninvasive and highly specific labeling of biological samples. The subset of "phototransformable" fluorescent proteins recently attracted a widespread interest, as their fluorescence state can be modified upon excitation at defined wavelengths. The fluorescence emission of Reversibly Switchable Fluorescent Proteins (RSFPs), in particular, can be repeatedly switched on and off. RSFPs enable many new exciting modalities in fluorescence microscopy and biotechnology, including protein tracking, photochromic Förster Resonance Energy Transfer, super-resolution microscopy, optogenetics, and ultra-high-density optical data storage. Photoswitching in RSFPs typically results from chromophore *cis–trans* isomerization accompanied by a protonation change, but other switching schemes based on, e.g., chromophore hydration/dehydration have also been discovered. In this chapter, we review the main structural features at the basis of photoswitching in RSFPs.

Key words Fluorescent proteins, Photoswitching, Dronpa, RSFPs, Protein dynamics, *cis–trans* Isomerization, Proton transfer, Super-resolution microscopy

Abbreviations

GFP	Green fluorescent protein
YFP	Yellow fluorescent protein
FPs	Fluorescent proteins
PTFPs	Phototransformable fluorescent proteins
RSFPs	Reversibly switchable fluorescent proteins
PCFPs	Photoconvertible fluorescent proteins
PAFPs	Photoactivatable fluorescent proteins
ESPT	Excited state proton transfer
KIE	Kinetic isotope effect
p-HBI	4-(*p*-Hydroxybenzylidene)-5-imidazolinone
pcFRET	Photochromic Förster resonance energy transfer
QM/MM	Quantum mechanics/molecular mechanics
SMLM	Single molecule localization microscopy
PALM	Photoactivated localization microscopy
STORM	Stochastic optical reconstruction microscopy
STED	Stimulated emission depletion

Sidney Cambridge (ed.), *Photoswitching Proteins: Methods and Protocols*, Methods in Molecular Biology, vol. 1148,
DOI 10.1007/978-1-4939-0470-9_12,

RESOLFT	Reversible saturable optical linear fluorescence transitions
SSIM	Saturated structured illumination microscopy
(pc)SOFI	(Photochromic) stochastic optical fluctuation imaging
IR	Infra-red
HSQC	Heteronuclear single quantum coherence
XFEL	X-Ray-free electron laser

1 Introduction

Fluorescent proteins (FPs) have become indispensable tools to investigate the interrelations between cell structure, function, and dynamics [1]. Their three-dimensional structure is quite simple: the peptide chain forms an 11-stranded β-barrel resembling a "soda can," which wraps around a three-residues-based endogenous chromophore (Fig. 1). This 4-(*p*-hydroxybenzylidene)-5-imidazolinone (*p*-HBI) chromophore only requires oxygen as an external cofactor to become mature. A stunning palette of fluorescent proteins displaying a wide range of emission colors (450–650 nm) has been engineered, typically by rational or random mutagenesis of the chromophore itself or of its close environment [2]. The discovery of FPs from Anthozoan species (e.g., corals or anemones), which exhibit a high structural similarity but only a small sequence identity (<30 %) with the more classical Hydrozoan FPs (e.g., jellyfishes), launched the development of red fluorescent proteins [3], and considerably boosted FP research in recent years.

In addition to suitable colors, useful FPs should exhibit a high expression level, fast maturation, and high fluorescence brightness so that they can be imaged with sufficient signal-to-noise ratio soon after cell transfection. Furthermore, they should be monomeric and should not induce cytotoxicity, to avoid cellular dysfunction. Importantly, they should be photostable and possible modifications of their fluorescence properties as a function of light excitation or environmental parameters (e.g., pH, redox potential, oxygen level) should be understood.

The protonation state of the *p*-hydroxybenzylidene moiety of the chromophore plays a key role in the fluorescence properties of FPs. Two protonation states can generally be adopted, the proportion of which is determined by the interactions with neighboring residues in the chromophore pocket and may (or not) vary with pH. The protonated (neutral) chromophore absorbs in the so-called "A-band," whereas the deprotonated (anionic) chromophore absorbs in the "B-band" (Fig. 1). For a green-emitting FP, those bands usually peak at ~400 nm and ~490 nm, respectively. In their anionic state, FPs are typically highly fluorescent, whereas in their neutral state they are dimly or not fluorescent. However, upon excitation of the neutral state, the FP chromophore becomes a strong acid with a p*K*a near zero. Ultrafast conversion to a

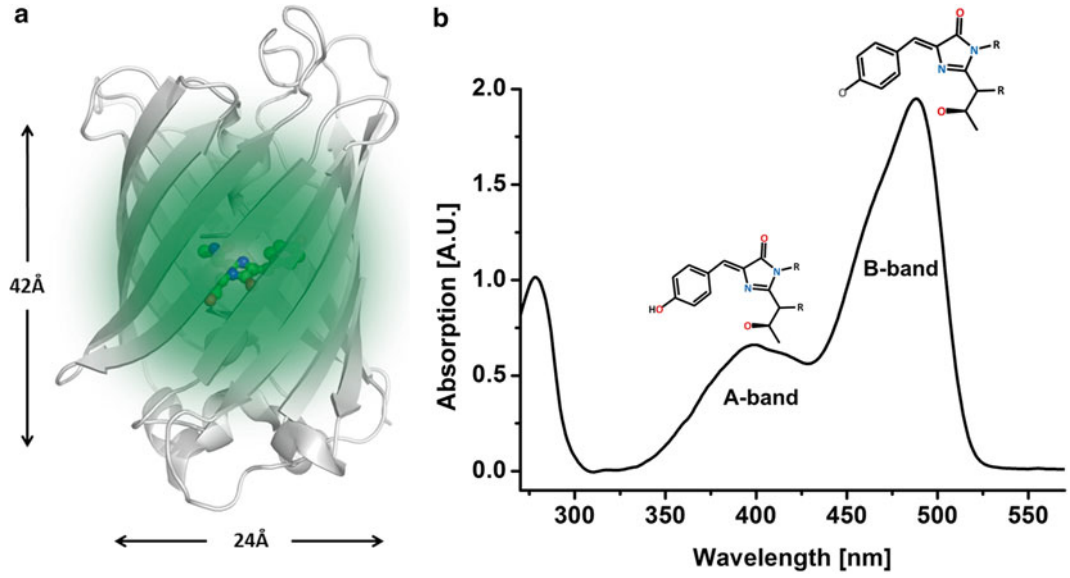

Fig. 1 Enhanced green fluorescent protein (EGFP). (**a**) The crystal structure (Protein Data Bank (PDB) ID 2Y0G) of a single chain is represented in *gray cartoons*. The green-glowing chromophore is represented in *balls* and *sticks* and *stands* in the center of the barrel. (**b**) Absorption spectrum of EGFP. Two bands are attributed to the neutral form (A-band) and the anionic form (B-band) of the chromophore. Lewis structures of the corresponding chromophore are represented as *insets*

deprotonated excited state may thus occur, resulting in high yield and strongly Stokes-shifted fluorescence.

The high fluorescence quantum yield of FPs (generally > ~0.5) is commonly attributed to the idea that the chromophore is held rigidly within the protein matrix through a set of tight non-covalent interactions. This is a too simplistic view. In fact, FPs exhibit a highly dynamic behavior, in line with their observed complex photophysics. Upon light absorption, and especially when intersystem crossing to the long-lived triplet state takes place, the FP structural plasticity may allow a number of photophysical or photochemical transformations to occur. For example, like any fluorophore, FPs undergo transient stochastic switching events to nonfluorescent dark states ("blinking"), and eventual conversion to a permanent off state ("bleaching").

In the subfamily of fluorescent proteins termed Phototransformable FPs (PTFPs), specific phototransformations can be quantitatively induced by light, which is at the basis of a number of revolutionary developments in advanced fluorescence microscopy. These PTFPs, mostly found in Anthozoan stony corals, but also engineered from Hydrozoan FPs have become the focus of intense research since a few years [4–6]. Three types of phototransformations may be distinguished in PTFPs (Fig. 2): nonreversible activation from a nonfluorescent to a fluorescent state (referred to as "photoactivation," fluorescent proteins of this

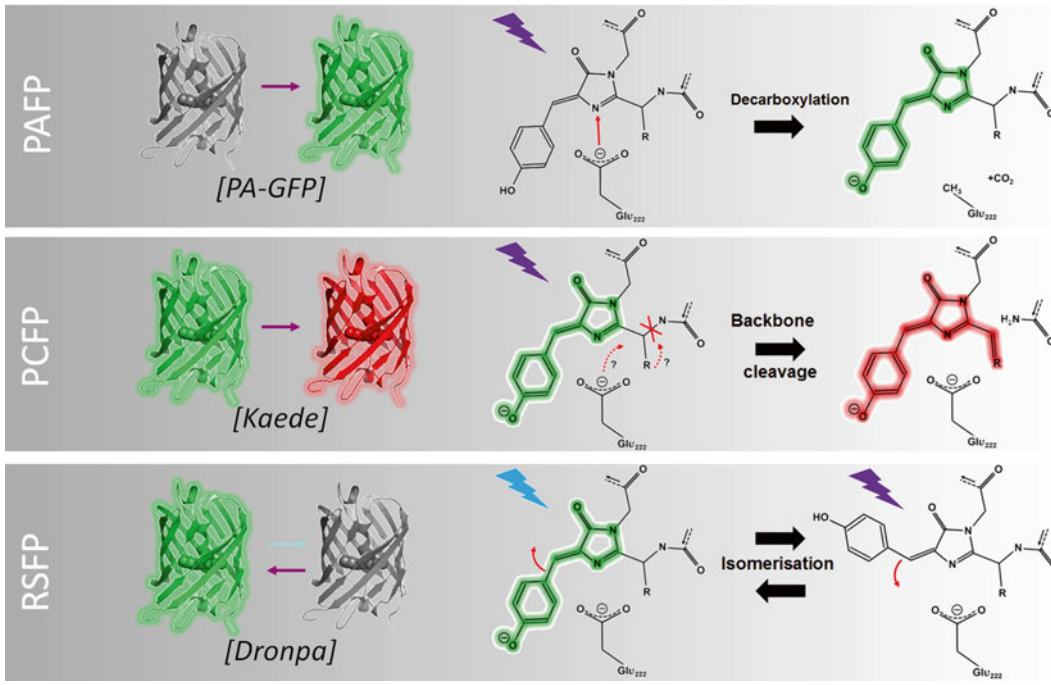

Fig. 2 Various possible reactions in phototransformable fluorescent proteins with typical examples of irreversibly photoactivatable fluorescent proteins (PAFP), irreversibly photoconvertible fluorescent proteins (PCFP), and reversibly switchable fluorescent proteins (RSFP). Photoinduced reactions occurring at the chromophore level are represented for each case. Figure reproduced from D. Bourgeois, A. Regis-Faro and V. Adam (2012), Biochemical Society Transactions, 40 531–538, © the Biochemical Society, with permission from Portland Press Limited

group are called Photoactivatable FPs (PAFPs)), nonreversible conversion between two fluorescent states with different emission colors ("photoconversion," fluorescent proteins of this group are called Photoconvertible FPs (PCFPs)), and reversible switching between a fluorescent on-state and a nonfluorescent off-state ("photoswitching," fluorescent proteins of this group are called Reversibly Switchable FPs (RSFPs)). In this chapter we give a structural perspective on the fascinating photophysical properties of RSFPs.

2 Discovery and Classification of RSFPs

A list of the currently developed RSFPs with their main photophysical properties is provided in Table 1.

The first observation of reversible photoswitching of a fluorescent protein at room temperature was made with yellow derivatives of *Aequora victoria* GFP at the single molecule [7] and at the ensemble levels [8–10]. However, photoswitching of these Hydrozoan FPs appeared limited, probably involving only minor

Table 1
Properties of well-characterized RSFPs developed to date

Class	Switching	Protein (oligomerization)	Parent protein [wild-type]	Source organism	Chromophore triad	λ_{max} ex/em[a](nm)	ε[a] ($M^{-1}.cm^{-1}$)	Φ_{fluo}[a]	Brightness[b]	pK_a	Φ_{sw}[a] On-off	Φ_{sw}[a] Off-on	Actinic light (nm) On-off	Actinic light (nm) Off-on	Ref.
Anthozoans	Negative	mTFP0.7 (M)	cFP484	*Clavularia* sp.	AYG	453/488	60,000	0.50	89 %	4.0	ND	ND	458	405	[31]
		mGeosC (M)	EosFP	*L. Hemprichii*	CYG	505/516	76,967	0.81	186 %	6.0	ND	ND	488	405	[34]
		mGeos-M (M)	EosFP	*L. Hemprichii*	MYG	503/514	51,609	0.85	130 %	4.5–5	ND	ND	488	405	[34]
		mGeos-S (M)	EosFP	*L. Hemprichii*	SYG	501/512	64,602	0.76	145 %	5–5.5	ND	ND	488	405	[34]
		Dronpa (M)	22G	*Echinophyllia* sp. *SC22*	CYG	503/517	94,100	0.67	188 %	5.3	3.0×10^{-4}	7.0×10^{-1}	488	405	[12, 36]
		Dronpa-2 (M)	Dronpa [22G]	*Echinophyllia* sp. *SC22*	CYG	489/515	56,000	0.28	47 %	ND	4.7×10^{-2}	ND	488	405	[29]
		Dronpa-3 (M)	Dronpa [22G]	*Echinophyllia* sp. *SC22*	CYG	489/515	58,000	0.33	57 %	ND	5.3×10^{-3}	ND	488	405	[29]
		rsFastLime (M)	Dronpa [22G]	*Echinophyllia* sp. *SC22*	CYG	496/518	39,094	0.77	89 %	ND	ND	ND	488	405	[20]
		bsDronpa (M)	Dronpa [22G]	*Echinophyllia* sp. *SC22*	CYG	460/504	45,000	0.50	67 %	ND	ND	ND	488	405	[20]
		rsCherryRev (M)	mCherry [DsRed]	*Discosoma* sp.	MYG	572/608	84,000	0.005	1 %	5.5	ND	ND	550	450	[77]
		rsTagRFP (M)	TagRFP [eqFP578]	*E. quadricolor*	MYG	567/585	36,800	0.11	12 %	6.6	ND	ND	570	445	[78]
		mEosFP M159A (M)	EosFP	*L. Hemprichii*	HYG	487/512	98,600	0.52	153 %	4.3	2.6×10^{-3}	1.5×10^{-1}	488	405	[36]
		IrisFP (T)	EosFP	*L. Hemprichii*	HYG	488/516	57,800	0.48	83 %	5.7	3.2×10^{-3}	1.5×10^{-1}	488	405	[35, 36]
		IrisFP (T)				551/580	27,000	0.50	40 %	6.8	2.0×10^{-3}	5.0×10^{-2}	561	440	
		mIrisFP (M)	EosFP	*L. Hemprichii*	HYG	486/516	74,000	0.60	132 %	5.7	2.2×10^{-3}	1.3×10^{-1}	488	405	[36, 71]
		mIrisFP (M)				546/578	26,000	0.44	34 %	7.0	4.0×10^{-4}	1.1×10^{-1}	561	440	
		NijiFP (M)	Dendra2 [DendGFP]	*Dendronephthya* sp.	HYG	469/507	41,100	0.64	78 %	7.0	1.8×10^{-3}	1.0×10^{-1}	488	405	[36]
		NijiFP (M)				526/569	42,000	0.65	81 %	7.3	1.0×10^{-3}	1.0×10^{-1}	561	440	
		Dendra2 M159A (M)	Dendra2 [DendGFP]	*Dendronephthya* sp.	HYG	471/504	51,100	0.55	84 %	6.5	1.1×10^{-3}	8.0×10^{-2}	488	405	[36]
		Dendra2 M159A (M)				528/562	45,000	0.75	100 %	6.8	3.2×10^{-3}	1.0×10^{-2}	561	440	
	Positive	Padron (M)	Dronpa [22G]	*Echinophyllia* sp. *SC22*	CYG	503/522	43,000	0.64	82 %	ND	ND	ND	405	488	[20]
		rsCherry (M)	mCherry [DsRed]	*Discosoma* sp.	MYG	572/610	80,000	0.02	5 %	6.0	ND	ND	450	550	[77]
		asFP595 (T)	–	*A. sulcata*	MYG	572/595	56,200	<0.001	<0.2 %	ND	ND	ND	450	568	[81]
		KFP1 (T)	asFP595	*A. sulcata*	MYG	590/600	59,000	0.07	12 %	ND	ND	ND	458	532	[11]
Hydrozoans	Negative	Mut2Q (M)	GFP	*A. victoria*	AYG	496/507	54,000	0.28	45 %	6.0	4.7×10^{-3}	2.6×10^{-2}	478	405	[37, 82]
		EYQ1 (M)	EYFP [GFP]	*A. victoria*	SYG	510/524	73,000	0.72	156 %	6.9	1.8×10^{-4}	6.0×10^{-2}	514	405	[37]
		rsEGFP (M)	EGFP [GFP]	*A. victoria*	TYG	493/510	47,000	0.36	50 %	6.5	ND	ND	488	405	[38]
		rsEGFP2(M)	EGFP [GFP]	*A. victoria*	AYG	478/503	61,300	0.3	60 %	5.8	ND	ND	491	405	[39]
	D[a]	Dreiklang (M)	Citrine [GFP]	*A. victoria*	GYG	511/529	83,000	0.41	101 %	7.2	ND	ND	405	365	[40]

Note: the table summarizes the photophysical properties of RSFPs in their fluorescent form

[a]Abbreviations: λ_{max} ex/em wavelength of maximum in excitation/emission spectrum; ε, molar extinction coefficient; Φ_{fluo}, fluorescence quantum yield; Φ_{sw}, photoswitching quantum yield; D, decoupled switching

[b]Brightness is the product of quantum yield and molar extinction coefficient divided by 1,000, expressed in % of the EGFP brightness

[c]Wavelengths required for reversible transitions. Background colors represent the emission colors of the proteins (left) and the colors of lights used to reversibly switch proteins (right). M, monomer; T, tetramer; NA, not applicable; ND, not determined

subpopulations of molecules. Efficient photoswitching was initially reported of the weakly fluorescent and tetrameric asFP595 from the Anthozoan sea anemone *Anemonia sulcata*. The phenomena was described as reversible "kindling," because the fluorescence emission from asFP595 was enhanced by the fluorescence excitation light (568 nm) and quenched by blue light (450 nm) [11]. The first RSFP of sufficient quality to successfully conduct biological experiments was obtained upon engineering a Pectiniidae coral FP, yielding the well-known Dronpa [12]. In contrast to asFP595, fluorescence emission in Dronpa is quenched by the excitation light (490 nm) and recovered by illumination with violet light (405 nm). A large number of mechanistic investigations were then performed on these two proteins [13–28].

In view of the growing interest of RSFPs for advanced fluorescence microscopy applications, substantial efforts were made in the last years to develop variants with improved properties such as higher fluorescence brightness (the product of fluorescence quantum yield and molar extinction coefficient), enhanced switching contrast (ratio of fluorescence emission of the on and off states), tunable switching quantum yields, increased photoresistance, or red-shifted emission (Table 1). Several new Anthozoan RSFPs were thus introduced such as a number of Dronpa variants [20, 29, 30], mTFP0.7 from *Clavuliara* sp. [31], rsTagRFP from *E. quadricolor* [32, 33], mGeos from *L. hemprichii* [34], and others (Table 1). An interesting case was IrisFP (and later NijiFP), which combines on–off photoswitching with green to red photo-conversion properties [35, 36], introducing the possibility to achieve dual color photoswitching with a single protein. Recently, Hydrozoan GFP-based RSFPs were also developed, showing that high-performance photoswitching is not restricted to Anthozoan FPs. Single-mutation of the strictly conserved Glu222 (GFP numbering) into Gln conferred high-contrast switching properties to variants of YFP [37], while a combined rational and random mutagenesis approach yielded the photoresistant rsEGFP [38] and rsEGFP2 [39].

All these RSFPs can be classified as "negative" or "positive." In negative RSFPs such as Dronpa, off-switching results from illumination at wavelengths absorbed by the protein in its on-state. In positive RSFPs such as asFP595, on-switching results from illumination at wavelengths absorbed by the protein in its on-state (Table 1). In all cases, switching is thought to primarily result from a light-induced *cis–trans* isomerization of the chromophore accompanied by a change of the *p*-hydroxybenzylidene protonation state. A different acid–base environment of the chromophore in the two isomeric states modulates its p*K*a and is key to the photoswitching function. In the fluorescent on-state, the chromophore is typically in an anionic *cis* configuration, whereas in the nonfluorescent off state it is found in a *trans* configuration, either neutral or anionic. In negative RSFPs, the *cis* configuration of the chromophore is the

thermodynamically stable form, so these proteins are typically highly fluorescent in their native state. In positive RSFPs, the nonfluorescent *trans* configurations tends to be more thermodynamically stable, although both states are sometimes observed at equilibrium, so these proteins are normally nonfluorescent or weakly fluorescent in their native state.

In 2011, Brakemann *et al.* [40] engineered YFP-derivatives previously shown to be partially switchable [10, 41] to elaborate Dreiklang, an RSFP that exhibits an entirely new mechanism which does not rely on *cis–trans* isomerization of the chromophore, but rather involves reversible chemical modifications of the imidazolinone moiety. In Dreiklang, photoswitching is neither positive nor negative but is "decoupled," meaning that fluorescence excitation exerts no influence on photoswitching.

3 Methodology for the Investigation of Photoswitching Mechanisms

Boosted by this rapidly evolving research field, increased attention has been devoted to mechanistic investigations of RSFPs with a dual goal: gaining fundamental insight into this intriguing phenomenon and rationally designing variants with enhanced photophysical properties. Several methods can be used that are briefly described below.

Confocal or wide-field fluorescence microscopy approaches based on single-molecule detection allow monitoring the stochastic nature of photoswitching. By recording many single-molecule fluorescence traces, histograms of on-times and off-times can be extracted from which key photophysical parameters such as switching quantum yields can be derived. Single-molecule investigations provide the essential advantage that subpopulations of molecules behaving differently from the average can be identified. The same illumination conditions as those used in cell microscopy experiments can be used and the influence of environmental conditions such as redox potential, pH, or oxygen level can be monitored. However, to study single molecule behavior, the RSFPs are typically attached to a glass coverslip or immobilized in a polymer substrate, which might induce deviations relative to the *in cellulo* behavior. Ultimately, despite complications due to a lower signal-to-noise ratio and a higher molecular density, these methods will be applied directly in the biological sample so as to evaluate RSFPs switching in genuine experimental conditions.

To get a high-resolution structural view of photoswitching, ensemble level techniques must be used, such as X-ray crystallography, NMR, UV–vis optical spectroscopy, or vibrational spectroscopy. The most direct view of the structural signature of photoswitching is provided by crystallography. However, the

nonstandard concepts of "kinetic" protein crystallography need to be used [42], whereby photoswitching is induced *in crystallo*. Indeed, the photoswitched chromophore is usually not stable for more than at most a few hours, a time much too short to achieve crystal growth. Thus, to generate the switched state, the crystalline sample is submitted to laser illumination, followed by flash cooling to prevent back switching and to minimize radiation damage effects during diffraction data collection. Fortunately, FPs are well-suited samples for kinetic protein crystallography, as conformational changes induced by light illumination are small enough to be compatible with crystal packing interactions, so that samples are usually not seriously deteriorated upon illumination. However, it should always be kept in mind that the crystalline state may exert an influence on the observed switching scenario, for example by selecting out a subset of conformational states not strictly representative of the in-solution behavior. This point has for example been a matter of debate concerning the structure of the off state of Dronpa [16]. 2D-NMR investigations (typically based on ^{1}H–^{15}N or ^{1}H–^{13}C HSQC experiments) have the advantage that no crystal constraints are present, so the observed conformational changes may be more genuine. However, the usually longer measuring times at room temperature make it trickier to maintain the photoswitched state in the sample. For example, prolonged illumination might be required and result in unwanted photobleaching. In all cases, X-ray or NMR structural views should be complemented by steady-state optical spectroscopy measurements so as to quantify the extent of photoswitching in the investigated samples. Optical microspectrophotometry can be applied *in crystallo*, in the absorbance, fluorescence [43], or even Raman mode [44]. It should be noted that careful spectroscopic investigations using relatively basic instruments can provide a wealth of insightful mechanistic information complementary to structural approaches [45, 46].

To gain further mechanistic insight, putative intermediate states along the photoswitching reaction pathway should be characterized in addition to the switching endpoints. Since photoswitching is typically a very rapid (subnanosecond) process, ultrafast pump-probe UV–vis or IR spectroscopy are the tools of choice to be used. However, a major difficulty is that photoswitching in RSFPs is a low yield process (10^{-4}–10^{-1}) so that the fraction of molecules that can simultaneously follow the desired photoswitching pathway is small (although a larger fraction may engage into the pathway but quickly return to the starting state or deviate to other photophysical states). This explains why almost all ultrafast spectroscopic investigations of RSFPs photoswitching so far concentrated on the back-photoswitching reaction of Dronpa which has a particularly high yield (>0.1).

Yet, another approach to track intermediates consists in performing temperature-controlled experiments. At sufficiently

low temperature, the switching reaction may not be able to be completed if thermal energy barriers are present along the pathway. In such a case, activated molecules may possibly get trapped and accumulate in an intermediate state that can then be probed structurally or spectroscopically. Such an approach was for example used to study the protein Padron [47]. Working at low temperature, however, always carries the danger that the protein conformational landscape may be altered.

Important insight into photoswitching mechanisms can also be obtained from theoretical investigations such as molecular dynamics simulations or reaction-path-finding techniques. In such studies, the RSFP is modeled with quantum mechanics/molecular mechanics (QM/MM) hybrid approaches: the chromophore and its nearby environment are described at the quantum level in the ground or excited state, whereas the rest of the protein is treated with classical force fields. Such investigations have provided a number of interesting details about fundamental properties of photoswitching [21, 27]. However, they strongly rely on available high-resolution crystallographic input structures, and it should be kept in mind that they remain restricted by necessary simplifications and assumptions, due to limited computing power. For example, modeling proton transfer reactions involving the RSFPs chromophore is difficult, as the number of atoms in the QM region can typically not be changed along simulations.

Ultrafast time-resolved crystallography experiments on RSFPs based on synchrotron Laue diffraction have so far remained unsuccessful. However, new XFEL sources offer exciting prospects to catch photoswitching in action. In the long term, the dream would be to watch single RSFPs in real time at atomic resolution, e.g., by combining femtosecond stimulated Raman scattering [48] with XFEL diffraction [49].

4 Photoswitching Mechanisms

In this section, we describe in more detail the photoswitching mechanisms as observed in negative, positive, and decoupled RSFPs. Three important remarks should be made beforehand.

First, the *p*-HBI chromophore in solution has been shown to undergo facile photoinduced *cis–trans* isomerization caused by twisting around the methylene bridge that links the two cyclic moieties (explaining the lack of fluorescence of the isolated *p*-HBI chromophore in solution) [50]. Thus, chromophore isomerization in RSFPs is primarily a manifestation of intrinsic excited state chromophore dynamics. This process is in general hindered by the protein scaffold in FPs, but it can still occur with low yield in RSFPs. Chromophore isomerization in RSFPs is a single-photon excitation process in both directions [13, 47]. However, back-switching is

also thermally driven and it should be kept in mind that some FPs are able to change the isomeric state of their chromophore in the ground state following pH changes [51, 52].

Second, the isomeric state of the chromophore in general does not dictate per se the occurrence or the lack of fluorescence. There exist FPs exhibiting strong fluorescence in the *trans* state [52, 53]. However, in positive or negative RSFPs, the nonfluorescent state has always been found to correspond to the *trans* configuration of the chromophore.

Third, the proton affinity of the chromophore hydroxybenzylidene group strongly depends on the local protein environment and therefore it is isomer dependent, both in the ground and in the excited states. Widely different chromophore p*K*a are therefore expected—and observed—in the *trans* or *cis* configurations. As chromophore protonation has a strong influence on the ability to fluoresce, this isomer-dependent p*K*a generally plays a key role in fluorescence switching.

4.1 Negative Anthozoan RSFPs: On and Off States

To describe the photoswitching mechanism in negative RSFPs, we take the example of IrisFP, which has been extensively characterized by us [35]. The X-ray structures and absorption/fluorescence spectra of the protein in its on and off states are presented in Fig. 3.

In both states, it can be seen that the chromophore is maintained by a complex set of H-bonding interactions involving Arg66, Ser142, Glu144, Ser173, Tyr177, His194, and Glu212, as well as water molecules. These residues are essentially conserved in all negative RSFPs from Anthozoa species. *cis–trans* Isomerization is accompanied by a substantial structural change of the chromophore pocket. The tightly H-bonded triad Glu144-His194-Glu212 in the *cis* configuration is replaced by the Glu144-Arg66-Glu212 triad in the *trans* configuration, with either His194 or Arg66 stabilizing the chromophore by π-stacking and π-cation interactions with the hydroxybenzylidene moiety, respectively. In the *cis* configuration, the chromophore phenolate interacts with Ser142 whose hydroxy group is protonated, thus favoring a deprotonated state. This anionic state is further favored by the interaction of Arg66 with the carbonyl group of the imidazolinone moiety, which retains electron density on that ring. Hence, the p*K*a of the *cis* chromophore in IrisFP ensures a predominantly deprotonated chromophore at physiological pH (p*K*a = 5.7). The chromophore is also found in a highly planar configuration. Thus, the conditions favoring a high fluorescence yield are fulfilled. In the *trans* configuration, a very different scenario is found, where the phenolate group is interacting with the deprotonated Glu144, and the interaction of Arg66 with the imidazolinone being disengaged. Consequently, there is a substantial change in the chromophore electrostatic environment, and the latter is found completely protonated at physiological pH, with a p*K*a > 10.

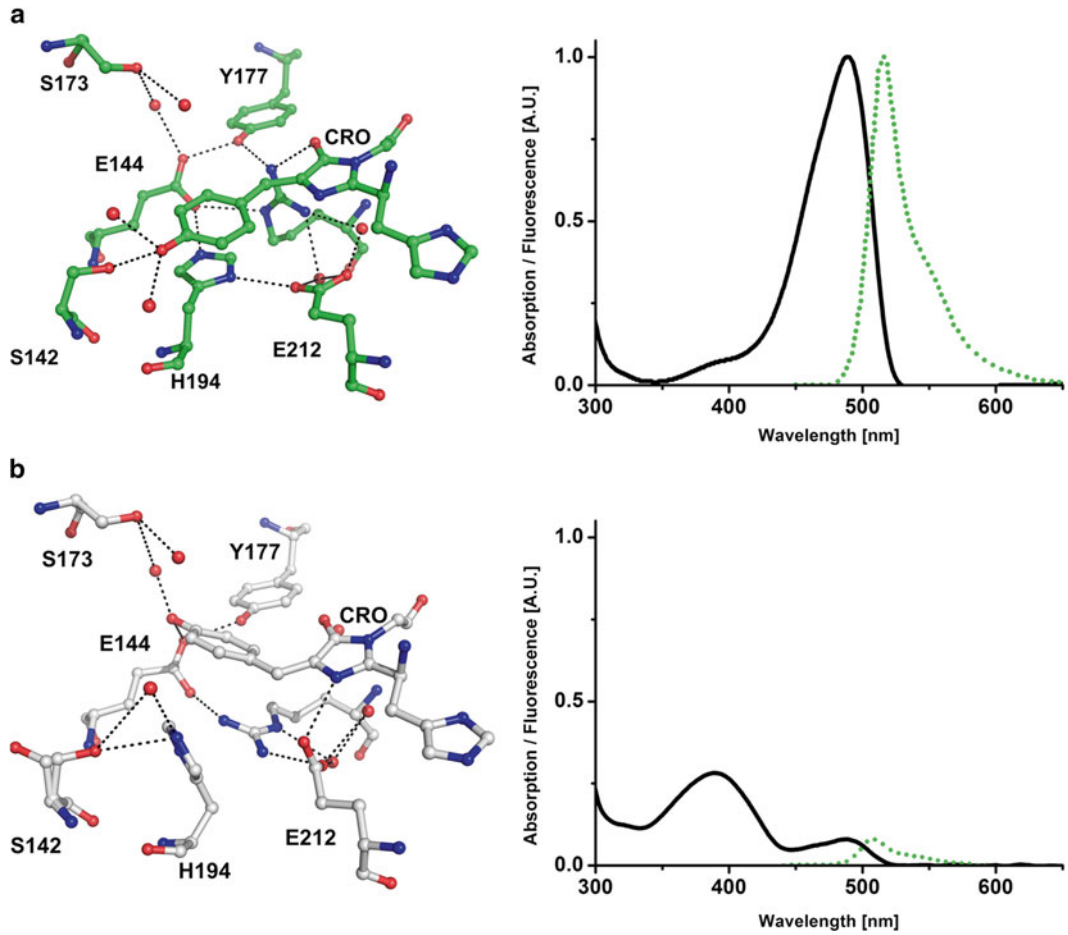

Fig. 3 Crystallographic structures of the chromophore, its microenvironment, and the corresponding spectra for IrisFP. (**a**) In the more stable fluorescent state (PDB ID 2VVH), the chromophore adopts a *cis* conformation and is deprotonated as observable by the major anionic absorption band peaking at 487 nm (*black spectrum*) that provides fluorescence peaking at 516 nm (*green dotted spectrum*). (**b**) In the dark state (PDB ID 2VVI), the 3D structure shows that the chromophore clearly adopts a *trans* conformation and is protonated as observable by the major neutral band peaking at 390 nm (*black spectrum*). The remaining fluorescence signal (*green dotted spectrum*) is due to a minor fraction of chromophores remaining in the *cis* conformation. Water molecules are represented as *red balls* and hydrogen bonds are represented as *black dotted lines*

No ESPT (excited state proton transfer) is observed and the chromophore is found to adopt a quite distorted geometry. Thus, the conditions favoring a high fluorescence yield are not fulfilled. The *trans*-conformation is thermodynamically quite stable, taking a few hours to return to the *cis*-conformation. This stems from the fact that the protein scaffold is able to accommodate the hydroxybenzylidene group of the *trans*-chromophore with overall little deformation, and by optimally rearranging the H-bond networks within the pocket. Some subtleties contribute to enhancing the stability of the *trans*-state: for example, Ser142, which maintains a strong

H-bond with the hydroxybenzylidene moiety in the *cis*-state, engages with another H-bonding partner once the chromophore has been isomerized, as a compensation. Also, Glu212 directly interacts with the imidazolinone nitrogen in the *trans*-state, providing further stabilization.

Similar schemes have been described for Dronpa [15] and mTFP0.7 [31], with some relatively minor variations. An important peculiarity of Dronpa is that upon off-photoswitching, the seventh β-strand near the chromophore becomes disordered, as shown by NMR experiments [16]. As this strand forms part of the cross-dimer interface in the tetrameric parent of Dronpa, Dronpa photoswitching modulates its propensity to multimerize at high concentration. This property was ingenuously used to develop a new optogenetic approach [54]. Likewise, researchers took advantage of the flexibility-mediated photoswitching of Dronpa to develop a viscosity measurement assay [55].

4.2 Positive Anthozoan RSFPs: On and Off States

Padron is a positive RSFP engineered from Dronpa [30, 56]. The two essential Met159Tyr and Val157Gly mutations were sufficient to completely reverse the switching properties of Dronpa (hence the name "Padron"). The X-ray structures and absorption/fluorescence spectra of Padron in its on and off states are presented in Fig. 4. In the on state, the configurations of the chromophore and of its immediate environment do not differ much from Dronpa or IrisFP. However, Ser142 adopts a different conformation than in Dronpa, which might be responsible for the substantial increase in the proton affinity of the chromophore hydroxybenzylidene moiety. Indeed, the chromophore exhibits a p*K*a of 6.0 (5.3 for Dronpa), meaning that at physiological pH a significant fraction of the switched-on Padron molecules are protonated and nonfluorescent. In the *trans* state, structural differences with negative RSFPs are striking: Tyr159 now establishes an H-bonding interaction with the chromophore phenolate, which maintains the latter in an anionic state, with a p*K*a of 4.5. His193, Arg66, and Glu211 (equivalent to His194, Arg66, and Glu212 in IrisFP) do not change their conformation relative to the *cis* state, possibly because of the shifted location of Ser142, and this may in turn result in the severe torsion of the *trans* chromophore. Thus, the *trans* chromophore is nonfluorescent but exhibits an absorption spectrum similar to that of the fluorescent on state (although somewhat broader presumably due to a larger conformational freedom).

4.3 Positive and Negative Anthozoan RSFPs: Reaction Pathways

Photoswitching kinetics and pathways in RSFPs are controlled by the potential energy surfaces that connect the on and off states of the chromophore. The chromophore isomer conformation and protonation, in the ground and excited state, as well as the protein environment, are all involved. Therefore, modifying the chromophore composition, or its environment, allows tuning properties

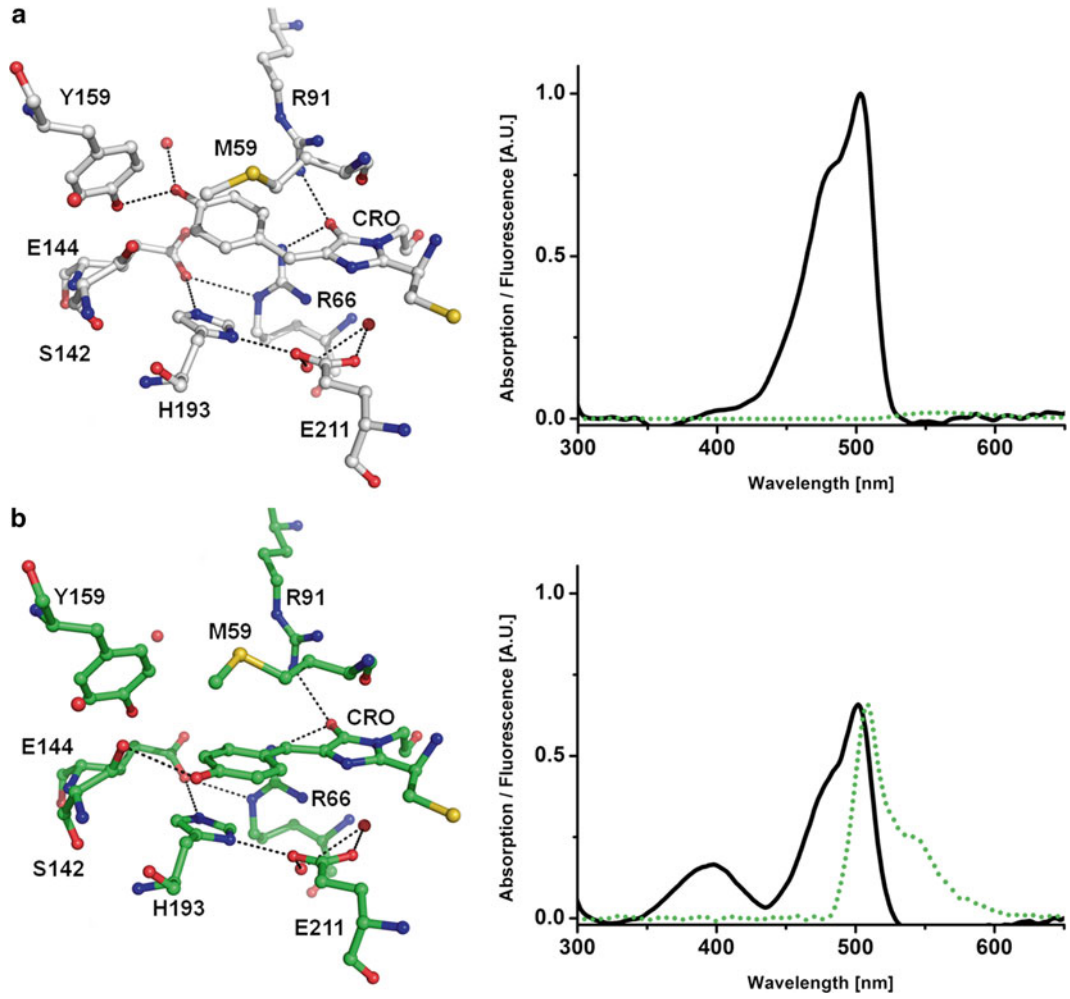

Fig. 4 Crystallographic structures of the chromophore, its microenvironment, and the corresponding spectra for Padron. (**a**) In the more stable dark state (PDB ID 3ZUF) the 3D structure shows that the chromophore adopts a trans conformation and is deprotonated as indicated by the major anionic absorption band peaking at 503 nm (*black spectrum*). (**b**) In the fluorescent state (PDB ID 3ZUJ) the chromophore clearly adopts a *cis* conformation. Absorption spectra reveal two bands, one peaking at 390 nm and corresponding to the neutral fraction and one peaking at 503 nm and corresponding to the anionic fluorescent fraction peaking at 518 nm. Water molecules are represented as red balls and hydrogen bonds are represented as *black dotted lines*

such as photoswitching rates, photon outputs, photostability, or pH-sensitivity. For example, Chang et al. [34] engineered the mGeos negative RSFPs by modifying the first position of the chromophore tripeptide and found that mGeos-M (with a methionine at this position) had the highest number of photons emitted per switching cycle amongst all green RSFPs. Likewise, Adam et al. [36] modified the protein environment of the photo-convertible EosFP and Dendra2 PCFPs to engineer bi-photochromic variants with differing properties.

In both positive and negative RSFPs, the exact order of events and the presence of intermediate states along the reaction pathway have been investigated. Because of its high quantum yield (~0.5), the back switching reaction in Dronpa could be experimentally interrogated by ultrafast spectroscopy. ESPT to an intermediate state I was proposed to occur, consistent with the observation of a significant kinetic isotope effect (KIE) using deuterated samples [18]. In line with this view, theoretical calculations proposed that isomerization and deprotonation events during Dronpa off-on switching are concerted [21]. This view is also consistent with the elegant theoretical model of Olsen et al. [57], which suggests that to promote efficient photoswitching, the protein environment should restrict torsion around the methylene phenoxy bond (P-bond) and promote torsion around the imidazolinone bond (I-bond) through suitable acid–base chemistry. However, these findings were recently questioned by a Fourier Transform infrared study (FTIR) in which a *cis* protonated ground state intermediate was evidenced, strongly suggesting that deprotonation of the chromophore rather occurs as a subsequent step to isomerization [23]. These contradictory observations show that the interpretation of ultrafast spectroscopic data is a delicate issue and corroborates the fact that many interrelated factors control photoswitching in RSFPs, the exact roles of which are difficult to disentangle. Moreover, hidden processes may take place and further complicate the matter: as an example, the recent study of Gayda et al. [45] on a mutant of IrisFP (called mIrisGFP) revealed that the neutral *cis* chromophore of mIrisGFP can isomerize to the neutral *trans* state much more efficiently than the anionic *cis* chromophore (consistent with a barrierless mechanism predicted by the Olsen model [57]). This phenomenon however typically remains unnoticed, as back switching by the same illumination wavelength (405 nm) is even more efficient, bringing back the neutral *trans* chromophore "immediately" to the *cis* configuration. Several different switching processes may thus occur in parallel, even if at the ensemble level the spectroscopic footprint remains steady. Overall, the precise photoswitching mechanism of negative RSFPs still remains to be elucidated completely.

In positive RSFPs, work has been done on Padron and asFP595. A study of the asFP595-Ala143Ser mutant (displaying an enhanced fluorescence quantum yield) by molecular dynamics suggested that on-switching was linked to chromophore *trans–cis* isomerization via a Hula-Twist mechanism, in which both I and P bonds change in a concerted manner to minimize the volume swept by the chromophore during switching [14]. This view is however difficult to reconcile with the Olsen theory of isomerization through I-bond flip. *Ab initio* calculations and QC/MM molecular dynamics simulations in asFP595 suggested that *trans–cis* isomerization occurs in the neutral state of the chromophore, followed by a dark state equilibration to a zwitterionic fluorescent *cis* state [27]. In Padron, a different scenario was observed: two fluorescent intermediates

along the on-switching pathway could be cryo-trapped [47]. The combined spectroscopic and crystallographic data suggested that *trans–cis* isomerization of the chromophore occurs entirely in the anionic state and precedes protonation. These experimental findings are in line with the latest results by FTIR in Dronpa [23]. They are also interesting in terms of structural protein dynamics. First, they reveal that full *trans–cis* isomerization of the Padron chromophore is possible at 100 K, a temperature at which protein dynamical breathing is essentially stalled. As heat dissipation upon photon absorption occurs on the picosecond timescale, a transiently "hot" chromophore could account for this observation. Second, it was observed that protonation of the chromophore following isomerization only took place above the glass transition temperature (~200 K), suggesting that protonation involves exchange with the surrounding solvent. The fact that Padron can be efficiently photoswitched at cryo-temperature opens interesting potential applications such as cryo-nanoscopy [47].

Overall, as for negative RSFPs, the mechanisms governing fluorescence switching in positive RSFPs are still not entirely understood. The extent by which these mechanisms differ between members of each family also remains to be evaluated.

4.4 Hydrozoan RSFPs

Surprisingly little structural information is available on RSFPs evolved from GFP derivatives. Amongst several pieces of indirect evidence, studies by vibrational spectroscopy [58] suggest that a chromophore *cis–trans* isomerization process similar to that found in Anthozoan RSFPs also takes place in these proteins. However structural evidence for a *trans* chromophore in Hydrozoan RSFPs is still lacking.

4.5 Decoupled Switching in Hydrozoan RSFPs: Dreiklang

Positive and negative RSFPs are not optimal in that laser-light used for fluorescence excitation also induces switching. The protein Dreiklang, evolved from the GFP variant Citrine, nicely overcomes this problem [40]. In Dreiklang, excitation at 514 nm does not induce significant off-switching, whereas near UV-light at 365 and 405 nm result in on and off switching, respectively. The existence of such decoupling had already been hinted at in previous experiments with EYFP [10, 41]. In Dreiklang, this behavior was deliberately exacerbated by random mutagenesis, resulting in an unprecedented switching mechanism. Combined crystallographic and mass spectroscopy analyzes provided evidence that light-induced hydration-dehydration of the chromophore caused switching by disrupting the π-conjugated electron system (Fig. 5). Hydration of the C_{65} atom of the imidazolinone moiety appeared to be facilitated by the proper positioning of a water molecule (Wat_A) held in place by hydrogen bonding between Tyr203 and Glu222 and putatively replaced in the switched-off state by another water molecule (Wat_B) garnered from the environment. However, the exact roles of the 4 mutations (Val61Leu, Phe64Ile, Tyr145His,

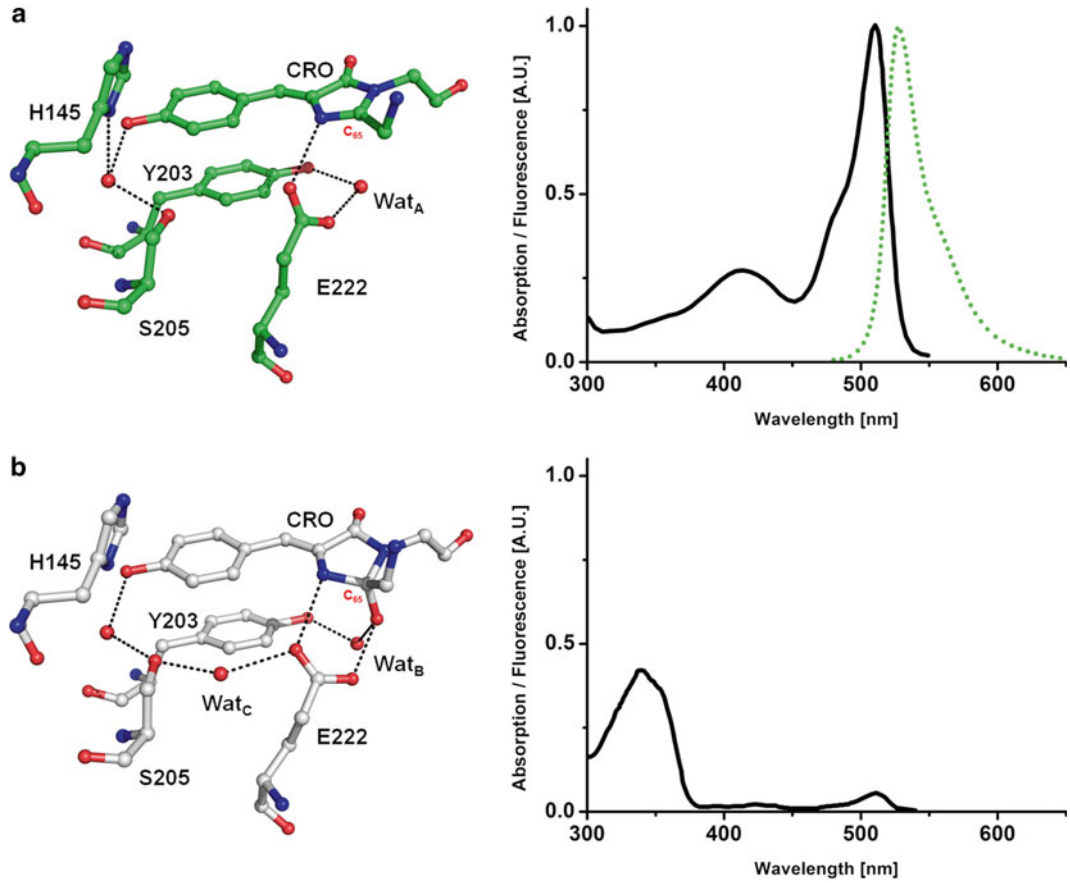

Fig. 5 Crystallographic structures of the chromophore, its microenvironment, and the corresponding spectra for Dreiklang. (**a**) In the more stable fluorescent state (PDB ID 3ST4), the chromophore adopts a *cis* conformation and is deprotonated as observable by the major anionic absorption band peaking at 515 nm (*black spectrum*) that provides fluorescence at 529 nm (*green dotted spectrum*). (**b**) In the dark state (PDB ID 3ST3) the water molecule Wat_A is found to hydrate the carbon C_{65}, distorting the geometry of the imidazolinone ring. Absorption spectra reveal that both the neutral and the anionic forms have been converted to a blue-shifted absorption band peaking at 340 nm. Water molecules are represented as *red balls* and hydrogen bonds are represented as *black dotted lines*

and Asn146Asp) relative to Citrine remain to be established. Also, the use of UV-light to induce on- and off-switching is prone to generate cytotoxicity. It is also not clear yet how the hydration/dehydration processes can be light-activated in the protonated state of the chromophore.

5 Using RSFPs in Advanced Fluorescence Applications

Many exciting fields of science are nowadays explored by using photoswitchable fluorescent proteins, including super-resolution fluorescence microscopy (*see* Chapter 16 of this volume),

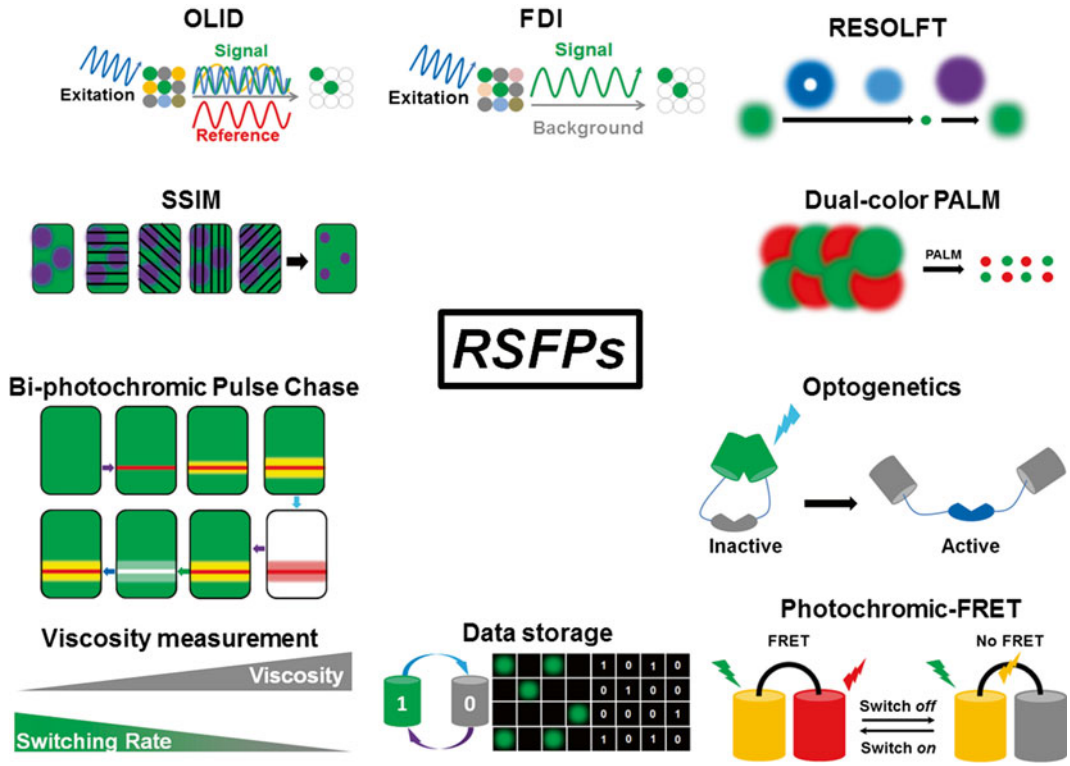

Fig. 6 Panoply of possible applications using RSFPs in super-resolution imaging and biotechnology. *OLID* optical lock-in detection, *FDI* frequency domain imaging

optogenetics, optical lock-in detection, frequency-domain imaging, sensor developments and biotechnological applications (Fig. 6). Some examples are described below.

5.1 Super-Resolution Fluorescence Microscopy by Single Molecule Localization

Single molecule localization microscopy (SMLM) was developed in 2006 with techniques such as photoactivated localization microscopy (PALM) [59, 60] and stochastic optical reconstruction microscopy (STORM) [61]. These super-resolution techniques are conceptually identical but use either phototransformable FPs (PALM) or blinking organic dyes (STORM) as highlighters. SMLM is nowadays very popular in that it does not require a complex instrumental setup and provides the best spatial resolutions currently achievable. Irreversible photoconvertible FPs are generally preferred for PALM applications over RSFPs because they typically emit more photons per localized spot and are less prone to complications due to multiple localizations of a single molecule. Multicolor PALM, however, is difficult to achieve with PCFPs only, as currently available members do not display a large spectral separation. A solution to this problem has been found by achieving dual-labeling with a green-to-red PCFP such as EosFP and an RSFP such as Dronpa. The method relies on a sequential acquisition protocol: all EosFP molecules are first photoconverted to

their red-emitting state by 405-nm irradiation and detected by 561-nm illumination with minimal effects on the Dronpa molecules that are visualized subsequently with alternating 488 and 405-nm illumination. This protocol succeeded in colocalizing a variety of proteins of interest [62, 63].

Interestingly, the rich photophysics of RSFPs also allow acquiring dual-labeling "false-multicolor" PALM data [30]. This can be accomplished by distinguishing RSFPs variants of similar colors based on properties such as positive vs. negative switching, or different photoswitching rates.

The capacity of RSFPs to produce intense fluctuations of their emission signal recently permitted their application into a variant of SMLM called stochastic optical fluctuation imaging (SOFI) (*see* Chapter 17 of this volume). In its standard version, SOFI takes advantage of natural fluorescence flickering to enhance image resolution [64]. Photochromic SOFI (pcSOFI) [65] demonstrates improved signal-to-noise contrast and a two- to threefold enhancement of the spatial resolution compared to diffraction-limited images, thanks to the possibility of precisely controlling the "flickering" (switching) of RSFPs.

5.2 Nonlinear Microscopy Applications

RSFPs can be advantageously used in nonlinear imaging because the saturation of their switching transitions leads to distinct minima/maxima of fluorescence depending on the illumination pattern, even with low light intensities.

In confocal illumination mode, the concept of REversible Saturable Optical Linear Fluorescence Transitions (RESOLFT) [66] has been proposed as an alternative to the well-known STimulated Emission Depletion (STED) microscopy. In STED, a donut-shaped laser spot applied immediately after excitation by a diffraction-limited laser spot depletes emission of a standard fluorophore except for the central zero-intensity region of the donut beam. The diameter of the resulting effective point spread function decreases with increasing intensities of the donut-shaped beam, thus providing enhanced resolution. However, an enormous power density is required for this beam (typically MW/cm^2). Instead, when RESOLFT is used in combination with RSFPs [67, 68], the donut-shaped beam serves to switch off the label, a process which is not limited by the fluorescence lifetime. Thus, albeit at the expense of a reduced time-resolution, this allows a huge decrease (up to six orders of magnitude) of the light intensity needed to break the diffraction barrier as compared to STED microscopy. This considerably reduces potential cytotoxic effects.

Increasing spatial resolution in RESOLFT implies achieving a higher number of switching cycles of the RSFP, while improving time resolution requires higher switching yields. The engineering of the well-known EGFP into rsEGFP [38] created an RSFP with much faster photoswitching rates than Dronpa and with a much

enhanced photoresistance, comparable to that of its parent EGFP. Recent modifications of this variant resulted in an even faster RSFP, named rsEGFP2, in which, as compared to rsEGFP, the mutations Val150Ala and Ser205Asn have been back-mutated and the first amino acid of the chromophore was modified (Thr65Ala) [39]. RsEGFP2 allows the application of RESOLFT microscopy with no more light than in conventional confocal microscopy and at unprecedented speed.

Similarly, very weak illumination intensities can be used when RSFPs are employed in combination with Saturated Structured Illumination Microscopy (SSIM), a nonlinear version of SIM [69]. In this wide-field imaging technique, the sample is illuminated with a sine-shaped wavefront (structured illumination) that is modulated in phase and angle. From the interferences between the patterned illumination and the spatial response of the fluorescent sample (Moiré fringes) a resolution increase by a factor of 2 can be achieved. To push the resolution further with standard fluorophores, very intense illumination is required to saturate the singlet excited state S_1, producing sharp fluorescent fringes. The use of RSFPs such as Dronpa relies on saturating the long-lived off state instead of the short-lived S_1, alleviating the need for high intensities [70].

5.3 Advanced Microscopy and Biotechnology with Bi-photochromic FPs

Biphotochromic FPs combine the photophysical properties of both PCFPs and RSFPs into single PTFPs. IrisFP [35] was the first member of this family: it can be irreversibly photoconverted from green to red and reversibly switched off in either the green or the red state. The monomeric variant mIrisFP was successfully used as a tool for two-color super-resolved pulse-chase imaging experiments [71]. In this technique, a fraction of the molecules are first photoconverted to their red-emitting state and let to diffuse within the cell. Using photochromic-based PALM, both the unphotoconverted (green) and photoconverted (red) molecules are then tracked at nanometric precision. Improved biphotochromic variants have been recently engineered [36]. In particular, NijiFP is a variant of the monomeric PCFP Dendra2 and demonstrated promising properties: low tendency to oligomerize, good spectral contrast between green and red states, and excellent photoswitching capability of the two forms.

PTFPs have been used to demonstrate the concept of biological data-storage, possibly in 3D [72]. Notably, rsEGFP has been shown to provide a remarkable support for rewritable ultrahigh density data storage [38]. Biphotochromic FPs open the route to quaternary data storage applications. Photoconverting to the red state half of a biphotochromic FP substrate spread on a surface, it becomes possible to achieve four optical combinations by switching off or on the green and red molecules. A base-4 encoding system is obtained: dark + dark = 0, dark + green = 1, dark + red = 2, red + green = 3, equivalent in binary code to 00, 01, 10, and 11, respectively.

5.4 Optogenetics

The use of RSFPs in optogenetics was recently introduced as an exquisite tool to control specific cellular activities through reversible photoswitching [54]. Dronpa is a monomeric RSFP, but it was derived from a tetrameric parent. A single mutant of Dronpa (Lys145Asn), called PDM1-4 [73], was shown to exhibit a propensity to tetramerize in the switched-on state, whereas it remains monomeric in the off state. The crystallographic structure of PDM1-4 revealed a rigidified tetramer interface, consistent with this finding [74]. A mixture of PDM1-4 and Dronpa was then shown to promote light-induced dimer-to-monomer conversion rather than tetramer-to-monomer conversion with PDM1-4 alone. The idea, then, consists in fusing a protein of interest (POI) at one end with PDM1-4 and at the other end with Dronpa. In the on-state, the two RSFP domains interact, "caging" the POI, while in their off state they split, restoring the POI activity. The method was applied to intersectin, a guanine nucleotide exchange factor that activates Cdc42. Upon 490-nm illumination, activation of Cdc42 by uncaged intersectin was monitored through the growth of filopodia, an obvious morphological change that was observed concomitantly with the disappearance of Dronpa fluorescence due to switching. Using the same concept, it was possible to design a light inducible NS3-4A protease in the hepatitis C virus (HCV).

5.5 Viscosity Sensing

The interrelation between Dronpa photoswitching and β-barrel plasticity allowed yet another surprising application of this RSFP, this time as a sensor for solvent viscosity. Hydrodynamic changes exerted on Dronpa by an increasing viscosity were found to reduce the photoswitching rate of its chromophore [55]. Moreover, the authors demonstrated that fast-switching variants and more specifically Dronpa[Val157Ile/Met159Ala], named Dronpa-3 [29], are especially sensitive to viscosity changes: the photoswitching rate of Dronpa-3 slowed down by a factor of 4 when the glycerol concentration was increased from 0 to 90 %. This makes Dronpa-3 an efficient genetically-encoded reporter for microviscosity in vivo as demonstrated in the case of chromatin: a slightly more viscous environment was repeatedly measured when cells were in mitosis.

5.6 Photochromic FRET (pcFRET)

The synthesis of photochromic organic fluorescent dyes allowed, a decade ago, the development of a novel approach for quantitative Förster resonance energy transfer (FRET) [75, 76]. In this photochromic FRET (pcFRET) approach, modulations of fluorescence emission by a donor molecule can be induced by reversible switching of a photochromic acceptor, allowing quantitative and repeatable determination of the FRET efficiency between two molecules without the need to apply corrections based on reference images.

The recent engineering of the red-shifted RSFPs rsCherryRev [77] and rsTagRFP [78] allowed the conception of similar pcFRET

experiments using solely genetically encoded reporters. Coupled to EYFP as a donor, rsTagRFP revealed to be an excellent photochromic acceptor [78] and allowed a precise quantification of protein–protein interactions within living cells.

6 Conclusion: Future Prospects for RSFPs

Reversibly switchable FPs are astonishing macromolecules that nowadays play a key role in state-of-the-art techniques based on light-induced protein manipulation.

In contrast to photoconvertible FPs that are found in nature, all RSFPs known so far are man-made, developed on the basis of FPs from both the Anthozoan and the Hydrozoan classes. Thus, there is probably little functional advantage to such switching capabilities in marine organisms. On the contrary, an incredibly wide palette of applications has already been found by researchers, in the fields of advanced fluorescence microscopy and biotechnology.

The mechanism underlying switching in RSFPs is generally based on *cis–trans* photoinduced isomerization of the chromophore coupled with a protonation change. However, there are subtle differences between members, and despite significant progress in the last years, reaction pathways and intermediate states possibly involved are still under debate.

An important aspect of future research in RSFPs photophysics will be to understand how blinking and bleaching, these phenomena that are so characteristic in all FPs, interfere with photoswitching. Although hints have been provided already [79, 80], these stochastic events are difficult to capture and characterize. Yet, they are fundamental in the quest for future optimization of RSFPs, together with other properties, such as red-shifted fluorescence or decoupled switching.

Our knowledge of fluorescent proteins is constantly growing. However, experience has shown that the complex architecture of the β-barrel and its links to the chromophore is intricate to a degree that success in developing improved variants on the basis of rational design alone has been so far the exception rather than the rule. It will be interesting to see if multi-residue rational design of a PTFP will eventually be successful, knowing that directed evolution approaches are currently bound to miss a large fraction of possible synergistic combinations of mutations.

Whatever the engineering approaches, surprising new properties will continue to emerge and, based on these, the palette of new RSFPs-based applications will continue to grow, so it is worth to stay tuned for amazing new developments.

References

1. Dedecker P, De Schryver FC, Hofkens J (2013) Fluorescent proteins: shine on, you crazy diamond. J Am Chem Soc 135(7):2387–2402. doi:10.1021/ja309768d
2. Chudakov DM, Matz MV, Lukyanov S, Lukyanov KA (2010) Fluorescent proteins and their applications in imaging living cells and tissues. Physiol Rev 90(3):1103–1163. doi:10.1152/physrev.00038.2009
3. Subach FV, Verkhusha VV (2012) Chromophore transformations in red fluorescent proteins. Chem Rev 112(7):4308–4327. doi:10.1021/cr2001965
4. Lippincott-Schwartz J, Patterson GH (2009) Photoactivatable fluorescent proteins for diffraction-limited and super-resolution imaging. Trends Cell Biol 19(11):555–565. doi:S0962-8924(09)00199-8 [pii]10.1016/j.tcb.2009.09.003
5. Bourgeois D, Adam V (2012) Reversible photoswitching in fluorescent proteins: a mechanistic view. IUBMB Life 64(6):482–491. doi:10.1002/iub.1023
6. Bourgeois D, Regis-Faro A, Adam V (2012) Photoactivated structural dynamics of fluorescent proteins. Biochem Soc Trans 40:531–538. doi:10.1042/bst20120002
7. Dickson RM, Cubitt AB, Tsien RY, Moerner WE (1997) On/off blinking and switching behaviour of single molecules of green fluorescent protein. Nature 388(6640):355–358
8. Sinnecker D, Voigt P, Hellwig N, Schaefer M (2005) Reversible photobleaching of enhanced green fluorescent proteins. Biochemistry 44(18):7085–7094
9. Nifosi R, Ferrari A, Arcangeli C, Tozzini V, Pellegrini V, Beltram F (2003) Photoreversible dark state in a tristable green fluorescent protein variant. J Phys Chem B 107(7):1679–1684. doi:10.1021/Jp0266852
10. McAnaney TB, Zeng W, Doe CF, Bhanji N, Wakelin S, Pearson DS, Abbyad P, Shi X, Boxer SG, Bagshaw CR (2005) Protonation, photobleaching, and photoactivation of yellow fluorescent protein (YFP 10C): a unifying mechanism. Biochemistry 44(14):5510–5524
11. Chudakov DM, Feofanov AV, Mudrik NN, Lukyanov S, Lukyanov KA (2003) Chromophore environment provides clue to "kindling fluorescent protein" riddle. J Biol Chem 278(9):7215–7219
12. Ando R, Mizuno H, Miyawaki A (2004) Regulated fast nucleocytoplasmic shuttling observed by reversible protein highlighting. Science 306(5700):1370–1373. doi:10.1126/science.1102506
13. Habuchi S, Ando R, Dedecker P, Verheijen W, Mizuno H, Miyawaki A, Hofkens J (2005) Reversible single-molecule photoswitching in the GFP-like fluorescent protein Dronpa. Proc Natl Acad Sci U S A 102(27):9511–9516
14. Andresen M, Wahl MC, Stiel AC, Grater F, Schafer LV, Trowitzsch S, Weber G, Eggeling C, Grubmuller H, Hell SW, Jakobs S (2005) Structure and mechanism of the reversible photoswitch of a fluorescent protein. Proc Natl Acad Sci U S A 102(37):13070–13074. doi:10.1073/pnas.0502772102
15. Andresen M, Stiel AC, Trowitzsch S, Weber G, Eggeling C, Wahl MC, Hell SW, Jakobs S (2007) Structural basis for reversible photoswitching in Dronpa. Proc Natl Acad Sci U S A 104(32):13005–13009. doi:10.1073/pnas.0700629104
16. Mizuno H, Mal TK, Walchli M, Kikuchi A, Fukano T, Ando R, Jeyakanthan J, Taka J, Shiro Y, Ikura M, Miyawaki A (2008) Light-dependent regulation of structural flexibility in a photochromic fluorescent protein. Proc Natl Acad Sci U S A 105(27):9227–9232. doi:0709599105 [pii] 10.1073/pnas.0709599105
17. Dedecker P, Hotta J, Ando R, Miyawaki A, Engelborghs Y, Hofkens J (2006) Fast and reversible photoswitching of the fluorescent protein Dronpa as evidenced by fluorescence correlation spectroscopy. Biophys J 91(5):L45–L47
18. Fron E, Flors C, Schweitzer G, Habuchi S, Mizuno H, Ando R, Schryver FC, Miyawaki A, Hofkens J (2007) Ultrafast excited-state dynamics of the photoswitchable protein Dronpa. J Am Chem Soc 129(16):4870–4871
19. Wilmann PG, Turcic K, Battad JM, Wilce MC, Devenish RJ, Prescott M, Rossjohn J (2006) The 1.7 A crystal structure of Dronpa: a photoswitchable green fluorescent protein. J Mol Biol 364(2):213–224
20. Stiel AC, Trowitzsch S, Weber G, Andresen M, Eggeling C, Hell SW, Jakobs S, Wahl MC (2007) 1.8 A bright-state structure of the reversibly switchable fluorescent protein Dronpa guides the generation of fast switching variants. Biochem J 402(1):35–42
21. Li X, Chung LW, Mizuno H, Miyawaki A, Morokuma K (2010) A theoretical study on the nature of on- and off-states of reversibly photoswitching fluorescent protein Dronpa: absorption, emission, protonation, and Raman. J Phys Chem B 114(2):1114–1126. doi:10.1021/jp909947c

22. Li X, Chung LW, Mizuno H, Miyawaki A, Morokuma K (2010) Primary events of photodynamics in reversible photoswitching fluorescent protein Dronpa. J Phys Chem Lett 1(23):3328–3333. doi:10.1021/Jz101419p
23. Warren MM, Kaucikas M, Fitzpatrick A, Champion P, Timothy Sage J, van Thor JJ (2013) Ground-state proton transfer in the photoswitching reactions of the fluorescent protein Dronpa. Nat Commun 4:1461. http://www.nature.com/ncomms/journal/v4/n2/suppinfo/ncomms2460_S1.html
24. Quillin ML, Anstrom DM, Shu X, O'Leary S, Kallio K, Chudakov DM, Remington SJ (2005) Kindling fluorescent protein from Anemonia sulcata: dark-state structure at 1.38 A resolution. Biochemistry 44(15): 5774–5787
25. Schüttrigkeit TA, von Feilitzsch T, Kompa CK, Lukyanov KA, Savitsky AP, Voityuk AA, Michel-Beyerle ME (2006) Femtosecond study of light-induced fluorescence increase of the dark chromoprotein asFP595. Chem Phys 323(2–3):149–160. doi:10.1016/j.chemphys.2005.09.039
26. Schafer LV, Groenhof G, Klingen AR, Ullmann GM, Boggio-Pasqua M, Robb MA, Grubmuller H (2007) Photoswitching of the fluorescent protein asFP595: mechanism, proton pathways, and absorption spectra. Angew Chem Int Ed 46(4):530–536
27. Schafer LV, Groenhof G, Boggio-Pasqua M, Robb MA, Grubmuller H (2008) Chromophore protonation state controls photoswitching of the fluoroprotein asFP595. PLoS Comput Biol 4(3):e1000034. doi:10.1371/journal.pcbi.1000034
28. Grigorenko BL, Polyakov IV, Savitsky AP, Nemukhin AV (2013) Unusual emitting states of the kindling fluorescent protein: appearance of the cationic chromophore in the GFP family. J Phys Chem B 117(24):7228–7234. doi:10.1021/jp402149q
29. Ando R, Flors C, Mizuno H, Hofkens J, Miyawaki A (2007) Highlighted generation of fluorescence signals using simultaneous two-color irradiation on Dronpa mutants. Biophys J 92(12):L97–L99. doi:biophysj.107.105882 [pii] 10.1529/biophysj.107.105882
30. Andresen M, Stiel AC, Folling J, Wenzel D, Schonle A, Egner A, Eggeling C, Hell SW, Jakobs S (2008) Photoswitchable fluorescent proteins enable monochromatic multilabel imaging and dual color fluorescence nanoscopy. Nat Biotechnol 26(9):1035–1040. doi:nbt.1493 [pii] 10.1038/nbt.1493
31. Henderson JN, Ai HW, Campbell RE, Remington SJ (2007) Structural basis for reversible photobleaching of a green fluorescent protein homologue. Proc Natl Acad Sci U S A 104(16):6672–6677
32. Subach FV, Zhang L, Gadella TW, Gurskaya NG, Lukyanov KA, Verkhusha VV (2010) Red fluorescent protein with reversibly photoswitchable absorbance for photochromic FRET. Chem Biol 17(7):745–755. doi:10.1016/j.chembiol.2010.05.022 S1074-5521(10)00213-9 [pii]
33. Pletnev S, Subach FV, Dauter Z, Wlodawer A, Verkhusha VV (2012) A structural basis for reversible photoswitching of absorbance spectra in red fluorescent protein rsTagRFP. J Mol Biol 417(3):144–151. doi:10.1016/j.jmb.2012.01.044
34. Chang H, Zhang M, Ji W, Chen J, Zhang Y, Liu B, Lu J, Zhang J, Xu P, Xu T (2012) A unique series of reversibly switchable fluorescent proteins with beneficial properties for various applications. Proc Natl Acad Sci U S A 109(12):4455–4460. doi:10.1073/pnas.1113770109
35. Adam V, Lelimousin M, Boehme S, Desfonds G, Nienhaus K, Field MJ, Wiedenmann J, McSweeney S, Nienhaus GU, Bourgeois D (2008) Structural characterization of IrisFP, an optical highlighter undergoing multiple photo-induced transformations. Proc Natl Acad Sci USA 105(47):18343–18348. doi:0805949105 [pii] 10.1073/pnas.0805949105
36. Adam V, Moeyaert B, David CC, Mizuno H, Lelimousin M, Dedecker P, Ando R, Miyawaki A, Michiels J, Engelborghs Y, Hofkens J (2011) Rational design of photoconvertible and biphotochromic fluorescent proteins for advanced microscopy applications. Chem Biol 18(10):1241–1251. doi:10.1016/j.chembiol.2011.08.007
37. Bizzarri R, Serresi M, Cardarelli F, Abbruzzetti S, Campanini B, Viappiani C, Beltram F (2010) Single amino acid replacement makes Aequorea victoria fluorescent proteins reversibly photoswitchable. J Am Chem Soc 132(1):85–95. doi:10.1021/ja9014953
38. Grotjohann T, Testa I, Leutenegger M, Bock H, Urban NT, Lavoie-Cardinal F, Willig KI, Eggeling C, Jakobs S, Hell SW (2011) Diffraction-unlimited all-optical imaging and writing with a photochromic GFP. Nature 478(7368):204–208. doi:10.1038/nature10497
39. Grotjohann T, Testa I, Reuss M, Brakemann T, Eggeling C, Hell SW, Jakobs S (2012) rsEGFP2 enables fast RESOLFT nanoscopy of living cells. ELife 1 1:e00248. doi:10.7554/eLife.00248.00001
40. Brakemann T, Stiel AC, Weber G, Andresen M, Testa I, Grotjohann T, Leutenegger M, Plessmann U, Urlaub H, Eggeling C, Wahl MC, Hell SW, Jakobs S (2011) A reversibly

photoswitchable GFP-like protein with fluorescence excitation decoupled from switching. Nat Biotechnol 29(10):942–947. doi:10.1038/nbt.1952

41. Faro AR, Adam V, Carpentier P, Darnault C, Bourgeois D, de Rosny E (2010) Low-temperature switching by photoinduced protonation in photochromic fluorescent proteins. Photochem Photobiol Sci 9(2):254–262. doi:10.1039/b9pp00121b
42. Bourgeois D, Royant A (2005) Advances in kinetic protein crystallography. Curr Opin Struct Biol 15(5):538–547. doi:S0959-440X(05)00150-8 [pii] 10.1016/j.sbi.2005.08.002
43. Royant A, Carpentier P, Ohana J, McGeehan J, Paetzold B, Noirclerc-Savoye M, Vernede X, Adam V, Bourgeois D (2007) Advances in spectroscopic methods for biological crystals. 1. Fluorescence lifetime measurements. J Appl Cryst 40:1105–1112. doi:10.1107/S0021889807044196
44. Carpentier P, Royant A, Ohana J, Bourgeois D (2007) Advances in spectroscopic methods for biological crystals. 2. Raman spectroscopy. J Appl Cryst 40:1113–1122. doi:10.1107/S0021889807044202
45. Gayda S, Nienhaus K, Nienhaus GU (2012) Mechanistic insights into reversible photoactivation in proteins of the GFP family. Biophys J 103(12):2521–2531
46. Adam V, Nienhaus K, Bourgeois D, Nienhaus GU (2009) Structural basis of enhanced photoconversion yield in green fluorescent protein-like protein dendra2. Biochemistry 48(22):4905–4915. doi:10.1021/bi900383a
47. Faro AR, Carpentier P, Jonasson G, Pompidor G, Arcizet D, Demachy I, Bourgeois D (2011) Low-temperature chromophore isomerization reveals the photoswitching mechanism of the fluorescent protein Padron. J Am Chem Soc 133(41):16362–16365. doi:10.1021/ja207001y
48. Fang C, Frontiera RR, Tran R, Mathies RA (2009) Mapping GFP structure evolution during proton transfer with femtosecond Raman spectroscopy. Nature 462(7270):200–204. doi:10.1038/nature08527
49. Chapman HN, Fromme P, Barty A, White TA, Kirian RA, Aquila A, Hunter MS, Schulz J, DePonte DP, Weierstall U, Doak RB, Maia FR, Martin AV, Schlichting I, Lomb L, Coppola N, Shoeman RL, Epp SW, Hartmann R, Rolles D, Rudenko A, Foucar L, Kimmel N, Weidenspointner G, Holl P, Liang M, Barthelmess M, Caleman C, Boutet S, Bogan MJ, Krzywinski J, Bostedt C, Bajt S, Gumprecht L, Rudek B, Erk B, Schmidt C, Homke A, Reich C, Pietschner D, Struder L, Hauser G, Gorke H, Ullrich J, Herrmann S, Schaller G, Schopper F, Soltau H, Kuhnel KU, Messerschmidt M, Bozek JD, Hau-Riege SP, Frank M, Hampton CY, Sierra RG, Starodub D, Williams GJ, Hajdu J, Timneanu N, Seibert MM, Andreasson J, Rocker A, Jonsson O, Svenda M, Stern S, Nass K, Andritschke R, Schroter CD, Krasniqi F, Bott M, Schmidt KE, Wang X, Grotjohann I, Holton JM, Barends TR, Neutze R, Marchesini S, Fromme R, Schorb S, Rupp D, Adolph M, Gorkhover T, Andersson I, Hirsemann H, Potdevin G, Graafsma H, Nilsson B, Spence JC (2011) Femtosecond X-ray protein nanocrystallography. Nature 470(7332):73–77. doi:10.1038/nature09750
50. Yang JS, Huang GJ, Liu YH, Peng SM (2008) Photoisomerization of the green fluorescence protein chromophore and the meta- and para-amino analogues. Chem Commun (Camb) 11:1344–1346. doi:10.1039/b717714c
51. Pletnev S, Shcherbo D, Chudakov DM, Pletneva N, Merzlyak EM, Wlodawer A, Dauter Z, Pletnev V (2008) A crystallographic study of bright far-red fluorescent protein mKate reveals pH-induced cis-trans isomerization of the chromophore. J Biol Chem 283(43):28980–28987. doi:M800599200 [pii] 10.1074/jbc.M800599200
52. Violot S, Carpentier P, Blanchoin L, Bourgeois D (2009) Reverse pH-dependence of chromophore protonation explains the large stokes shift of the red fluorescent protein mKeima. J Am Chem Soc 131(30):10356–10357. doi:10.1021/ja903695n
53. Petersen J, Wilmann PG, Beddoe T, Oakley AJ, Devenish RJ, Prescott M, Rossjohn J (2003) The 2.0-A crystal structure of eqFP611, a far red fluorescent protein from the sea anemone Entacmaea quadricolor. J Biol Chem 278(45):44626–44631
54. Zhou XX, Chung HK, Lam AJ, Lin MZ (2012) Optical control of protein activity by fluorescent protein domains. Science 338(6108):810–814. doi:10.1126/science.1226854
55. Kao Y-T, Zhu X, Min W (2012) Protein-flexibility mediated coupling between photoswitching kinetics and surrounding viscosity of a photochromic fluorescent protein. Proc Natl Acad Sci U S A. doi:10.1073/pnas.1115311109
56. Brakemann T, Weber G, Andresen M, Groenhof G, Stiel AC, Trowitzsch S, Eggeling C, Grubmuller H, Hell SW, Wahl MC, Jakobs S (2010) Molecular basis of the light-driven switching of the photochromic fluorescent protein Padron. J Biol Chem 285(19):14603–14609. doi:M109.086314 [pii] 10.1074/jbc.M109.086314

57. Olsen S, Lamothe K, Martinez TJ (2010) Protonic gating of excited-state twisting and charge localization in GFP chromophores: a mechanistic hypothesis for reversible photoswitching. J Am Chem Soc 132(4):1192–1193. doi:10.1021/ja907447k
58. Luin S, Voliani V, Lanza G, Bizzarri R, Amat P, Tozzini V, Serresi M, Beltram F (2009) Raman study of chromophore states in photochromic fluorescent proteins. J Am Chem Soc 131(1):96–103. doi:10.1021/ja804504b 10.1021/ja804504b [pii]
59. Betzig E, Patterson GH, Sougrat R, Lindwasser OW, Olenych S, Bonifacino JS, Davidson MW, Lippincott-Schwartz J, Hess HF (2006) Imaging intracellular fluorescent proteins at nanometer resolution. Science 313(5793):1642–1645
60. Hess ST, Girirajan TP, Mason MD (2006) Ultra-high resolution imaging by fluorescence photoactivation localization microscopy. Biophys J 91(11):4258–4272
61. Rust MJ, Bates M, Zhuang X (2006) Sub-diffraction-limit imaging by stochastic optical reconstruction microscopy (STORM). Nat Methods 3(10):793–796
62. Shroff H, Galbraith CG, Galbraith JA, White H, Gillette J, Olenych S, Davidson MW, Betzig E (2007) Dual-color superresolution imaging of genetically expressed probes within individual adhesion complexes. Proc Natl Acad Sci U S A 104(51):20308–20313. doi:10.1073/pnas.0710517105
63. Hsu CJ, Baumgart T (2011) Spatial association of signaling proteins and F-actin effects on cluster assembly analyzed via photoactivation localization microscopy in T cells. PLoS One 6(8):e23586. doi:10.1371/journal.pone.0023586
64. Dertinger T, Colyer R, Iyer G, Weiss S, Enderlein J (2009) Fast, background-free, 3D super-resolution optical fluctuation imaging (SOFI). Proc Natl Acad Sci U S A 106(52):22287–22292. doi:10.1073/pnas.0907866106
65. Dedecker P, Mo GCH, Dertinger T, Zhang J (2012) Widely accessible method for superresolution fluorescence imaging of living systems. Proc Natl Acad Sci U S A 109(27):10909–10914. doi:10.1073/pnas.1204917109
66. Hell SW, Dyba M, Jakobs S (2004) Concepts for nanoscale resolution in fluorescence microscopy. Curr Opin Neurobiol 14(5):599–609
67. Dedecker P, Hotta J, Flors C, Sliwa M, Uji-i H, Roeffaers MB, Ando R, Mizuno H, Miyawaki A, Hofkens J (2007) Subdiffraction imaging through the selective donut-mode depletion of thermally stable photoswitchable fluorophores: numerical analysis and application to the fluorescent protein Dronpa. J Am Chem Soc 129(51):16132–16141. doi:10.1021/ja076128z
68. Hofmann M, Eggeling C, Jakobs S, Hell SW (2005) Breaking the diffraction barrier in fluorescence microscopy at low light intensities by using reversibly photoswitchable proteins. Proc Natl Acad Sci U S A 102(49):17565–17569
69. Gustafsson MG (2005) Nonlinear structured-illumination microscopy: wide-field fluorescence imaging with theoretically unlimited resolution. Proc Natl Acad Sci U S A 102(37):13081–13086. doi:10.1073/pnas.0406877102
70. Rego EH, Shao L, Macklin JJ, Winoto L, Johansson GA, Kamps-Hughes N, Davidson MW, Gustafsson MG (2011) Nonlinear structured-illumination microscopy with a photoswitchable protein reveals cellular structures at 50-nm resolution. Proc Natl Acad Sci U S A 109:E135–E143. doi:10.1073/pnas.1107547108
71. Fuchs J, Bohme S, Oswald F, Hedde PN, Krause M, Wiedenmann J, Nienhaus GU (2010) A photoactivatable marker protein for pulse-chase imaging with superresolution. Nat Methods 7(8):627–630. doi:10.1038/nmeth.1477
72. Adam V, Mizuno H, Grichine A, Hotta JI, Yamagata Y, Moeyaert B, Nienhaus GU, Miyawaki A, Bourgeois D, Hofkens J (2010) Data storage based on photochromic and photoconvertible fluorescent proteins. J Biotechnol 4(6):377–390. doi:S0168-1656(10)00186-0 [pii] 10.1016/j.jbiotec.2010.04.001
73. Mizuno H, Dedecker P, Ando R, Fukano T, Hofkens J, Miyawaki A (2010) Higher resolution in localization microscopy by slower switching of a photochromic protein. Photochem Photobiol Sci 9(2):239–248. doi:10.1039/b9pp00124g
74. Nguyen Bich N, Moeyaert B, Van Hecke K, Dedecker P, Mizuno H, Hofkens J, Van Meervelt L (2012) Structural basis for the influence of a single mutation K145N on the oligomerization and photoswitching rate of Dronpa. Acta Crystallogr D Biol Crystallogr 68(12):1653–1659. doi:10.1107/s0907444912039686
75. Giordano L, Jovin TM, Irie M, Jares-Erijman EA (2002) Diheteroarylethenes as thermally stable photoswitchable acceptors in photochromic fluorescence resonance energy transfer (pcFRET). J Am Chem Soc 124(25):7481–7489
76. Song L, Jares-Erijman EA, Jovin TM (2002) A photochromic acceptor as a reversible light-driven switch in fluorescence resonance energy transfer (FRET). J Photochem Photobiol Chem 150:177–185
77. Stiel AC, Andresen M, Bock H, Hilbert M, Schilde J, Schonle A, Eggeling C, Egner A, Hell SW, Jakobs S (2008) Generation of monomeric

reversibly switchable red fluorescent proteins for far-field fluorescence nanoscopy. Biophys J 95(6):2989–2997.doi:doi:biophysj.108.130146 [pii] 10.1529/biophysj.108.130146

78. Subach OM, Malashkevich VN, Zencheck WD, Morozova KS, Piatkevich KD, Almo SC, Verkhusha VV (2010) Structural characterization of acylimine-containing blue and red chromophores in mTagBFP and TagRFP fluorescent proteins. Chem Biol 17(4):333–341. doi:S1074-5521(10)00086-4 [pii] 10.1016/j.chembiol.2010.03.005
79. Adam V, Carpentier P, Violot S, Lelimousin M, Darnault C, Nienhaus GU, Bourgeois D (2009) Structural basis of X-ray-induced transient photobleaching in a photoactivatable green fluorescent protein. J Am Chem Soc 131(50):18063–18065. doi:10.1021/ja907296v
80. Roy A, Field MJ, Adam V, Bourgeois D (2011) The nature of transient dark states in a photoactivatable fluorescent protein. J Am Chem Soc 133(46):18586–18589. doi:10.1021/ja2085355
81. Lukyanov KA, Fradkov AF, Gurskaya NG, Matz MV, Labas YA, Savitsky AP, Markelov ML, Zaraisky AG, Zhao X, Fang Y, Tan W, Lukyanov SA (2000) Natural animal coloration can be determined by a nonfluorescent green fluorescent protein homolog. J Biol Chem 275(34):25879–25882
82. Abbruzzetti S, Grandi E, Viappiani C, Bologna S, Campanini B, Raboni S, Bettati S, Mozzarelli A (2005) Kinetics of acid-induced spectral changes in the GFPmut2 chromophore. J Am Chem Soc 127(2):626–635. doi:10.1021/ja045400r

Chapter 13

Using Photoactivatable GFP to Track Axonal Transport Kinetics

Archan Ganguly and Subhojit Roy

Abstract

The advent of photoactivatable tools has revolutionized imaging of dynamic cellular processes. One such application is to visualize axonal transport—an intricate and dynamic process by which proteins and other macromolecules are conveyed from their sites of synthesis in the cell bodies to their destinations within axons and synapses. High-quality dynamic imaging of axonal transport using photoactivatable vectors can now be routinely performed using epifluorescence microscopes and CCD cameras that are standard in most laboratories, yet this is largely underutilized. Here we describe detailed protocols for imaging cargoes moving in fast and slow axonal transport in axons of cultured hippocampal neurons.

Key words Cytosolic proteins, Soluble proteins, Slow axonal transport, Photoactivation, PAGFP, Synapsin, Neurofilaments, APP

1 Introduction

Typically, neurons have two distinct anatomical and functional domains—somato-dendritic and axonal. Axons usually extend for long distances, but the vast majority of proteins in a neuron are synthesized in the cell bodies. Therefore, neurons have intricate transport machineries that deliver proteins to distant sites within axons and synapses. Termed axonal transport, it is important to remember that this is not a developmental process, but is constitutive, occurring throughout the life of the neuron. Classic pulse-chase radiolabeling studies defined the phenomenon of axonal transport. In these experiments, radiolabeled amino acids were injected into the vicinity of neuronal cell bodies in mice in vivo [1]. These amino acids were subsequently incorporated into newly synthesized proteins in the perikarya and transported into axons by the cell's innate transport machinery. By isolating axons and examining the radiolabeled profiles at various time points after injection, researchers identified two overall "waves" of movement that they termed fast and slow axonal transport. The faster population

Sidney Cambridge (ed.), *Photoswitching Proteins: Methods and Protocols*, Methods in Molecular Biology, vol. 1148,
DOI 10.1007/978-1-4939-0470-9_13,

moved at overall rates of 50–200 mm/day and was composed of membranous proteins; and the slower population moved only at overall rates of 2–10 mm/day and was composed of cytoskeletal and cytosolic (or soluble) proteins [2].

Even though radiolabeling studies characterized overall axonal transport, these methods could not visualize the movement, thus the identity of cargoes moving in slow and fast transport-components remained unclear. With advances in live imaging and development of fluorescent-probes, many vesicular cargoes moving in fast axonal transport have been directly visualized [3–6]. However, cargoes moving in slow axonal transport have been difficult to see. The main reason is that unlike vesicles that have discrete, punctate profiles that can be easily tracked, slow transport cargoes such as cytoskeletal and cytosolic proteins are evenly distributed in axons, precluding visualization of individual moving elements. Moreover, the latter can have freely diffusible protein pools that make optical imaging challenging. To circumvent these issues, we and others have been using photoactivatable vectors to image such cargoes. The most commonly used photoactivatable vector is PAGFP (PhotoActivatable GFP). This is a modified form of the GFP protein which has low basal fluorescence in the native state, but upon activation by violet light (405 nm), there is a 100-fold increase in its fluorescence. The basic idea is to photoactivate a small population of a given protein within an axon and to then track its dynamic behavior over time. These approaches can overcome some of the caveats mentioned above with slow-transport imaging and have proven to be useful [7–13].

Here we describe detailed protocols for axonal and somatic photoactivation of slow- and fast-component proteins tagged to PAGFP. The method uses a standard epifluorescence microscope and cultured hippocampal neurons, but can be applied to other cultured cells as well.

2 Materials

2.1 Neuronal Culture and Transfection Reagents

2.1.1 Reagents

1. Glass-bottomed dishes, uncoated (Mattek, Catalog# P35G-1.5-10-C).
2. Poly-D-Lysine (Sigma–Aldrich).
3. 0.25 % Trypsin–EDTA (Invitrogen).
4. HBSS (GIBCO).
5. D-Glucose (Sigma–Aldrich).
6. HEPES (Sigma–Aldrich).
7. Pen-Strep (GIBCO).
8. NaCl (Sigma–Aldrich).
9. Boric acid (Sigma–Aldrich).
10. Borax—Sodium Tetraborate anhydrous (Fluka).

11. B27 (Invitrogen, Catalog# 17504-044).
12. GlutaMAX (Sigma–Aldrich).
13. Fetal bovine serum (FBS, Hyclone).
14. 10× PBS (Invitrogen).
15. Opti-MEM (Invitrogen).
16. Lipofectamine 2000 (Invitrogen).
17. Laminar flow hood for sterile tissue culture conditions.
18. 5 % CO_2 incubator.
19. Hemocytometer (for cell counting).
20. 1.5 in. coverslips.
21. 70 μm filter.
22. Constructs for protein of interest tagged to PAGFP.
    (a) PAGFP–synapsin—a gift from George Augustine, Duke University.
    (b) APP:PAGFP—a gift from Christoph Kaether, Jena, Germany.
    (c) PAGFP–Neurofilament-M (PAGFP–NFM)—a gift from Anthony Brown, Ohio State University.
23. Hibernate-E low fluorescence medium (Brainbits, Catalog# HE-lf).

2.1.2 Buffers and Solutions

1. *Borax Buffer*: 51.4 mM Boric acid, 23.6 mM Borax, ddH_2O. Adjust pH to 8.5 and sterilize using a 0.22 μm syringe filter. Store at 4 °C for long-term use.
2. *HBSS* (*Dissection buffer*): HBSS, 4.44 mM D-Glucose, 6.98 mM HEPES. Adjust pH—7.3 and filter sterilize. Store at 4 °C for long-term use.
3. *Poly-D-Lysine solution*: Dissolve to obtain a final concentration of 1 mg/mL in borax buffer.
4. *Neurobasal/B27* (*NB/B27-neuronal culture media*): Neurobasal, 2 % B27, 1 % Glutamax and filter sterilized. Aliquots of NB/B27 are kept frozen at −20 °C for long-term use and at 4 °C for short-term use (up to a week).
5. *Blocking buffer*: 30 % FBS, 70 % 1× PBS, filter sterilize using a 0.22 μm syringe filter.
6. *Plating medium*: 10 % FBS, 90 % Neurobasal/B27, filter sterilize using a 0.22 μm syringe filter.
7. *Live imaging solution* (*HELF*): Hibernate-E medium, 2 mM GlutaMAX, 0.4 % D-Glucose, 37.5 mM NaCl, 2 % B27. Ensure that the components are thoroughly mixed. Filter sterilize by using a 0.22 μm filter. Aliquot and store at −20 °C. Once thawed, each aliquot can be stored at 4 °C for up to 1 week.

2.2 Live Imaging Equipment and Reagents

2.2.1 Microscope Setup

1. An inverted epifluorescence microscope (Olympus) equipped with 40× and 100× oil-immersion objectives, a dual light source fluorescence illuminator IX2-RFAW (Olympus), a CCD camera (CoolSnap HQ2 or similar), shutters IX2-SHA, a filter wheel and a pinhole.
2. Mercury lamp (HBO 100 W).
3. Violet excitation filter (D405/40, Chroma).
4. Smart Shutter (Sutter Instruments).
5. GFP cube set (Chroma, cat. no. U-N41001).
6. Dichroic mirror (T495pxr, Chroma).
7. Emission filter (HQ535/50).

The details of our microscope setup have been recently described in Roy et al. [8] and are not elaborated here. We use a custom-built device as described in Roy et al., but excellent photoactivation devices are also available commercially (Andor Technology, UK).

2.2.2 Live Imaging Setup and Solutions

1. Hibernate-E low fluorescence medium (Brainbits, Catalog# HE-lf).
2. Weather Station (Precision Control LLC) air stream incubator.
3. Vibration-isolation table (TMC).
4. Nitrogen tank.

2.2.3 Image Acquisition and Analysis Tools

1. MetaMorph imaging software (acquisition module and offline module; MolecularDevices LLC, USA).
2. MATLAB software, basic package (Math Works, USA).

3 Methods

The overall goal is to obtain cultured neurons from hippocampi of mouse (or rat) brains, allow the neurons to grow to maturity, transfect the neurons with photoactivatable vectors tagged to the protein of interest, and then study the kinetics of the photoactivated protein pools over time.

3.1 Hippocampal Neuronal Culture

1. Before dissection, add 100 µL of 1 mg/mL Poly-D-Lysine solution on to the inner well of each Mattek dish. Spread evenly and allow the coating to proceed for 2 h at room temperature. After 2 h wash the dishes thrice with ddH_2O. Dry the dishes thoroughly using an aspirator and let them sit in the hood until neurons are ready to be plated.
2. Dissect out the hippocampus from the P0–P1 mice pups after rapid decapitation using a standard dissection protocol [14]. A good tutorial video demonstrating the procedure for hippocampal neuronal culture is available on the following

website: http://www.ejnblog.org/2011/11/04/preparation-of-neuronal-cell-cultures/. Place the dissected hippocampi in ice-cold HBSS buffer before enzymatic treatment (*see* **Notes 1** and **2**). Two hippocampi from each brain yield approximately 60,000 cells after dissociation. Around 25,000 cells are plated per dish, so the number of hippocampi to be dissected needs to be calculated according to the number of dishes being plated. All dissections are carried out in ice-cold HBSS buffer.

Caution: Follow all relevant governmental and institutional ethics guidelines on the use of animals in research.

3. Once the desired number of hippocampi have been collected in ice-cold HBSS transfer them to 10 mL of pre-warmed 0.25 % Trypsin–EDTA at 37 °C. Incubate the hippocampi for 15 min at 37 °C in a water bath. After 15 min, stop enzymatic digestion by transferring the hippocampi to 10 mL blocking buffer.
4. Transfer the hippocampi from the blocking solution to 5 mL of 1× PBS. Carry out two more washes in 5 mL 1× PBS. Transfer the hippocampi to a vial containing 1 mL of plating media for dissociation (*see* **Note 3**).
5. Dissociate hippocampi in 1 mL plating media by triturating 5–8 times with an unused P1000 pipette tip. The plating media should turn slightly turbid during the dissociation process. Once this is achieved and no large chunks of tissue are seen floating in the media, the cell suspension is passed through a 70 μm filter. 10 μL of the sterile cell suspension is then used to count cells on a standard hemocytometer.

   Caution: **steps 1–4** are strictly carried out in a laminar flow fume hood to maintain sterile cultures.
6. After counting, about 25,000 cells/100 μL of the cell suspension are plated on to the center well of each poly-D-lysine coated dish. Adjust the cell dilution close to this value before plating.
7. After plating, allow the cells to recover for 1 h in an incubator (5 % CO_2, 37 °C). Then add 1.5 mL of neurobasal/B27 (NB/B27) media to the culture dish and place the dish back in the CO_2 incubator. The health of the neurons is monitored for the next 7–8 days (days in vitro; DIV7–DIV8) and 0.5 mL of fresh NB/B27 is added to each dish every 48 h up to DIV7 (*see* **Note 4**). We usually study neurons that are at least DIV7–8, with well-defined axons and dendrites.

3.2 Transfection and Live-Cell Imaging

1. A day before imaging, transfect the neurons with the desired PAGFP construct (PAGFP–synapsin, APP:PAGFP, or PAGFP–NFM) and a soluble, cytoplasmic red fluorescent protein to visualize the axons. Since the PAGFP constructs have minimal fluorescence before photoactivation, co-transfection with fluorescent markers such as monomeric red fluorescent protein (mRFP) or mCherry is essential to identify axons suitable for photoactivation.

2. To transfect five dishes, aliquot 125 μL of OPTI-MEM into two 1.5 mL Eppendorf tubes. To the first tube add 7.5 μL of Lipofectamine 2000 and mix well by pipetting. To the second tube add a total of 1.2 μg DNA of the desired PAGFP and soluble mRFP construct (in a ratio of 1:1) and mix well. Mix the contents of the two tubes and let them sit at room temperature for 15 min.
3. Meanwhile, warm NB/B27 in the water bath to 37 °C. After 15 min add 5 mL of warmed NB/B27 to the OPTI-MEM mixture. Once this is done, collect and save the conditioned medium from each culture dish so that it can be added back to the cultures after the completion of transfection. Add 1 mL of the NB/B27 OPTI-MEM mix to each culture dish to be transfected. Incubate the dishes at 37 °C, 5 % CO_2 in the incubator for 3 h with the transfection mix.
4. After 3 h, remove the transfection media from each dish and wash the cells with 1 mL fresh pre-warmed NB/B27. Remove the NB/B27 and replace with the conditioned media collected from each dish before transfection. Allow at least 4–6 h post-transfection before imaging the cells; for most experiments, we image neurons 16–24 h post-transfection (*see* **Notes 5**–**7**).
5. On the morning of imaging, turn on the stage incubator (Weatherstation) and let it equilibrate to 37 °C (this may take up to 1 h). Warm up the HELF (live imaging buffer) to 37 °C in a water bath. Now remove the NB/B27 in each transfected dish and rinse three times with 1 mL of pre-warmed HELF buffer. After the fourth rinse move the dishes to the Weatherstation and begin imaging (*see* **Notes 8** and **9**).
6. Identify transfected neurons by looking at the soluble mRFP signal, using the 40× oil immersion objective. DIV8 neurons should have several dendrites and one single axon emanating from the soma. Avoid neurons which have an overtly complex morphology, especially those in which the morphological distinction between axons and dendrites is not clear. Usually, a long straight axon with minimal morphological variations is selected as indicated in Fig. 1a. Axons are identified based on their morphology alone, and this requires some practice (*see* **Note 10**).
7. Once an axon is selected, switch to the 100× oil-immersion objective and first determine the axonal region of interest (ROI) to be photoactivated. This is done by using the soluble mRFP signal of the selected axon (*see* **Notes 11** and **12**), and an image is taken in the red channel (Fig. 1a, upper panel). The exact photoactivated ROI will depend on the instrument used. In our system (described in ref. [7]), the photoactivated area is a fixed circular ROI, determined by a pinhole situated in the optical path. In other commercial instruments (Andor Instruments),

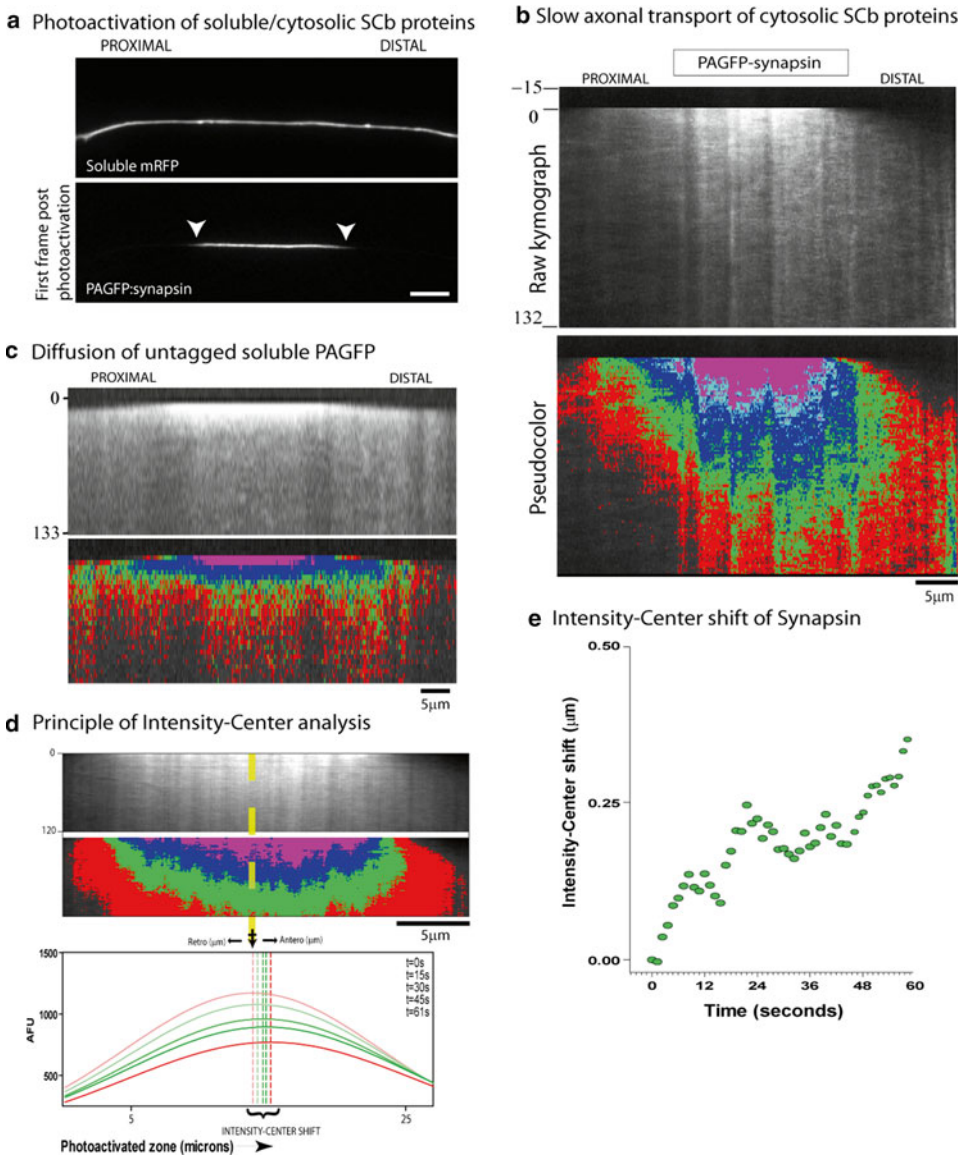

Fig. 1 Photoactivation strategy to visualize synapsin transport in axons. (**a**) Representative images of an axon co-transfected with soluble mRFP and PAGFP–synapsin showing the photoactivated GFP ROI immediately after photoactivation. *Arrowheads* denote the boundaries of the photoactivated zone. (**b**) Kymographs of photoactivated PAGFP:synapsin. Note that the synapsin fluorescence disperses bidirectionally, but has an anterograde (distal) bias. The anterogradely biased plume of fluorescence is better seen in the pseudocolor image of the kymograph above, where intensity ranges are represented by colors (*red*: lowest intensity bin, *pink*: highest intensity bin above background). Elapsed time in seconds shown on *left*, scale bar is 5 μm. (**c**) Unlike the slow, anterogradely biased flow of synapsin, the free diffusion of untagged PAGFP is very rapid and unbiased. Elapsed time in seconds is shown on *left*, scale bar is 5 μm. (**d**) Principle of the intensity center shift assay used to analyze axonal transport of soluble (SCb) proteins. PAGFP:synapsin kymographs (*above*), and its quantification (*below*). The *curves* below are overlays of selected line-scan intensities from successive frames in the PAGFP:synapsin movie that was used to generate the kymograph above. The *dashed vertical lines* mark the center of mass (centroid or "intensity-center") of the line scan fluorescence. Note the anterograde shift in the intensity-center over time. Gaussian curves are shown for clarity, but raw data are used for actual calculations. *AFU* arbitrary fluorescence units. (**e**) The "intensity-center shift" curve for the example shown in (**d**). The numerical intensity-center value in each frame of the movie is plotted over elapsed time; note the anterograde bias of the fluorescent population. Images adapted with permission from Scott et al. [9]

almost any desired region or shape can be photoactivated. Once this is done, the ROI in the axon is ready for photoactivation.

8. For PAGFP, photoactivation is carried out by violet (405 nm excitation wavelength) light. The goal here is to photoactivate a subpopulation of molecules, so that they can be visualized reliably. The time of photoactivation for the sample is important, as less than optimal activation would produce a poor signal, whereas excessive exposure of the sample to incident light may cause bleaching, or even toxicity. Accordingly, the exact time for which a sample needs to be activated has to be empirically determined by the user (*see* **Note 13**). In our setup (using a 100 W mercury lamp), we typically use 1 s of photoactivation to obtain a 10-bit GFP image for PAGFP–synapsin (Fig. 1a, lower panel). Following this, we acquire a movie which captures the movement of the activated protein over time. To track PAGFP–synapsin movement, we typically collect ~30–65 s movies of 60–130 frames, at an interval of 500 ms using 2 × 2 camera binning (*see* **Note 14**). The movies are then used to generate a line scan kymograph with a built-in function in MetaMorph. A line scan kymograph is a tool to depict motion of molecules in a linear structure (axon in this case). In our kymographs, time is depicted on the Y-axis and distance on the X-axis. A greyscale kymograph of the photoactivated PAGFP–synapsin subpopulation and its corresponding pseudocolor heat map are shown in Fig. 1b. Note the anterograde bias in the PAGFP–synapsin fluorescence over time. In contrast, soluble PAGFP disperses bi-directionally, without any bias (Fig. 1c). An intensity center shift assay was developed to calculate the rate of movement of the photoactivated protein along the axon (Fig. 1d, *see* Subheading 3.3 for details of this analysis). The overall rate of movement for synapsin (0.1–0.3 μm/s) population (Fig. 1e) is strikingly similar to rates seen with radiolabeling experiments [9].
9. In addition to axons, neuronal cell bodies can also be photoactivated using similar protocols. Figure 2 shows experiments where neurons were transfected with either PAGFP-tagged neurofilament M or APP:PAGFP and the perikarya were selectively photoactivated. Thereafter, the egress of photoactivated neurofilaments (Fig. 2a) was visualized in the dendrites. Kinetics of photoactivated APP:GFP vesicles in soma and axons can also be seen by these methods (Fig. 2b, c). The movement of individual GFP-tagged APP particles can be tracked along the axon by live imaging as indicated by the colored arrows on the line scan kymograph (Fig. 2c).

3.3 Image Analysis

1. For photoactivated proteins where individual GFP-tagged particles are seen post photoactivation (APP-GFP) a simple line scan kymograph is generated using the built-in function in

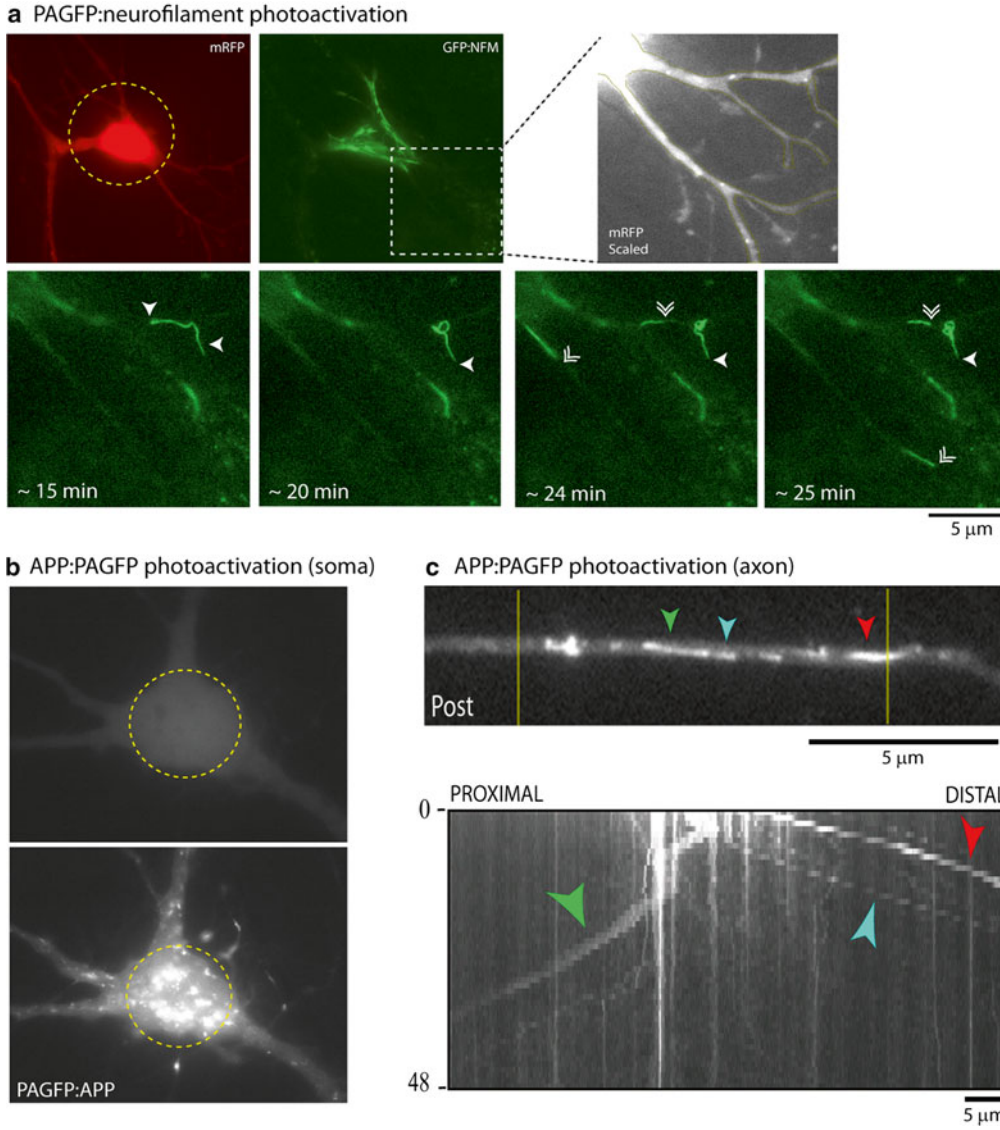

Fig. 2 Visualizing neurofilament and APP movement after somatic photoactivation. (**a**) *Top left panels*: Neurons were transfected with soluble mRFP and PAGFP–neurofilament-M (NFM), and the neuronal cell body was specifically photoactivated (*dashed circle* in mRFP image represents photoactivated ROI at 40× magnification). Note the expected filamentous appearance of GFP:NFM in the image immediately after activation. The *boxed* region was selected for dynamic imaging, and the *bottom panels* show selected frames from the corresponding time-lapse movie (the scaled mRFP image on *upper right* shows the emerging dendrites from this cell that were imaged). *Bottom panels*: Sequence of images from a time-lapse movie of the dendrites within the boxed ROI above; elapsed time after photoactivation is shown on the *bottom left. Arrowheads* mark several neurofilaments entering into the dendrites from the cell body. *Single arrowheads* mark a filament that entered into the top dendrite and paused for several minutes (note the elastic "curling" of the lagging end during the pause). The *double-arrowheads* mark other neurofilaments that moved during this time-lapse movie. Note the infrequent and intermittent nature of this transport in dendrites, as described by Brown and colleagues in the axon [11]. (**b**) Somatic photoactivation of PAGFP:APP (*dashed yellow circles* represent photoactivated ROI before and after photoactivation at 100× magnification). Note the egress of APP vesicles into dendrites. (**c**) Axonal photoactivation of PAGFP:APP, *vertical yellow lines* mark photoactivated ROI at 100× magnification (*upper panel*). Several discrete vesicles are photoactivated, some marked by *arrowheads*. In the kymograph below, note the vectorial movement of discrete vesicles (elapsed time in seconds shown on *left*). Scale bars, 5 μm

Metamorph (Fig. 2c, lower panel). Such kymographs provide sufficient information about the movement of labeled particles along the axons/dendrites—for instance the slope of the moving particles represents their velocities, where steeper slopes indicate higher velocities. For example, *see* the analyses in Tang et al. [6].

2. For soluble proteins like synapsin where fluorescent molecules disperse as a plume of fluorescence, a combination of imaging functions in Metamorph and custom written code in Matlab are used to determine the overall bias along an axon. The main goal here is to measure the position of the fluorescence intensity-peak (centroid) along the axon, for every frame of a given movie. If there is a bulk movement of fluorescence, then there would also be a corresponding shift in the centroid (*see* Fig. 1d and ref. [7] for more details). To measure the centroid, first, determine the boundaries of the photoactivated zone by thresholding the first frame of the time-lapse image series. Use a standard drop-down function in Metamorph to generate average intensity kymographs. This kymograph has information about each successive X-axis and Y-axis coordinates which carry information about the time points of imaging and successive distance from the proximal region of the axon. This generates a time distance plot which compresses the movie into a series of 2D images, facilitating further quantification.
3. Using a custom written code in Matlab basic package, the change in the center of fluorescence mass is calculated for each time point in the movie. Briefly, the center of mass for each individual horizontal line scan of a kymograph is calculated. Then the center of mass of the photoactivated region (first frame) is subtracted from the center of mass for each subsequent frame. A shift in the center of mass with each subsequent frame in either direction represents a directional bias (Fig. 1d). When line scans are drawn from the proximal to the distal direction a net anterograde bias is seen for a sample PAGFP–synapsin kymograph (Fig. 1e). For a detailed description of the analysis and videos refer to refs. [7, 9]. We can provide Matlab codes upon request.

4 Notes

1. To obtain consistent hippocampal neurons with good cell viability and transfection efficiency, we prefer using early P0-early P1 mice pups. Older pups result in higher cell death and poor viability. An alternative is to use neurons from embryonic (E18) pups.
2. During the hippocampi dissection, care should be taken to remove the fimbriae attached to the hippocampi. If not

removed properly, this results in hippocampi aggregating during dissociation, which leads to a lower cell yield.

3. We recommend dissociating not more than ten hippocampi from five brains in 1 mL of plating media for best cell yields. If more hippocampi are dissected, the dissociation should be carried out in incremental amounts of plating media.
4. Neuronal cultures are fed with 0.5 mL of fresh NB/B27 per dish every 2–3 days without removing any of the old medium for the first week (DIV7). This is essential to maintain neurons in optimal health. Letting the neurons stay in the incubator for a long time without adding fresh media leads to evaporation and change in the pH of the media.
5. The amount of DNA to be transfected needs to be optimized for each PAGFP-tagged protein and soluble marker. Too much PAGFP-tagged protein leads to high basal levels of GFP fluorescence prior to photoactivation in the axons, which may cause inconsistent results after the intensity center shift analysis.
6. Imaging should be performed between 16 and 24 h post transfection for consistent results.
7. As a negative control for imaging soluble proteins by photoactivation, one can co-transfect neurons with the empty PAGFP and soluble mRFP constructs using the transfection protocol described earlier.
8. The Weatherstation (on-stage incubator) should be equilibrated to 37 °C before performing experiments and sudden changes in the temperature of the station should be avoided during the imaging session to prevent focal drift.
9. The HELF medium maintains a pH similar to NB/B27 at atmospheric CO_2 levels, eliminating the need for a CO_2 delivery system during live imaging for several hours. Neurons in HELF survive and axons continue to grow for at least 24–48 h [11, 15].
10. Rigorous selection criteria should be implemented before axons are selected for photoactivation, especially for imaging cytosolic proteins which also invariably have a diffusible fraction. Since the axon selection is carried out based on the soluble mRFP signal it is important to select axons showing an optimal amount of RFP fluorescence. It is important to exclude neurons expressing very high or very low levels of RFP, and this needs to be empirically determined by the user. In our case, we routinely determine the entire range of RFP signals from the transfected neurons in each dish and select axons with moderate fluorescence in the RFP channel.
11. We recommend selecting a region of the axon at least 200–600 μm away from the soma of the neuron.

12. Neurons with complex morphology and axons with several bends along the primary axon should be avoided. The reason is that although movement can still be seen in those axons, analysis will be difficult—particularly in the case of soluble proteins. Ideally, linear axons with a uniform diameter should be selected. The region of the axon to be photoactivated should be fully in focus with the 100× objective throughout imaging period. In case of soluble proteins, even very small defocused areas will render the time-lapse movies unfit for analysis. Also, axons with low amounts of photoactivated GFP signal should be avoided but if necessary, the photoactivation time can be increased.
13. (Intensity of photoactivated zone) vs. (time of 405 nm light exposure) curves can be generated for each PAGFP-tagged protein to empirically determine the time required for photoactivation.
14. The parameters above are specific to our settings and should be used only as a general guideline.

Acknowledgments

Past and ongoing work on slow axonal transport in the Roy lab is supported by grants from the NIH (R01NS075233), the March of Dimes (Basil O' Connor), and start-up funds from UCSD to SR. The authors thank the many researchers who have generously shared constructs with us.

Conflict of interest: The authors declare no conflict of interest.

References

1. Droz B, Leblond CP (1962) Migration of proteins along the axons of the sciatic nerve. Science 137(3535):1047–1048
2. Black MM, Lasek RJ (1980) Slow components of axonal transport: two cytoskeletal networks. J Cell Biol 86(2):616–623
3. Brown A (2003) Axonal transport of membranous and nonmembranous cargoes: a unified perspective. J Cell Biol 160(6):817–821. doi:10.1083/jcb.200212017, jcb.200212017 [pii]
4. Goldstein AY, Wang X, Schwarz TL (2008) Axonal transport and the delivery of pre-synaptic components. Curr Opin Neurobiol 18(5):495–503. doi:10.1016/j.conb.2008.10.003, S0959-4388(08)00130-X [pii]
5. Roy S, Zhang B, Lee VM, Trojanowski JQ (2005) Axonal transport defects: a common theme in neurodegenerative diseases. Acta Neuropathol 109(1):5–13. doi:10.1007/s00401-004-0952-x
6. Tang Y, Scott DA, Das U, Edland SD, Radomski K, Koo EH, Roy S (2012) Early and selective impairments in axonal transport kinetics of synaptic cargoes induced by soluble amyloid beta-protein oligomers. Traffic 13(5):681–693. doi:10.1111/j.1600-0854.2012.01340.x
7. Gauthier-Kemper A, Weissmann C, Golovyashkina N, Sebo-Lemke Z, Drewes G, Gerke V, Heinisch JJ, Brandt R (2011) The frontotemporal dementia mutation R406W blocks tau's interaction with the membrane in an annexin A2-dependent manner. J Cell Biol 192(4):647–661. doi:10.1083/jcb.201007161, jcb.201007161 [pii]
8. Roy S, Yang G, Tang Y, Scott DA (2011) A simple photoactivation and image analysis module for visualizing and analyzing axonal transport with high temporal resolution. Nat Protoc 7(1):62–68. doi:10.1038/nprot.2011.428, nprot.2011.428 [pii]

9. Scott DA, Das U, Tang Y, Roy S (2011) Mechanistic logic underlying the axonal transport of cytosolic proteins. Neuron 70(3): 441–454. doi:10.1016/j.neuron.2011.03.022, S0896-6273(11)00295-9 [pii]
10. Tang Y, Das U, Scott DA, Roy S (2012) The slow axonal transport of alpha-synuclein—mechanistic commonalities amongst diverse cytosolic cargoes. Cytoskeleton (Hoboken) 69(7):506–513. doi:10.1002/cm.21019
11. Trivedi N, Jung P, Brown A (2007) Neurofilaments switch between distinct mobile and stationary states during their transport along axons. J Neurosci 27(3):507–516. doi:10.1523/JNEUROSCI.4227-06.2007, 27/3/507 [pii]
12. Weissmann C, Reyher HJ, Gauthier A, Steinhoff HJ, Junge W, Brandt R (2009) Microtubule binding and trapping at the tip of neurites regulate tau motion in living neurons. Traffic 10(11):1655–1668. doi:10.1111/j.1600-0854.2009.00977.x, TRA977 [pii]
13. Taylor NJ, Wang L, Brown A (2012) Neurofilaments are flexible polymers that often fold and unfold, but they move in a fully extended configuration. Cytoskeleton (Hoboken) 69(7): 535–544. doi:10.1002/cm.21039
14. Fath T, Ke YD, Gunning P, Gotz J, Ittner LM (2009) Primary support cultures of hippocampal and substantia nigra neurons. Nat Protoc 4(1):78–85. doi:10.1038/nprot.2008.199, nprot.2008.199 [pii]
15. Roy S, Winton MJ, Black MM, Trojanowski JQ, Lee VM (2007) Rapid and intermittent cotransport of slow component-b proteins. J Neurosci 27(12):3131–3138

Chapter 14

In Vivo Cell Tracking Using PhOTO Zebrafish

William P. Dempsey, Hanyu Qin, and Periklis Pantazis

Abstract

By combining the strength of previously described in vivo cell tracking methodologies, we have recently generated a set of transgenic zebrafish lines, called "PhOTO (*ph*otoconvertible *o*ptical *t*racking *o*f…)" zebrafish. PhOTO zebrafish lines are suitable for cell tracking during highly dynamic events, including gastrulation, tissue regeneration, tumorigenesis, and cancer/disease progression. Global monitoring of cell shape, cell interactions, e.g., cell intercalations, coordinated division, and cell dynamics are accomplished by using fluorescence imaging of nuclear and plasma membrane fluorescent protein labeling. The irreversible green-to-red photoconversion property of Dendra2 fusions enables noninvasive, specific and high-contrast selection of targeted cells of interest, which greatly simplifies cell tracking and segmentation in time and space. Here we demonstrate photoconversion and in vivo cell tracking using PhOTO zebrafish.

Key words Photoconversion, Dendra2, Cerulean, Lineage tracing, Segmentation

1 Introduction

The understanding of vertebrate development and disease has advanced considerably in recent years primarily due to two key advantages the zebrafish possesses as a model organism: The short life-cycle (i.e., the embryo develops to an adult fish in approximately 12 weeks) [1] and the ease to carry out classical forward genetic analysis has rendered the zebrafish a powerful vertebrate model organism to study human disease mechanisms in large-scale genetic screens [2]. In addition, the transparency of the developing embryo allows observing the fate and movement of single cells during development [3], providing insight into the formation of individual tissues, organs, and neural networks [4–7].

To elucidate the complex cell dynamics (i.e., divisions, movement, morphological changes) underlying zebrafish embryonic development, different experimental approaches have been devised to track cells with high fidelity in space and time. These methods can be classified into two main categories: sparse/partial and global labeling and tracking. Partial labeling techniques have been

Sidney Cambridge (ed.), *Photoswitching Proteins: Methods and Protocols*, Methods in Molecular Biology, vol. 1148,
DOI 10.1007/978-1-4939-0470-9_14,

accomplished either by expressing fluorescent proteins in certain cell types or tissue structures by genetic means (e.g., tissue specific promoter [8–10], random gene insertion [11, 12]) or by precise cell/tissue/organ injection of dyes or chemicals [13–15]. Global labeling takes advantage of ubiquitously expressing fluorescent proteins under the control of a constitutive promoter [16, 17]. Whereas partial labeling introduces a high signal-to-noise ratio by tagging exclusively cells/tissue of interest, the acquired image sequences do not provide information about the context of the surrounding tissue microenvironment. Global labeling provides opportunities to study the whole cell population, yet requires the use of sophisticated volumetric imaging setups and demands considerable computational efforts for cell segmentation and tracking.

To combine the strengths of both partial and global labeling, we have recently generated transgenic zebrafish lines, collectively called the PhOTO [18] lines, that permit photoconvertible optical tracking of cell dynamics in vivo. PhOTO zebrafish ubiquitously express targeted blue fluorescent protein Cerulean [19] and green-to-red photoconvertible Dendra2 fusions [20]. By photoconverting Dendra2 noninvasive, nonrandom mosaic labeling of any subset of cells could be achieved at any time during development. Simultaneous monitoring of global cell behavior and morphology is achieved by visualizing spectrally distinct unconverted Dendra2 and Cerulean fusion proteins, thereby improving accuracy for segmentation and tracking of cells in vivo. We introduced two stable transgenic lines: PhOTO-N zebrafish (*Tg*(*βactin2*:*memb-Cerulean-2A-H2B-Dendra2*)^{zh21}) constitutively expressing H2B-Dendra2 to label all nuclei and memb-Cerulean to label all membranes, and the complementary PhOTO-M zebrafish (*Tg*(*βactin2*:*memb-Dendra2-2A-H2B-Cerulean*)^{zh22}) expressing H2B-Cerulean and memb-Dendra2 [21, 22]. Given that their expression persists throughout the lifecycle of the PhOTO zebrafish, lineage-tracing experiments can be performed during any stage in the lifetime of the zebrafish.

In this chapter, we describe a protocol to identify the optimal photoconversion conditions for Dendra2 exemplified in mosaic PhOTO-N Casper zebrafish [23]. Casper (*mitfa*$^{w2/w2}$;*roy*$^{a9/a9}$) zebrafish provide a unique transparent optical basis for deep tissue imaging throughout all developmental stages. The photoconversion is rapid and nontoxic, circumventing experimental shortcomings such as long incubation time or potential cytotoxicity seen with heat shock or drug inducible promoters for mosaic labeling. Photoconversion allows in vivo cell tracking during early stages of embryo gastrulation using PhOTO-N embryos. We anticipate that using PhOTO zebrafish for lineage tracing at the systems-level in the early embryo as well as in the adult fish will greatly facilitate research efforts to understand development, traumatic injury and regeneration, cancer progression, and stem cell behavior [24–28].

2 Materials

Standard materials commonly available in a zebrafish lab can be used for the following protocol. In addition, a laser scanning confocal microscope with an image processing workstation is required to perform cell-specific photoconversion of the fluorescent protein H2B-Dendra2 in the living PhOTO-N zebrafish embryo and further tracking of photoconverted proteins at later developmental stages. Alternatives of materials and equipment can be utilized according to experimenter's purpose:

2.1 Solutions and Reagents

1. Egg water: 20 mM NaCl; 2.2 mM $CaSO_4 \cdot 2H_2O$; 265 μL Methylene Blue solution 5 L deionized water.
2. 1 M 4-(2-Hydroxyethyl)piperazine-1-ethanesulfonic acid (HEPES) buffer, pH 7.5.
3. 30× Danieau's solution: 1,740 mM NaCl; 21 mM KCl; 12 mM $MgSO_4 \cdot 7H_2O$; 18 mM $Ca(NO_3)_2$; 150 mM 1 M HEPES buffer; add deionized water to 1 L and adjust to pH 7.6.
4. 1 % Low melting temperature agarose in 30× Danieau's solution: 5 g Low melting point agarose (SeaPlaque® Agarose, Cat.# 50100, Lonza); 500 mL 30× Danieau's solution; Storage temperature 45 °C.
5. 0.5 % 25× Tricaine storage solution: Tricaine methanesulfonate (Finquel®/MS-222, AGENT Chemical Laboratories).
6. 25× PTU solution: 0.075 % (W/V) 1-phenyl-2-thiourea in egg water without Methylene Blue (*see* **Note 1**).
7. Embryo tested mineral oil.
8. 0.5 % Phenol red solution in Dulbecco's Phosphate-Buffered Saline (DPBS) (Cat.# P0290, Sigma Life Science).
9. Nuclease-free water.

2.2 Fish Breeding Materials

1. WT:AB zebrafish.
2. PhOTO-N(*Tg*(*βactin2*:*memb-Cerulean-2A-H2B-Dendra2*)^{zh21}) transgenic zebrafish line.
3. Casper (*mitfa*$^{w2/w2}$;*roy*$^{a9/a9}$) mutant zebrafish line.
4. 1.0 L clear polycarbonate breeding tank sets with lid and insert (AQUANEERING, Part No.# ZHCT100).
5. Plastic plants and nets.
6. 7 mL, non-sterile, graduated Pasteur pipettes.

2.3 Microinjection Equipment and Materials

1. PhOTO-N vector.
2. *Tol2* Transposase vector.
3. mMESSAGE mMACHINE® High Yield Capped RNA Transcription SP6 Kit (Life Technologies™ Ambion®, Cat.#1340).

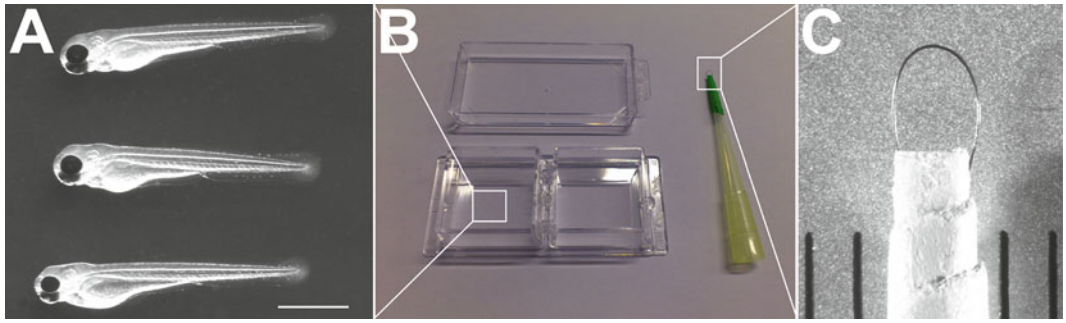

Fig. 1 Embedding mosaic PhOTO-N Casper larvae. Lab-TEEK Chambered #1.0 Borosilicate Coverglass System (coverglass and chamber) (**b**) with embedded 2 dpf PhOTO-N Casper larvae (magnified view shown in **a**). Hair loop (**b**, *right*) was made of a 200 μL tip (*yellow*) and human hair (magnified end of the hair loop is shown in **c**, hair loop diameter: 1.5 mm). Scale bar (**a**): 500 μm (Color figure online)

4. Nanoinject II Auto-Nanoliter injector (Drummond Scientific Company).
5. 3.5″ Drummond#3-000-203-G/X replacement tubes (Drummond Scientific Company).
6. P-1000 Flaming/Brown Micropipette Puller (Stutter Instrument).
7. Embryo injection mold (TU-1, AdaptiveScienceTools).

2.4 Imaging Equipment and Materials

1. Two-well glass chambers (Lab-TEK Chambered #1.0 Borosilicate Coverglass System, Cat.#155380, Thermo Fisher Scientific) (*see* Fig. 1b).
2. 150 mm disposable glass Pasteur pipettes (*see* **Note 2** and **Note 3**).
3. Pipetting pump.
4. Hair loop (*see* Fig. 1b, c).
5. Immersol™ W immersion fluid (Carl Zeiss AG).
6. Laser scanning microscope Zeiss LSM 780 with a 405 nm Diode laser, a 561 nm DPSS laser, and a 458 nm, 488 nm, 514 nm argon laser (Carl Zeiss AG).
7. Zeiss LSM 710 confocal microscope (Carl Zeiss AG).
8. Olympus MVX10 Fluorescence MacroZoom stereomicroscope (Olympus Inc.) with X-Cite Series 120Q excitation light source (Lumen Dynamics).
9. LD LCI PlanApo 25×/0.8 W objective (Carl Zeiss AG).
10. 20×/0.8NA Plan-Apochromat air objective (Carl Zeiss AG).
11. ZEN 2011 software (Carl Zeiss AG).
12. Imaris software (Bitplane AG).
13. Photoshop CS6 (Adobe).

3 Methods

All animal procedures detailed below were performed in accordance with official animal care guidelines and were approved by the Veterinary Department of the Canton of Basel-Stadt (Switzerland).

3.1 Preparation of PhOTO-N Casper Zebrafish Larvae for Photoconversion

1. Maintain fish at 14-h on/10-h off light cycle at 28 °C and pH ~7.4, with salinity-controlled water conditions. Use adult fish (≥3 months old) for breeding.
2. Static-tank spawning: Add one male and one female Casper zebrafish in each mating tank and separate the male from the female with a transparent plastic divider. Keep the zebrafish together for at least 12 h (i.e., overnight) prior to mating. Add plastic plants in the breeding tank to enrich the mating environment. Remove the divider when the light turns on (*see* **Note 4**).
3. Preparation of injection mixture: Produce *Tol2* Transposase mRNA from *Tol2* Transposase vector by using the mMESSAGE mMACHINE® SP6 Kit. A 5 μL injection mixture consists of 1 μL PhOTO-N plasmid DNA (100 ng/μL), 1 μL *Tol2* Transposase mRNA (400 ng/μL), 1 μL Phenol Red (0.1 %, in DPBS), and 2 μL nuclease-free water. Keep the injection mixture on ice before loading the solution into the injection needle. Prefill the injection needle with mineral oil. Unload a certain volume (~3 μL) of mineral oil and then load the prepared injection mixture into the injection needle.
4. Microinjection to generate mosaic PhOTO-N Casper zebrafish: Harvest fertilized embryos within 15 min after the removal of the divider. Align fertilized embryos in the embryo holder filled with egg water. Find an appropriate position for the injection needle and perform microinjection at the zygote stage. Tol2 transposase proteins, translated during the early zebrafish development, recognize the *Tol2* elements flanking the coding region of PhOTO-N. When the plasmid is present within a cell expressing these transposase proteins, the coding region of the PhOTO-N plasmid can be inserted randomly into the genome.
5. Positive embryo screening: Screen embryos using a fluorescence stereomicroscope approximately 4–6 h after injection for early gastrulation experiments or 24 h for other embryonic and larval stage experiments. Select brightly expressing mosaic embryos (positive embryos can make up to 30–50 % of the screened population depending on the experimenter's injection skill and embryo quality) from the injected population and raise them in egg water at 28 °C until imaging at 2–5.5 day post fertilization (dpf) (*see* **Note 5**).
6. Embedding larvae: Anesthetize larvae in 0.015–0.03 % (w/v) Tricaine. Embed the larvae in 1 % (w/v) low melting temperature

agarose with 30× Danieau's solution containing 0.02 % Tricaine and place them laterally in the Lab-TEK Chambered #1.0 Borosilicate Coverglass System using the hair loop [29] (*see* Fig. 1).

3.2 Dendra2 Photoconversion in PhOTO-N Casper Zebrafish Larvae

1. Image acquisition of Dendra2 before photoconversion: Choose an appropriate objective for H2B-Dendra2 photoconversion (e.g., LD LCI PlanApo 25×/0.8 W objective [Carl Zeiss AG]). For water objectives, apply one drop of water or one drop of immersion oil having the same refractive index of water (e.g., Immersol™ W immersion fluid for the water objective (Carl Zeiss AG)) onto the objective. The following parameters were used in the in-house Zeiss 780 microscope system for image acquisition: 1 % of 488 nm laser power (~0.01 mW) and 20 % of 561 nm laser power (~0.4 mW) (power before the objective). Add a bright-field channel if the overview of the gross anatomical structure is desired (*see* **Notes 6–8**).
2. Define one or more regions of interest (ROI) for photoconversion using the Zen 2011 software (*see* **Notes 9** and **10**).
3. Photoconversion of Dendra2: Determine the power of the laser and the number of iterations empirically for each experimental

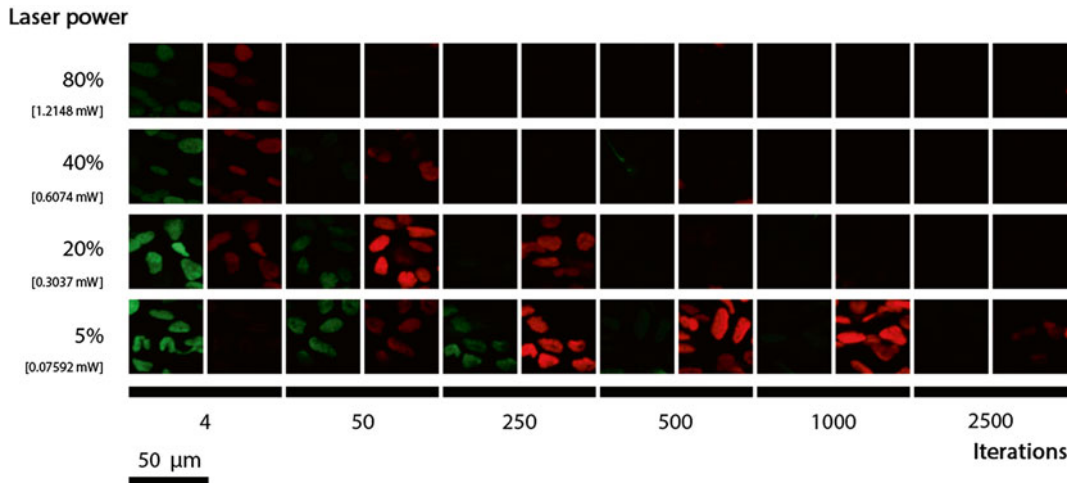

Fig. 2 Photoconversion of nuclear Dendra2 in mosaic PhOTO-N Casper zebrafish using different combinations of laser power and iterations. Photoconversion efficiencies were tested using different laser powers and iterations. *Green* and *red* H2B-Dendra2 fluorescence was acquired post conversion. The *green* fluorescence shows remaining unconverted Dendra2 and the *red* fluorescence indicates converted Dendra2. Five percentage laser excitation in the software shows efficient photoconversion around 250–1,000 iterations. Iterations between 50 and 250 result in efficient photoconversion using 20 % laser excitation. In contrast to low and medium laser excitation power levels, high software power levels (40 and 80 % in our experimental setup) show poor photoconversion efficiencies. We defined the photoconversion efficiency as the intensity of vanishing *green* and increasing *red* fluorescence. Fluorescence intensity acquisition was taken within in the linear range of the detector (i.e., no pixels are saturated). Size of ROI for photoconversion: 75 × 75 pixel. Pixel dwell time: 3.15 µs. Scale bar: 50 µm

imaging setting (*see* Fig. 2). Based on our results, complete photoconversion from green to red fluorescence of H2B-Dendra2 of the PhOTO-N Casper zebrafish larva within an ROI is achieved with low to medium excitation power settings combined with medium to low scan iterations, respectively (*see* Fig. 2). Under these photoconversion conditions, no phototoxic effects were observed. In contrast, high-energy excitation power settings (e.g., 40 or 80 %) usually provided inefficient photoconversion with considerable phototoxicity (i.e., a noticeable developmental delay) (*see* **Notes 11** and **12**). This observation is in contrast to experiments performing photoactivation of photoactivatable GFP (paGFP) in tissue [30, 31].

4. Perform image acquisition of Dendra2 after photoconversion with the imaging parameters provided under Subheading 3.2, **step 1**.

Here, we demonstrate the feasibility of using PhOTO zebrafish to track individual cells in vivo by photoconverting nuclear H2B-Dendra2 in PhOTO-N zebrafish at early gastrula stage.

3.3 In Vivo Cell Tracking During Early Gastrula Stage in Transgenic PhOTO-N Zebrafish

1. Preparation of PhOTO-N F1 embryos for time-lapse imaging: Obtain PhOTO-N F1 embryos from crossing PhOTO-N founders with WT zebrafish.
2. Raise embryos in egg water at 28 °C.
3. Screen and identify embryos positive for green fluorescence (488 nm channel) with a fluorescence stereomicroscope before the imaging experiment.
4. Embed dechorionated positive embryos in 1 % (w/v) low melting temperature agarose with 30× Danieau's solution (*see* **Note 2** and **Note 3**).
5. In vivo cell tracking during embryo gastrulation: Keep embryos between 26 and 32 °C throughout time-lapse experiments, if possible using a heated chamber around the imaging stage. Note that for long-term time-lapse experiments, lower temperatures in this range are more optimal to reduce the metabolism of the embryo during imaging (*see* **Note 13**).
6. Figure 3 is an example of successful photoconversion [18]. To generate this time-lapse, we used a 20×/0.8NA Plan-Apochromat air objective on a Zeiss LSM 710 (Carl Zeiss AG) confocal microscope (*see* Fig. 3a, b). The photoconversion of Dendra2 seen in Fig. 3 was carried out by 405 nm laser illumination of a set of nucleus-sized, circular regions of interest by defining an ROI within the zebrafish sample at the late gastrulation period on a Leica True Confocal Scanner SP5 Spectral High-Speed Confocal System with an acousto-optical beam splitter (AOBS) (Leica Microsystems, Inc., Deerfield, IL) (*see* **Note 14**).

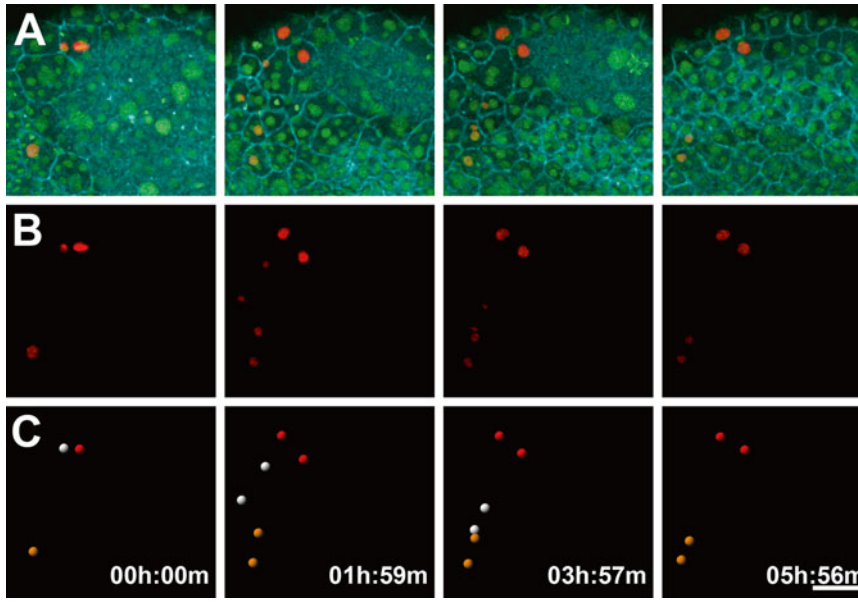

Fig. 3 Achieving high-contrast photoconversion of individual nuclei containing nuclear targeted mDendra2 within a live, multi-color labeled embryo. This is a cropped view of the animal pole region of an ~6 h time-lapse movie of cells within a transgenic PhOTO-N zebrafish embryo at the late gastrula period. Each image is a maximum intensity projection of 10.5 μm in depth, and four frames from the video are shown. (**a**) In the merged image of each color channel gives context to the photoconverted cells of the embryo. Membranes (*cyan*) outline each cell within the embryo, and both photoconverted (*red*) and non-photoconverted (*green*) nuclei can be seen throughout the projected images. (**b**) In the segmented photoconverted (*red*) channel alone, one can easily make out the three individually photoconverted nuclei with high contrast within the embryo. (**c**) Each nucleus can be given a distinct identity (in this case *red*, *white*, and *yellow* coloring) so that the cell divisions that occur between the first and second panel are easily distinguished. Note that one cell and its daughter migrate below the field of view between the third and fourth panels. Scale bar: 50 μm. This figure has been modified from Dempsey et al. [1]

7. Depending on the depth of the cells and the dynamic nature of the process in the *z*-direction, differing *z*-extents for optical stacks will be necessary. In this case, since there are few cell layers throughout much of the gastrulating embryo, we only required a *z*-extent of ~10 μm. This enabled us to perform multicolor imaging to see all three fluorescence channels, as well (*see* Fig. 3a) (*see* **Note 15**).
8. Image processing and analysis: Process images and time-lapse data of embryo gastrulation using Imaris (Bitplane AG) or a comparable image processing software that can handle four dimensional (*x*, *y*, *z*, and *t*) images. Cell segmentation and tracking in Fig. 3c was achieved in a semi-automated manner using the spot-tracking tool (for PhOTO-N nuclei) within Imaris (Bitplane AG). Similar tracking tools can be utilized for the membranes in PhOTO-M photoconverted cells, such as with the recently published automated cell morphology extractor (ACME) software [32] (*see* **Note 16**).

4 Notes

1. 25× is an appropriate concentration for the PTU stock solution, since it has a high solubility at this concentration. 25× PTU can be kept at 4 °C.
2. Avoid exposing dechorionated embryos to air (especially at the air–water interface, where there is high surface tension) or plastic surfaces, since the embryos can easily break when exposed to mechanical stress.
3. Plastic Pasteur pipettes are suitable for transferring embryos that have not been dechorionated. Once dechorionated, they tend to stick to plastic, so always use glass Pasteur pipettes (preferably with slightly fire-polished ends in order to avoid damaging the fish).
4. Tilt the breeding tank insert to create a shallow water area to promote females laying eggs during fish mating.
5. Imaging in the absence of pigmentation can be achieved by using the transparent Casper zebrafish. Alternatively, inhibition of pigmentation can be achieved by incubating the zebrafish in 1× PTU in egg water starting at 24 hpf, changing the solution once daily [33].
6. We recommend using 20–63× objectives for efficient photoconversion. Please note that water immersion objectives are expected to yield a more efficient photoconversion with the same imaging conditions than air objectives because of the reduction in refractive index mismatch between the sample medium and the objective.
7. Perform a red fluorescence pre-scan prior to the experiment to (1) ascertain whether there is any unexpected previously photoconverted Dendra2 in the sample and (2) establish a background level of red for comparison after the sample is photoconverted.
8. For quantitative imaging, it is necessary to maintain the fluorescence intensity of especially the photoconverted species within the linear range of the detector. Calibration of the linear range of the detector using recombinant fluorescent proteins can enable accurate quantitative imaging of expressed protein species, if desired [31].
9. We noticed that photoconversion is not precisely confined and often leads to significant bleaching at the focus within the chosen ROI when using an objective with NA > 0.8. Since the double-cone of excitation is much larger for high NA objectives and the focal spot is tighter, there is a larger area of photoconversion outside of the focus and higher nonlinear effects within the focus itself. Consequently, when using high NA

objectives, define a smaller region of interest than you would for a lower NA objective (e.g., a circle defining 80–90 % of a nucleus instead of the entire nucleus itself) to reduce this excess off-target photoconversion and to reduce bleaching at the focus. Also, adjust the number of scan iterations and the laser power accordingly—usually, the reduction of both parameters is necessary.

10. We noticed that the shape of the ROI affects the photoconversion because of the directionality of laser scanning. In most commercial systems, scanning proceeds from left to right along the *x*-axis before moving down the *y*-axis, similar to your reading of this protocol now. Thus, the movement in the *y*-direction proceeds much more slower than in the *x*-direction. Consequently, shapes that have a high aspect ratio should be designed to have the longer side in the *x*-direction. For example, when designing a long rectangular region of interest, try to make sure that the long side of the rectangle is in the *x*-direction, while the short end is in the *y*-direction to allow faster scanning and more efficient photoconversion.
11. Photoconversion of Dendra2 can be accomplished by either 405 nm laser power or high intensity 488 nm laser power. However, in our experience, pronounced photobleaching is favored over efficient photoconversion at high power or long-term exposure at 488 nm. We suggest using 405 nm laser power to achieve an efficient photoconversion. When taking the pre-photoconversion images, use low 488 nm laser power to avoid unexpected increases in photoconverted species during long-term time-lapse imaging.
12. To photoconvert molecules or cells that are highly dynamic, the use of medium excitation laser energy combined with minimal scan iterations (i.e., 4–8) is recommended. For relatively slow dynamic events (e.g., long-term regeneration), the use of low excitation laser energy with prolonged illumination is more suitable.
13. Add embryo tested mineral oil onto the surface of fully solidified low melting temperature agarose for long-term imaging to reduce evaporation while still allowing gas diffusion (e.g., O_2) to the sample.
14. Because of the single-photon nature of the photoconversion process at 405 and 488 nm, it is often desirable to target small populations of nuclei that are sparsely localized in the *z*-direction (e.g., on the lateral or ventral sides of the embryo during epiboly) to limit unwanted photoconversion of cells above or below a given desirable focal plane.
15. For long-term time-lapse imaging of dynamic processes on a commercial laser scanning microscope system, we recommend

focusing on as small of a z extent as possible (up to around 50 μm in the z-direction) to allow reasonable time resolution between frames to enable accurate segmentation even after cell division. Slower dynamic processes could require many fewer frames, and greater depths within the embryo can be visualized.

16. Use a cell-tracking software such as Imaris or plugins for FIJI/ImageJ to segment and keep track of photoconverted nuclei and the progeny of photoconverted cells from the PhOTO-N zebrafish lines.

Acknowledgment

We thank Michel Haffner for fish care and for assisting in taking Fig. 1. WPD was supported by the Swiss National Center of Competence in Research (NCCR) "Nanoscale Science".

References

1. Kimmel CB, Ballard WW, Kimmel SR et al (1995) Stages of embryonic development of the zebrafish. Dev Dyn 203:253–310
2. Patton EE, Zon LI (2001) The art and design of genetic screens: zebrafish. Nat Rev Genet 2:956–966
3. Keller PJ, Schmidt AD, Wittbrodt J, Stelzer EH (2008) Reconstruction of zebrafish early embryonic development by scanned light sheet microscopy. Science 322:1065–1069
4. Kirby BB, Takada N, Latimer AJ et al (2006) In vivo time-lapse imaging shows dynamic oligodendrocyte progenitor behavior during zebrafish development. Nat Neurosci 9:1506–1511. doi:10.1038/nn1803
5. Yaniv K, Isogai S, Castranova D et al (2006) Live imaging of lymphatic development in the zebrafish. Nat Med 12:711–716. doi:10.1038/nm1427
6. Laughlin ST, Baskin JM, Amacher SL, Bertozzi CR (2008) In vivo imaging of membrane-associated glycans in developing zebrafish. Science 320:664–667. doi:10.1126/science.1155106
7. Mikut R, Dickmeis T, Driever W et al (2013) Automated processing of zebrafish imaging data: a survey. Zebrafish 10(3):401–421. doi:10.1089/zeb.2013.0886, 130612061407002
8. Long Q, Meng A, Wang H et al (1997) GATA-1 expression pattern can be recapitulated in living transgenic zebrafish using GFP reporter gene. Development 124:4105–4111
9. Caron SJC, Prober D, Choy M, Schier AF (2008) In vivo birthdating by BAPTISM reveals that trigeminal sensory neuron diversity depends on early neurogenesis. Development 135:3259–3269. doi:10.1242/dev.023200
10. Rodrigues FSLM, Doughton G, Yang B, Kelsh RN (2012) A novel transgenic line using the Cre-lox system to allow permanent lineage-labeling of the zebrafish neural crest. Genesis 50:750–757. doi:10.1002/dvg.22033
11. Tryon RC, Higdon CW, Johnson SL (2011) Lineage relationship of direct-developing melanocytes and melanocyte stem cells in the zebrafish. PLoS ONE 6:e21010. doi:10.1371/journal.pone.0021010.s001
12. Caneparo L, Pantazis P, Dempsey W, Fraser SE (2011) Intercellular bridges in vertebrate gastrulation. PLoS ONE 6:e20230. doi:10.1371/journal.pone.0020230.g001
13. Schilling TF, Kimmel CB (1994) Segment and cell type lineage restrictions during pharyngeal arch development in the zebrafish embryo. Development 120:483–494
14. Woo K, Shih J, Fraser SE (1995) Fate maps of the zebrafish embryo. Curr Opin Genet Dev 5:439–443
15. Vogeli KM, Jin S-W, Martin GR, Stainier DYR (2006) A common progenitor for haematopoietic and endothelial lineages in the

zebrafish gastrula. Nature 443:337–339. doi:10.1038/nature05045

16. Burket CT, Montgomery JE, Thummel R, Kassen SC, LaFave MC, Langenau DM, Zon LI, Hyde DR (2008) Generation and characterization of transgenic zebrafish. lines using different ubiquitous promoters. Transgenic Res 17:265–279
17. Mosimann K, Kaufman CK, Li PL, Pugach EK, Tamplin OJ, Zon LI (2011) Ubiquitous transgene expression and Cre-based recombination driven by the ubiquitin promoter in zebrafish. Development 138(1):169–177
18. Dempsey WP, Fraser SE, Pantazis P (2012) PhOTO zebrafish: a transgenic resource for in vivo lineage tracing during development and regeneration. PLoS ONE 7:e32888. doi:10.1371/journal.pone.0032888.s008
19. Rizzo MA, Springer GH, Granada B, Piston DW (2004) An improved cyan fluorescent protein variant useful for FRET. Nat Biotechnol 22:445–449. doi:10.1038/nbt945
20. Gurskaya NG, Verkhusha VV, Shcheglov AS et al (2006) Engineering of a monomeric green-to-red photoactivatable fluorescent protein induced by blue light. Nat Biotechnol 24:461–465. doi:10.1038/nbt1191
21. Donnelly ML, Hughes LE, Luke G et al (2001) The 'cleavage' activities of foot-and-mouth disease virus 2A site-directed mutants and naturally occurring '2A-like' sequences. J Gen Virol 82:1027–1041
22. Zacharias DA (2002) Partitioning of lipid-modified monomeric GFPs into membrane microdomains of live cells. Science 296:913–916. doi:10.1126/science.1068539
23. White RM, Sessa A, Burke C et al (2008) Transparent adult zebrafish as a tool for in vivo transplantation analysis. Cell Stem Cell 2:183–189. doi:10.1016/j.stem.2007.11.002
24. Traver D, Paw BH, Poss KD et al (2003) Transplantation and in vivo imaging of multilineage engraftment in zebrafish bloodless mutants. Nat Immunol 4:1238–1246. doi:10.1038/ni1007
25. Lieschke GJ, Currie PD (2007) Animal models of human disease: zebrafish swim into view. Nat Rev Genet 8:353–367. doi:10.1038/nrg2091
26. Stoletov K, Montel V, Lester RD et al (2007) High-resolution imaging of the dynamic tumor cell–vascular interface in transparent zebrafish. Proc Natl Acad Sci 104:17406–17411
27. Kissa K, Murayama E, Zapata A et al (2007) Live imaging of emerging hematopoietic stem cells and early thymus colonization. Blood 111:1147–1156. doi:10.1182/blood-2007-07-099499
28. Lee SLC, Rouhi P, Jensen LD et al (2009) Hypoxia-induced pathological angiogenesis mediates tumor cell dissemination, invasion, and metastasis in a zebrafish tumor model. Proc Natl Acad Sci 106:19485–19490
29. Woo K, Fraser SE (1995) Order and coherence in the fate map of the zebrafish nervous system. Development 121:2595–2609
30. Pantazis P, González-Gaitán M (2007) Localized multiphoton photoactivation of paGFP in Drosophila wing imaginal discs. J Biomed Opt 12:044004. doi:10.1117/1.2770478
31. Plachta N, Bollenbach T, Pease S et al (2011) Oct4 kinetics predict cell lineage patterning in the early mammalian embryo. Nat Cell Biol 13:117–123. doi:10.1038/ncb2154
32. Mosaliganti KR, Noche RR, Xiong F et al (2012) ACME: automated cell morphology extractor for comprehensive reconstruction of cell membranes. PLoS Comput Biol 8:e1002780. doi:10.1371/journal.pcbi.1002780.s007
33. Karlsson J, von Hofsten J, Olsson P-E (2001) Generating transparent zebrafish: a refined method to improve detection of gene expression during embryonic development. Mar Biotechnol 3:0522–0527. doi:10.1007/s1012601-0053-4

Chapter 15

In Vivo Optogenetics for Light-Induced Oxidative Stress in Transgenic Zebrafish Expressing the KillerRed Photosensitizer Protein

Cathleen Teh and Vladimir Korzh

Abstract

Optogenetic methods are gaining broad recognition. The zebrafish is particularly useful for these applications as a model vertebrate due to a unique combination of translucent embryos/larvae and efficient transgenesis. Here, we describe a zebrafish model of light-induced cardiac deficiency. Upon illumination with intense green light, the membrane-tethered photosensitizer protein KillerRed acts as a photoinducer of reactive oxygen species which in turn cause changes in heart rate and contractility in hearts that express this transgene.

Key words Membrane-tethered photosensitizer, ROS, Heart rate and contractility

1 Introduction

Zebrafish, *Danio rerio*, is a popular vertebrate model animal with well-established tools for transgenesis [1–3]. It is compatible with in vivo imaging as the optically translucent larvae develop externally. The 5 days old and 4 mm long free swimming larvae are amenable to whole body imaging using standard microscopy techniques. Optical translucence of embryos and larvae allows the non-invasive photo-induction of oxidative stress in transgenic larvae expressing the genetically encoded photosensitizer, KillerRed [4]. Here, reactive oxygen species (ROS) are produced upon KillerRed illumination with intense green light [5]. ROS production occurs near the chromophore of KillerRed [6]. Overt ROS production ultimately destroys the chromophore and results in photobleaching of KillerRed, a useful readout of oxidative stress. Hence, a typical illumination experiment requires a transgenic larvae expressing at least two fluorescent proteins, the first being KillerRed, and a second—a photostable fluorescent reporter protein that tolerates prolonged green light illumination, such as enhanced green fluorescent protein (EGFP) [5, 7]. The second reporter is necessary for

Sidney Cambridge (ed.), *Photoswitching Proteins: Methods and Protocols*, Methods in Molecular Biology, vol. 1148,
DOI 10.1007/978-1-4939-0470-9_15,

morphological and physiological analysis of illuminated tissue after KillerRed bleaching. Some outcomes of oxidative stress induced by KillerRed illumination include, but are not limited to, morphological changes, cell death, abnormal heart beat [4, 8], behavioral changes [9, 10], etc. In this chapter the induction and analysis of heart failure are discussed in detail. The key characteristic of light-induced ROS production in the KillerRed transgenic zebrafish is the rapid and noninvasive nature of experiment. This allows following the recovery response of illuminated tissue for days and the reiterative induction of oxidative stress in the same tissue after recovery of KillerRed fluorescence. Of course, a prerequisite is that all experimental transgenic animals must be healthy so that photoinduction of oxidative stress can truly model the transition to a diseased state. Here, we describe in detail the procedure of generating and growing transgenics, conducting a tissue-targeted illumination that elicits light-induced ROS production in the KillerRed transgenics, and optimizing larval survival despite repeated mounting and immobilization in low melting point agarose.

2 Materials

2.1 Setting Up Zebrafish Crosses and Growing Embryos

1. Crossing tank consists of two compatible containers with the smaller mesh-bottom container placed on top of the holding one. The mesh separates the adults from the embryos until their collection.
2. Plastic and glass petri dishes 90 × 15 mm for embryo culture.
3. Incubator to culture zebrafish embryos at 28.5 °C.
4. Transfer pipettes to pick up unfertilized/dead embryos.
5. Egg water for growing zebrafish embryos: 0.6 g of aquarium salt (Red Sea Fish Pharm, Israel) per 1,000 ml of deionized water.
6. Egg water with 1-Phenyl-2-thiourea, PTU (Sigma-Aldrich, USA). 50× stock is made by dissolving 0.15 g PTU in 50 ml of deionized water. 1× egg water with PTU is prepared by adding 1 ml of PTU stock solution to 50 ml of egg water.
7. Zebrafish were maintained according to established protocols in agreement with Institutional Animal Care and Use Committee regulations (Biological Resource Center of Biopolis, license no. 050096) and rules of the Institute of Molecular and Cell Biology zebrafish facility.

2.2 Screening Transgenic Larvae

1. We recommend the use of KillerRed and EGFP transgenic lines with well characterized spatial temporal expression patterns. In this study, we describe two transgenic lines: first, SqKR15 (http://plover.imcb.a-star.edu.sg/webpages/memKR15.html), which expresses the membrane-tethered KillerRed in

the heart and retina, lens, pigmented epithelium, olfactory placode, telencephalon (olfactory bulb), hindbrain (cerebellum, r3, r5-6, radial cells), jaws, enveloping layer, and notochord [5]; second, SqET33-mi3a with strong EGFP expression in the heart ventricle [11].

2. Fluorescence stereo dissecting microscope equipped with fluorescence filter sets for detection of green and red fluorescent proteins (MVX10® MacroView, Olympus, Japan).
3. Petri dishes (90 mm) for larvae collection.
4. 3 ml Transfer pipettes to pick up larvae.
5. Egg water with PTU (to block melanin formation).

2.3 Mounting Transgenic Larvae for Tissue Targeted Illumination

1. 1 % UltraPure™ low melting point agarose in water.
2. 250 ml Duran® screw cap laboratory glass bottle.
3. Uncoated glass bottom culture dishes (35 mm; MatTek Corporation, USA) for microscopic imaging.
4. 150 mm glass transfer pipette.
5. Rubber bulbs for glass transfer pipettes.
6. 3 ml and 1 ml transfer pipettes.
7. 1 ml syringe with detachable 30G×1/2 in. needle.

2.4 Tissue-Specific Illumination to Induce Oxidative Stress

1. Upright compound microscope (Zeiss Axioplan 2) with Zeiss filter sets [38HE (EGFP/FITC/ALEXA488; ex470/40, em525/50) and 43HE (Cy3/DsRed/Rhodamine; ex550/25, em605/70); Zeiss, Germany].
2. A 5×/0.12 objective of the upright compound microscope (Zeiss, Germany).
3. AxioVision image acquisition software (Zeiss, Germany).
4. Illuminator power supply (ebq100 dc).
5. Illuminator with mercury short arc lamp with reflector (HBO103W/2; OSRAM, Germany).
6. Microscope glass slide (clear glass with ground edges).
7. Glass-bottom petri dishes with agarose-mounted transgenic larvae.
8. 1 ml syringe with detachable 30G×1/2 in. needle.

2.5 Image Acquisition and Data Analysis of Larvae Heartbeat

1. Zeiss Axiovert 200 M Cell Imaging System microscope.
2. AxioCam HSm (high-speed camera; Zeiss, Germany).
3. Colibri LED illumination setup (470 nm to visualize GFP; Zeiss, Germany).
4. AxioVision image acquisition software.
5. LSM 5 LIVE high speed confocal laser scanning microscopy (Zeiss, Germany) with 488 nm and 532 nm laser lines.

6. 20×/0.5 objective for embryo imaging.
7. Zeiss LSM software for image acquisition using LSM5 LIVE (Zeiss, Germany).
8. Zeiss LSM software (Zeiss, Germany) or Image J (NIH, USA) to retrieve and process images in database.

3 Methods

3.1 Growing Transgenic Larvae

1. Crosses are set up in the evening after adult fish completed daily meals. Transfer system water into the crossing tank such that the mesh-bottom container is immersed in approximately 3–4 cm of system water before transferring transgenic males and females into the crossing tank using a fish net. Clearly label the crossing tank stating the identity of male and female transgenic parents used for the cross so that the adults can be correctly transferred back to the system tank after breeding.
2. Transfer embryos from the bottom of crossing tank into a sieve. Wash embryos with tap water before transfer into 90 mm plastic/glass petri dishes (50–100 of embryos per dish) containing 20 ml of 1× egg water (buffer) to ensure normal development (*see* **Note 1**). Culture embryos in a 28.5 °C incubator (*see* **Note 2**). Unfertillized eggs and dead embryos can be identified using a stereomicroscope and should be removed with a transfer pipette to ensure healthy growth of larvae.
3. Melanin interferes with photo-induction of oxidative stress and optical imaging. To inhibit melanin formation, change water to egg water containing 1× PTU (*see* **Note 3**) after embryos reach 22 h post fertilization stage.

3.2 Screening of Transgenic Larvae

1. Use a fluorescent stereomicroscope equipped to visualize KillerRed and EGFP. A clutch of transgenic embryos must be screened to identify and isolate those with dual expression of KillerRed and EGFP. First transfer all KillerRed-positive transgenic larvae into a separate 90 mm petri dish containing egg water with 1×PTU using a 3 ml transfer pipette. Screen these for EGFP expression. Transfer the double transgenics into a separate petri dish containing egg water with PTU using a 3 ml transfer pipette (*see* **Note 4**).
2. Transfer the siblings expressing only EGFP into a separate petri dish containing egg water with 1×PTU. These larvae will be used as the illuminated control (*see* **Note 5**).
3. Unless larvae hatched on their own, remove chorions manually with sharp forceps or needles (in a non-sticky glass petri dish) for subsequent mounting of larvae in the low melting point agarose.

3.3 Mounting Transgenic Larvae for Tissue-Specific Illumination

1. Add 100 ml of deionized water to 1 g of low melting point agarose granules in a 250 ml screw-capped laboratory glass bottle. Microwave the agarose mix until the agarose granules completely dissolve. Swirl the agarose granules and reheat the agarose mix until it bubbles. This process is repeated twice. Transfer 1.5 ml aliquots of liquid agarose into Eppendorf tubes and store at 37 °C (*see* **Note 6**). Aliquots for mounting transgenic larvae should be kept at 30 °C at least 30 min before mounting to make agarose more viscous. Although embryos tolerate limited exposure to temperature up to 40 °C, this causes heat shock (also *see* **Note 2**).
2. An upright microscope is used to conduct the illumination experiment and the larvae must be positioned and mounted before illumination in such a way that the target tissue is positioned as close to the agarose surface as possible. Transfer 4–5 transgenic larvae into a glass-bottom culture dish and remove as much egg water as possible using a glass transfer pipette attached to a rubber bulb (*see* **Note 7**). Use a 1 ml transfer pipette to dispense a drop of the viscous low melting point agarose into the glass-bottom culture dish holding the larvae. Use the 1 ml transfer pipette to position the larvae near the agarose surface. Use the 1 ml syringe with needle to position and align the larvae as close to each other as possible and the tissue targeted for illumination, in this case the heart, should be as close to agarose surface as possible. To prevent mounted larvae from drying, add 1 ml of water to the dish of mounted larvae after the agarose has completely set, usually 10 min after immobilization of larvae in agarose.

3.4 Tissue-Specific Illumination to Induce Oxidative Stress

1. Turn on the mercury lamp illuminator power supply 15 min before conducting the illumination experiment to achieve a stable light output.
2. Move the stage away from the 5× objective and place the petri dish with closely aligned, mounted larvae on the microscopic stage (*see* **Note 8**). Adjust the light path to direct 100 % light to the eyepiece, turn a condensor into the "bright field" position, and place the cluster of mounted larvae in the beam of light. Position a block under the 5× objective so all mounted zebrafish larvae will be seen. Use the AxioVision image acquisition software to capture a fluorescent image of the mounted embryos in both channels before prolonged exposure to green light to trigger oxidative stress (ex550/25 nm). Turn on the Rhodamine filter and focus on the target KillerRed-positive tissue (heart). Illuminate larvae with intense green light of the mercury lamp until obvious photobleaching of KillerRed starts. Acquire an image of larvae after KillerRed bleaching (Fig. 1). Under these conditions with several larvae simultaneously

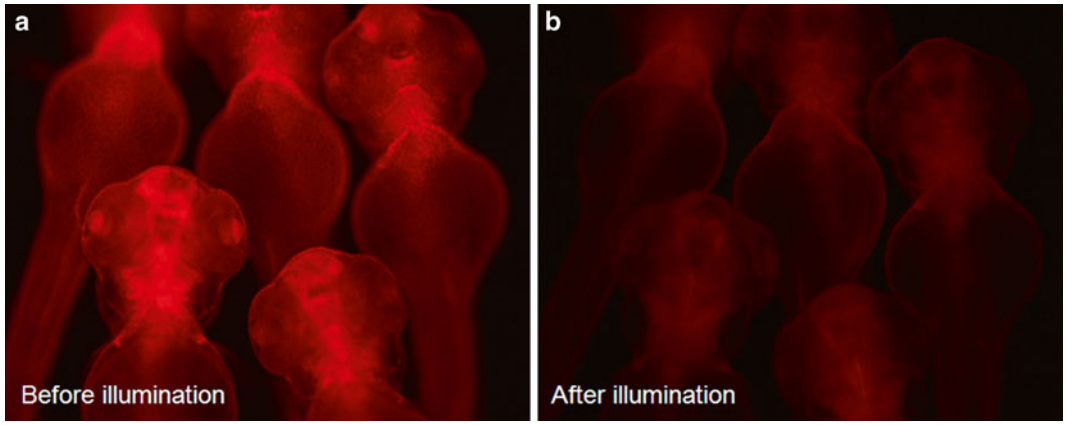

Fig. 1 Illumination of KillerRed transgenic larvae by intense green light bleaches KillerRed. Images of transgenic larvae (KR15) before illumination (**a**) and 40 min after illumination (**b**). Images are acquired under identical settings to illustrate a similar decrease in fluorescence intensity in all larvae. A ×5 objective was used for illumination with intense green light

exposed to intense green light, the duration of illumination varies from 30 min to an hour. Some level of photobleaching must be observed to indicate that sufficient ROS have been produced to degrade KillerRed chromophore. The length of illumination will depend upon the intensity of light generated by the mercury lamp. Hence, a decrease in KillerRed intensity after exposure to green light must be noted to standardize treatment (*see* **Notes 9** and **10**).

3. High-speed image acquisition is required to accurately follow cardiac contraction and dilation. Illuminated larvae have to be remounted if the high-speed camera is attached to the inverted microscope as image acquisition requires mounted zebrafish larva to be positioned as close to the bottom of the glass-bottom dish as possible. First add 2 ml of water into each dish of mounted larvae. Then use a 1 ml syringe attached to a 30G × 1/2 in. needle to dislodge agarose surrounding the larvae cluster. Transfer freed larvae into another glass-bottom petri dish. Remove as much water as possible before adding a viscous drop of low melting point agarose (*see* **Note 11**). Use the needle to position each embryo as close to the bottom of the dish as possible until agarose has set. Cover the agarose drop with water 10 min after agarose has set.

3.5 Image Acquisition and Data Analysis of Larvae Heartbeat

1. For image acquisition of the beating heart, the Axiocam HSm camera (18 frames/s) attached to an inverted Zeiss Axiovert 200 M microscope or LSM5 LIVE high-speed laser-scanning microscope (60 frames/s) has been used. Time-lapse movies of the EGFP-positive heart are recorded for both control and experimental larvae (*see* **Note 12**). EGFP illumination is powered by a 470 nm LED from the Colibri LED illumination

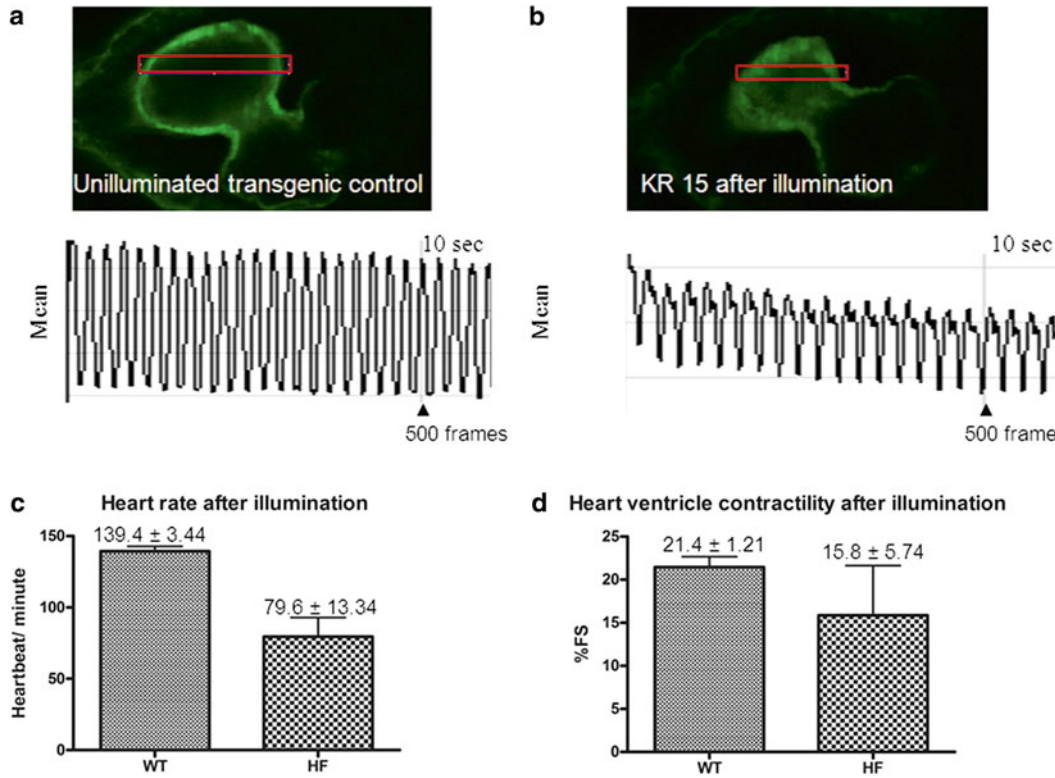

Fig. 2 Illumination of KillerRed transgenic larvae by intense green light causes cardiac deficiency. Changes in dynamic mean intensity illustrated by graphs generated using Image J. Changes in frequency of peak intensity and range of mean intensity in unilluminated transgenic control larvae (**a**) and after induction of heart failure in KR15 larvae (**b**). Note the decrease in the frequency of the peak mean intensity, an indicator of reduced heartbeat, after illuminating KR15 transgenic line. The ventricle also cannot contract or dilate as much when compared to unilluminated transgenic control larvae resulting in a small ventricle (**b**). A bar chart summarizing a decrease in heart rate (**c**) and contractility (**d**) observed in five illuminated larvae after photo-induction of oxidative stress in heart expressing the KillerRed photosensitizer. Values are presented as mean ± SEM. *P* values are derived from unpaired *t* tests and significant decrease in heart rate ($P = 0.0025$) was observed after illumination. The decrease in contractility is not significant ($P = 0.37$) due to phenotype variation

setup attached to the Zeiss Axiovert 200 M microscope or the 489 nm laser line in LSM5 LIVE. Continuous image acquisition over 30 s is recorded and saved as a .zvi file or .lsm files.

2. Open the .zvi or .lsm file using Image J software and select the rectangle area selection tool to demarcate the region of interest, where contraction and dilation of the heart ventricle are at their maximum. To plot dynamic changes in pixel intensity over time, select Image > Stacks > Plot *z*-axis profile. This generates a graph documenting a variation of mean pixel intensity over a 30 s interval (Fig. 2). The graph file is accompanied by the text file, which contains mean intensity values in the rectangular area of all analyzed frames. This allows identification of frames illustrating contraction (maximal mean intensity) and dilation (minimal mean intensity) of the ventricle.

3. To export all image sequences as Tiff files, first select Image > Type to set the image format to 8 bit. Then select File > Save as > Image sequence > Start at 1 to export all the images into a folder for follow-up heartbeat and contractility analysis. The frame number in each image should now be related to a mean intensity reading recorded in the raw data text file. In the raw data text file, note down 5 consecutive frame numbers with maximal (ventricle contraction; systole) and minimal (ventricle dilation; diastole) mean intensity values, where the maximal and minimal values are represented by peaks and dips in the graph. Take note of the number of frames required to complete one heartbeat, which is defined by the completion of one systole-diastole cycle. Now heartbeat per minute = total number of frames per minute/number of frames per heartbeat. Contractility of the heart ventricle can be calculated based on the image sequence, where images with the maximal (systole) and minimal values (diastole) in one heartbeat are opened using Image J software. Mark the ventricle diameter with the line selection tool then select Analyze > Measure to record the diastolic and systolic diameters of 5 consecutive heartbeats. Measurements recorded in the raw data text file are required for calculation of heart contractility using the % of fractional shortening (%FS) formula = [(diastolic diameter − systolic diameter)/diastolic diameter] × 100. Mean values for heartbeat and contractility (%FS) based on 5 consecutive heart contractions can then be compared between different experimental groups (Fig. 2).

4 Notes

1. Do not add too much water into a petri dish for zebrafish cultivation; the volume of egg water should not exceed half petri dish volume. Periodically remove dead embryos and unfertilized eggs and replace water. Follow these rules to ensure optimal aeration and facilitate healthy embryo growth.
2. Zebrafish larvae can be cultured at a range of temperature (22–30 °C) without compromising their survival.
3. Preparation of 50×PTU stock solution (0.15 g per 100 ml water) requires long stirring. This stock solution can be stored at room temperature. Effective inhibition of melanin formation requires egg water with 1×PTU to be added to larvae starting from 22 h post fertilization (hpf). When starting suppression of melanin formation in older embryos (before 32 hpf), increase PTU concentration 2×. This delay will result in incomplete inhibition of melanin formation.

4. Study the spatial temporal expression pattern of each transgene in advance. For example, if the eye is the first tissue that expresses KillerRed followed by that in the heart, the transgenic could be first identified by eye expression before the heart expression becomes obvious during later development. The early identified transgenics will express KillerRed in the heart later on. It is more difficult to screen older larvae under a fluorescent stereomicroscope after they hatch and swim freely in the dish. Immobilization of larvae with MS222 (tricaine, 3-amino-benzoic acidethylester) during screening for transgene expression is not recommended, since this drug may affect results of illumination.
5. Transgenic larvae expressing only EGFP are used as illumination control.
6. Dissolve low melting point agarose in deionized water. A fresh batch of 1 % low melting point agarose must be prepared by reheating when it takes a longer time to position the mounted larvae in agarose. Remove residual water from the culture dish after larvae transfer since it will dilute the agarose and slow down its polymerization.
7. If an upright compound microscope is used to induce ROS production in transgenic zebrafish larvae expressing KillerRed, the larvae must be aligned close to each other and mounted at the same height within the agarose block so the light beam will illuminate all of them with the same intensity. For best aeration and illumination larvae are placed as close to the top of agarose block as possible. Hence, a beginner may start with mounting a single embryo and increase larval number as skills mature.
8. To mount the glass-bottom culture dish onto a microscope use the specimen holder. In its absence a microscopic glass slide can be placed underneath the glass-bottom dish.
9. Light intensity can be measured with a fiber optic power meter (Thorlabs, USA). The mercury short arc lamp must be changed once its life-span ends or when KillerRed photobleaching becomes inefficient.
10. The illumination experiment requires standard illumination regimen for transgenic larvae expressing the GFP reporter in the target tissue (negative illumination control), double (KillerRed-EGFP) transgenic larvae with both transgenes expressed in the same target tissue (experimental sample) and non-illuminated KillerRed/EGFP transgenic larvae (negative control).
11. Do not add more than 50 μl of agarose when larvae are mounted for imaging using the inverted microscope as older larvae do not survive well upon prolonged incubation. Only add enough agarose to immobilize the larvae.

12. It is not possible to record heartbeat in the red channel due to low fluorescence. This results in longer exposure to capture an image, which becomes too slow to match the heart movement. Hence, the EGFP reporter is used to document changes in heartbeat and contractility.

Acknowledgements

We thank the personnel at the Institute of Molecular and Cell Biology facilities for the maintenance of zebrafish lines. This work was supported by an Institute of Molecular and Cell Biology institutional grant from the Agency for Science, Technology, and Research (A*STAR) of Singapore and A*STAR-BMRC-Mindef grant (to V.K.).

References

1. Kawakami K (2007) Tol2: a versatile gene transfer vector in vertebrates. Genome Biol 8 Suppl 1: S7
2. Korzh V (2007) Transposons as tools for enhancer trap screens in vertebrates. Genome Biol 8 Suppl 1: S8
3. Sivasubbu S, Balciunas D, Amsterdam A et al (2007) Insertional mutagenesis strategies in zebrafish. Genome Biol 8 Suppl 1: S9
4. Teh C, Chudakov DM, Poon KL et al (2010) Optogenetic in vivo cell manipulation in KillerRed-expressing zebrafish transgenics. BMC Dev Biol 10:110
5. Bulina ME, Chudakov DM, Britanova OV et al (2006) A genetically encoded photosensitizer. Nat Biotechnol 24(1):95–99
6. Pletnev S, Gurskaya NG, Pletneva NV et al (2009) Structural basis for phototoxicity of the genetically encoded photosensitizer KillerRed. J Biol Chem 284(46):32028–32039
7. Korzh V, Teh C, Kondrychyn I et al (2011) Visualizing compound transgenic zebrafish in development: a tale of green fluorescent protein and KillerRed. Zebrafish 8(1):23–29
8. Yan H, Teh C, Sreejith S et al (2012) Functional mesoporous silica nanoparticles for photothermal-controlled drug delivery in vivo. Angew Chem Int Ed Engl 51(33):8373–8377
9. Lee A, Mathuru AS, Teh C et al (2010) The habenula prevents helpless behavior in larval zebrafish. Curr Biol 20(24):2211–2216
10. Del Bene F, Wyart C, Robles E (2010) Filtering of visual information in the tectum by an identified neural circuit. Science 330(6004): 669–673
11. Poon KL, Liebling M, Kondrychyn I et al (2010) Zebrafish cardiac enhancer trap lines: new tools for in vivo studies of cardiovascular development and disease. Dev Dyn 239(3): 914–926

Chapter 16

Photoactivatable Fluorescent Proteins for Super-resolution Microscopy

Yuji Ishitsuka, Karin Nienhaus, and G. Ulrich Nienhaus

Abstract

Super-resolution fluorescence microscopy techniques such as simulated emission depletion (STED) microscopy and photoactivated localization microscopy (PALM) allow substructures, organelles or even proteins within a cell to be imaged with a resolution far below the diffraction limit of ~200 nm. The development of advanced fluorescent proteins, especially photoactivatable fluorescent proteins of the GFP family, has greatly contributed to the successful application of these techniques to live-cell imaging. Here, we will illustrate how two fluorescent proteins with different photoactivation mechanisms can be utilized in high resolution dual color PALM imaging to obtain insights into a cellular process that otherwise would not be accessible. We will explain how to set up and perform the experiment and how to use our latest software "a-livePALM" for fast and efficient data analysis.

Key words Photoactivatable fluorescent protein, Photoswitching, Photoconversion, Super-resolution microscopy, PALM, RESOLFT, STED, a-livePALM

1 Introduction

Optical microscopy is arguably the method of choice for visualizing biological structures and processes inside living organisms. The method is minimally invasive and fast enough to monitor many biological processes in real time. Optical microscopy using fluorescence detection has proven to be particularly powerful for cellular imaging. It relies on the reemission of light by fluorophores that are specifically attached to structures of interest to make them visible. However, the resolution of optical microscopy is restricted to about half the wavelength of visible light (~200 nm) due to fundamental physical laws governing wave optics [1], which obviously presents a major obstacle because many subcellular structures have dimensions below 100 nm.

During the past decade, a variety of innovative super-resolution fluorescence microscopy techniques have been developed that circumvent the diffraction barrier [2, 3]. They provide the capability

Sidney Cambridge (ed.), *Photoswitching Proteins: Methods and Protocols*, Methods in Molecular Biology, vol. 1148,
DOI 10.1007/978-1-4939-0470-9_16,

to visualize the distribution, dynamics, and interactions of individual molecules in cells under physiological conditions with a spatial resolution down to ~10 nm. All these novel techniques rely on switching fluorophores between an "on" and an "off" state, so that the emission from fluorophores that are closer in distance than ~200 nm is not detected simultaneously but sequentially. Three principal strategies can be distinguished: In the targeted approach, applied in stimulated emission depletion (STED [4]) or, more generally, in reversible saturable optical fluorescence transitions (RESOLFT [5, 6]) microscopy, a spatial light intensity distribution with areas of zero intensity in space switches the fluorescent markers such that only a minor fraction, located in a region of sub-diffraction extension, is either in the on or off state. In the localization approach, utilized in photoactivation localization microscopy (PALM [7]), fluorescence photoactivation localization microscopy (FPALM [8]), and stochastic optical reconstruction microscopy (STORM [9]), individual molecules are photoactivated, for instance, switched to the fluorescent state (on), randomly in space, while the surrounding molecules remain in the dark (off) state, so that the positions of the individual emitters can be determined with high precision. The fluctuation approach, utilized in super-resolution optical fluctuation imaging (SOFI [10]), relies on the statistical analysis of spatiotemporal fluctuations, i.e., the blinking of fluorophores, to obtain subdiffraction optical resolution in all three dimensions (*see* Chapter 17 for details).

All super-resolution techniques have greatly benefited from the rapid development of novel photoactivatable fluorescence markers, where the emission properties can be controlled by light irradiation. Among the different labels presently available, photoactivatable fluorescent proteins (PA-FPs) of the GFP family have the key advantage of being genetically encodable. Fused to their target in a 1:1 relation, these proteins enable unprecedented insights into the living cell. Photoactivation of PA-FPs can either be irreversible or reversible. Irreversible photoactivation, also known as photoconversion, involves a permanent photochemical modification of the FP. As a consequence, a nonfluorescent (dark) state may get permanently activated to a fluorescent (bright) state, or one bright state may be turned into another bright state with a different emission wavelength (Fig. 1). Reversible photoactivation, also known as photoswitching, typically arises from chromophore isomerization between two conformations only one of which emits fluorescence with high quantum yield (Fig. 1). In the so-called positive photoswitchers, irradiation with light within the fluorescence excitation band increases the fraction of molecules in the on-state; in negative switchers, this fraction is reduced by irradiation with light within the excitation wavelengths [11]. The body of acquired knowledge on photoactivation of FPs has been summarized in several excellent reviews [12–17] including Chapter 12 of this volume.

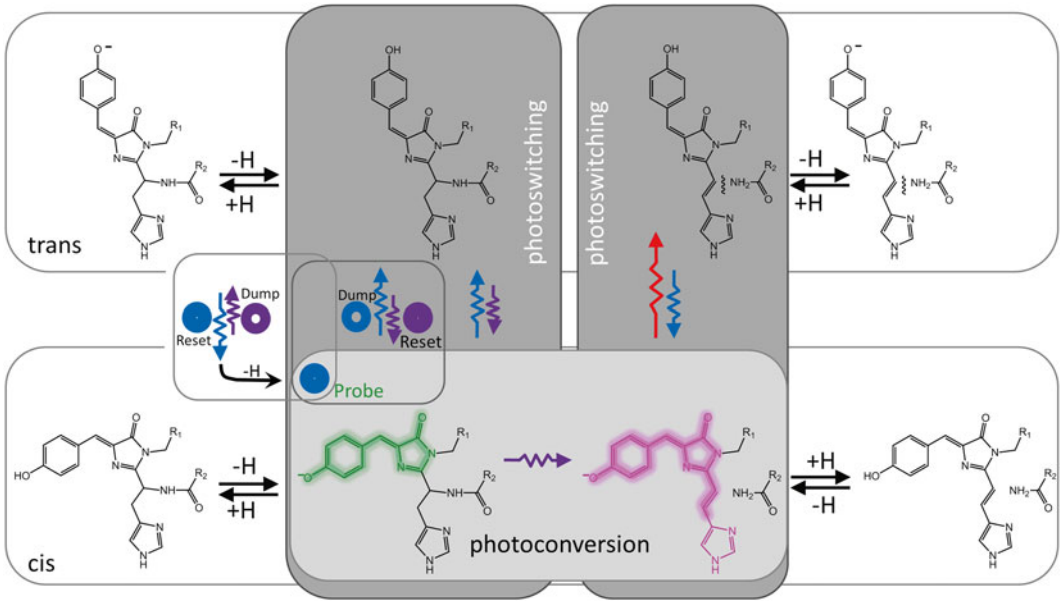

Fig. 1 Photoactivation mechanisms, explained using mIrisFP as an example. Reversible photoswitching occurs between the anionic, fluorescent *cis*, and the neutral, nonfluorescent *trans* chromophores (*dark gray boxes*). Irreversible photoconversion from the green-emitting to the red-emitting state (*light gray box*) extends the conjugated π-electron system of the chromophore. *Straight arrows*: protonation reaction. *Jagged arrows*: Light-activated transition. *Colors* and *lengths* indicate the wavelength of the activation light: *violet/short*: 405 nm, *blue/medium*: 473 (488) nm, *red/long*: 561 (532) nm

Independent of the activation mode, any FP used in fluorescence microscopy applications should feature a large extinction coefficient and fluorescence quantum yield to produce strong signals above background. Moreover, it should mature quickly and efficiently at 37 °C to be applicable in live-cell experiments. For fusion constructs, monomeric variants are preferred to avoid adverse effects, such as oligomerization and aggregation. One should also consider that the cell provides a rather complex and heterogeneous environment, which may influence the properties of the FP under study. In the next sections, we focus on those marker properties that are essential for successful RESOLFT and PALM applications. For a more detailed discussion, we refer the reader to recent review papers and the references therein [16, 18, 19].

1.1 Photoactivatable FPs in RESOLFT

Targeted illumination-based super-resolution microscopy utilizes the nonlinear (switching) response of fluorophores to light irradiation. STED microscopy was the first actual demonstration of this principle. In a STED microscope, the focused laser spot that excites the fluorophores is spatially overlayed with a depletion beam that has a doughnut-like cross-section in the focal plane, with zero intensity in the center. Fluorophores in the periphery of the

excitation spot are efficiently deexcited by stimulated emission. Only fluorophores close to the center escape depletion and can thus spontaneously emit fluorescence photons. Therefore, the effective size of the excitation point spread function (PSF), i.e., the image of a point-like object, is smaller than the diffraction-limited PSF. Due to the short lifetime of the excited electronic state, STED beam laser powers of several MW/cm^2 are required to achieve sufficient deexcitation, which may pose a problem when FPs are to be used because they have a lower photostability than organic fluorophores. The high powers may also cause photodamage in the biological samples.

Instead of depleting the active state of the fluorescent markers by stimulated emission, one can also rely on pumping of a triplet state [20] or exploit a photoswitching mechanism, e.g., *cis-trans* isomerization of fluorophores between bright and dark states [21]. This generalization has been termed RESOLFT [5, 6]. The isomeric states of reversibly photoswitchable FPs (PS-FPs) are long-lived, so that depletion of the fluorescent state by off-switching is possible with beam intensities of only a few kW/cm^2.

The RESOLFT image is acquired by raster scanning the excitation and depletion beams across the sample, with a step size of, at most, half the desired spatial resolution. Therefore, the FPs have to undergo many light-activated transitions between the fluorescent and nonfluorescent states to contribute appreciably to the image. Reversible photoswitching is mandatory. In addition, spontaneous interconversion between active and inactive forms must be slow compared with photoactivation. Photoconvertible FPs cannot be used at all because they can perform only a single, irreversible switching act.

In the experiment, all FPs within a diffraction-limited spot are first reset by a pulse of activating light to establish a uniform chromophore state (Fig. 1, reset). Subsequently, the doughnut-shaped, red-shifted depletion beam is applied to deactivate molecules in the periphery (Fig. 1, dump). Finally, the molecules in the center are probed by a short pulse of excitation light (Fig. 1, probe), again with a diffraction-limited spot size. As there are several fluorophores in the excitation spot that contribute to the signal the brightness of the individual molecule is less important than a high resistance to switching fatigue.

The repetition rate of the illumination sequence and, therefore, the scanning speed of the method, is limited by the transition rates between the activated and the deactivated states. For imaging negative photoswitchers, dump and probe require the same laser wavelength, but different beam profiles. In contrast, reset and probe are achieved with the same diffraction-limited laser, when positive photoswitchers are used (*see* Fig. 1). This concurrent activation and photoexcitation is especially favorable as it reduces the image acquisition time.

1.2 Photoactivatable FPs in PALM

In conventional fluorescence microscopy, many fluorophores are excited simultaneously and, consequently, their PSFs overlap in the resulting image. The image appears blurred. If, however, the fluorophores can be externally controlled, for example by light, so that only a small subset of markers is fluorescent at any given point in time, the individual loci can be determined with a precision well above the resolution limit. This is the basic principle applied in PALM imaging: A subpopulation of marker molecules is stochastically switched on for sequential single-molecule readout.

In a typical experiment, all markers are initially switched to their inactive (off) state. Subsequently, they are sparsely activated by properly adjusting the intensity of the photoactivating light, so that only a few fluorophores appear in each image frame in a wide-field microscope. They can easily and precisely be localized. By repeated image acquisition (10–100 frames/s), a large number of frames (10^2–10^4) are collected and analyzed individually. The final image is, in fact, a density map depicting all molecule positions. To generate these high-resolution density maps, a careful analysis of all individual frames is required. These calculations are computationally demanding, and, until recently, image reconstruction took much longer than data acquisition. Over the past few years, however, the data processing time has been reduced by orders of magnitude, so that localization can keep up with data acquisition [22, 23].

The localization precision of each molecule is roughly proportional to the inverse square root of the acquired photon count. Therefore, a high photon yield in the activated state is essential to achieve a good resolution. In addition, the dynamic range, i.e., the contrast ratio between the fluorescence of the activated (on) and deactivated (off) states, has to be high for precise localization, especially in densely marked samples, to be able to distinguish the single activated fluorophore from the background. These criteria are best met by photoconvertible FPs. Before activation, they are nonfluorescent at the probe wavelength. After activation and upon excitation, they emit photons until they are irreversibly bleached. In fact, irreversible photobleaching is the rate-limiting step because each activated fluorophore has to be bleached before the next fluorophore within the same diffraction-limited spot can be activated—otherwise their PSFs would overlap. Note that, in principle, these FPs should enable an exact molecule counting. In practice, however, blinking of FPs in their photoactivated state has been a major obstacle to the use of PALM for accurate counting [7, 24–26].

PS-FPs are not only excited but also photoswitched by the excitation light. Positive photoswitchers are activated, imaged and bleached by the excitation light. Therefore, they can be considered "photoconvertible." Negative photoswitchers are deactivated by the excitation light. The number of photons detected in each switching cycle is limited by the off-switching rate: the slower the

isomerization kinetics, the higher the photon counts per cycle and the lower the overall number of cycles, but the better the localization precision. Therefore, these PS-FPs can undergo multiple switching cycles, e.g., appear in multiple frames, before falling victim to photodestruction.

1.3 Photoactivatable FPs in Dual-Color PALM

In the following protocol, we shall illustrate how two FPs with different photoactivation mechanisms can be utilized in high-resolution dual-color PALM imaging to obtain insights into a cellular substructure that otherwise would not be accessible.

The green-to-red photoconvertible mEosFP*thermo* (Table 1) and the reversibly photoswitchable green fluorescent mIrisGFP (Table 1) are variants of EosFP [27, 28] and IrisFP [29, 30], respectively. They were fused to mutant and wild-type desmin proteins, respectively. Desmin forms intermediate filaments in cardiac, skeletal, and smooth muscle cells. Certain point mutations in the desmin gene cause desmin aggresomes to form. Individuals who carry these mutations suffer from arrhythmogenic right ventricular cardiomyopathy. To understand the pathogenesis of this disease, it is essential to analyze desmin filament structures under conditions in which both healthy (wild-type) and mutant desmin are present in a cell. Therefore, desmin mutant N116S and wild-type desmin were co-expressed in living SW-13 cells, which lack endogenous desmin, to investigate their mutual effects on filament assembly [31].

Dual-color PALM is a serial approach. The experiment is started by imaging mEosFP*thermo*. The initially green-fluorescent mEosFP*thermo* molecules are activated, i.e., turned red-fluorescent, localized based on their red emission and bleached by continuous exposure to activation (405 nm) and excitation light (561 nm). Eventually, over the course of thousands of frames, the supply of mEosFP*thermo* molecules is exhausted. Subsequently, the mIrisGFP molecules are imaged. After switching all molecules off, activation (405 nm) and excitation (473 nm) light are applied until all

Table 1
Optical properties of mEosFP*thermo* and mIrisGFP

	Exc. max (nm)	Em. max (nm)	On switch (nm)	Off switch (nm)	Exc. max (nm)	Em. max (nm)	ε (M^{-1} cm^{-1})	QY	References
Fluorescent protein	**Inactivated**				**Activated**				
mEosFP*thermo* (G)	506	516	405	–	–	–	72,000	0.70	[47, 48]
mEosFP*thermo* (R)					569	581	41,000	0.55	[47, 48]
mIrisGFP (G)	–	–	405	473	488	516	47,000	0.63	[49]

G green, *R* red

mIrisGFP molecules have been activated, e.g., photoswitched to the on state, localized based on their green emission, and bleached. Finally, the localization maps obtained for the two FPs are superimposed to yield the dual-color PALM image of the relative distributions of the two target proteins, desmin-N116S and wild-type desmin, within the filaments. Note that the sequence of measurements is important because otherwise the large pool of pre-activated green mEosFP*thermo* molecules may form a bright background that impedes the localization of single activated mIrisGFP molecules based on their green fluorescence.

2 Materials

2.1 Reagents

1. SW-13 cells (LGC Standards, Middlesex, UK).
2. Cell culture medium without phenol red, such as Dulbecco's Modified Eagle Medium (DMEM) supplemented with 10 % fetal bovine serum (FBS).
3. Penicillin–Streptomycin.
4. Dulbecco's Phosphate-Buffered Saline (DPBS).
5. Transfection reagent, such as Lipofectamine 2000 (Invitrogen, Life Technologies GmbH).
6. Plasmids (pmEosFP*thermo*-Desmin-N116S and pmIrisGFP-Desmin [31]).
7. LabTek chambered cover glasses (#1, Nunc, 155383 or 155411, Thermo Scientific, Dreieich, Germany).
8. 4 % (w/v) paraformaldehyde (PFA) in DPBS (*see* **Note 1**).
9. 100-nm fluorescent microspheres as fiducial markers (TetraSpeck, T7279, Invitrogen).

2.2 Instrumentation

In principle, PALM images of thin biological samples may be obtained with any inverted epifluorescence/TIRF (Total internal reflection fluorescence) microscope setup. Some companies offer microscope systems specifically designed for localization based super-resolution imaging. In this section, we provide some general guidelines for choosing key components and present a list of components of the microscope that we use in our laboratory (Table 2). A schematic depiction is provided in Fig. 2.

2.2.1 Microscope Body

Any commercial inverted microscope frame that is compatible with epifluorescence/TIRF measurements may be used. Multiple ports (side, back, bottom) may be useful to perform experiments that require different optical detection pathways, such as multicolor or 3D PALM measurements. An automated axial drift correction device will help to maintain the focus throughout the experiment. For 3D PALM measurements, which are not addressed in this

Table 2
Components of our current PALM setup

Microscope		
Microscope body	Axiovert 200	Zeiss, Jena, Germany
Axial drift correction	Definite Focus	Zeiss
Objective scanner	Fast PIFOC® Piezo Nanofocusing Z-Drive, PD72Z1	Physik Instrumente, Karlsruhe, Germany
Dichroic filter	zt405/488/561/640rpc TIRF	Chroma (via AHF), Tübingen, Germany
Objective		
	Alpha Plan-Apochromat 63×, NA 1.46 Oil	Zeiss
Illumination		
Lasers	405 nm, CLASII 405-50	Blue Sky Research, Milpitas, CA, USA
	473 nm, LSR473-200-T00	Laserlight, Berlin, Germany
	561 nm, GCL-150-561	CrystaLaser, Reno, NV, USA
	642 nm, LBX-642	Oxxius, Lannion, France
Laser intensity control	Acousto optic tunable filter AOTFnC-400.650, A-A	Opto-Electronic, Orsay Cedex, France
Dichroic filters	R405, R473, R561	Semrock (via AHF)
Detection		
	Optosplit II	Cairn Research, UK
Filter	535/70 bandpass (HQ 535/70)	Chroma (via AHF)
	610/75 bandpass (HQ 610/75)	Chroma (via AHF)
Beam splitter	Zeiss FT 580 (dichroic)	Zeiss
Camera	EMCCD iXon^{EM} + DU-860 (128 × 128 pixel chip)	Andor Technology, Belfast, Northern Ireland
	EMCCD DV887ECS-BV (512 × 512 pixel chip)	
Computer hardware		
Instrument control	Intel(R) Core(TM)2 Quad CPU Q9650 (3.00 GHz), 4.0 GB memory	
Data analysis	Intel(R) Core(TM) i7-2600 processor (3.40 GHz), 8.0 GB memory	
Software		
	Andor Solis	Andor Technology
	LabView	National Instruments, Munich, Germany
	Matlab with DIP*image*	The MathWorks, Natick, MA, USA Delft University of Technology, Delft, Netherlands
	ImageJ	National Institutes of Health, MD, USA

protocol, a high precision objective scanner will be necessary in addition. For localization-based super-resolution microscopy measurements on thick samples, one can alternatively use selective plane illumination microscopy (SPIM) [32, 33].

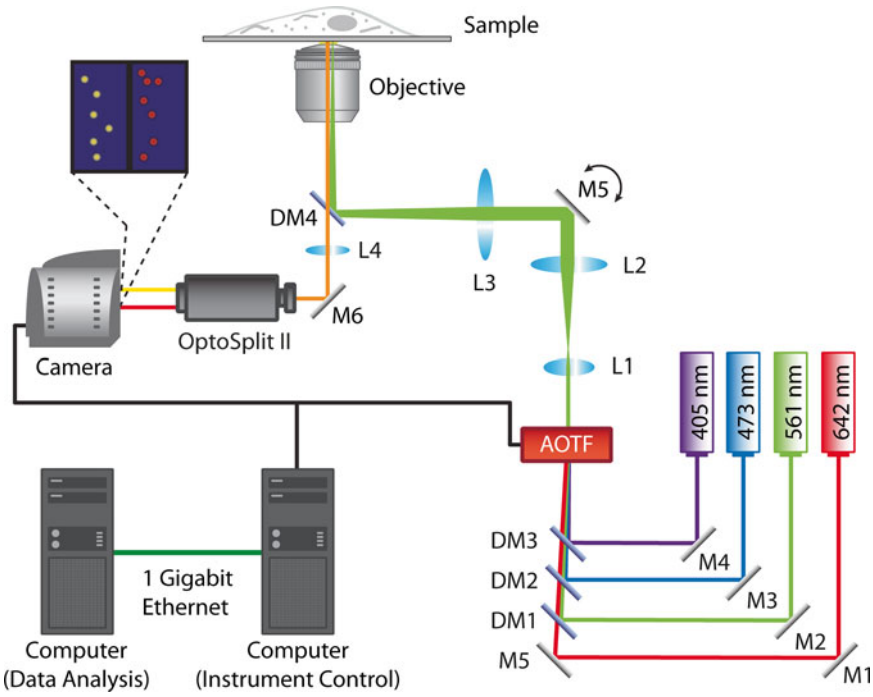

Fig. 2 An instrumentation schematic for 2D PALM imaging experiments. *M* mirror, *DM*, dichroic mirror, *L* lens, *AOTF* acousto-optical tunable filter

2.2.2 Objective Lens

The NA of the objective lens must be greater than the refractive index, n, of the sample to be able to achieve TIRF (for cellular components, $n \approx 1.38$). Therefore, oil immersion objective lenses with NA 1.45, 1.49, or 1.65 are required (*see* **Note 2**). The higher the NA, the better is the photon collection efficiency of the objective and, consequently, the signal-to-noise ratio (SNR) and the localization precision.

2.2.3 Illumination Sources

Common diode-pumped solid-state lasers used for conventional fluorescence microscopy may also be used for PALM experiments. Laser sources with powers >100 mW are recommended so that the setup is flexible enough to accommodate a wide variety of fluorophores. Most PA-FPs are activated with 405-nm light. Therefore, a laser with this wavelength is mandatory. Green and red-orange FPs are typically excited with 473-nm (or 488-nm) and 561-nm (532-nm) light, respectively. The same set of lasers is also necessary for activation and deactivation of green and red PS-FPs.

Preferentially, all laser sources should be coupled into an acousto-optical tunable filter (AOTF) for convenient wavelength selection and fast adjustment of their intensities. The device also enables fast switching between lasers. In addition, the AOTF allows illumination of the sample according to pre-programmed

illumination schemes, e.g., alternating excitation with two lasers. The AOTF may also be synchronized with the data acquisition cycle of the camera to minimize photobleaching during camera read-out.

2.2.4 Fluorescence Detection

State of the art back-illuminated EMCCD cameras provide near 100 % quantum efficiency and very low background noise. They have been the standard in single molecule measurements. They are equipped with chips of 128×128 pixels up to 1024×1024 pixels, with a typical pixel size of 16×16 μm^2. Smaller chips have reduced acquisition times (128×128 pixel: ~500 frames/s, 512×512 pixel: ~30 frames/s) and data file sizes. It is also possible to use only a small region of a large chip. The performances of sCMOS cameras have been continually improving in recent years. They may also be used for PALM experiments [34, 35].

2.2.5 Computer

It is advisable to have two desktop computers, one for the instrument control and the second one for the "online" data analysis. In our setup, the instrument computer runs Andor Solis (Andor Technologies) for controlling the camera and LabView for controlling the lasers. As the cameras typically come with their own computer card, one has to make sure that the computer has an appropriate empty slot. The raw data recorded by the camera are transferred immediately from the instrument computer to the data analysis computer via a 1-Gbit ethernet cable to permit PALM data analysis during data acquisition without increasing the processing load on the instrument computer. Because we use graphics processing units (GPUs) to run some routines of our data analysis software, it is crucial for the data analysis computer to be equipped with a CUDA enabled graphics card, such as the NVIDIA GeForce GTX 560Ti and GTS 450. For an image of 128×128 (512×512) pixels acquired by the camera, the processing time is 2–5 (15–30) ms, depending on its complexity. The speed is comparable to the maximum frame rate of current EMCCD cameras and, therefore, allows real-time data processing.

3 Methods

3.1 Sample Preparation

1. Culture SW-13 cells to an optimal density (20–30 % surface coverage to avoid multiple cell layers) in a chambered cover glass system in DMEM supplemented with 10 % FBS and penicillin/streptomycin according to standard cell culturing procedures (*see* **Note 3**).
2. Transfect the cells with 800 ng of plasmid DNA for a single transfection and 400 ng of each plasmid for co-transfections, using Lipofectamine 2000 according to the manufacturer's protocol. Prepare cells without transfection (negative control),

with pmEosFP*thermo*–Desmin-N116S only (mEosFP*thermo* control), with pmIrisGFP–Desmin only (mIrisGFP control) and with both pmEosFPthermo–Desmin-N116S/pmIrisGFP–Desmin. Replace the medium 8 h after transfection.

3. For sample stabilization, fix the cells by incubating them in 4 % PFA for 30 min (*see* **Note 4**). Then wash thoroughly with DPBS. Omit the fixation step for live-cell imaging experiments.
4. Suspend fluorescent microspheres in DPBS (*see* **Note 5**). Exchange the DPBS covering the fixed cells with microsphere-containing buffer, incubate for 10 min and wash with DPBS. Adding fiducials is especially important for long acquisition times. For dual-color experiments, it is essential that the fiducials show up in both color channels.

3.2 Data Acquisition

1. Instrument warm up. Turn on the microscope system and the lasers at least 1 h prior to beginning the experiment (*see* **Note 6**).
2. For live cells, record a bright-field image before and after PALM data collection to control cell viability.
3. Sample validation. With low 473-nm illumination, identify a cell that expresses a high level of fluorophores. Be aware that, at this point, mEosFP*thermo* and mIrisGFP cannot be distinguished based on their emission. Collect 50 image frames with 100 ms exposure time each. Sum these images and check for the proper protein expression level and the phenotype of the target protein (*see* **Note 7**).
4. Laser intensity adjustment to image mEosFP*thermo* (*see* **Note 8**). Focus onto a cell that is transfected with mEosFP*thermo* only (mEosFP*thermo* control chamber). Initially, illuminate the sample with the 561-nm laser to bleach the small population of mEosFP*thermo* that is already activated, e.g., emits red fluorescence. Then add the 405-nm laser for photoconversion of additional molecules and adjust the 405- and 561-nm illumination powers such that signals from individual red fluorescent mEosFP*thermo* molecules are detectable by the analysis software (*see* **Note 9**). With our instrumental setup and an integration time of 3 ms per frame, sufficient green-to-red photoconversion is achieved with 405-nm light at 0–0.2 kW/cm^2. The red form of mEosFP*thermo* is imaged with 561 nm at 2.5–4.5 kW/cm^2. As the pool of inactivated mEosFP*thermo* is more and more depleted, it is advisable to increase the power of the activation laser to keep the number of activated fluorophores per frame constant.
5. Laser intensity adjustment to image mIrisGFP (*see* **Note 10**). Focus onto a cell that is transfected with mIrisGFP only (mIris GFP control chamber). Initially, most mIrisGFP molecules will be in the activated form and contribute to a bright green background signal. Illuminate the sample with 473-nm light to reduce the

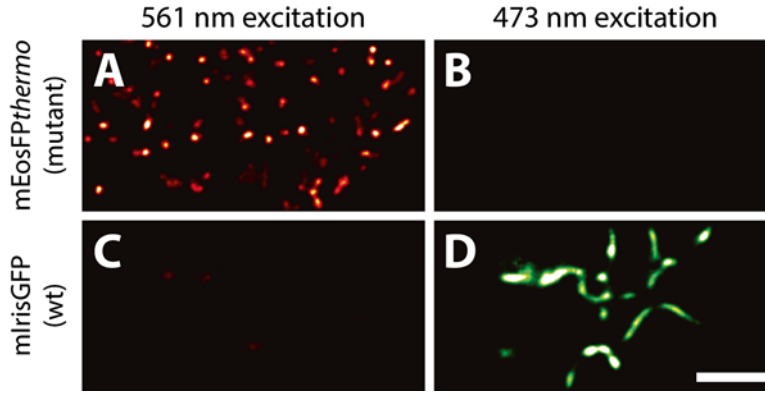

Fig. 3 Cross talk control. (**a**) PALM image of activated mEosFP*thermo* fused to desmin mutant N116S in the red channel. (**b**) The control image in the green channel reveals that mEosFP*thermo* has been fully activated. No residual green signal is detectable. (**d**) PALM image of mIrisGFP fused to (wild-type) desmin in the green channel. (**c**) The control image of mIrisGFP in the red channel verifies that photoconversion to the red-emitting form is absent. Scale bar: 2 μm

number of activated mIrisGFP molecules. Then adjust the 405-nm and 473-nm illumination powers such that single mIrisGFP signals are detectable by the analysis software. With our instrument, on switching requires 0–0.2 kW/cm^2 of 405-nm light (for an exposure time of 3 ms/frame). Imaging and off-switching of mIrisGFP is performed at epifluorescence excitation of 2.8–3.6 kW/cm^2 at 473 nm.

6. Turn on the drift control device.
7. Cross-talk control—part I. By focusing on a new cell in the mEosFP*thermo* control chamber, collect 5,000–20,000 image frames (depending on the protein expression level) until no further molecules are observable in the red channel using the selected laser intensities. To confirm that all mEosFP*thermo*-molecules are indeed converted to their red-emitting forms, turn off the 561-nm laser and turn on the 473-nm laser. Make sure that there is no residual signal in the green channel (Fig. 3a, b). This step guarantees that no EosFP*thermo* molecules are incorrectly identified as mIrisGFP molecules (*see* **Note 11**).
8. Cross-talk control—part II. To make sure that mIrisGFP is not converted to a red emitting form, image cells transfected only with mIrisGFP with the appropriate illumination protocol (as determined in **step 5**). Upon completion of the illumination series, use the 561-nm laser to ensure that there is no signal detectable in the red channel (Fig. 3c, d).
9. Dual-color PALM data acquisition. On a co-transfected cell in the mEosFP*thermo*–Desmin-N116S/mIrisGFP–Desmin chamber, collect 5,000–20,000 frames (depending on the protein expression level) using the laser intensity settings for

mEosFP*thermo* (*see* **step 4**). If no more molecules are detectable in the red channel with photoconverting 405-nm irradiation, obtain 5,000–20,000 frames using the illumination settings determined for mIrisGFP (**step 5**, *see* **Note 12**).

3.3 Data Analysis

The raw data of a single PALM measurement consist of a stack of several thousand diffraction-limited images. The information stored in each frame has to be extracted and subsequently combined to yield the reconstructed image, e.g., the map of all molecule locations. In a first step, regions where single molecules are present have to be filtered out of the background within each individual frame. Typically, the molecule detection algorithm in the analysis software package utilizes a certain set of initial parameters to define a threshold. Each signal above this threshold is considered a molecule. However, setting the proper threshold turns out to be a major challenge when working with biological samples because both the SNR and the signal-to-background ratio (SBR) are often heterogeneous, even within the same imaging area, and, in addition, may fluctuate over time, for example due to photobleaching of the fluorophores or fluctuations in the laser intensity. Improper thresholding, however, will result either in missing valid molecules or in mistaking noise for real molecules (*see* **Note 13**).

We have recently developed a GPU-based software called "a-livePALM" with significant improvements in the molecule detection efficiency while maintaining high precision and fast processing speed (Fig. 4) [36]. Briefly, the algorithm subdivides the raw image into many subregions to characterize the local background level (the standard deviation and the mean). Using this information, the probability of each pixel to be part of the surrounding background is computed in the form of a P value ($P = 1 -$ normal cumulative distribution function, Fig. 5). This approach is insensitive to changes in the SNR and the SBR (either between frames or even within a single image) and, therefore, significantly enhances the signal contrast without distorting the image. Local maxima with a P value below a certain threshold are considered to be molecule candidates (*see* **Note 14**, Fig. 5). Conventional molecule detection algorithms require a homogeneous background, both within the image and over the course of the experiment, or a continuous manual adjustment of the threshold values in order to achieve a similar performance.

In the following, we will guide the reader through the basic steps of the a-livePALM software (which is available upon request). Additional details regarding parameter selection and software installation may be found in the associated software manual.

1. Data loading. In the "a-live PALM Analyzer" panel (see screenshot of the user interface in Fig. 6), load the image file (stacked tif file format), select the output directory and enter the output file name (*see* **Note 15**).

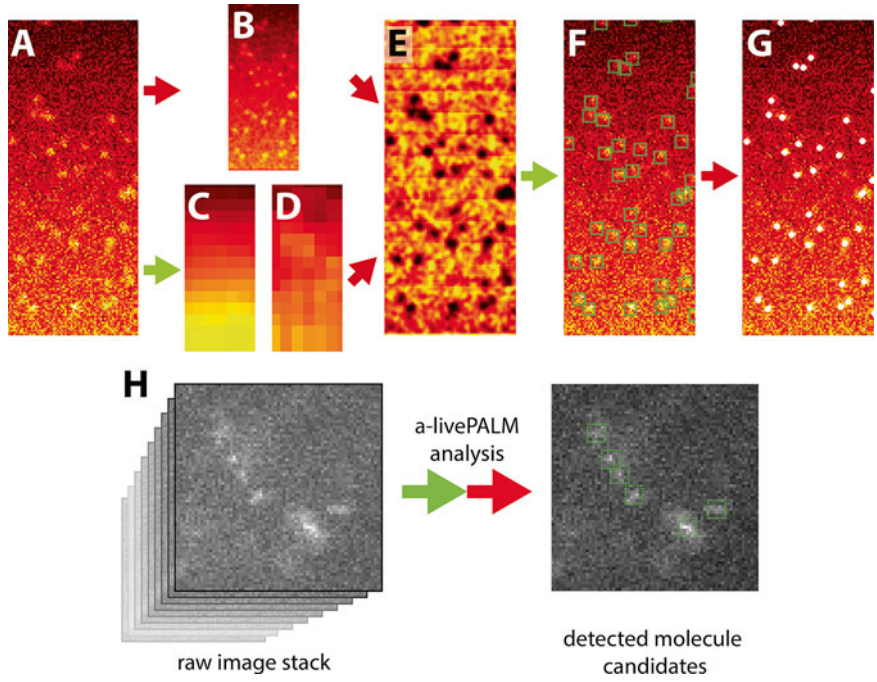

Fig. 4 Molecule detection by a-livePALM. For noise reduction, the raw image (**a**) is smoothed with a Gaussian kernel (**b**). In addition, each image is subdivided into small local areas, and the background within these areas is quantified by the mean value (**c**) and the standard deviation (**d**). (**e**) The *P* value, which represents the probability of a pixel to be part of the surrounding background, is calculated for each pixel in the smoothed image (**d**), using the obtained background information (**c** and **d**). (**f**) Local maxima with a *P* value below a threshold (compare Fig. 6) are assigned to molecule candidates. (**g**) *Circles* mark the final molecule locations obtained from the analysis. (**h**) The preview image allows controlling the molecule candidate selection step. *Green (light gray) arrows*: CPU-based computation. *Red (dark gray) arrows*: GPU-based computation

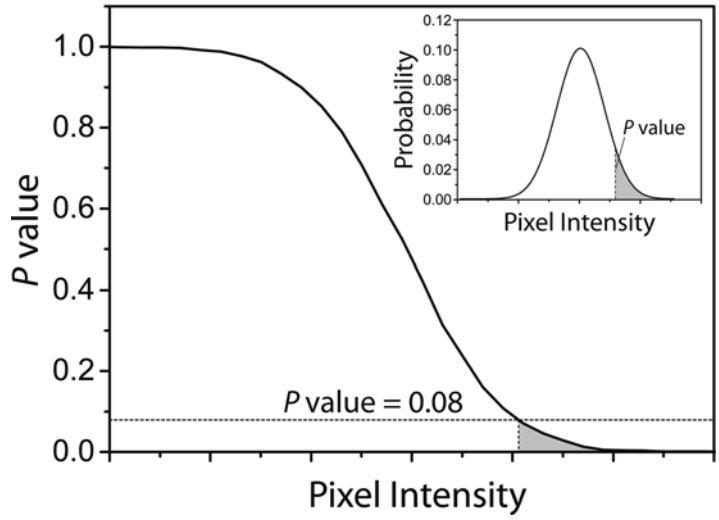

Fig. 5 Visualization of the *P* value. The *P* value is given by $P = 1 - \mathrm{CDF}$. It describes the probability that a certain pixel intensity is part of the surrounding background. *Inset*: Probability density distribution of the measured pixel intensities. The population with a *P* value below the assigned threshold (here: $P = 0.08$) is shaded in *gray*

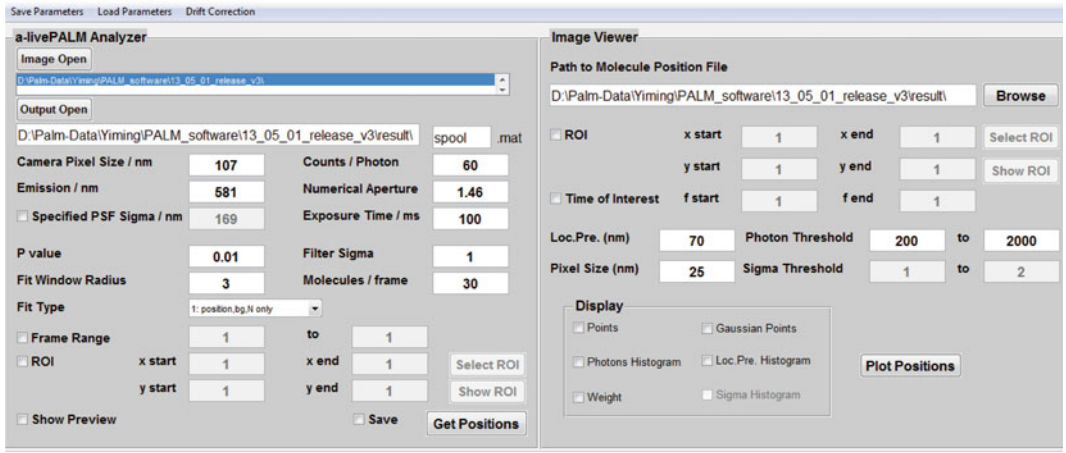

Fig. 6 User interface of the a-livePALM analysis software. The *left* and *right panels* are used for data analysis and image visualization, respectively

2. Basic analysis parameters. Enter basic experimental parameters (camera pixel size, counts/photon conversion factor, detection wavelength, numerical aperture of the objective lens, and the camera exposure time, *see* **Note 16**).
3. Thresholding. Enter a *P* value of 0.08 as a start, select five to ten representative frames via the "Frame range" option, and checkmark the "Show Preview" option. Press "Get Positions" to analyze the selected frames. As a result, the preview image will be displayed, with the detected molecule regions marked by a square. Make sure that all molecules are properly selected. Enter a different *P* value if necessary. Repeat these steps until a proper *P* value is selected (*see* **Note 17**).
4. Data Processing. Uncheck the "Frame range" and the "Show Preview" options, check the "Save" option and press "Get Positions" to analyze the entire image stack. The output file, which is essentially a list of molecule coordinates, photon counts, localization precisions, sigma widths, and photon appearance times, will be saved in the selected directory.
5. Image visualization. The output file may easily be visualized using the right hand panel of the software user interface. Load the output file, check the desired display options and press "Plot Positions" to view the reconstructed image (*see* **Note 18**). Different threshold parameters (photon threshold, localization precision, and sigma width) may be applied.
6. Image overlay. In the final step, the PALM images obtained in the green and red channels have to be superimposed (Fig. 7). Therefore, three fiducials visible in both channels are selected. Their positions are used to calculate an affine transform matrix which is then applied to one of the output files to map it onto

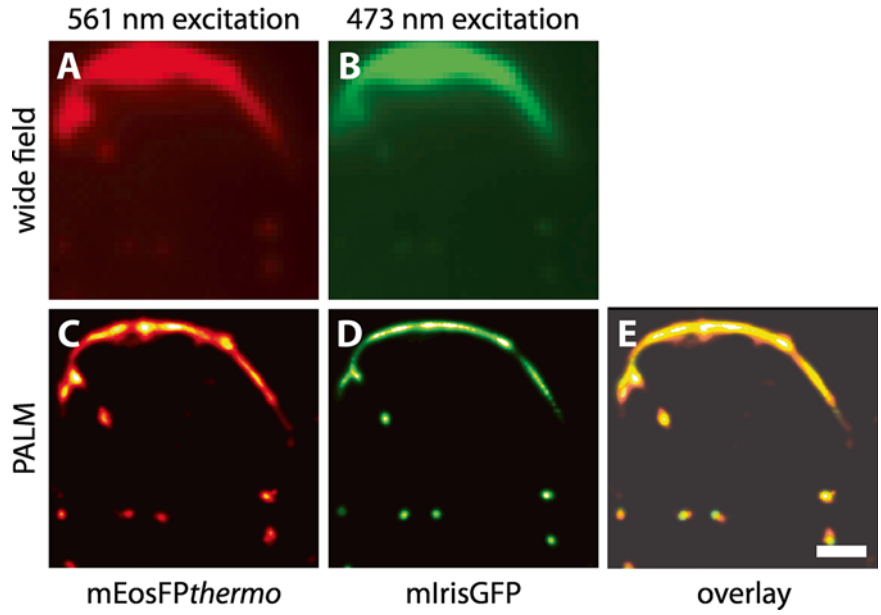

Fig. 7 Dual color PALM images of SW-13 cells co-expressing wild-type desmin fused to mIrisGFP and desmin mutant N116S labeled with mEosFP*thermo*. (**a**, **b**) Wide-field images, (**c**, **d**) individual PALM images, (**e**) dual-color PALM image. Scale bar: 1 μm. Wild-type desmin typically assembles into filamentous networks in SW-13 cells, whereas desmin mutant N116S in SW-13 cells forms cytoplasmic aggregates upon homozygous transient expression [31]. Co-expression of desmin mutant N116S and wild-type desmin, as shown here, leads to both filament and aggregate formation within the same cell, and all structural features seen in the image contain both desmin types; no segregation occurs. Compared with conventional microscopy, PALM imaging provides a higher confidence level of colocalization and more accurate structural information. In fact, closely spaced punctate aggregates arranged along a line could be mistaken as filaments when using conventional microscopy techniques. Slight displacements of the mutant and wild-type desmin signals likely arise from cell movement while the images in the green and red channels were acquired in sequence

the other output file. Coordinate-corrected images may be overlaid using ImageJ.

7. Extended PALM data analysis. Apart from plotting the data stored in the output file as a super-resolution image, this information may also be used to plot trajectories of individual molecules [37] or to quantify the local concentration of molecules [38–40] (*see* **Note 19**). The dual-color PALM data may also be used to obtain super-resolution co-localization data by applying a conventional analysis to the high resolution data.

4 Notes

1. This chemical is poisonous. Make sure that you wear appropriate protective equipment to avoid direct skin or eye contact.
2. Make sure to use the correct immersion oil and coverslips of suitable thickness to minimize image abberations.

3. Thin, adherent mammalian cell types, such as HeLa, HEK293 and COS7 cells, are ideal for PALM imaging. To enhance surface adhesion of the cells, the coverslip may be coated with poly-L-lysine or fibronectin. Make sure that there are no fluorescent contaminants in these reagents by imaging the surface-coated coverslip before adding the cells.
4. Image the fixed cells as soon as possible because some FPs will degrade after fixation.
5. Typically, the stock solution is diluted 1:1,000 to have only a few fiducials (two to five) appear in the field of view. Depending on the batch and the surface condition, this ratio may have to be adjusted.
6. This step will minimize the instrument drift.
7. It is important to see a cellular feature typically obtained by epifluorescence/TIRF microscopy at this point. Otherwise, it is highly unlikely to obtain a super-resolution image. Summing up frames may easily be accomplished by an image processing software such as ImageJ.
8. Essentially the same procedure can be followed to record single-color PALM images. Instead of mEosFP*thermo*, other photoconvertible FPs may be used. However, the laser wavelengths and the laser powers have to be adjusted with respect to the chosen FP and the experimental boundary conditions. If time resolution is not important, the exposure times may be increased to 50 ms/frame. Concomitantly, lower laser powers are sufficient (e.g., for mEosFP*thermo*: 405 nm: 0–0.02 kW/cm^2, 561 nm: 0.3–0.5 kW/cm^2).
9. The density of activated molecules should be <0.5 molecules/μm^2 to attain >90 % detection efficiency using our software. With the 128 × 128 pixel camera (pixel size 14.72 × 14.72 μm^2), this is equivalent to ~100 molecules per field of view. For imaging a dense filament-like structure, the local fluorophore density should be used for the estimation rather than the overall density. The preview feature of the software is a useful tool to visually check how well molecules are being detected.
10. Essentially the same procedure can be used to obtain single-color PALM images using other negatively photoswitching green FPs. Again, laser wavelength and power have to be adjusted for the individual experiment. For a positive photoswitcher, photoactivation, fluorescence excitation, and photobleaching are achieved with light of the same wavelength. Therefore, it may be possible to adjust the laser power such that the equilibrium between photobleaching of the fluorescent molecules and photoactivation of the nonfluorescent molecules keeps the number of molecules in the on-state constant, in a perfect range for PALM experiments so that a second, deactivating laser becomes obsolete.

11. Only green-to-red photoconvertible FPs that can be fully converted to the red state should be used.
12. The OptoSplit II device is part of our setup, but it is not required for serial dual-color PALM data collection. It allows recording the fluorescence emission in two separate channels simultaneously on the same camera. Care must be taken to ensure that the focal planes of the two channels are well aligned to each other. Problems may arise when dichroic mirrors with hard coatings are used. While these mirrors often perform better in terms of transmission/reflection and sharpness of the cutoff, the coating may introduce a slight curvature to the mirror and, thus, change the focal length of the transmitted light to create a mismatch between the channels.
13. The performance of a search algorithm is evaluated by two parameters, "recall" and "precision." Recall is defined as the ratio of the number of true positive molecules to the total number of molecules. Precision is defined as the ratio of the number of true positive molecules to the number of all detected molecules (i.e., true + false). It is obvious that a high precision is easily achieved by setting the threshold to a high value. The trade-off is a low recall. And vice versa, a low threshold results in a high recall and a low precision. To judge and compare the overall performance of different algorithms, the so-called *F*-measure or *F*-score is calculated, with $F = 2 \times \text{precision} \times \text{recall}/(\text{precision} + \text{recall})$. It can be interpreted as a weighted average of the precision and the recall, with $F = 1$ for the best performance. In the past few years, many different software packages for PALM data analysis have been presented. Most of them, including our older algorithm, utilize variations of the so-called DAOFIND algorithm for molecule detection [7, 9, 23, 41–44]. We found that all left room for improvement in either processing speed or molecule recall.
14. As image reconstruction requires processing thousands of image frames, it is desirable that the analysis algorithm can run at high speed to keep up with the image acquisition to allow for intuitive and interactive data acquisition. However, the added data processing steps (as implemented in our new algorithm) obviously increase the computational load. By parallelizing molecule localization using GPUs instead of the conventional central processing units (CPUs), our data analysis software runs at similar speeds as any other freely available fast software.
15. At this point, a region of interest (ROI) may be selected by using the "Select ROI" feature. Limiting the size of the image reduces the data processing time.
16. It is especially important to correctly enter the camera pixel size and counts/photon conversion factor to determine the scale of the final image and the localization accuracy. The camera pixel

size may be measured using a standard microscope calibration grid, and the conversion factor may be obtained by following the camera manufacturer's protocol. For analyzing the data using a fixed sigma, detection wavelength and the NA of the objective lens are necessary to compute the sigma value of a theoretical PSF. Alternatively, one can manually specify the sigma value of the PSF after tickmarking "Specified PSF Sigma."

17. Based on previous analyses of experimental and simulated images, a *P* value in the range 0.01–0.08 is appropriate for a typical PALM data analysis. With a properly selected *P* value, all molecules displayed in the preview panel should be selected (indicated by the red boxes, *see* Fig. 4f), and a minimal number of empty boxes should be present.
18. If necessary, the drift correction may be performed at this point. During long acquisition times, mechanical drifts on the order of >100 nm occur rather frequently. An uncorrected drift will lead to blurring of the final PALM picture. In the menu bar, select "Drift Correction > Select a Bead" to open a single raw image out of the stack of raw images that was just analyzed. Press "Select" in the menu bar and manually select the center of a fiducial marker in the image. Press "Confirm" to compute its lateral drift in each frame (relative to the initial position) and to automatically correct the molecule positions recorded in the output file for this drift.
19. Recently, it was reported that even photoconvertible FPs can be activated more than once because, instead of being permanently bleached by the excitation light, they may enter a long-lived dark state [45, 46]. In a molecule counting experiment, the actual number of fluorophores may, therefore, be overestimated unless the transient dark state is taken into account.

Acknowledgments

This work was supported by the Deutsche Forschungsgemeinschaft (DFG) and the State of Baden-Württemberg through the Center for Functional Nanostructures (CFN) and by DFG grant Ni 291/9.

References

1. Abbe E (1873) Beiträge zur Theorie des Mikroskops und der mikroskopischen Wahrnehmung. Arch Mikr Anat 9:413–468. doi:10.1007/BF02956173
2. Hedde PN, Nienhaus GU (2010) Optical imaging of nanoscale cellular structures. Biophys Rev 2:147–158. doi:10.1007/s12551-010-0037-0
3. Hell SW (2007) Far-field optical nanoscopy. Science 316(5828):1153–1158. doi:10.1126/science.1137395
4. Hell SW, Wichmann J (1994) Breaking the diffraction resolution limit by stimulated emission: stimulated-emission-depletion fluorescence microscopy. Opt Lett 19(11):780–782. doi:10.1364/OL.19.000780

5. Bossi M, Fölling J, Dyba M, Westphal V, Hell SW (2006) Breaking the diffraction resolution barrier in far-field microscopy by molecular optical bistability. New J Phys 8:275. doi:10.1088/1367-2630/8/11/275
6. Hofmann M, Eggeling C, Jakobs S, Hell SW (2005) Breaking the diffraction barrier in fluorescence microscopy at low light intensities by using reversibly photoswitchable proteins. Proc Natl Acad Sci U S A 102(49):17565–17569. doi:10.1073/pnas.0506010102
7. Betzig E, Patterson GH, Sougrat R, Lindwasser OW, Olenych S, Bonifacino JS, Davidson MW, Lippincott-Schwartz J, Hess HF (2006) Imaging intracellular fluorescent proteins at nanometer resolution. Science 313(5793):1642–1645. doi:10.1126/science.1127344
8. Hess ST, Girirajan TP, Mason MD (2006) Ultra-high resolution imaging by fluorescence photoactivation localization microscopy. Biophys J 91(11):4258–4272. doi:10.1529/biophysj.106.091116
9. Rust MJ, Bates M, Zhuang X (2006) Sub-diffraction-limit imaging by stochastic optical reconstruction microscopy (STORM). Nat Methods 3(10):793–795. doi:10.1038/nmeth929
10. Dertinger T, Colyer R, Iyer G, Weiss S, Enderlein J (2009) Fast, background-free, 3D super-resolution optical fluctuation imaging (SOFI). Proc Natl Acad Sci U S A 106(52):22287–22292. doi:10.1073/pnas.0907866106
11. Stiel AC, Andresen M, Bock H, Hilbert M, Schilde J, Schönle A, Eggeling C, Egner A, Hell SW, Jakobs S (2008) Generation of monomeric reversibly switchable red fluorescent proteins for far-field fluorescence nanoscopy. Biophys J 95(6):2989–2997. doi:10.1529/biophysj.108.130146
12. Lukyanov KA, Chudakov DM, Lukyanov S, Verkhusha VV (2005) Innovation: photoactivatable fluorescent proteins. Nat Rev Mol Cell Biol 6(11):885–891. doi:10.1038/nrm1741
13. Lippincott-Schwartz J, Patterson GH (2009) Photoactivatable fluorescent proteins for diffraction-limited and super-resolution imaging. Trends Cell Biol 19(11):555–565. doi:10.1016/j.tcb.2009.09.003
14. Bourgeois D, Adam V (2012) Reversible photoswitching in fluorescent proteins: a mechanistic view. IUBMB Life 64(6):482–491. doi:10.1002/iub.1023
15. Finan K, Flottmann B, Heilemann M (2013) Photoswitchable fluorophores for single-molecule localization microscopy. Methods Mol Biol 950:131–151. doi:10.1007/978-1-62703-137-0_9
16. Chudakov DM, Matz MV, Lukyanov S, Lukyanov KA (2010) Fluorescent proteins and their applications in imaging living cells and tissues. Physiol Rev 90(3):1103–1163. doi:10.1152/physrev.00038.2009
17. Wiedenmann J, Nienhaus GU (2006) Live-cell imaging with EosFP and other photoactivatable marker proteins of the GFP family. Expert Rev Proteomics 3(3):361–374. doi:10.1586/14789450.3.3.361
18. Day RN, Davidson MW (2009) The fluorescent protein palette: tools for cellular imaging. Chem Soc Rev 38(10):2887–2921. doi:10.1039/b901966a
19. Patterson GH (2011) Highlights of the optical highlighter fluorescent proteins. J Microsc 243(1):1–7. doi:10.1111/j.1365-2818.2011.03505.x
20. Bretschneider S, Eggeling C, Hell SW (2007) Breaking the diffraction barrier in fluorescence microscopy by optical shelving. Phys Rev Lett 98(21):218103. doi:10.1103/PhysRevLett.98.218103
21. Dedecker P, Hotta J, Flors C, Sliwa M, Uji-i H, Roeffaers MB, Ando R, Mizuno H, Miyawaki A, Hofkens J (2007) Subdiffraction imaging through the selective donut-mode depletion of thermally stable photoswitchable fluorophores: numerical analysis and application to the fluorescent protein Dronpa. J Am Chem Soc 129(51):16132–16141. doi:10.1021/ja076128z
22. Hedde PN, Fuchs J, Oswald F, Wiedenmann J, Nienhaus GU (2009) Online image analysis software for photoactivation localization microscopy. Nat Methods 6(10):689–690. doi:10.1038/nmeth1009-689
23. Quan T, Li P, Long F, Zeng S, Luo Q, Hedde PN, Nienhaus GU, Huang Z-L (2010) Ultrafast, high-precision image analysis for localization-based super resolution microscopy. Opt Express 18(11):11867–11876. doi:10.1364/OE.18.011867
24. Subach FV, Patterson GH, Manley S, Gillette JM, Lippincott-Schwartz J, Verkhusha VV (2009) Photoactivatable mCherry for high-resolution two-color fluorescence microscopy. Nat Methods 6(2):153–159. doi:10.1038/nmeth.1298
25. Flors C, Hotta J, Uji-i H, Dedecker P, Ando R, Mizuno H, Miyawaki A, Hofkens J (2007) A stroboscopic approach for fast photoactivation-localization microscopy with Dronpa mutants. J Am Chem Soc 129(45):13970–13977. doi:10.1021/ja074704l
26. Lee SH, Shin JY, Lee A, Bustamante C (2012) Counting single photoactivatable fluorescent molecules by photoactivated localization microscopy (PALM). Proc Natl Acad Sci U S A 109(43):17436–17441. doi:10.1073/pnas.1215175109
27. Nienhaus GU, Nienhaus K, Hölzle A, Ivanchenko S, Renzi F, Oswald F, Wolff M, Schmitt F, Röcker C, Vallone B, Weidemann W,

Heilker R, Nar H, Wiedenmann J (2006) Photoconvertible fluorescent protein EosFP: biophysical properties and cell biology applications. Photochem Photobiol 82(2):351–358. doi:10.1562/2005-05-19-RA-533

28. Nienhaus K, Nienhaus GU, Wiedenmann J, Nar H (2005) Structural basis for photo-induced protein cleavage and green-to-red conversion of fluorescent protein EosFP. Proc Natl Acad Sci U S A 102(26):9156–9159. doi:10.1073/pnas.0501874102
29. Adam V, Lelimousin M, Boehme S, Desfonds G, Nienhaus K, Field MJ, Wiedenmann J, McSweeney S, Nienhaus GU, Bourgeois D (2008) Structural characterization of IrisFP, an optical highlighter undergoing multiple photo-induced transformations. Proc Natl Acad Sci U S A 105(47):18343–18348. doi:10.1073/pnas.0805949105
30. Fuchs J, Böhme S, Oswald F, Hedde PN, Krause M, Wiedenmann J, Nienhaus GU (2010) A photoactivatable marker protein for pulse-chase imaging with superresolution. Nat Methods 7:627–630. doi:10.1038/nmeth.1477
31. Brodehl A, Hedde PN, Dieding M, Fatima A, Walhorn V, Gayda S, Saric T, Klauke B, Gummert J, Anselmetti D, Heilemann M, Nienhaus GU, Milting H (2012) Dual color photoactivation localization microscopy of cardiomyopathy-associated desmin mutants. J Biol Chem 287(19):16047–16057. doi:10.1074/jbc.M111.313841
32. Huisken J, Stainier DY (2009) Selective plane illumination microscopy techniques in developmental biology. Development 136(12):1963–1975. doi:10.1242/dev.022426
33. Cella Zanacchi F, Lavagnino Z, Perrone Donnorso M, Del Bue A, Furia L, Faretta M, Diaspro A (2011) Live-cell 3D super-resolution imaging in thick biological samples. Nat Methods 8(12):1047–1049. doi:10.1038/nmeth.1744
34. Huang ZL, Zhu H, Long F, Ma H, Qin L, Liu Y, Ding J, Zhang Z, Luo Q, Zeng S (2011) Localization-based super-resolution microscopy with an sCMOS camera. Opt Express 19(20):19156–19168. doi:10.1364/OE.19.019156
35. Long F, Zeng S, Huang ZL (2012) Localization-based super-resolution microscopy with an sCMOS camera part II: experimental methodology for comparing sCMOS with EMCCD cameras. Opt Express 20(16):17741–17759. doi:10.1364/OE.20.017741
36. Li Y, Ishitsuka Y, Hedde PN, Nienhaus GU (2013) Fast and efficient molecule detection in localization-based super-resolution microscopy by parallel adaptive histogram equalization. ACS Nano 7(6):5207–5214. doi:10.1021/nn4009388
37. Manley S, Gillette JM, Patterson GH, Shroff H, Hess HF, Betzig E, Lippincott-Schwartz J (2008) High-density mapping of single-molecule trajectories with photoactivated localization microscopy. Nat Methods 5(2):155–157. doi:10.1038/nmeth.1176
38. Veatch SL, Machta BB, Shelby SA, Chiang EN, Holowka DA, Baird BA (2012) Correlation functions quantify super-resolution images and estimate apparent clustering due to over-counting. PLoS One 7(2):e31457. doi:10.1371/journal.pone.0031457
39. Sengupta P, Jovanovic-Talisman T, Skoko D, Renz M, Veatch SL, Lippincott-Schwartz J (2011) Probing protein heterogeneity in the plasma membrane using PALM and pair correlation analysis. Nat Methods 8(11):969–975. doi:10.1038/nmeth.1704
40. Owen DM, Rentero C, Rossy J, Magenau A, Williamson D, Rodriguez M, Gaus K (2010) PALM imaging and cluster analysis of protein heterogeneity at the cell surface. J Biophotonics 3(7):446–454. doi:10.1002/jbio.200900089
41. Henriques R, Lelek M, Fornasiero EF, Valtorta F, Zimmer C, Mhlanga MM (2010) QuickPALM: 3D real-time photoactivation nanoscopy image processing in ImageJ. Nat Methods 7(5):339–340. doi:10.1038/nmeth0510-339
42. Holden SJ, Uphoff S, Kapanidis AN (2011) DAOSTORM: an algorithm for high-density super-resolution microscopy. Nat Methods 8(4):279–280. doi:10.1038/nmeth0411-279
43. Wolter S, Schuttpelz M, Tscherepanow M, Van de Linde S, Heilemann M, Sauer M (2010) Real-time computation of subdiffraction-resolution fluorescence images. J Microsc 237(1):12–22. doi:10.1111/j.1365-2818.2009.03287.x
44. York AG, Ghitani A, Vaziri A, Davidson MW, Shroff H (2011) Confined activation and subdiffractive localization enables whole-cell PALM with genetically expressed probes. Nat Methods 8(4):327–333. doi:10.1038/nmeth.1571
45. Annibale P, Vanni S, Scarselli M, Rothlisberger U, Radenovic A (2011) Identification of clustering artifacts in photoactivated localization microscopy. Nat Methods 8(7):527–528. doi:10.1038/nmeth.1627
46. Roy A, Field MJ, Adam V, Bourgeois D (2011) The nature of transient dark states in a photoactivatable fluorescent protein. J Am Chem Soc 133(46):18586–18589. doi:10.1021/ja2085355
47. Wiedenmann J, Ivanchenko S, Oswald F, Schmitt F, Röcker C, Salih A, Spindler KD, Nienhaus GU

(2004) EosFP, a fluorescent marker protein with UV-inducible green-to-red fluorescence conversion. Proc Natl Acad Sci U S A 101(45):15905–15910. doi:10.1073/pnas.0403668101

48. Wiedenmann J, Gayda S, Adam V, Oswald F, Nienhaus K, Bourgeois D, Nienhaus GU (2011) From EosFP to mIrisFP: structure-based development of advanced photoactivatable marker proteins of the GFP-family. J Biophotonics 4(6):377–390. doi:10.1002/jbio.201000122
49. Gayda S, Nienhaus K, Nienhaus GU (2012) Mechanistic insights into reversible photoactivation in proteins of the GFP family. Biophys J 103(12):2521–2531. doi:10.1016/j.bpj.2012.11.011

Chapter 17

pcSOFI as a Smart Label-Based Superresolution Microscopy Technique

Benjamien Moeyaert and Peter Dedecker

Abstract

Stochastic optical fluctuation imaging (SOFI) is a superresolution imaging technique that uses the flickering of fluorescent labels to generate a microscopic image with a resolution better than what the diffraction limit allows. Its adaptation towards fluorescent protein-labeled samples (called photoconversion SOFI or pcSOFI) allows for a straightforward and easily accessible way of generating superresolution images. In this protocol, we will discuss how so-called "smart labels," and specifically the reversibly switchable fluorescent proteins, have opened doors towards superresolution imaging in general and we provide a protocol on how to perform pcSOFI on HeLa cells expressing human β-actin labeled with the reversibly photoswitchable fluorescent protein Dronpa.

Key words Diffraction limit, Superresolution microscopy, Imaging, Smart labels, Fluorescent proteins, Reversible photoswitching, pcSOFI

1 Introduction

1.1 Breaking an Unbreakable Barrier

Nature is intrinsically complex on many scales. While macroscopic phenomena are readily observed by the naked eye, the microscope has provided great insights into nature at a much smaller and somehow more fundamental level. For decades, fluorescence microscopy has been the technique of choice for studying biological phenomena at the micrometer and sub-micrometer scale. However, the spatial resolution of light-based microscopy is restricted by what is called the diffraction limit.

Visible light is an electromagnetic wave with wavelengths in the 400–700 nm range. As a result of this wave-like nature, light emitted by a point source will be detected as a spatial intensity distribution rather than a single point (Fig. 1a). This distribution is a direct consequence of diffraction. In the second half of the nineteenth century, Ernst Abbe found that the lateral dimensions of this distribution can be approximated as a spot with radius $\lambda/(2\ \mathrm{NA})$. In this equation, NA is the numerical aperture of the

Sidney Cambridge (ed.), *Photoswitching Proteins: Methods and Protocols*, Methods in Molecular Biology, vol. 1148,
DOI 10.1007/978-1-4939-0470-9_17,

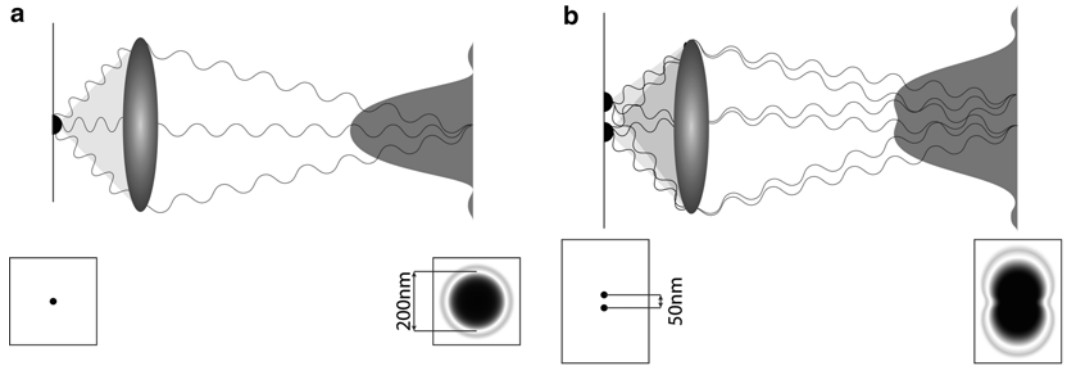

Fig. 1 Diffraction and resolution. (**a**) The wave-like nature of light leads to diffraction. As a result, the emission of an infinitesimally small emitter describes a point spread function of typically 200 nm in diameter. (**b**) Point sources closer than the diffraction limit (e.g., 50 nm) cannot be resolved due to overlapping point spread functions

objective, a measure for the size of the cone of light that can be collected by the objective, with a value that is usually less than 1.5. This diffraction-limited spot is often referred to as the "point spread function".

As a result of point spreading, two emitters that are sufficiently close to each other project overlapping intensity profiles (Fig. 1b). When two such emitters are close enough, the individual projections can no longer be discriminated and the individual emitters cannot be resolved. This so-called diffraction limit is wavelength- and NA-dependent; a typical value is about 200–250 nm. As a consequence, at large magnifications, the image is inevitably blurred. Given that the scale of many biological structures and processes is smaller than this diffraction limit, the implications for biological fluorescence microscopy applications are obvious.

Point spreading is an unavoidable barrier in far-field fluorescence microscopy. However, recent scientific developments offered ways to reduce this problem. One solution is to reduce or prevent fluorescence emission from emitters that would otherwise overlap. This is an interesting paradox. High label densities are needed to image fine structures, but detecting labels at lower densities seems to open doors for higher resolution imaging. The solution to this apparent contradiction is to *temporarily* reduce the detected label density. In other words, classical labels, following a fixed and well defined chain of events (they are irradiated, get excited, and emit fluorescence) are insufficient. Their direct linear coupling between irradiated light and fluorescence emission leaves no room to avoid the consequences of diffraction.

Increasingly however, new fluorescent labels are being discovered that display a nonlinear relationship between the intensity of excitation light they receive and the intensity of the emitted fluorescence. In other words, these labels do not inevitably process an incoming photon into an emitted photon, but can use the energy of the

incoming photon to access a range of different states with different emissive properties. Because their emissive properties can be altered effectively at will, they have been referred to as "smart labels" [1].

Using these smart labels, it is possible to come up with techniques that temporarily reduce the local density of emissive labels and perform repeated measurements to build up a superresolution image. There are roughly two ways of doing this. The first idea is to use patterned illumination to locally and temporarily alter the emissive properties of a subset of labels. The labels respond differently depending on their position relative to the pattern, which provides a means of sharpening the resulting excitation or emission distributions. The second idea is to apply a uniform illumination to the sample and use the stochastical nature of the photophysical processes in the smart labels to create evolving fluorescence distributions in which different combinations of emitters are active at any given instant. However, at the core of every superresolution technique is the use of "smart labels" not just as passive photon sources, but as active partners in the measurement.

Rather than giving a complete overview of superresolution imaging techniques, which has already been presented in several review papers [2–5], we will, guided by a few examples, demonstrate how these techniques crucially depend on smart labels, with a particular emphasis on smart fluorescent protein labels.

1.2 Smart Fluorescent Proteins

Fluorescent proteins (FPs) are genetically encoded labels that have been successfully used in numerous life science research settings [6]. Interestingly, some of these FPs were found to display so-called photoactivation properties, meaning that their fluorescence emission can be altered by irradiating them with light of specific wavelengths (Fig. 2) [7]. Not only are these smart fluorescent proteins interesting from a biophysical and photophysical point of view, they above all are pivotal in superresolution imaging of living systems.

The first example of superresolution imaging with smart fluorescent protein labels is based on reversibly switchable fluorescent proteins (RSFPs), which can be reversibly switched between a bright fluorescent and a dim, nonfluorescent state (Fig. 2a). This behavior is used in reversible saturable optical fluorescence transitions (RESOLFT) microscopy (Fig. 3) [8]. In this technique, a light pattern is applied onto the sample in order to bring a subset of emitters to a non-emissive state. For example, quenching light can be focused into a special intensity distribution that irradiates only molecules towards the edges of the focal volume of a confocal microscope. As a result, only those labels are switched off, and fluorescence from the labels residing in a center area arbitrarily smaller than the diffraction limit can be excited and detected, while the off-center molecules do not contribute. The sample is point scanned and although the excitation beam used to read out the fluorescence is diffraction limited, the detected point spread function is effectively reduced

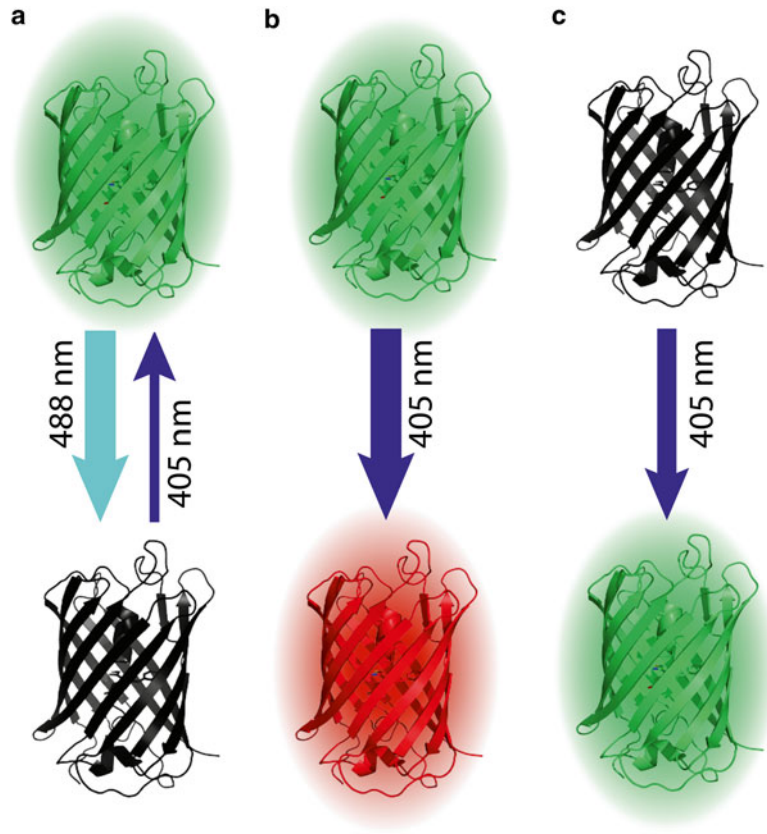

Fig. 2 (**a**) Reversibly photoswitchable fluorescent proteins (RSFPs) can be switched off from a bright, green-emissive state to a dark, non-emissive state with high intensity 488 nm light. The dark state is efficiently returned to the bright state with low-intensity 405 nm light. (**b**) Green-to-red photoconvertible fluorescent proteins (PCFPs) exist as green-emissive species that can irreversibly be converted to a red-emissive state by applying 405 nm light. (**c**) Photoactivatable fluorescent proteins (PAFPs) are initially in a nonfluorescent state. Upon activation with 405 nm light, they irreversibly become fluorescent

thanks to the fluorescence depletion. A similar technique is STED [9], which makes use of stimulated emission depletion instead of photoswitching. As a result, this technique is somewhat less flexible when used with fluorescent proteins. Patterned illumination is also the basis for some diffraction-unlimited wide-field applications such as nonlinear structured illumination microscopy (NSIM) [10] or wide-field applications of RESOLFT [11].

Two other interesting classes of smart fluorescent proteins are the irreversibly photoconvertible fluorescent proteins (PCFPs) (Fig. 2b) and the irreversibly photoactivatable fluorescent proteins (PAFPs) (Fig. 2c). The former class consists of initially green fluorescent proteins that upon irradiation with 405-nm light convert

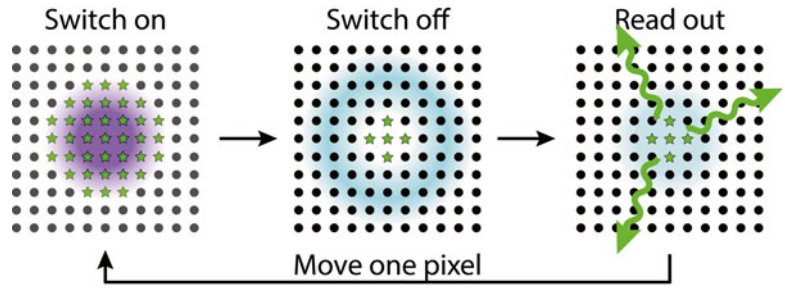

Fig. 3 The RESOLFT technique. In the diffraction-limited focal spot, all molecules are switched on with 405 nm light. Next, a donut-shaped beam of 488 nm light is applied, bringing off-center molecules to a non-emissive state. In the last step, the emission of the center molecules, located in an area smaller than the diffraction limit, is collected. This process is repeated for every pixel until the entire region of interest is imaged

to a red fluorescent state, while the latter class consists of initially nonfluorescent proteins that become fluorescent upon activation with 405-nm light. These two classes open doors for a different kind of superresolution imaging approach. Since they can both be turned on from a non-detected to a detected state, it is possible to image only a subset of labels by tuning the activation light. When in every frame no two emitters overlap, every molecule can be detected individually. Furthermore, since the shape of the point-spread function is known, the physical position of an emitter can be perfectly determined if its emission spot is directly recorded. By tuning the photoactivation such that the emitters are slowly activated over the course of many acquired fluorescence images, the emission spot of each emitter can be clearly resolved. These images can then be subjected to an automated analysis, where a computer program automatically analyzes the resulting fluorescence images and determines the precise position of every fluorophore. These positions are then used to create synthetic superresolution images. A number of different techniques, collectively known as "localization microscopy" [12], exploit this principle, though in the context of fluorescent proteins this concept is typically known as photoactivated localization microscopy (PALM) (Fig. 4) [13]. It is seen here that reversibility of the activation is not strictly required. However, RSFPs can be useful for PALM, for instance for repeated imaging of the same sample.

Localization microscopy requires that the observed label density is as low as possible, so that the emission of the individual molecules does not overlap. In fact, localization microscopy is simply an example of the more fundamental underlying concept: taking advantage of the fluorescence dynamics of the fluorophores to record multiple, complementary views of the same (stationary) sample. Superresolution information can be extracted by comparing the

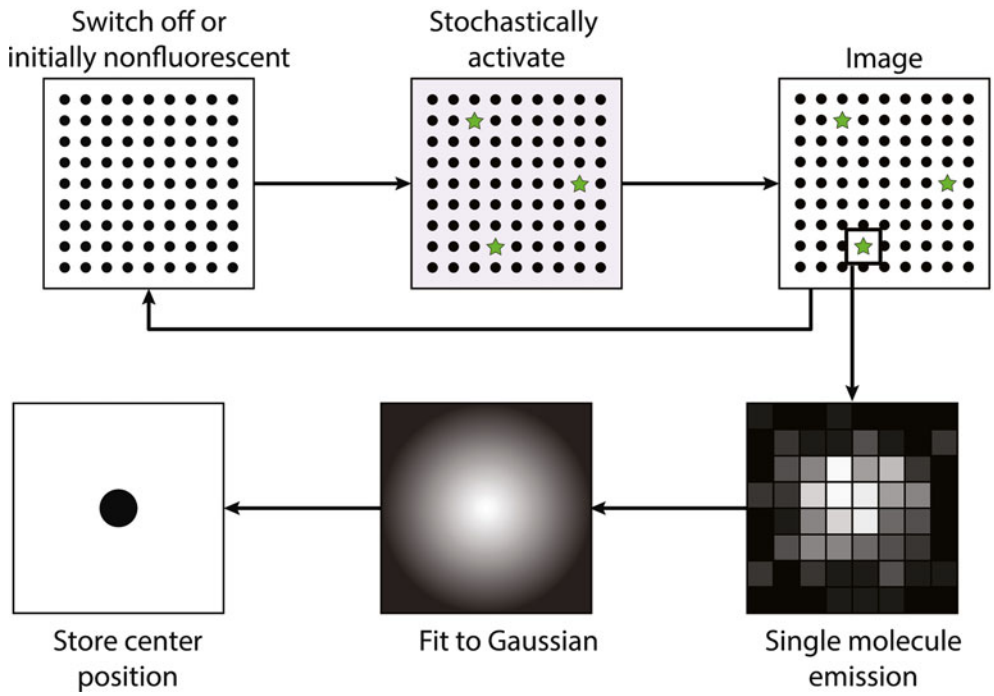

Fig. 4 The technique of PALM. All molecules in the field of view are brought to a non-emissive state or are already nonfluorescent. By applying very low doses of activation light, some molecules are stochastically brought to a detectable state. The sample is visualized and the cycle repeats until all emitters have been visualized. Afterwards, in every recorded image the single molecule emitters are identified, fitted to a 2D-Gaussian function and their center position is stored. A diffraction-unlimited image is reconstructed from these center positions

resulting images with one another. PALM is a powerful example, but there is a wide range of conditions under which individually resolvable emitters cannot be prepared, though overlapping and apparently highly complex fluctuations in emitter emission can be observed. One way of creating such images would be to irradiate an RSFP-labeled sample with both off- and on-switching light. The resulting "flickering" images can be used to obtain a superresolution image using a technique called stochastic optical fluctuation imaging or SOFI [14, 15], even when the emission of individual molecules is not resolvable at all. When using RSFPs, SOFI microscopy is typically known as pcSOFI [16].

The principle behind pcSOFI is conceptually straightforward (Fig. 5). When excitation light is applied onto an RSFP-labeled sample, the labels continuously cycle between the fluorescent and nonfluorescent state (Fig. 2a), determined by the off-switching induced by the excitation light and the thermal or light-induced recovery of the fluorescent state. If the rates of off- and on-switching are well tuned, then a sustained flickering of the RSFP labels can be seen. In every pixel, the measured intensity is the sum of the intensities of several neighboring molecules. Since the fluctuations of every emitter are independent from all

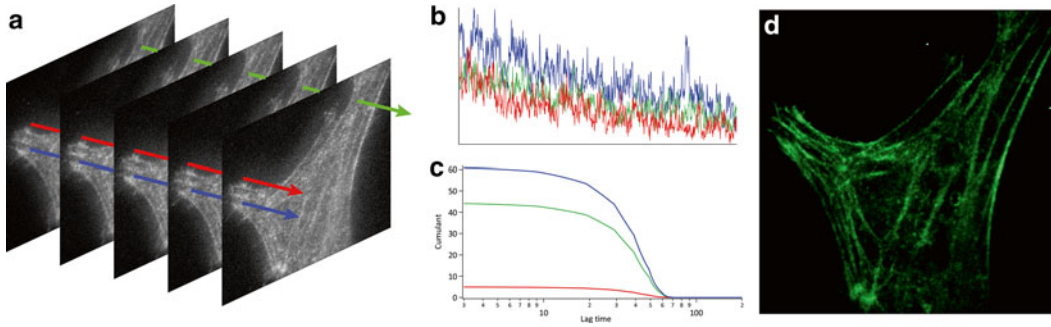

Fig. 5 The SOFI technique. (**a**) A stack of images showing flickering fluorescent labels is recorded. (**b**) For every pixel, an intensity trace is generated and (**c**) the cumulant is calculated. The magnitude of this cumulant is then used to reconstruct (**d**) a diffraction-unlimited image

the other emitters, their contributions can be more selectively extracted using a cumulant analysis, which is analogous to a correlation analysis (see Box: Cumulants? Orders?: How SOFI Works). Plotting the cumulant instead of the intensity results in an image that displays a reduced background, a better contrast, and a higher spatial resolution.

The most attractive aspects of pcSOFI are its ability to provide repeated imaging (including 3D imaging) with comparatively fast temporal resolution (compared to PALM) under a wide range of conditions. The imaging can be performed using a range of RSFPs and is very well accessible for nonexpert users. Because of its wide range of applications in biological superresolution imaging, we will discuss pcSOFI with some of its practicalities and end this chapter with a hands-on protocol for pcSOFI imaging of RSFP-labeled human β-actin in cultured HeLa cells.

1.3 Requirements and Deliverables for pcSOFI

In this second part, we discuss what can be expected from and what is needed for pcSOFI. We discuss the spatial and temporal resolution, which labels are suitable for pcSOFI, what equipment is needed, and lastly we provide some information concerning the data analysis.

1.4 Spatial and Temporal Resolution

Theoretically the resolution of pcSOFI is unlimited, but in practice, a threefold resolution increase, up to 70 nm, is what is readily achievable with the current FPs. This is less than can be achieved with PALM (for which a typical resolution is around 20 nm), which is probably the closest relative to pcSOFI in terms of experimental hardware and imaging strategy. As we have outlined above, this discrepancy is due to the much lower requirements that pcSOFI imposes on the imaging: instead of requiring individually resolvable emitters, only observable fluctuations in fluorescence are needed, and the imaging can therefore be performed under conditions where PALM imaging would fail. This also means that the imaging can be performed with many more labels active in any

given image, and as a consequence, a small image sequence containing 500 frames is enough to generate superresolution data. With as little as 100 frames, a significant resolution enhancement can already be obtained. This allows for the diffraction-unlimited visualization of dynamic processes in living systems with temporal resolutions of a few seconds or less.

1.5 Available Labels

Sample preparation and labeling have to be well adapted to both the sample and the imaging technique in question. In addition to fluorescent proteins, SOFI imaging has been performed using synthetic dyes [17] and quantum dots [14]. In combination with antibodies or other targeting strategies, they can be specifically and efficiently targeted to any structure of choice, and can allow excellent imaging. However, some of these labeling strategies have low biocompatibility for example because of potential toxicity when brought into the cell.

For live cell experiments, fluorescent proteins are the typical labels of choice. For pcSOFI, the repertoire of labels that can be used is broad. While originally only the RSFPs Dronpa [18] and rsTagRFP [19] (green- and red-emitting, respectively) were reported, we have found that a broad range of RSFPs and even non-switchable FPs (for instance Emerald [20]) display the kind of flickering that can be processed via pcSOFI into high resolution data (unpublished findings).

1.6 Required Equipment

pcSOFI has only modest technical requirements, and can often be performed on hardware that is readily available. For optimal imaging, excitation light should be provided by lasers, coupled into an inverted fluorescence microscope equipped with a high-NA objective and appropriate filters. A 488 nm laser line can be used for Dronpa and other GFPs, while a 561 nm laser line can be used for rsTagRFP or other RFPs. An EMCCD camera is the detector of choice, because of the good signal-to-noise ratio that can be obtained, coupled with the high speed of acquisition. If the sample can be analyzed by TIRF imaging then a TIRF illumination system can be advantageous, though it is not required.

We have used a variety of setups to acquire pcSOFI data. Good quality data could be obtained with home-built setups with different brands of optics, microscope bodies, lasers, and cameras. Also, we used two commercial wide-field fluorescence microscopes (Nikon Eclipse and Olympus cell^tirf) and found them to be very well suited for pcSOFI microscopy. Overall, any sufficiently sensitive microscope with the ability to acquire images at fairly high rates should be suitable.

1.7 Data Analysis

As a statistical technique, SOFI is based on computational processing of the acquired data. In a nutshell, SOFI software calculates for any given pixel the intensity fluctuation in time upon which an

auto- or cross-correlation analysis is performed. From the correlation function then, the cumulant (a parameter that has the same value as the correlation for second and third order correlation analysis) is extracted and used as intensity value for that specific pixel (Fig. 5). In order to get the most out of the analysis, an extra calculation, such as a so-called Richardson-Lucy deconvolution, has to be performed. More information can be found in the Box and in references [14, 15, 17].

The actual cumulant analysis requires only a very limited number of parameters and settings, such as the order of the calculation, and can therefore be performed even with comparatively little experience. Higher order calculations allow a higher resolution improvement to be realized, though at the cost of increased sensitivity to noise, requiring the acquisition of more fluorescence images during the experiment. With the current FPs, second- and third-order SOFI calculations are possible.

By virtue of the underlying concepts, SOFI calculations are unlikely to induce artificial structuring or biasing into the resulting output images. In other words, SOFI should not introduce spurious structural features or details into the superresolution image. Furthermore, if the sample is uniformly illuminated and the fluorophores display similar fluctuations and brightnesses then the observed signal is proportional to the local concentration of the fluorophore. However, if these assumptions are not true then these differences can be amplified in the output SOFI image.

The actual calculations used in SOFI imaging are not particularly difficult to implement. However, we have created a freely available and open-source implementation of the SOFI analysis, which is described in further detail below.

Cumulants? Orders?: How SOFI Works

The key requirement for SOFI microscopy is the stochastical fluctuation of the individual fluorescent emitters. Because of the stochasticity and reversibility of the process underlying fluorescence blinking, one can record many images, every one of them representing the same structure but with a different subset of emitting molecules.

So what happens in the "black box" of a SOFI calculation? Say that we acquired a fluorescence movie consisting of 100 images using a camera that has 512×512 pixels (262,144 pixels in total). That means that for every one of those 262,144 pixels, we recorded 100 intensity values. We can now characterize each of those 262,144 series of 100 intensity values using a statistical approach known as *cumulants*. Cumulants are simply numbers that tell us something about what a particular distribution looks like. In fact, there is a whole family of cumulants, known as different *orders*. The second-order cumulant is the most simple, followed by the third order cumulant, up to a cumulant of any order n. This concept of orders is no different from what you may have encountered in everyday statistics: the mean of a distribution is also known as its first moment, while its variance is

(continued)

known as the second moment, the skewness as the third moment, and so on for a theoretically unlimited number of moments.

So what do these cumulants look like in practice? They are somewhat difficult to write down straightforwardly, so instead we usually compute them by calculating correlation functions. Here is the expression for the second order cumulant $C_2(\tau)$, which is the most simple one that we use in SOFI:

$$C_2(\tau) = \langle \delta F(t) \cdot \delta F(t+\tau) \rangle \quad (1)$$

In this expression $F(t)$ is simply the fluorescence intensity (the pixel value) in the image acquired at time t. δ means "fluctuation of", so $\delta F(t)$ can be read as "the fluctuation of the fluorescence at time t". In other words, we simply take the pixel value at time t and subtract the average of all values that we recorded for that pixel, which then gives us the fluctuation. The notation $\langle \cdots \rangle$ means that we average whatever is between the angle brackets over all the acquired images. Lastly, the τ parameter is known as the time lag. It means that we can multiply a fluctuation at time t with a fluctuation at time $t+\tau$ if we choose to do so. However, we usually set τ equal to zero, so we obtain:

$$C_2 = \langle \delta F(t)^2 \rangle. \quad (2)$$

It may not seem like it yet, but this formula gives us a very simple recipe to calculate SOFI images! Basically, here is what it says: for every one of those 262,144 pixels, convert the 100 intensity values to fluctuations (deviations from the average) by subtracting the average value for that pixel. Next take the square of each of those fluctuations, and calculate the average. The resulting number is the value of that pixel in the SOFI image. Seems familiar? Could be, because this is simply the calculation of the variance of the pixel values! The superresolution information comes from the fact that we square the fluctuations in Eq. 2, which results in an image of which the effective point spread function is narrower. While taking the square of all the values in an image will lead to peaks becoming sharper, it will not cause them to become more resolved, and that is why we need to include multiple image acquisitions.

Now we take a look at what the third order cumulant in the simplest case looks like also compare it with Eq. 2:

$$C_3 = \langle \delta F(t)^3 \rangle. \quad (3)$$

In this case we are working with the cube of the fluctuations, so we end up with more resolution improvement. However, as also the noise is cubed, the third order cumulant is more susceptible to this noise. In general, higher cumulant orders produce a more substantial resolution improvement, but either requires higher-quality input data or the acquisition of more images to counteract this increased susceptibility to noise in the measurement. This concept generalizes to the higher cumulant orders, though orders of four and above the mathematical expressions are no longer as simple as they are for second and third orders. For order n, we can expect a factor $\sqrt{n}$ improvement in resolution. Using deconvolution or Fourier reweighing, this can be extended to a factor n improvement. In practical experiments we will also typically use *crosscumulants* to create additional, "virtual", pixels that provide additional information but require a somewhat more complex calculation.

1.8 A Basic Protocol for SOFI Imaging

Here, we will describe a short protocol on how to image the β-actin fiber network in HeLa cells using pcSOFI. We used vector Dronpa-β-actin/pMC1 [21], containing the green RSFP Dronpa N-terminally linked to human β-actin. For dual-color imaging, we find rsTagRFP to be a suitable red RSFP.

2 Materials

2.1 Cell Culture

1. HeLa cells.
2. Growth medium: Dulbecco's modified Eagle's medium (DMEM) supplemented with 10 % fetal bovine serum (FBS), 1 % GlutaMAX, and 0.1 % gentamycin.
3. Hank's buffered salt solution (HBSS).
4. Phosphate buffered saline (PBS).
5. Fixation buffer: freshly prepared 4 % paraformaldehyde in PBS.
6. Plasmid DNA: Dronpa-β-actin/pMC1. This vector is based on the phKikGR-I-MCI vector (Amalgaam, Tokyo, Japan) in which the gene coding for human β-actin was introduced between the BamHI and the NotI site and in which the gene coding for KikGR was replaced by the gene coding for Dronpa [21].
7. 35 mm glass bottom culture dishes (MatTek Corporation, Ashland, MA, USA).

As for any superresolution imaging technique, pcSOFI benefits from careful and clean sample preparation. However, there are different degrees of "cleanliness". Single molecule clean sample preparation is rather difficult to achieve when working with biological samples. Growth media, transfection agents, and most importantly the cells themselves can generate background fluorescence. We therefore advise to work as clean as possible without overdoing it. A good way to confirm the cleanliness of the sample is to image non-transfected cells. These should give a low or negligible SOFI signal compared to transfected cells.

2.2 Microscope Setup

Although many different setups can be used for pcSOFI, we describe a home-built wide-field setup routinely used for pcSOFI with Dronpa and/or rsTagRFP as well as for PALM-type experiments using RSFPs or PCFPs. We describe the setup as we follow the light path.

1. A 404-nm (100 mW, CUBE, Coherent, Santa Clara, CA, USA), 488-nm (100 mW, Sapphire, Coherent) and 561-nm laser (200 mW, Sapphire, Coherent) are combined using appropriate dichroic mirrors (e.g., a 455 long pass and 550 long pass (all filters and dichroics from Chroma, Bellows Falls, VT, USA)) (*see* **Note 1**). The power of the 404-nm laser is reduced using ND (neutral density) filters.
2. The linearly polarized laser light is circularized using a half-wave and a quarter-wave plate (both Newport, Irvine, CA, USA)

(*see* **Note 2**) before passing two diaphragms spaced approximately 20 cm apart. These two diaphragms help in aligning the laser lines perfectly on top of each other.

3. A 5× beam expander and two 2-in. mirrors guide the light to the backport of an inverted microscope (IX83, Olympus, Hamburg, Germany) equipped with appropriate dichroics, a high-NA objective, typically a 60× NA 1.35 objective (UPLSAPO 60XO, Olympus) for measurements in epifluorescence mode or a 60× NA 1.49 TIRF objective (APON 60XOTIRF, Olympus) and emission filters.
4. The light leaving the microscope is magnified another 2.5× before being projected onto an EMCCD camera (ImagEM, Hamamatsu, Japan).

2.3 Software

We will describe the analysis using the Localizer software [22], which comes in a number of different flavors. We will use the plug-in for Igor Pro (Wavemetrics, Portland, OR, USA), a powerful visualization and analysis program. While Igor Pro is a commercial program, a free 30-day trial version is available, and should allow plenty of time to get a feel for SOFI imaging.

1. Igor Pro, available from http://www.wavemetrics.com.
2. The Localizer plug-in can be downloaded from https://bitbucket.org/pdedecker/localizer, where installation instructions are also provided.

3 Methods

3.1 Cell Culture

1. Grow HeLa cells at 37 °C with 5 % CO_2 in growth medium (*see* **Note 3**).
2. When the cells reach 80–90 % confluency, transfer 300,000 cells to a glass bottom dish.
3. Transfect the cells with the method of choice immediately after the cells have been plated. Our preferred method is the calcium phosphate method [23] with up to 5 μg of DNA for 100,000 cells.
4. Incubate the cells for 16–24 h, after which time the cells are nicely fluorescent.
5. Wash the imaging dish containing the transfected cells three times with HBSS preheated to 37 °C (*see* **Note 4**).

At this time, there are two options.

6. The live cells are imaged right away.
7. The cells are fixed. Add 2 ml of fixation buffer to the cells and incubate at 37 °C for 30 min. Wash the sample three times with PBS of 4 °C. The cells can now be stored in the fridge for later use (*see* **Note 5**).

3.2 Image Acquisition

Acquisition parameters should always be optimized depending on the setup and label used as described below.

1. Configure the camera to maximum acquisition speed, typically 30 ms. While electron multiplication is not necessarily required for pcSOFI, it can help in improving the signal-to-noise ratio, facilitating data analysis and interpretation.
2. Find a representative cell using the lowest possible light intensity (*see* **Note 6**).
3. Starting from the lowest light intensity, gradually increase the laser power until you see a uniform blinking. The image should resemble the snowy noise as seen on an analog television (*see* **Note 7**). This blinking should be consistent for more than 500 frames. Find a good balance between fluorescence intensity and bleaching rate (*see* **Note 8**).
4. Having found the optimal imaging conditions, find a representative region of interest and focus using as little light as possible.
5. Start the camera and the laser illumination simultaneously. Acquire between 200 and 2,000 frames. At first, we recommend to try recording 1,000 frames, which is more than is usually required.

3.3 Data Analysis

1. Download and install Igor Pro, available from http://www.wavemetrics.com. The Localizer plug-in can be downloaded from https://bitbucket.org/pdedecker/localizer, where installation instructions are also provided.
2. Load the data into the Localizer plug-in. This can take a few seconds depending on the number of images.
3. In the SOFI tab, several options are available. Start with a second-order cross-correlation analysis with 500–1,000 images. The software provides other options such as the time lag, the type of analysis (auto- or cross-correlation) and the order of the correlation analysis, whose parameters can be modified in order to identify the analysis settings that give the best obtainable image.
4. We recommend generating an average image using the "Also average image" option. In this case the software returns two images. One is the average image which is diffraction limited, the other is the high-resolution pcSOFI image. Comparing the average image with the pcSOFI image provides a qualitative idea of the resolution enhancement.
5. Perform a Richardson-Lucy deconvolution in order to utilize the full potential of the SOFI analysis.
6. Use the functionalities of Igor Pro as a data analysis program to create an image that suits your likes and needs.

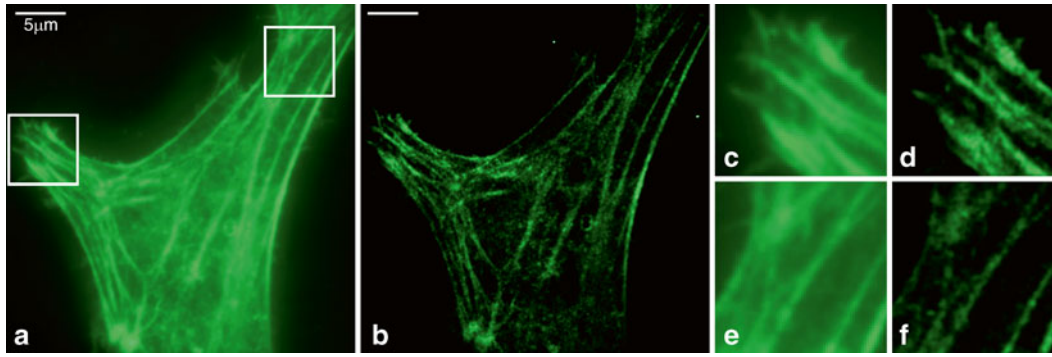

Fig. 6 Typical pcSOFI image of Dronpa-labeled human β-actin fibers in cultured HeLa cells. (**a**) Average image of 1,000 wide-field images. (**b**) Second order cross-correlation SOFI-analyzed image. (**c**)–(**f**) *Insets* highlight background reduction, contrast increase, and resolution enhancement due to the SOFI analysis

3.4 A Typical Result

A typical pcSOFI image of Dronpa-labeled human β-actin fibers in cultured HeLa cells can be found in Fig. 6. Both the average image and the pcSOFI image are displayed.

4 Notes

1. To combine one laser line with another using a dichroic mirror, it is instrumental to do so using at least two rotatable mirrors per laser. This will greatly facilitate the alignment process, as one can now rotate and move the laser line with great precision.
2. In an ideal case, one quarter-wave plate is added in front of each laser.
3. Do not add phenol red, as this is a source of background fluorescence that can heavily interfere with the imaging.
4. Changing the growth medium for HBSS ensures that the cells are in viable in atmospheric conditions. In case 5 % CO_2 incubation is applied at the microscope, cells in HBSS will die; use for example DMEM instead.
5. Fixed cells provide some temporal flexibility for example when setups are heavily booked and measurement days are limited. However, make sure not to use cells fixed more than 2 weeks ago.
6. If your microscope is equipped with an additional fluorescence lamp, use this. It will provide a bigger field of view and less intense light.
7. For examples of such flickering, see the movies in the Supplementary Information of reference [16].
8. If the fluorescence intensity decreases very fast due to fast off-switching, applying very low doses of 405-nm light can be a good idea.

Acknowledgments

The authors thank Susana Rocha and Jeroen Vangindertael for setting up and maintaining some of the microscope setups, Doortje Borrenberghs for help with the cell culture, and Hideaki Mizuno for the Dronpa-β-actin/pMC1 construct. B.M. is funded by a Ph.D. grant from the Agency for Innovation by Science and Technology (IWT) Flanders. P.D. is a postdoctoral fellow of the Research Foundation–Flanders (FWO).

References

1. Dedecker P, De Schryver FC, Hofkens J (2013) Fluorescent proteins: shine on, you crazy diamond. J Am Chem Soc 135:2387–2402. doi:10.1021/ja309768d
2. Heilemann M, Dedecker P, Hofkens J, Sauer M (2009) Photoswitches: key molecules for subdiffraction-resolution fluorescence imaging and molecular quantification. Laser Photon Rev 3:180–202. doi:10.1002/lpor.200810043
3. Huang B (2010) Super-resolution optical microscopy: multiple choices. Curr Opin Chem Biol 14:10–14. doi:10.1016/j.cbpa.2009.10.013
4. Heilemann M (2010) Fluorescence microscopy beyond the diffraction limit. J Biotechnol 149:243–251. doi:10.1016/j.jbiotec.2010.03.012
5. Hell SW (2007) Far-field optical nanoscopy. Science 316:1153–1158. doi:10.1126/science.1137395
6. Chudakov DM, Matz MV, Lukyanov S, Lukyanov KA (2010) Fluorescent proteins and their applications in imaging living cells and tissues. Physiol Rev 90:1103–1163. doi:10.1152/physrev.00038.2009
7. Lukyanov KA, Chudakov DM, Lukyanov S, Verkhusha VV (2005) Innovation: photoactivatable fluorescent proteins. Nat Rev Mol Cell Biol 6:885–891. doi:10.1038/nrm1741
8. Hofmann M, Eggeling C, Jakobs S, Hell SW (2005) Breaking the diffraction barrier in fluorescence microscopy at low light intensities by using reversibly photoswitchable proteins. Proc Natl Acad Sci U S A 102:17565–17569. doi:10.1073/pnas.0506010102
9. Hell SW, Wichmann J (1994) Breaking the diffraction resolution limit by stimulated emission: stimulated-emission-depletion fluorescence microscopy. Optic Lett 19:780–782
10. Gustafsson MGL (2005) Nonlinear structured-illumination microscopy: wide-field fluorescence imaging with theoretically unlimited resolution. Proc Natl Acad Sci U S A 102:13081–13086. doi:10.1073/pnas.0406877102
11. Schwentker MA, Bock H, Hofmann M et al (2007) Wide-field subdiffraction RESOLFT microscopy using fluorescent protein photoswitching. Microsc Res Tech 70:269–280. doi:10.1002/jemt.20443
12. Herbert S, Soares H, Zimmer C, Henriques R (2012) Single-molecule localization super-resolution microscopy: deeper and faster. Microsc Microanal 18:1419–1429. doi:10.1017/S1431927612013347
13. Betzig E, Patterson GH, Sougrat R et al (2006) Imaging intracellular fluorescent proteins at nanometer resolution. Science 313:1642–1645. doi:10.1126/science.1127344
14. Dertinger T, Colyer R, Iyer G et al (2009) Fast, background-free, 3D super-resolution optical fluctuation imaging (SOFI). Proc Natl Acad Sci U S A 106:22287–22292. doi:10.1073/pnas.0907866106
15. Dertinger T, Pallaoro A, Braun G et al (2013) Advances in superresolution optical fluctuation imaging (SOFI). Q Rev Biophys 46(2):210–221. doi:10.1017/S0033583513000036
16. Dedecker P, Mo GCH, Dertinger T, Zhang J (2012) Widely accessible method for superresolution fluorescence imaging of living systems. Proc Natl Acad Sci U S A 109:10909–10914. doi:10.1073/pnas.1204917109
17. Dertinger T, Heilemann M, Vogel R et al (2010) Superresolution optical fluctuation imaging with organic dyes. Angew Chem Int Ed Engl 49:9441–9443. doi:10.1002/anie.201004138
18. Ando R, Mizuno H, Miyawaki A (2004) Regulated fast nucleocytoplasmic shuttling observed by reversible protein highlighting. Science 306:1370–1373. doi:10.1126/science.1102506
19. Pletnev S, Subach FV, Dauter Z et al (2012) A structural basis for reversible photoswitching of absorbance spectra in red fluorescent protein rsTagRFP. J Mol Biol 417:144–151. doi:10.1016/j.jmb.2012.01.044

20. Cubitt AB, Woollenweber LA, Heim R (1999) Understanding structure-function relationships in the Aequorea victoria green fluorescent protein. Meth Cell Biol 58:19–30
21. Mizuno H, Dedecker P, Ando R et al (2010) Higher resolution in localization microscopy by slower switching of a photochromic protein. Photochem Photobiol Sci 9:239–248. doi:10.1039/b9pp00124g
22. Dedecker P, Duwé S, Neely RK, Zhang J (2012) Localizer: fast, accurate, open-source, and modular software package for superresolution microscopy. J Biomed Optic 17:126008. doi:10.1117/1.JBO.17.12.126008
23. Sambrook J, Fritsch EF, Maniatis T (1989) Molecular cloning a laboratory manual. Cold Spring Harbor Laboratory Press, New York, pp 931–957

Index

Sidney Cambridge (ed.), *Photoswitching Proteins: Methods and Protocols*, Methods in Molecular Biology, vol. 1148, DOI 10.1007/978-1-4939-0470-9, © Springer Science+Business Media New York 2014

M

N

O

P

R

S

T

V

Z